AD NUMBER

AD920282

NEW LIMITATION CHANGE

TO

Approved for public release, distribution unlimited

FROM

Distribution authorized to U.S. Gov't. agencies only; Test and Evaluation; Oct 1973. Other requests shall be referred to Air Force Flight Dynamics Laboratory, Attn: AFFDL/FY, Wright-Patterson AFB, OH 45433.

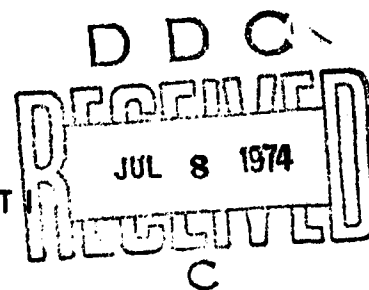## AUTHORITY

AFFDL ltr, 27 Aug 1979

AD920282

ACOUSTIC FATIGUE OF AIRCRAFT STRUCTURES AT ELEVATED TEMPERATURES

CECIL W. SCHNEIDER

LOCKHEED-GEORGIA COMPANY

D D C

JUL 8 1974

C

TECHNICAL REPORT AFFDL-TR-73-155, PART I

MARCH 1974

AIR FORCE FLIGHT DYNAMICS LABORATORY
AIR FORCE SYSTEMS COMMAND
WRIGHT-PATTERSON AIR FORCE BASE, OHIO

NOTICE

When Government drawings, specifications, or other data are used for any purpose other than in connection with a definitely related Government procurement operation, the United States Government thereby incurs no responsibility nor any obligation whatsoever; and the fact that the government may have formulated, furnished, or in any way supplied the said drawings, specifications, or other data, is not to be regarded by implication or otherwise as in any manner licensing the holder or any other person or corporation, or conveying any rights or permission to manufacture, use, or sell any patented invention that may in any way be related thereto.

ACOUSTIC FATIGUE OF AIRCRAFT STRUCTURES AT ELEVATED TEMPERATURES
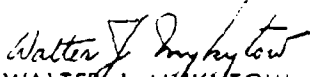
CECIL W. SCHNEIDER

FOREWORD

This report was prepared by the Lockheed-Georgia Company, Marietta, Georgia, for the Aero-Acoustics Branch, Vehicle Dynamics Division, Air Force Flight Dynamics Laboratory, Wright-Patterson Air Force Base, Ohio, under Contract F33615-72-C-1141. The work described herein is a continuing part of the Air Force Systems Command's exploratory development program to establish tolerance levels and design criteria for acoustic fatigue prevention for flight vehicles. The work was directed under Project 1471, "Aero-Acoustic Problems in Air Force Flight Vehicles," Task 147101, "Sonic Fatigue". Mr. Davey L. Smith (AFFDL/FYA) was the Task Engineer.

This report concludes the work on Contract F33615-72-C-1141, which covered a period from April 1972 to December 1973. This report is one of two issued under this contract; AFFDL-TR-73-155, Part II, is a design handbook which contains the essential design criteria of this report.

The analytical development for this program was accomplished by Mr. F. F. Rudder of Acoustics and Vibration Associates, Inc., Smyrna, Georgia, under a subcontract from the Lockheed-Georgia Company; their report identification number is AVA/TR 72-184. The Lockheed-Georgia Company report identification for this AFFDL Document is LG73ER0182.

This manuscript was submitted by the author 31 October 1973.

This technical report has been reviewed and is approved.

WALTER J. MYKYTOW
Asst. for Research and Technology
Vehicle Dynamics Division
Air Force Flight Dynamics Laboratory

ABSTRACT

An analytical and experimental program was conducted to develop acoustic fatigue design criteria for aircraft structures subjected to intense noise in a high temperature environment. Equations for the dynamic response of a buckled panel were formulated for simply supported boundary conditions using large deflection plate theory. Random amplitude acoustic fatigue testing of representative aircraft structure was accomplished at temperatures up to 600°F to provide data for correlation with the analytical results. Empirical design criteria are presented in the form of design equations and nomographs for predicting the combined thermal and dynamic response of aircraft structures.

TABLE OF CONTENTS

TABLE OF CONTENTS (Continued)

LIST OF ILLUSTRATIONS

LIST OF ILLUSTRATIONS (Continued)

LIST OF ILLUSTRATIONS (Continued)

LIST OF ILLUSTRATIONS (Continued)

LIST OF TABLES

LIST OF TABLES (Continued)

LIST OF SYMBOLS

A	Y-intercept of regression line equation
AR	Aspect ratio function $= 3(b/a)^2 + 3(a/b)^2 + 2$
A_x, A_y	Cross section area of stiffening member – in^2
a, a_i	Dimension of panel in the x-direction – inch
B	Slope of regression line equation
b, b_i	Dimension of panel in the y-direction – inch
C_{ij}	Slope compatibility coefficients, see Table I
C_{mn}	Aspect ratio scale parameter, see Equation (5)
C_x, C_y, C_z	Dimension from stiffening member shear center to centroid – inch
D	Panel flexural rigidity $= Eh^3/12(1 - \nu^2)$ – in.-lb
d	Stiffener height – inch
d_{ij}	Scale parameter for temperature rise, see Equation (35)
$_k d_{ij}$	Scale parameter for temperature rise of box structure, see Appendix I
E	Modulus of elasticity – psi
E_o	Modulus of elasticity at ambient temperature – psi
e_x, e_y, e_z	Dimension from stiffening member centroid to attachment point with skin – inch
$_1 e_i, _2 e_i$	Scale parameter for box structure, see Appendix I
F_{mn}	Aspect ratio function $= m^2(b/a) + n^2(a/b)$
F, F_1	Stress functions, see Equation (10)
F^*, F_1^*, F_2^*	Skin stiffness terms, see Equations (36) and (56)
f	Frequency – Hz
f_{ij}	Fourier coefficients for stress function

f_o Room temperature fundamental mode response frequency – Hz

G Shear Modulus – psi

G^* Modal parameter for cylindrical structure, see Appendix II

h Skin thickness – inch

h_1 Depth of box structure rib, see Appendix I

h_r Thickness of stiffening member – inch

I_{px}, I_{py} Cross-section polar moment of inertia of stiffening member – in^4

I_{xx}, I_{yy}, etc.   Cross-section second area moment of inertia of stiffening member – in^4

I^* Cross-section moment of inertia of stiffening member, see Equation (70) – in^4

J St. Venant's torsion constant for stiffening member – in^4

K_{sx}, K_{sy} Substructure stiffness terms

K^*, K^{**} Skin stiffness terms for box structure, see Appendix I

K_1 Modal stiffness of nine-bay panel below critical temperature

K_2 Modal stiffness of nine-bay panel above critical temperature

$_1K_s, _1K_r$ Skin stiffness terms for box structure, see Appendix I

K_{111} Modal stiffness for box structure below critical temperature

k_{xi}, k_{yj} Substructure stiffness terms

k_m, k_n Modal parameters for cylindrical structure, see Appendix II

M_1 Modal mass of nine-bay panel

M_{111} Modal mass of box structure, see Appendix I

M_r, M_s Mass terms for box structure, see Appendix I

m Mode number for x-direction

$\bar{m}$ Slope of approximate regression line through the origin and the data centroid $(\bar{x}, \bar{y})$

LIST OF SYMBOLS (Continued)

N_x, N_y, N_{xy} In-plane skin loading – lb/in

N_T Thermal loading on skin due to non-uniform heating

N Cycles to failure

n Mode number for y-direction

P Internal pressure on cylindrical structure, see Appendix II

p Mode number for z-direction (box structure only), see Appendix I

q, q_{mn} Generalized coordinate for transverse dynamic displacement

R, R_{ij} Aspect ratio function, see Equations (19a) and (34b)

R_c Correlation coefficient

R^* Stiffness parameter for nine-bay structure; also for box structure, see Appendix I

R^{**} Stiffness parameter for box structure, see Appendix I

r Temperature ratio $= T/T_c$

r_c Radius of curvature for cylindrical structure, see Appendix II

r_{ij} Temperature ratio for elements of nine-bay panel

r_m Temperature ratio for nine-bay panel $= T/T_{c_m}$

r_o Value of r for which nine-bay panel buckles

S_x, S_y, S_z Dimension from stiffening member shear center to the attachment point with the skin – inch

T Kinetic energy; temperature increase (note context)

T_1, T_2 Temperature of box structure skins, see Appendix I

T_p Kinetic energy of plate element

T_r Temperature of box structure rib, see Appendix I

T_{sx}, T_{sy}	Kinetic energy of substructure
T_c	Critical buckling temperature of skin - $^{\circ}F$ above ambient
T_{c_m}	Critical buckling temperature of center bay of nine-bay panel - $^{\circ}F$ above ambient
T_{c_s}	Ciritical buckling temperature of simple panel - $^{\circ}F$ above ambient
t	Time
$_i t_r, _i t_s$	Thickness of box structure ribs and skin, see Appendix I
U	Strain energy
U_p	Strain energy of plate element
U_{sx}, U_{sy}	Strain energy of substructure elements
u, v, w	In-plane displacements in x, y and z-directions
W_o	Skin thermal buckling amplitude of simple panel or center bay of nine-bay panel - inch
$_{ij} W_o$	Skin thermal buckling amplitude of plate elements of nine-bay panel
W_{ij}	Total transverse displacement of vibrating panel
x, y, z	Coordinate direction
x_c, y_c, z_c	Coordinate direction from stiffening member centroid
$\bar{x}, \bar{y}, \bar{z}$	Coordinate direction from stiffening member shear center
$\bar{x}, \bar{y}$	Centroid of data set, see Section IV
α	Coefficient of thermal expansion - $(in/in)/^{\circ}F$
Γ_e	Cross-section warping constant of substructure about shear center - in^6
Γ_x^*, Γ_y^*	Cross-section warping constants of substructure about the skin attachment points - in^6
γ	Mass density - $lb\text{-}sec^2/in^4$

LIST OF SYMBOLS (Continued)

γ_{xy} — Shear strain in x-y plane

δ_m, δ_n — Modal parameters for cylindrical structure, see Appendix II

ϵ_x, ϵ_y — Normal strain in the x and y-directions

ζ — Damping ratio

μ — Micro - 10^{-6}

ν — Poisson's ratio

π — 3.1415927

σ_c — Standard deviation from the mean

σ_m — Mean stress - psi (or ksi)

σ_T — Thermal expansion stress - psi (or ksi)

σ_x, σ_y — Normal stress in the x and y-directions - psi (or ksi)

$\bar{\sigma}_x, \bar{\sigma}_y$ — Thermal mean stress in x and y-directions - psi (or ksi)

$\sigma_{x_b}, \sigma_{y_b}$ — Thermal buckling stress in x and y-directions - psi (or ksi)

$\tilde{\sigma}_x, \tilde{\sigma}_y$ — Dynamic stress in x and y-directions - psi (or ksi) rms

τ_{xy} — Shear stress in the x-y plane - psi

$\Phi(f)$ — Acoustic pressure density - psi/$\sqrt{Hz}$

ϕ — Sector angle of cylindrical structure, see Appendix II

Mathematical Notation

$$( )_{,x}; ( )_{,xy} = \frac{\partial( )}{\partial x}; \frac{\partial^2( )}{\partial x\,\partial y}$$

$$\dot{( )} = \frac{d( )}{dt}$$

$$\ddot{( )} = \frac{d^2( )}{dt^2}$$

$$\nabla^2(\ ) = (\ )_{,xx} + (\ )_{,yy}$$

$$\nabla^4(\ ) = (\ )_{,xxxx} + 2(\ )_{,xxyy} + (\ )_{,yyyy}$$

Abbreviations

dB	Decibel (Re: 0.0002 microbar)
F	Fahrenheit
ksi	1000 psi
psi	lb/in^2
rms	Root mean square
RT	Room temperature
SPL	Sound pressure level

I - INTRODUCTION

The development of acoustic fatigue design criteria has historically followed on empirical approach, since many of the factors that affect high cyclic fatigue are not predictable. Early efforts[1] were directed toward establishment of a broad base of general design information in the form of empirical design nomographs, applicable to several structural configurations. These design charts were based on discrete frequency fatigue data that had been converted to an equivalent random amplitude fatigue curve through the use of Miles[2] single degree-of-freedom theory and the Miner-Palmgren[3] cumulative damage concept. The aircraft designer found these criteria to be of considerable value and he could, with a certain amount of individual judgment and experience, effectively control acoustic fatigue problems for conventional subsonic aircraft. However, increasing aircraft performance and size, coupled with increasingly stringent requirements for structural efficiency, created a need to refine these conservative criteria to eliminate unnecessary weight from structural designs.

Subsequent programs[4-9] were accomplished to refine and extend the range of application of the then-existing design criteria. These later programs included acoustic fatigue tests of structural panels using random amplitude excitation. The program of Reference 4 included fatigue tests of flat, stiffened-skin and honeycomb panels. A subsequent program[8] continued the refinement of stiffened-skin design criteria by developing empirical design methods for the structural support members.

The results of these previous programs have considerably reduced the uncertainties involved in predicting dynamic response and life characteristics of conventional structures subjected to both propulsion system and aerodynamic noise at ambient temperatures. However, when unusual structural configurations or environmental conditions are encountered, the applicability of existing design methodology decreases, and the judgment of the design engineer must be relied on more heavily. Structural applications are commonly encountered today in the near field of an operating turbojet or turbofan engine where severe noise, high temperatures, static loading, and vibratory buffet occur simultaneously or in conjunction with each other.

At least one attempt[6] has been made to define the effects of low frequency dynamic loads and elevated temperatures on the acoustic fatigue resistance of flat and curved simple panels, and curved honeycomb structures. One of the significant conclusions from this program was that combined environments should be investigated in limited combinations; the combined environment problem should be approached gradually and systematically. The primary cause of the fatigue failures experienced during this program was dynamic response due to acoustic excitation, acting in combination with thermal mean stresses caused by the structural heating.

The program described in this report was undertaken to extend the basic design technology for stiffened structures at ambient temperatures to include the effects of simultaneous application of thermal and acoustic environments. An analytical development is described in Section II for the dynamic response of heated structures before and after

thermal buckling. The primary purpose of the analytical effort was to identify the parameters which describe the structural response; then the data requirements for the experimental program (Section III) were defined in detail. Measured data were correlated with the analytical results in Section IV; these empirical relations were then used to establish the design methods and nomographs presented in Section V. A preliminary analytical development for the dynamic response of heated box and curved structures is presented in Appendices I and II.

The results of this investigation are also summarized in a design handbook for ease of application by the design engineer. That report, AFFDL-TR-73-155, Part II, contains the empirical equations, design nomographs, and computer programs described herein.

II - ANALYTICAL

The emphasis of the analytical effort was placed upon developing techniques for under-standing the vibration of heated structures through maximum utilization of available ana-lytical results reported in the literature. Since the beginning point of this development was the analysis previously developed by Rudder,[8] the primary task was the modification of the room temperature stiffened panel analysis to include the effect of a spatially uniform temperature increase upon the dynamic characteristics of the structure.

It was assumed that the panel vibration modes and the panel buckled modes are such that the stiffeners remain straight along the axial direction and only rotate about the attach-ment line of the stiffener and the cover sheet. The analytical model considers an array of simply supported panels constrained at the boundaries so that the slopes between adjacent panels are compatible (zero shear condition). This permits the use of sinusoidal mode shapes below and above the panel buckling temperature. The validity of this assumption was checked by using the results presented by Timoshenko[10] for a stiffened panel uniformly compressed by inplane edge forces.

The Rayleigh-Ritz method is used to derive the equations of motion for the structure. An expression is developed for predicting the temperature increase required to cause the panel to buckle; this temperature increase is defined as the critical temperature. The tempera-ture increase is defined relative to a room (or ambient) temperature at which no thermal mean stresses are present. Below the critical temperature the panel dynamic response is calculated utilizing linear small deflection plate theory. Above the critical temperature, large deflection (von Karman) plate theory is used. The large deflection plate analysis is linearized to obtain first order effects for estimating the panel dynamic response above the critical temperature. All of the assumptions are discussed as they are introduced. The effect of a temperature increase upon material properties is also considered (i.e., the temperature dependence of Young's Modulus and the coefficient of expansion).

Based on the simple panel analysis, expressions for the frequency and buckling amplitude of a flat, stiffened, nine-bay panel structure are developed. These relations include the effect of substructure stiffness and mass; however, the substructure is assumed to be temperature-independent.

A. Simple Panel Response

The geometry, nomenclature, and sign convention for the inplane forces is indicated in Figure 1, which shows the simple panel configuration. Assuming simple supports at the edges of the panel, the dynamic and buckled modes of the panel can be described by sinusoidal functions in the inplane coordinates. The analysis assumes a spatially uniform temperature increase, T, over the surface of the panel. Below the critical temperature, the thin panel is assumed to be initially flat, and small deflection plate theory is used to develop

3

the equations of motion. Above the critical temperature, the thin panel is assumed to have a buckled shape, and the equations of motion are developed by application of large deflection (von Karman) plate theory.
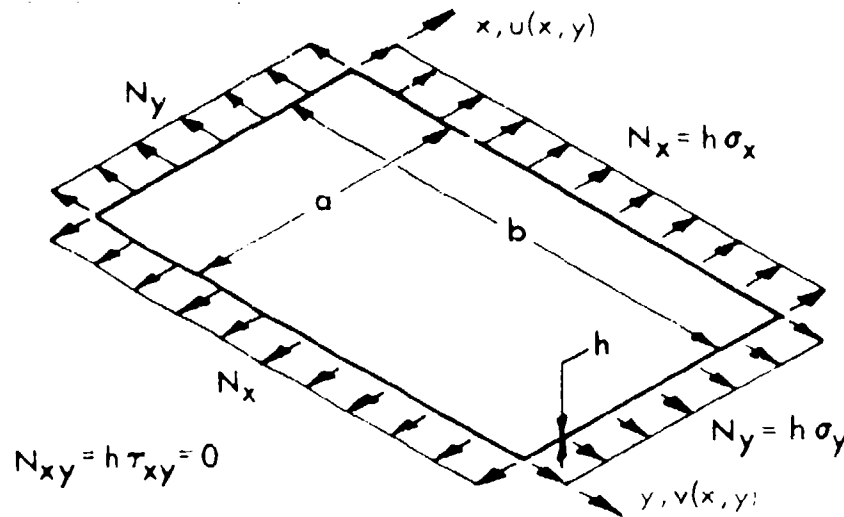
FIGURE 1. SIMPLE PANEL GEOMETRY AND NOTATION

1. Pre-Buckled Response

In the following discussion, the panel skin temperature, T, refers to the temperature increase relative to a predefined zero mean stress condition (i.e., ambient temperature).

Assuming a transverse displacement function of the form

$$w(x,y,t) = \sum_m \sum_n \sin\left(\frac{m\pi x}{a}\right) \sin\left(\frac{n\pi y}{b}\right) q_{mn}(t) \tag{1}$$

and using small displacement plate theory, the strain energy of the simple panel has the form

$$U = \frac{1}{2}D \int_0^a \int_0^b (\nabla^2 w)^2 \, dy\, dx + \frac{1}{2}h \int_0^a \int_0^b \left[\bar{\sigma}_x w_{,x}^2 + \bar{\sigma}_y w_{,y}^2\right] dy\, dx \tag{2}$$

while the kinetic energy has the form

$$T = \frac{1}{2}\gamma h \int_0^a \int_0^b \dot{w}^2 \, dy\, dx \tag{3}$$

4

Here, and throughout this development, the spatial and time dependence functions have been dropped from the basic parameter after the initial introduction to simplify the expressions.

For small deflection plate theory, the mean stresses are defined in terms of the temperature increase, T, as

$$\bar{\sigma}_x = \bar{\sigma}_y = -\frac{E\alpha T}{(1 - \nu)} \tag{4}$$

Substituting the assumed displacement function and the above mean stresses into the strain and kinetic energy expressions, the equation of motion for the (m,n) mode is determined by Lagrange's equation, and is

$$\ddot{q}_{mn} + \frac{\pi^4 D F_{mn}^2}{\gamma h a^2 b^2}(1 - C_{mn}r)q_{mn} = 0 \qquad (0 \le C_{mn}r < 1) \tag{5}$$

where $C_{mn} = F_{11}/F_{mn}$; $F_{mn} = (b/a)m^2 + (a/b)n^2$; $r = T/T_c$; and the critical buckling temperature, T_c, is

$$T_c = \frac{\pi^2 h^2 F_{11}}{12\alpha a b(1 + \nu)} \tag{5a}$$

Assuming simple harmonic motion, the expression for the natural frequency is

$$f(r) = \frac{\pi}{2ab}\left[\left(\frac{D}{\gamma h}\right)(1 - C_{mn}r)\right]^{1/2} F_{mn} \qquad (C_{mn}r < 1) \tag{6}$$

It is now advantageous to discuss certain features of these results. First, the critical temperature, T_c, is defined in terms of the panel geometry, with the only material properties being the coefficient of linear expansion, α, and Poisson's ratio, ν. Noting that the frequency expression, given by Equation (6), is a function of the mode number (m,n), it is obvious that the frequency squared for a given mode decreases linearly with an increase in temperature. The magnitude of the temperature differential required to yield a zero natural frequency for a given mode is broadly defined as the critical buckling temperature for that mode. However, from Equation (5) it is seen that the lowest critical temperature occurs for the fundamental mode (m = n = 1), and that the critical temperatures for the higher modes are related to the fundamental mode critical temperature by the panel aspect ratio and mode numbers.

Since the frequency expression given by Equation (6) is limited to positive or zero values, this analysis will be used to estimate the panel fundamental frequency response for a range of temperature such that $T \le T_c$. In other words, this analysis will be limited to temperature increases below the critical temperature. Also, all references to the critical temperature will imply the temperature increase required to cause the fundamental frequency to equal zero.

5

Finally, it should be noted that the equations of motion for each mode are uncoupled below the critical temperature. Above the critical temperature, Shulman[11] shows that the buckled panel dynamic response is coupled for the dynamic modes different from the buckled mode, but the dynamic mode corresponding to the buckled mode is uncoupled from all other dynamic modes. This result will be applied to estimate the simple panel response above the critical temperature.

2. Post-Buckled Response

The analysis presented here is a simplication of the analytical approach developed by Shulman[11] for calculating the dynamic response of a thin, rectangular panel subjected to a spatially uniform temperature increase. Since the dynamic response of the buckled panel is required, large deflection plate theory is used. Basically, the von Karman theory[12,13] is used with an assumed displacement and Airy stress function.[11] The expression for the strain energy of the buckled panel is formulated from the assumed displacement mode shape and the stress function. The nonlinear form of the stress function is linearized to obtain a first order approximation for the equations of motion.

Since this analysis is aimed at providing approximate results, certain assumptions will be introduced based on the pre-buckled analysis (below the critical temperature). First, it is assumed that the panel buckles in the fundamental mode (m = n = 1) corresponding to the lowest buckling temperature. Then, it is assumed that the only significant dynamic mode is the fundamental mode of the panel.

The amplitude of the buckled vibrating panel is defined by

$$W_{11}(t) = W_o + q(t)$$

where W_o is the static buckled panel amplitude, and $q(t)$ is the dynamic panel amplitude (both corresponding to the fundamental mode of the panel). The assumed transverse displacement has the form

$$w(x,y,t) = \sin\left(\frac{\pi x}{a}\right) \sin\left(\frac{\pi y}{b}\right) W_{11}(t) \tag{7}$$

For the panel, the stress-strain relationships are

$$\sigma_x = -\frac{E T}{(1-\nu)} + \frac{E}{(1-\nu^2)}\left[\epsilon_x + \nu\epsilon_y\right] , \quad \tau_{xy} = \frac{E}{2(1+\nu)}\gamma_{xy}$$

$$\sigma_y = -\frac{E T}{(1-\nu)} + \frac{E}{(1-\nu^2)}\left[\nu\epsilon_x + \epsilon_y\right] \tag{8}$$

and the strain-displacement relationships are

$$\epsilon_x = u,_x + \frac{1}{2} w,_x^2 \quad ; \quad \gamma_{xy} = u,_y + v,_x + w,_x w,_y$$

$$\epsilon_y = v,_y + \frac{1}{2} w,_y^2$$

(9)

For the assumed mode given by Equation (7), a suitable choice for the stress function has the form[11,12]

$$F(x,y,t) = \frac{h}{2} (\bar{\sigma}_x y^2 + \bar{\sigma}_y x^2) + F_1(x,y,t)$$

(10)

where

$$F_1(x,y,t) = Eh \sum_{m=0} \sum_{n=0} \left[\left(\frac{b}{a}\right) m^2 + \left(\frac{a}{b}\right) n^2 \right]^{-2} \cos\left(\frac{m\pi x}{a}\right) \cos\left(\frac{n\pi y}{b}\right) f_{mn}(t)$$

and (m,n) take on integer values. The significance of the mean stresses $\bar{\sigma}_x$ and $\bar{\sigma}_y$ will appear shortly. The stress function (10) and the displacement function (7) are related by

$$\nabla^4 F = -\nabla^2 N_T + Eh(w,_{xy}^2 - w,_{xx} w,_{yy})$$

(11)

where

$$N_T = \alpha E \int_{-h/2}^{h/2} T(x,y,z)dz$$

For a spatially uniform temperature increase, $\nabla^2 N_T \equiv 0$.

The relationships between the stress function, F, and the stresses given in Equation (8) are

$$h\sigma_x = F,_{yy} \quad ; \quad h\sigma_y = F,_{xx} \quad ; \quad h\tau_{xy} = -F,_{xy}$$

(12)

Substituting the assumed stress function, Equation (10), into Equations (12), it is evident that the shear stress vanishes along the edges of the panel.

The coefficients f_{mn} are obtained by substituting the assumed mode, Equation (7), into Equation (11), with the result that

$$f_{02} = \frac{1}{2} W_{11}^2 \quad ; \quad f_{20} = \frac{1}{2} W_{11}^2$$

while all other coefficients vanish identically.

Substituting these coefficients into Equation (10), the stress function becomes

7

$$F(x,y,t) = \frac{h}{2}\left(\bar{\sigma}_x y^2 + \bar{\sigma}_y x^2\right) + F_1(x,y,t)$$

(13)

$$F_1(x,y,t) = \frac{Eh}{32}\left[\left(\frac{a}{b}\right)^2 \cos\left(\frac{2\pi x}{a}\right) + \left(\frac{b}{a}\right)^2 \cos\left(\frac{2\pi y}{b}\right)\right] W_{11}^2$$

Substitution of the stress function into Equations (12) results in the static stress relations

$$\sigma_x = \frac{1}{h}F_{,yy} = \bar{\sigma}_x - \frac{\pi^2 E}{8a^2}\cos\left(\frac{2\pi y}{b}\right)W_{11}^2$$

$$\sigma_y = \frac{1}{h}F_{,xx} = \bar{\sigma}_y - \frac{\pi^2 E}{8b^2}\cos\left(\frac{2\pi x}{a}\right)W_{11}^2$$

(14)

$$\tau_{xy} \equiv 0$$

Now, substituting the strain-displacement relationships for ε_x and ε_y, Equation (9), into the stress-strain relationships for σ_x and σ_y, Equation (8), and solving for the displacements $u_{,x}$ and $v_{,y}$ gives

$$u_{,x} = \alpha T \cdot \frac{1}{E}\sigma_x - \frac{\nu}{E}\sigma_y - \frac{1}{2}w_{,x}^2$$

$$v_{,y} = \alpha T - \frac{\nu}{E}\sigma_x + \frac{1}{E}\sigma_y - \frac{1}{2}w_{,y}^2$$

(15)

Integrating these displacements and assuming that the edges of the panel are rigidly restrained from moving in the (x,y) plane yields

$$\int_0^a u_{,x}dx = u(a) - u(0) = 0 = a\alpha T + \frac{1}{E}\int_0^a \sigma_x dx - \frac{\nu}{E}\int_0^a \sigma_y dx - \frac{1}{2}\int_0^a w_{,x}^2 dx$$

(16)

$$\int_0^b v_{,y}dy = v(b) - v(0) = 0 = b\alpha T - \frac{\nu}{E}\int_0^b \sigma_x dy + \frac{1}{E}\int_0^b \sigma_y dy - \frac{1}{2}\int_0^b w_{,y}^2 dy$$

Combining the expressions for the stresses from Equation (14) and the assumed displacement function from Equation (7) with Equations (16) and solving for the thermally induced mean stresses, $\bar{\sigma}_x$ and $\bar{\sigma}_y$, produces

$$\bar{\sigma}_x = -\frac{E\alpha T}{(1-\nu)} + \frac{\pi^2 E}{8ab(1-\nu^2)}\left[\left(\frac{b}{a}\right) + \nu\left(\frac{a}{b}\right)\right]W_o^2$$

(17)

$$\bar{\sigma}_y = -\frac{E\alpha T}{(1-\nu)} + \frac{\pi^2 E}{8ab(1-\nu^2)}\left[\nu\left(\frac{b}{a}\right) + \left(\frac{a}{b}\right)\right]W_o^2$$

To summarize the results thus far, it is seen that for the assumed displacement and stress functions the stresses are given by Equation (14) with the mean stresses defined by Equation (17). The shear stresses vanish identically for the assumed form of the stress function. Figure 2 illustrates the thermal stress variation with temperature for a typical panel.

Now, in terms of the displacement function, w, and the stress function, F, the expression for the strain energy is taken in the form presented by Shulman[11]

$$U = \frac{D}{2}\int_0^a\int_0^b (\nabla^2 w)^2 dy\,dx + \frac{1}{2Eh}\int_0^a\int_0^b (\nabla^2 F_1)^2 dy\,dx$$

$$+ \frac{h}{2}\int_0^a\int_0^b [\bar{\sigma}_x w_{,x}^2 + \bar{\sigma}_y w_{,y}^2]dy\,dx$$

(18)

Substituting the displacement and stress functions, together with the mean stresses, the above strain-energy expression becomes

$$U = \frac{\pi^4 D}{8ab}\left[F_{11}^2(1-r) + \frac{1}{8}R\left(\frac{W_{11}}{h}\right)^2\right]W_{11}^2$$

(19)

where

$$R = 3[(5-\nu^2)F_{11}^2 - 2(5+\nu)(1-\nu)]$$

(19a)

and r and T_c remain as previously defined.

Now the displacement function was assumed to have an amplitude of the form $W_{11}(t) = W_o + q(t)$, where W_o is the static buckled panel amplitude and $q(t)$ is the dynamic (vibratory) panel amplitude. Then, expansion of the displacement function gives

$$W_{11}^2 = W_o^2 + 2W_o q + q^2$$

$$W_{11}^4 = W_o^4 + 4W_o^3 q + 6W_o^2 q^2 + 4W_o q^3 + q^4$$

(20)

Considering the static problem, the dynamic amplitude $q(t)$ in Equations (20) is set to zero and the strain energy minimized with respect to the buckle amplitude, W_o, to obtain

9
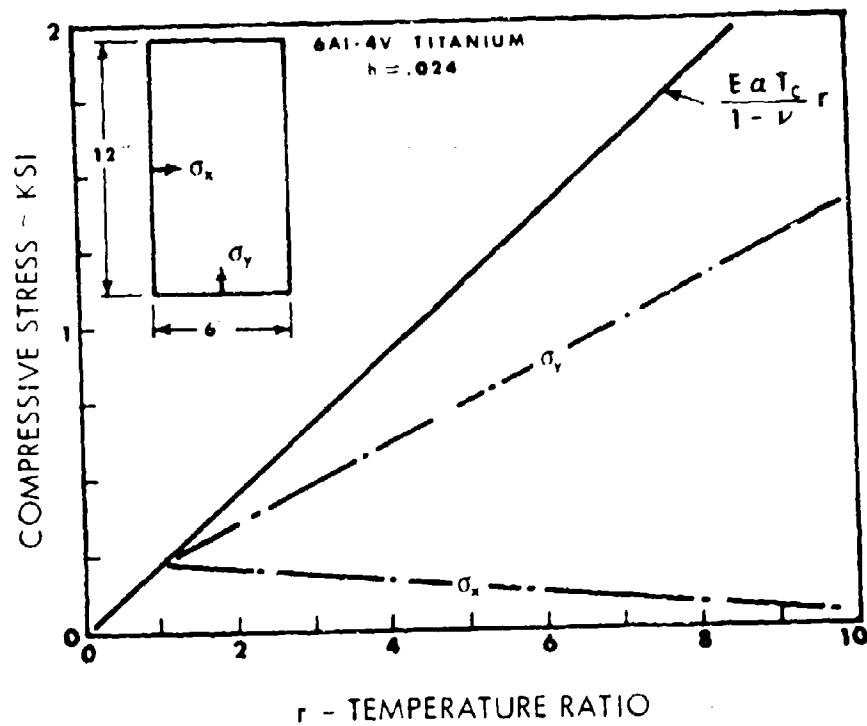
FIGURE 2. ANALYTICAL THERMAL STRESS VARIATION WITH TEMPERATURE

$$\frac{\partial U}{\partial W_o} = \frac{\pi^4 D W_o}{4ab} \left[F_{11}^2 (1 - r) + \frac{1}{4} R \left(\frac{W_o}{h} \right)^2 \right] = 0 \qquad (r \geq 1) \qquad (21)$$

Then

$$W_o = 2h \, F_{11} [(r - 1)/R]^{1/2} \qquad (22)$$

describes the panel static buckling amplitude as a function of the temperature increase. The effect of increasing temperature on buckling amplitude is shown in Figure 3 for various aspect ratios.

Now, it is clear that if the expanded forms of the displacement function, Equations (20), are used to obtain the modal stiffness of the panel, the stiffness will be nonlinear in the coordinate $q(t)$. Assuming that the static buckled amplitude is much greater than the dynamic amplitude ($W_o \gg |q(t)|$), then expressions for W_{11}^2 and W_{11}^4 can be approximated by

$$W_{11}^2 \approx W_o^2 + q^2$$

$$W_{11}^4 \approx W_o^4 + 6 W_o^2 q^2 \qquad (23)$$

Substituting these approximations in Equation (19), the expression for the strain energy becomes

$$U = \frac{\pi^4 D}{8ab} \left\{ \left[F_{11}^2 (1 - r) + \frac{R}{8} \left(\frac{W_o}{h} \right)^2 \right] W_o^2 + \left[F_{11}^2 (1 - r) + \frac{3R}{4} \left(\frac{W_o}{h} \right)^2 \right] \right\} q^2 \qquad (24a)$$

or

$$U = \frac{\pi^4 D}{8ab} \left[\frac{1}{2} F_{11}^2 (1 - r) W_o^2 + 2 F_{11}^2 (r - 1) q^2 \right] \qquad (24b)$$

where Equation (22) has been used to obtain the simplified Equation (24b).

The kinetic energy of the buckled panel has the form

$$T = \frac{1}{2} \gamma h \int_0^c \int_0^b \dot{w}^2 \, dy \, dx \qquad (25)$$

Substituting Equation (7) into Equation (25) and performing the indicated operations yields the result

$$T = \frac{1}{8} \gamma h a b \dot{q}^2 \qquad (26)$$

11
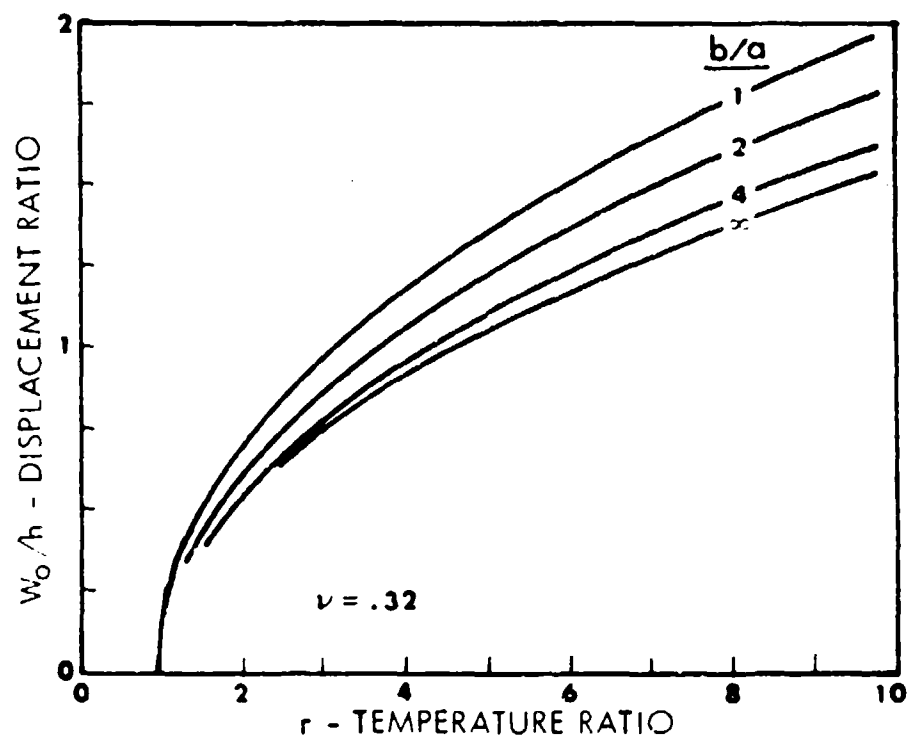
FIGURE 3. ANALYTICAL BUCKLING AMPLITUDE VARIATION WITH TEMPERATURE

The equation of motion is obtained by using Lagrange's equation and expressions (26) and (24) for the kinetic and strain energy, respectively.

$$\frac{1}{4} \gamma h a b \ddot{q} + \frac{\pi^4 D}{4ab} 2F_{11}^2 (r - 1)q = 0 \tag{27}$$

or

$$\ddot{q} + \frac{2\pi^4 D}{\gamma h a^2 b^2} F_{11}^2 (r - 1)q = 0 \qquad (r \geq 1) \tag{28}$$

Assuming harmonic motion, the expression for the response frequency is

$$f(r) = \frac{\pi}{2ab} F_{11} \left[\left(\frac{2D}{\gamma h} \right) (r - 1) \right]^{1/2} \qquad (r \geq 1) \tag{29}$$

Comparing this result to the fundamental frequency below the critical temperature, Equation (6), it will be noted that as the panel temperature is increased from the room temperature condition (zero thermal stress), the panel fundamental mode decreases to zero at the critical temperature. Above the critical temperature (after the panel buckles), the fundamental frequency increases at a rate 1.414 times that of the sub-critical temperature frequency decrease. Defining the room temperature fundamental mode frequency as f_o, and using Equations (6) and (29), the fundamental frequency can be simplified to

$$f_o = \frac{\pi F_{11}}{2ab} \left[\frac{D}{\gamma h} \right]^{1/2} \qquad (r = 0)$$

$$f(r) = f_o [1 - r]^{1/2} \qquad (0 \leq r \leq 1) \tag{30}$$

$$f(r) = f_o [2(r - 1)]^{1/2} \qquad (r \geq 1)$$

These results are graphically shown in Figure 4; the frequency ratio decreases to zero at buckling and then increases after buckling.

3. Summary of Simple Panel Results

For ease of comparison and reference, the following results are presented in terms of the panel temperature increase, T, relative to the critical temperature increase, T_c, for the panel.

Critical Temperature Increase, T_c:

$$T_c = \frac{\pi^2 h^2 F_{11}}{12 \alpha a b (1 + \nu)} \quad ; \quad F_{11} = (b/a) + (a/b)$$

13
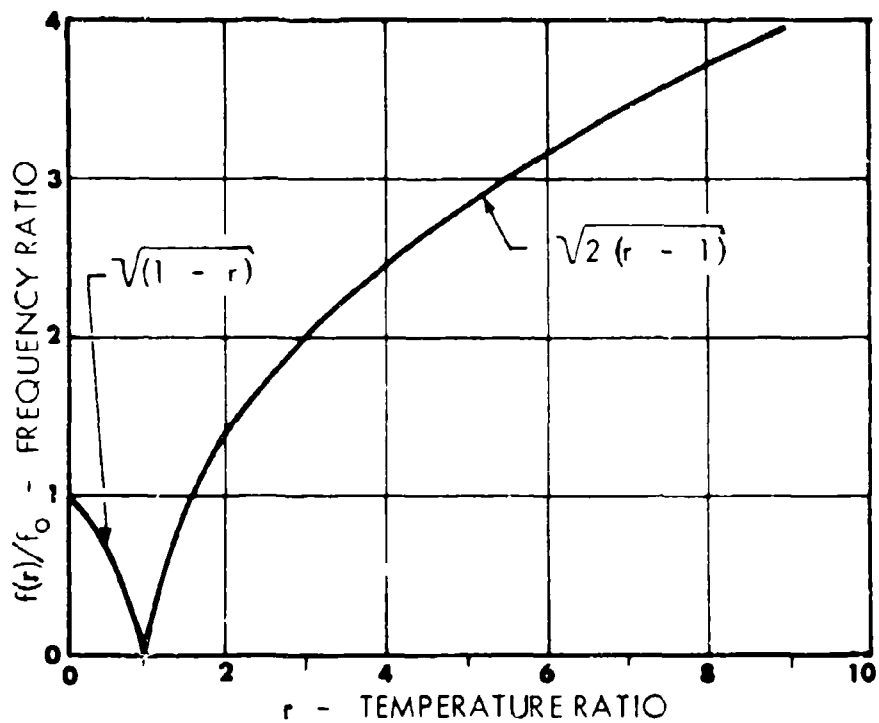
FIGURE 4. ANALYTICAL FREQUENCY VARIATION WITH TEMPERATURE

14

Panel Temperature Ratio:

$$r = T/T_c$$

Strain Energy (Linearized):

$$U = \frac{\pi^4 D}{8ab} F_{11}^2 (1 - r) q^2 \qquad (0 < r \le 1)$$

$$U = \frac{\pi^4 D}{8ab} \left| \frac{1}{2} F_{11}^2 (1 - r) W_o^2 + 2F_{11}^2 (r - 1) q^2 \right| \qquad (r \ge 1)$$

Panel Buckling Amplitude:

$$W_o = 0 \qquad (0 \le r \le 1)$$

$$W_o = 2hF_{11} \left[(r-1)/R \right]^{1/2} \qquad (r > 1)$$

$$R = 3 \left[(5 - \nu^2) F_{11}^2 - 2(5 + \nu)(1 - \nu) \right]$$

Mean Stresses:

$$\bar{\sigma}_x = \bar{\sigma}_y = - \frac{E\alpha T}{(1 - \nu)} \qquad (0 \le r \le 1)$$

$$\bar{\sigma}_x = - \frac{E\alpha T}{(1 - \nu)} + \frac{\pi^2 E}{8ab(1 - \nu^2)} \left[\left(\frac{b}{a} \right) + \nu \left(\frac{a}{b} \right) \right] W_o^2 \qquad (r \ge 1)$$

$$\bar{\sigma}_y = - \frac{E\alpha T}{(1 - \nu)} + \frac{\pi^2 E}{8ab(1 - \nu^2)} \left[\nu \left(\frac{b}{a} \right) + \left(\frac{a}{b} \right) \right] W_o^2$$

Thermal Stresses:

$$\sigma_x = \bar{\sigma}_x - \frac{\pi^2 E}{8a^2} \cos \left(\frac{2\pi y}{b} \right) W_o^2 \qquad (r \ge 1)$$

$$\sigma_y = \bar{\sigma}_y - \frac{\pi^2 E}{8a^2} \cos \left(\frac{2\pi x}{a} \right) W_o^2$$

15

Equation of Motion (Linear Free Vibration):

$$\ddot{q} + \frac{\pi^4 D F_{11}^2}{\gamma h a^2 b^2} (1 - r)q = 0 \qquad (0 \leq r \leq 1)$$

$$\ddot{q} + \frac{\pi^4 D F_{11}^2}{\gamma h a^2 b^2} 2(r - 1)q = 0 \qquad (r \geq 1)$$

Response Frequency:

$$f_o = \frac{\pi F_{11}}{2ab} \left[\frac{D}{\gamma h}\right]^{1/2} \qquad (r = 0)$$

$$f(r) = f_o [1 - r]^{1/2} \qquad (0 \leq r \leq 1)$$

$$f(r) = f_o [2(r - 1)]^{1/2} \qquad (r \geq 1)$$

B. Nine-Bay Panel Response

The simple panel analysis described in the previous section will now be used to develop a model of a flat, nine-bay stiffened panel configuration, illustrated in Figure 5. This analysis is based upon the results developed by Rudder,[8] and follows the basic assumptions that slope compatibility relations are preserved across the attachment line of the stiffener to the skin panel and that the stiffeners remain straight (i.e., no bending or buckling of the stiffeners is allowed).

The nine-bay panel analysis will be presented in terms of the temperature increase of the panel, similar to that for the simple panel analysis. Since the simple panel analysis assumed a uniform temperature distribution over the surface area and the thickness of the panel, it is likewise assumed that the temperature distribution over the surface and through the thickness of the sheet (see Figure 5) of the nine-bay panel is uniform. This assumption implies that the edges and the stiffeners of the nine-bay panel are insulated from the cover sheet.

1. Substructure Characteristics

The results presented in Reference 8 can be used directly, since the substructure is assumed to remain at room temperature.

Assuming that the stiffeners only rotate, and imposing slope compatibility for the cover sheet across the stiffeners, the expression for the strain energy of stiffeners parallel to the x-axis is

16

UNIFORM TEMPERATURE, T
OVER SURFACE OF CENTER BAY
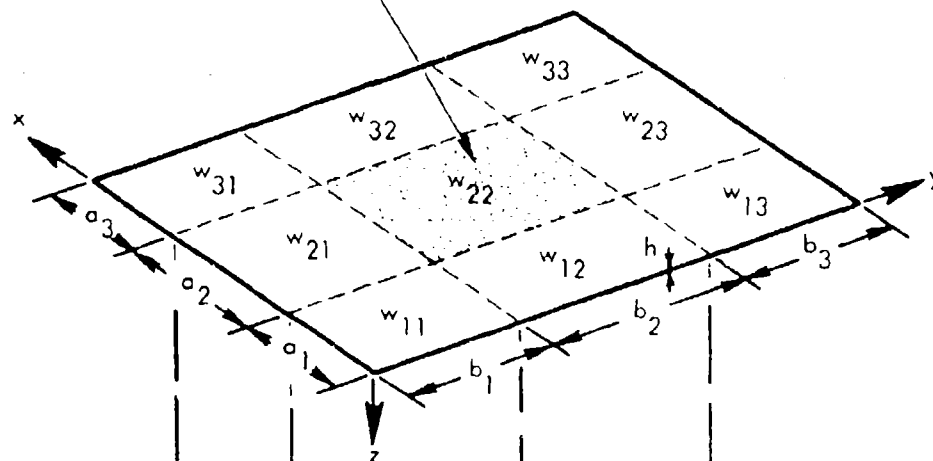
a) PLATE GEOMETRY
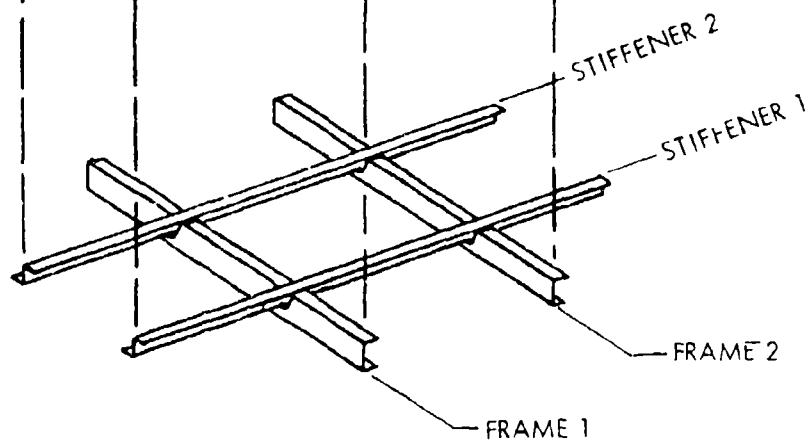
b) SUPPORT STRUCTURE GEOMETRY

FIGURE 5. NINE-BAY FLAT STIFFENED PANEL CONFIGURATION

$$U_{sx} = \frac{\pi^6 E \Gamma_x^*}{4a_2^3 b_2^2}\left[1 + k_{x2}^2 + 2\left(\frac{a_2}{a_1}\right)(1 + k_{x1}^2)\right]W_{22}^2 \tag{31a}$$

and for stiffeners parallel to the y-axis

$$U_{sy} = \frac{\pi^6 E \Gamma_y^*}{4a_2^2 b_2^3}\left[1 + k_{y2}^2 + 2\left(\frac{b_2}{b_1}\right)(1 + k_{y1}^2)\right]W_{22}^2 \tag{31b}$$

where the displacement of the center bay, $W_{22}(t)$, is

$$W_{22}(t) = W_o + q(t)$$

The kinetic energy of the stiffeners parallel to the x-axis is

$$T_{sx} = \frac{\pi^2}{4} \gamma I_{px} \frac{a_2}{b_2^2}\left[1 + 2\left(\frac{a_1}{a_2}\right)^3\right]\dot{W}_{22}^2 \tag{32a}$$

and for stringers parallel to the y-axis

$$T_{sy} = \frac{\pi^2}{4} \gamma I_{py} \frac{b_2}{a_2^2}\left[1 + 2\left(\frac{b_1}{b_2}\right)^3\right]\dot{W}_{22}^2 \tag{32b}$$

A fundamental mode of the nine-bay panel has been assumed for the above results (i.e., $(m,n) = (1,1)$).

The stiffener cross-sectional properties and elastic constants are defined as:

$$\Gamma_x^* = \Gamma_e + S_z^2 I_{zz} - 2S_y S_z I_{yz} + S_y^2 I_{yy}$$

$$\Gamma_y^* = \Gamma_e + S_z^2 I_{zz} - 2S_x S_z I_{xz} + S_x^2 I_{xx}$$

$$k_{xi}^2 = (GJ/E\Gamma^*)_x (a_i/\pi)^2 \quad ; \quad k_{yi}^2 = (GJ/E\Gamma^*)_y (b_i/\pi)^2$$

GJ = torsional stiffness of stiffener (note that $G/E = 1/2(1 + \nu)$)

$$I_{px} = I_{yy} + I_{zz} + (e_y^2 + e_z^2)A_x \quad ; \quad e_x = C_x - S_x$$

$$e_y = C_y - S_y$$

$$I_{py} = I_{xx} + I_{zz} + (e_x^2 + e_z^2)A_y \quad ; \quad e_z = C_z - S_z$$

18

The stiffener cross-section geometry and nomenclature is illustrated in Figure 6.

2. Skin Characteristics

Since the kinetic energy of the cover sheet is independent of temperature, this result will be presented first. Assuming a fundamental mode response for the nine-bay sheet (i.e., each bay responds in its fundamental mode) and applying slope compatibility relations, Table I, across the stiffener attachment lines, the kinetic energy is

$$T_p = \frac{1}{8}\gamma h a_2 b_2 \left[1 + 2\left(\frac{b_1}{b_2}\right)^3 + 2\left(\frac{a_1}{a_2}\right)^3 + 4\left(\frac{a_1 b_1}{a_2 b_2}\right)^3 \right] \dot{W}_{22}^2 \tag{33}$$

TABLE I

SLOPE COMPATIBILITY RELATIONS FOR A NINE-BAY STIFFENED PANEL

VALUES OF C_{ij}/W_{mn}

	$i = 1$	$i = 2$	$i = 3$
$j = 1$	$(-1)^{m+n}(a_1 b_1/a_2 b_2)$	$(-1)^n(b_1/b_2)$	$(-1)^{m+n}(a_1 b_1/a_2 b_2)$
$j = 2$	$(-1)^m(a_1/a_2)$	1	$(-1)^m(a_1/a_2)$
$j = 3$	$(-1)^{m+n}(a_1 b_1/a_2 b_2)$	$(-1)^n(b_1/b_2)$	$(-1)^{m+n}(a_1 b_1/a_2 b_2)$

Expressions for the strain energy of the cover sheet as a function of the temperature increase can be developed by using the results from Equation (2) for temperatures below the critical temperature, and from Equations (19) and (23) for temperatures above the critical temperature.

For a panel bay with dimensions a x b and thickness h, the expression for the strain energy of the fundamental mode as a function of the temperature ratio, r, is

$$U_{p_{ij}} = \frac{\pi^4 D}{8 a_i b_i} F_{11}^2(b_i, a_i)(1 - r_{ij})q_{ij}^2 \qquad (0 \le r \le 1) \tag{34a}$$

19
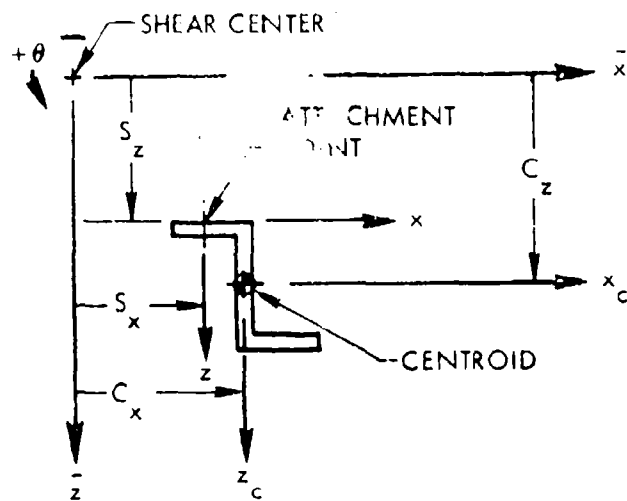
a) STIFFENER GEOMETRY AND NOTATION
   PARALLEL TO Y-AXIS
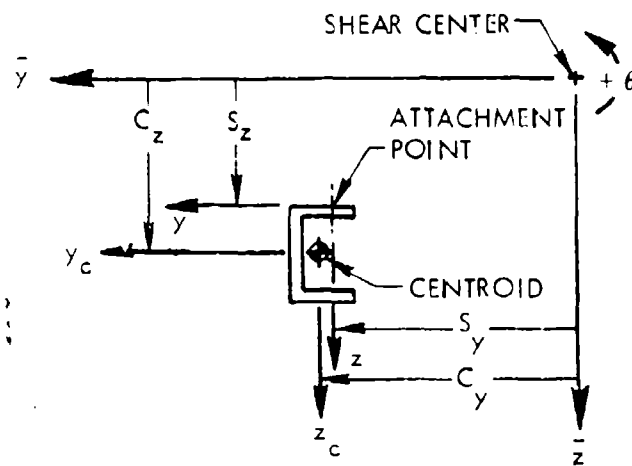
b) FRAME GEOMETRY AND NOTATION
   PARALLEL TO X-AXIS

FIGURE 6. SUBSTRUCTURE CROSS SECTION GEOMETRY

20

$$U_{p_{ij}} = \frac{\pi^4 D}{8a_i b_i} \left\{ \left[F_{11}^2(b_i, a_i)(1 - r_{ij}) + \frac{1}{8} R_{ij} \left(\frac{_{ij}W_o}{h} \right)^2 \right] {_{ij}}W_o^2 \right. \tag{34b}$$

$$\left. + \left[F_{11}^2(b_i, a_i)(1 - r_{ij}) + \frac{3}{4} R_{ij} \left(\frac{_{ij}W_o}{h} \right)^2 \right] q_{ij}^2 \right\} \quad (r \geq 1)$$

where

$$F_{11}(b_i, a_i) = (b_i/a_i) + (a_i/b_i)$$

$$R_{ij} = 3\left[(5 - \nu^2)F_{11}^2(b_i, a_i) - 2(5 + \nu)(1 - \nu) \right]$$

The slope compatibility coefficients can now be used to obtain the structural response in terms of the amplitude of the center bay. It is also necessary to scale the temperature parameter, r_{ij}, since the critical temperature is a function of the panel area (see Equation (5)). The scale factors on r are referenced to the critical temperature of the center bay.

It is now convenient to introduce the notation

$$r_{ij} = d_{ij} r \qquad d_{ij} = \frac{a_i b_i F_{11}(b_2, a_2)}{a_2 b_2 F_{11}(b_i, a_i)} \tag{35}$$

$$_{ij}W_o = W_o C_{ij} \qquad q_{ij}(t) = q(t) C_{ij}$$

where r is the critical temperature ratio of the center bay, d_{ij} are the scale parameters for the temperature rise, C_{ij} are the slope compatibility coefficients, and W_o and $q(t)$ represent the static buckling and vibration amplitudes, respectively, of the fundamental mode of the center bay. (The constants C_{ij} are defined in Table 1.)

Introducing this notation into Equation (34a) and summing all terms for each of the nine panel bays (see Figure 5), the expression for the total strain energy of the cover sheet for temperatures below the critical temperature becomes

$$U_p = \frac{\pi^4 D}{8a_2 b_2} F^*(r) q^2 \qquad (0 \leq r \leq r_o) \tag{36}$$

where

$$F^*(r) = F_{11}^2(b_2, a_2)(1 - r) + 2\left(\frac{b_1}{b_2} \right) F_{11}^2(b_1, a_2)(1 - d_{21}r)$$

$$+ 2\left(\frac{a_1}{a_2} \right) F_{11}^2(b_2, a_1)(1 - d_{12}r) + 4\left(\frac{a_1 b_1}{a_2 b_2} \right) F_{11}^2(b_1, a_1)(1 - d_{11}r)$$

21

The parameter r_o is the value of the temperature ratio for which the strain energy is zero, and will be evaluated later. For $r = 0$ (ambient temperature) this expression is identical to Equation (17) of Reference 8.

Likewise, introducing the notation of Equation (35) into Equation (34b) and summing all terms for each of the nine panel bays, the expression for the strain energy of the cover sheet for temperatures above the critical temperature becomes

$$U_p = \frac{\pi^4 D}{8 a_2 b_2} \left\{ \left[F^*(r) + \frac{1}{8} R^* \left(\frac{W_o}{h} \right)^2 \right] W_o^2 + \left[F^*(r) + \frac{3}{4} R^* \left(\frac{W_o}{h} \right)^2 \right] q^2 \right\} \qquad (r \geq r_o) \tag{37}$$

where

$$R^* = R_{22} + 2 \left(\frac{b_1}{b_2} \right)^3 R_{2i} + 2 \left(\frac{a_1}{a_2} \right)^3 R_{12} + 4 \left(\frac{a_1 b_1}{a_2 b_2} \right) R_{11}$$

$$R_{ij} = 3[(5 - \nu^2) F_{11}^2 (b_i, a_i) - 2(5 + \nu)(1 - \nu)]$$

Equation (36) represents the strain energy of the heated skin for temperatures below the critical temperature while Equation (37) is the strain energy of the heated skin for temperatures above the critical temperature.

3.   Frequency Response

The equation of motion for the fundamental mode of the nine-bay panel is obtained by summing the strain energy terms and the kinetic energy terms for the cover sheet and the stiffeners, and then applying Lagrange's equation.

Since the kinetic energy is independent of the temperature increase, this result will again be presented first. The kinetic energy for the fundamental mode of the nine-bay panel structure is, from Equations (32) and (33),

$$T = \frac{1}{8} \left\{ \nu h a_2 b_2 \left[1 + 2 \left(\frac{a_1}{a_2} \right)^3 + 2 \left(\frac{b_1}{b_2} \right)^3 + 4 \left(\frac{a_1 b_1}{a_2 b_2} \right)^3 \right] \right. $$
$$\left. + 4\pi^2 \gamma I_{px} \frac{a_2}{b_2^2} \left[1 + 2 \left(\frac{a_1}{a_2} \right)^3 \right] + 4\pi^2 \gamma I_{py} \frac{b_2}{a_2^2} \left[1 + 2 \left(\frac{b_1}{b_2} \right)^3 \right] \right\} \dot{W}_{22}^2 \tag{38}$$

Below the critical temperature $(0 \leq r < r_o)$, the strain energy for the fundamental mode of the nine-bay panel is

$$U = \frac{\pi^4 D}{8a_2 b_2} [F^*(r) + K_{sx} + K_{sy}] W_{22}^2 \qquad (0 \le r \le r_o) \qquad (39)$$

where Equations (31) and (36) have been used to obtain this result, and again, r_o is the value of r such that $U(r_o) = 0$.

The substructure stiffness terms in the preceding equation are

$$K_{sx} = \frac{4\pi^2 E \Gamma_x^*}{D a_2^2 b_2} \left[1 + k_{x2}^2 + 2\left(\frac{a_2}{a_1}\right)(1 + k_{x1}^2) \right] \qquad (40)$$

$$K_{sy} = \frac{4\pi^2 E \Gamma_y^*}{D a_2 b_2^2} \left[1 + k_{y2}^2 + 2\left(\frac{b_2}{b_1}\right)(1 + k_{y1}^2) \right] \qquad (41)$$

Equations (38) and (39) may be reduced to the following conventional forms

$$T = \frac{1}{2} M_1 \dot{W}_{22}^2 \quad \text{and} \quad U = \frac{1}{2} K_1(r) W_{22}^2 \qquad (0 \le r \le r_o) \qquad (42)$$

where the mass and stiffness are defined by

$$M_1 = \frac{1}{4} \left\{ \gamma h a_2 b_2 \left[1 + 2\left(\frac{a_1}{a_2}\right)^3 + 2\left(\frac{b_1}{b_2}\right)^3 + 4\left(\frac{a_1 b_1}{a_2 b_2}\right)^3 \right] \right.$$
$$\left. + 4\pi^2 \gamma I_{px} \frac{a_2}{b_2^2} \left[1 + 2\left(\frac{a_1}{a_2}\right)^3 \right] + 4\pi^2 \gamma I_{py} \frac{b_2}{a_2^2} \left[1 + 2\left(\frac{b_1}{b_2}\right)^3 \right] \right\} \qquad (43)$$

$$K_1(r) = \frac{\pi^4 D}{4a_2 b_2} [F^*(r) + K_{sx} + K_{sy}] \qquad (44)$$

The equation of motion of the nine-bay panel below the critical temperature is then, for free vibration,

$$M_1 \ddot{q} + K_1(r)q = 0 \qquad (0 \le r \le r_o) \qquad (45)$$

and assuming simple harmonic motion, the response frequency is given by

$$f(r) = \frac{1}{2\pi} [K_1(r)/M_1]^{1/2} \qquad (0 \le r \le r_o) \qquad (46)$$

23

For a temperature increase above the critical temperature, the kinetic energy expression, Equation (38), is still valid and Equations (31) and (37) are used to obtain the expression for the strain energy. As indicated in the development of Equation (37) the following approximations are assumed

$$W_{22}^2 \approx W_o^2 + q^2$$

$$W_{22}^4 \approx W_o^4 + 6W_o^2 q^2$$

(47)

where W_o is the buckling amplitude of the center bay and $q(t)$ is the dynamic amplitude of the center bay for the fundamental mode (see Equation 23).

It is evident that the kinetic energy expression is then simply

$$T = \frac{1}{2} M_1 \dot{q}^2 \qquad (r \ge r_o)$$

(48)

where M_1 is defined by Equation (43) since the mass is independent of temperature.

The strain energy of the nine-bay panel is obtained by using Equations (31) and (37), and is

$$U = \frac{\pi^4 D}{8a_2 b_2} \left\{ \left[\left[F^*(r) + \frac{1}{8} R^* \left(\frac{W_o}{h} \right)^2 \right] + K_{sx} + K_{sy} \right] \right.$$

$$\left. + \left[\left[F^*(r) + \frac{3}{4} R^* \left(\frac{W_o}{h} \right)^2 \right] + K_{sx} + K_{sy} \right] q \right\} \qquad (r \ge r_o)$$

(49)

Setting $q(t) = 0$ and minimizing the result with respect to W_o,

$$\frac{\partial U}{\partial W_o} = \frac{\pi^4 D W_o}{8a_2 b_2} \left\{ 2F^*(r) + 2K_{sx} + 2K_{sy} + \frac{1}{2} R^* \left(\frac{W_o}{h} \right)^2 \right\} = 0$$

(50)

Then neglecting the trivial case of $W_o = 0$, the displacement ratio (W_o/h) is obtained as

$$\left(\frac{W_o}{h} \right)^2 = -\frac{4}{R^*} [F^*(r) + K_{sx} + K_{sy}] \qquad (r \ge r_o)$$

(51)

where $F^*(r)$ is defined by Equation (36) and R^* is defined by Equation (37).

Applying Lagrange's equation to the kinetic and strain energy, the equation of motion for the fundamental mode of the buckled nine-bay panel is derived for free vibration and takes the conventional form

24

$$M_1 \ddot{q} + K_2(r)q = 0 \qquad (52)$$

where the mass was identified previously and the stiffness is

$$K_2(r) = -\frac{\pi^4 D}{2a_2 b_2} [F^*(r) + K_{sx} + K_{sy}] \qquad (53)$$

Comparison of the expressions for $K_1(r)$ and $K_2(r)$ reveals that both vanish for the same value of r, which is to be expected. Indeed, the result simplifies to

$$K_2(r) = -2K_1(r)$$

$$K_2(r_o) = K_1(r_o) = 0 \qquad (54)$$

The response frequency is determined from Equation (50) to be

$$f(r) = \frac{1}{2\pi} [K_2(r)/M_1]^{1/2} = \frac{1}{2\pi} [-2K_1(r)/M_1]^{1/2} \quad (r \geq r_o) \qquad (55)$$

The results presented to this point may be simplified by returning to Equations (35) and (36). Using the definition for d_{ij} and $F_{11}(b_i, a_i)$ the plate stiffness parameter may be expressed as

$$F^*(r) = F_1^* - F_2^* r \qquad (56)$$

where

$$F_1^* = F_{11}^2(b_2, a_2) + 2\left(\frac{b_1}{b_2}\right)F_{11}^2(b_1, a_2) + 2\left(\frac{a_1}{a_2}\right)F_{11}^2(b_2, a_1) + 4\left(\frac{a_1 b_1}{a_2 b_2}\right)F_{11}^2(b_1, a_1)$$

$$F_2^* = F_{11}(b_2, a_2)\left[F_{11}(b_2, a_2) + 2\left(\frac{b_1}{b_2}\right)^2 F_{11}(b_1, a_2) + 2\left(\frac{a_1}{a_2}\right)^2 F_{11}(b_2, a_1) \right.$$

$$\left. + 4\left(\frac{a_1 b_1}{a_2 b_2}\right)^2 F_{11}(b_1, a_1) \right]$$

Finally, the value of r at which the strain energy of the structure becomes zero is derived from Equation (39), and is

$$r_o = \frac{1}{F_2^*}(F_1^* + K_{sx} + K_{sy}) \qquad (57)$$

Using this definition of r_o, the previous results for stiffness may be further simplified to

25

$$K_1(r) = \frac{\pi^4 D}{4a_2 b_2} F_2^*(r_o - r) \qquad (0 \le r \le r_o) \qquad (58a)$$

$$K_2(r) = \frac{\pi^4 D}{4a_2 b_2} 2F_2^*(r - r_o) \qquad (r \ge r_o) \qquad (58b)$$

Likewise, the expressions for the response frequency of the heated nine-bay panel buckled into and vibrating in its fundamental mode is

$$f_o = \frac{\pi}{4} \left[\frac{D F_2^* r_o}{M_1 a_2 b_2} \right]^{1/2} \qquad (r = 0)$$

$$f(r) = f_o \left[1 - \frac{r}{r_o} \right]^{1/2} \qquad (0 \le r \le r_o) \qquad (59)$$

$$f(r) = f_o \left[2\left(\frac{r}{r_o} - 1 \right) \right]^{1/2} \qquad (r \ge r_o)$$

26

III - EXPERIMENTAL

This overall program was primarily experimental, with the preceding analysis serving as the means of establishing parameters to be measured during the test program for later correlation with the analytical results. The experimental program was conducted in two phases: (1) vibratory fatigue tests of coupon specimens, and (2) acoustic fatigue tests of multi-bay stiffened panels. Both series of tests were conducted at room and elevated temperatures with specimens fabricated of 7075-T6 aluminum and 6Al-4V titanium (mill-annealed) alloys.

Coupon vibratory fatigue tests were conducted to generate basic material fatigue properties for each alloy at room and elevated temperatures in the absence of mean (thermal) stresses. These data were used in the design of stiffened-skin specimens which were fatigue tested under random amplitude acoustic loading. The stiffened panel test program provided static (thermal) and dynamic test data for correlation with the analytical results.

A. Coupon Fatigue Tests

Fatigue tests were conducted on cantilever beam specimens to develop random loading fatigue properties at room and elevated temperatures. The two alloys were tested at the following temperatures:

7075-T6 Aluminum - Room temperature and 300°F

6Al-4V Titanium - Room temperature and 600°F

Cantilever beam specimens were used to develop zero mean stress fatigue data and to evaluate the thermal degradation effects on each alloy. The plain (unnotched) and riveted specimens are detailed in Figure 7. The riveted specimens incorporated two rivets to represent the stress concentration in the stiffened-skin test specimens.

All specimens were fabricated from close tolerance sheet using standard manufacturing and quality control processes and procedures. Each specimen was sheared oversize and milled to the final size to remove deformed or compressed material from the edges caused by the shearing operation. All holes were located relative to the free end of the beam and jig-drilled to provide close control over specimen cantilever length. Rivets were installed by a Drivematic riveting machine to give uniform rivet installation.

1. Test Procedure

Three specimens were fatigue tested simultaneously in each set-up, using random amplitude vibratory excitation. The room temperature test set-up is shown in Figure 8. The specimens were supported by steel clamp blocks (detailed in Appendix III) attached to the table of an MB Electronics C-10E electro-mechanical shaker. Phenolic inserts were used for room temperature tests, while steel inserts, with asbestos insulation on each side of the specimen, were used for all elevated temperature tests to minimize heat flow from the specimen to the clamp blocks.
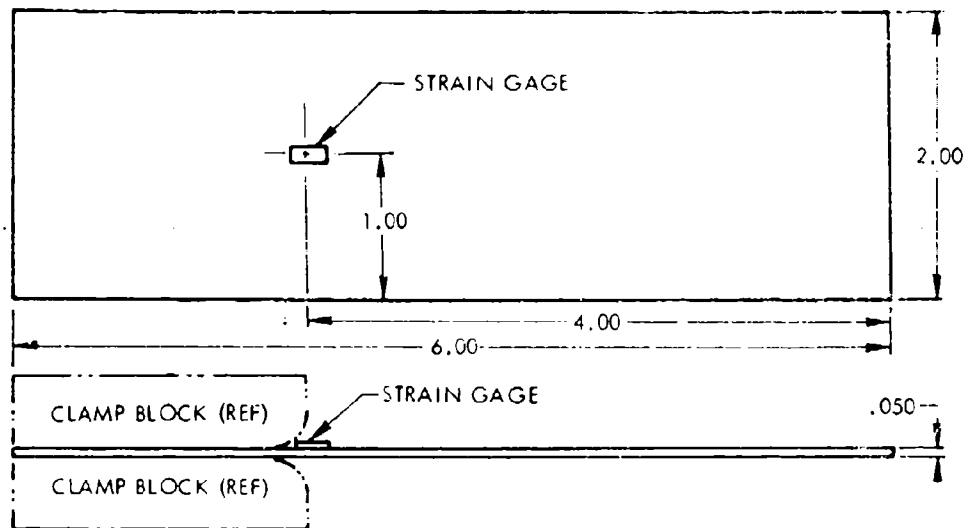
a) PLAIN SPECIMEN
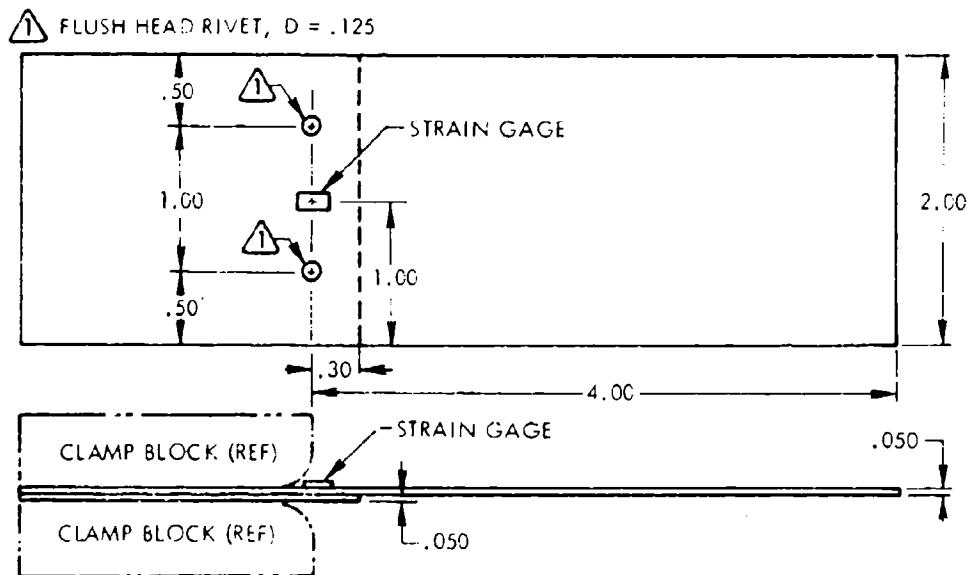
b) RIVETED SPECIMEN

FIGURE 7. COUPON SPECIMEN CONFIGURATION

28
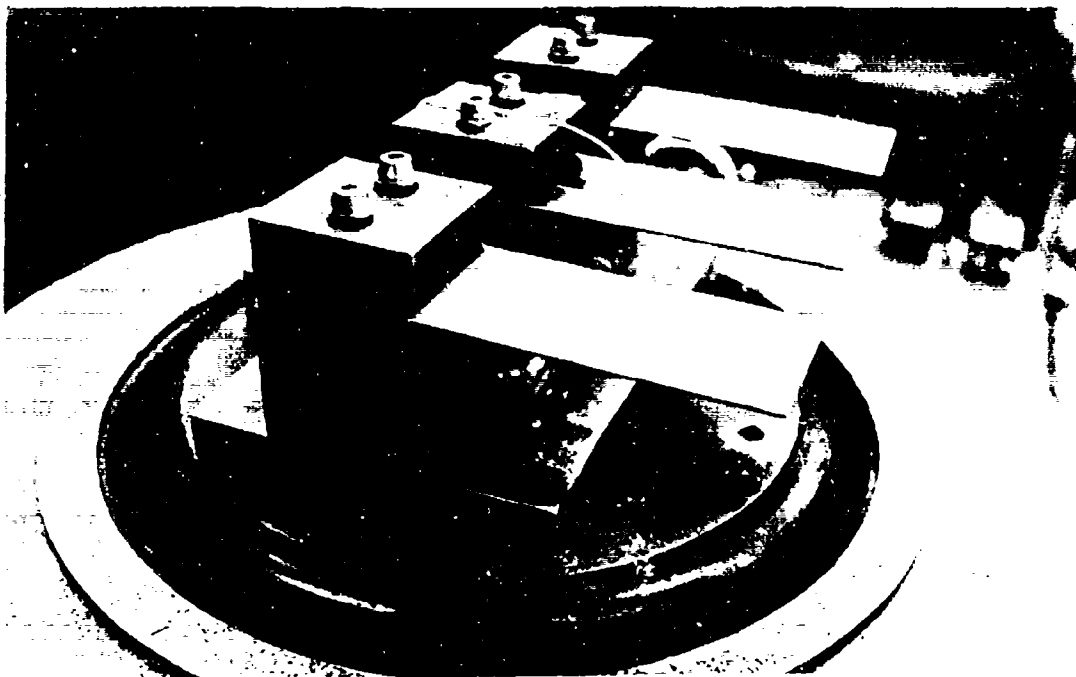
FIGURE 8. RC M TEMPERATURE SET-UP FOR COUPON FATIGUE TESTS
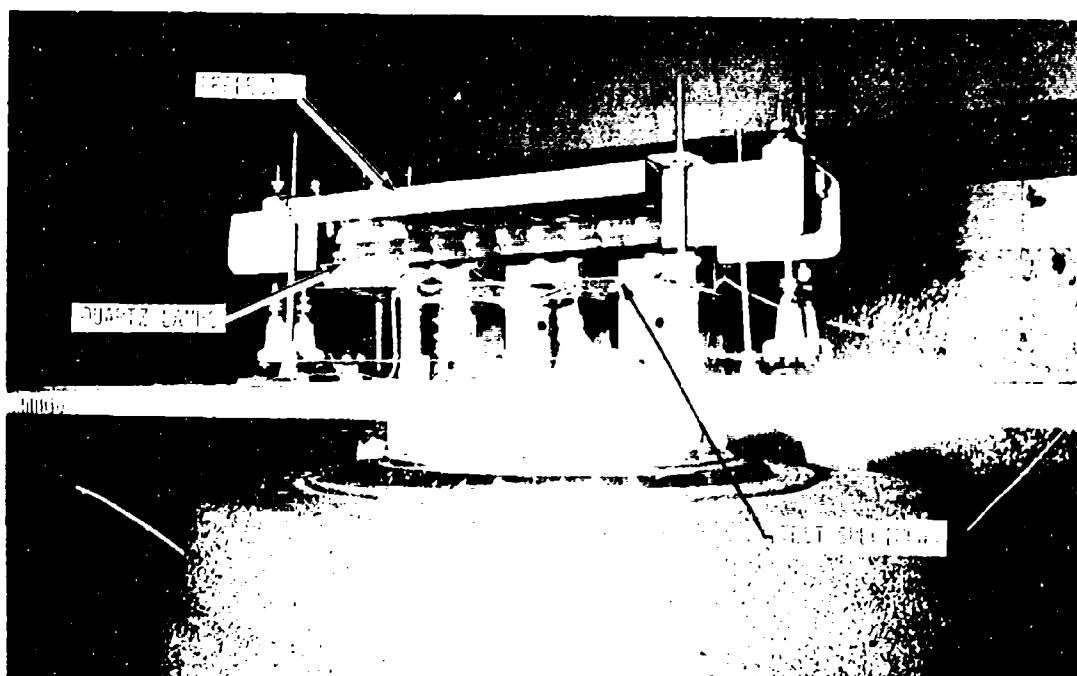
FIGURE 9. ELEVATED TEMPERATURE SET-UP FOR COUPON FATIGUE TESTS

The room temperature set-up was duplicated for the elevated temperature tests, with tungsten-filament quartz lamps and a thermal enclosure added. Two quartz lamps were located above the specimens to provide heat, as shown in Figure 9. The specimens and lamps were contained in an enclosure, shown in Figure 10, to maintain a uniform thermal environment around the specimens. A slot in the front of the enclosure allowed visual observation of the specimen response at the elevated temperatures.

Specimen temperatures were monitored by a thermocouple attached to a 1/2 inch wide strip of the specimen alloy rigidly fixed between adjacent specimens at the clamp line.

Strain levels were measured with uniaxial strain gages bonded to the specimen at the locations shown in Figures 7 and 11. Generally, only the center specimen was instrumented since specimen responses were essentially identical. Room temperature curing adhesives were used to bond all gages.

Excitation levels were monitored by means of an accelerometer attached directly to the shaker table.

a.   Strain/Acceleration Calibration - The strain gage fatigue life was limited by the high acceleration forces experienced during resonance testing. Also, the gages could only be used at ambient temperatures, since a room temperature curing adhesive was used to bond the gages to the specimens. This required establishment of a strain/acceleration transfer function for use in maintaining specimen strain levels after gage failure.

Narrow-band random input spectra were used for all tests, with a typical bandwidth of 30 Hz. The specimen resonances were located just below the upper cut-off frequency to maintain uniform input levels as the resonant frequency decreased during failure.

Simultaneous overall strain response and input acceleration levels were measured at various input levels, using the test spectrum described above. These data were plotted as shown in Figure 12 to produce an excitation versus response curve for each set of specimens. The acceleration level then became the control parameter for maintaining constant strain levels for the duration of the test.

2.   Fatigue Tests

The specimens were fatigue tested at the appropriate test temperature with the excitation spectrum used for the strain/acceleration calibration. The specimen temperature was allowed to stabilize prior to application of vibration for the elevated temperature tests. Periodic inspections were performed during testing to detect initiation of fatigue failure. During these inspections, the test was stopped, and the random excitation source was replaced with sinusoidal motion in order to accurately determine the resonant frequency. The specimen temperature was maintained during these inspections. A visual inspection was also performed on the room temperature specimens at this time.

Fatigue failure was defined as the time at which the resonant frequency decreased 2% below its initial value. This was determined from a plot of frequency versus test time for each specimen, as shown in Figure 13.
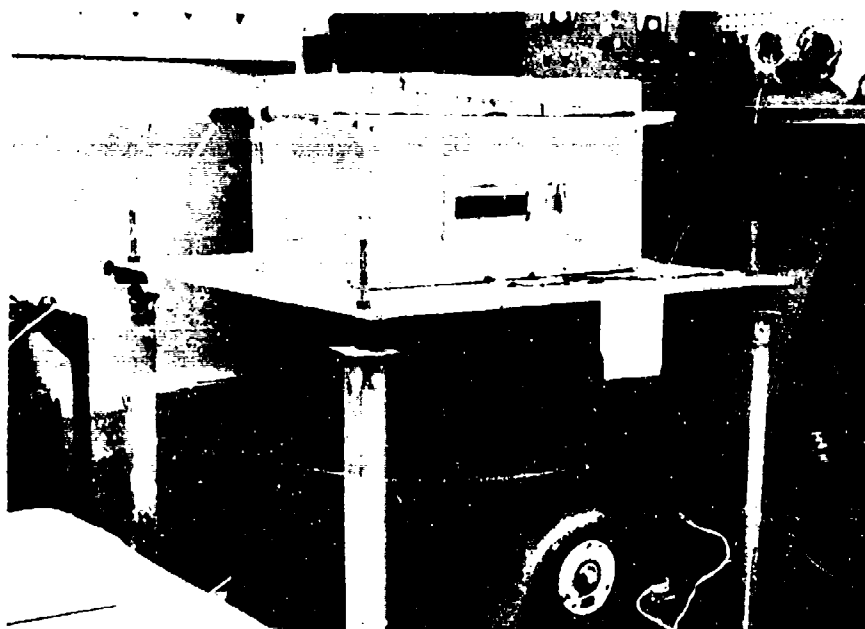
FIGURE 10. ELEVATED TEMPERATURE TEST THERMAL ENCLOSURE
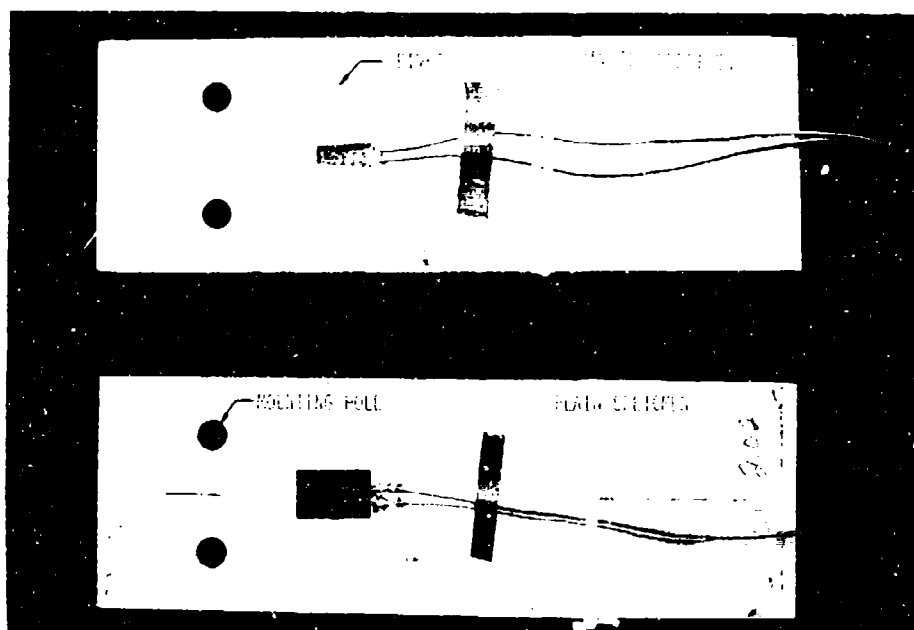
FIGURE 11. STRAIN GAGE INSTALLATION ON COUPON FATIGUE SPECIMENS

31
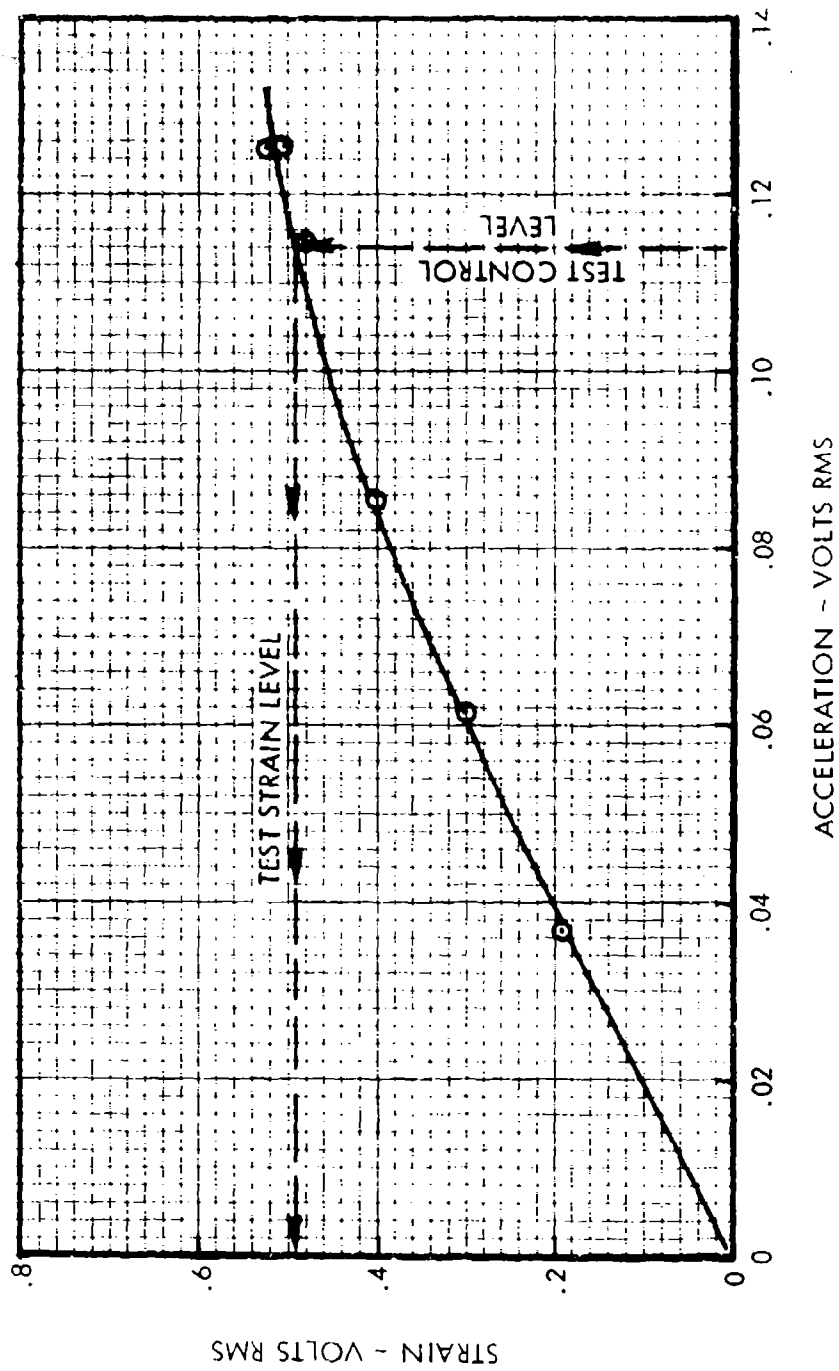
FIGURE 12. STRAIN/ACCELERATION CALIBRATION CURVE
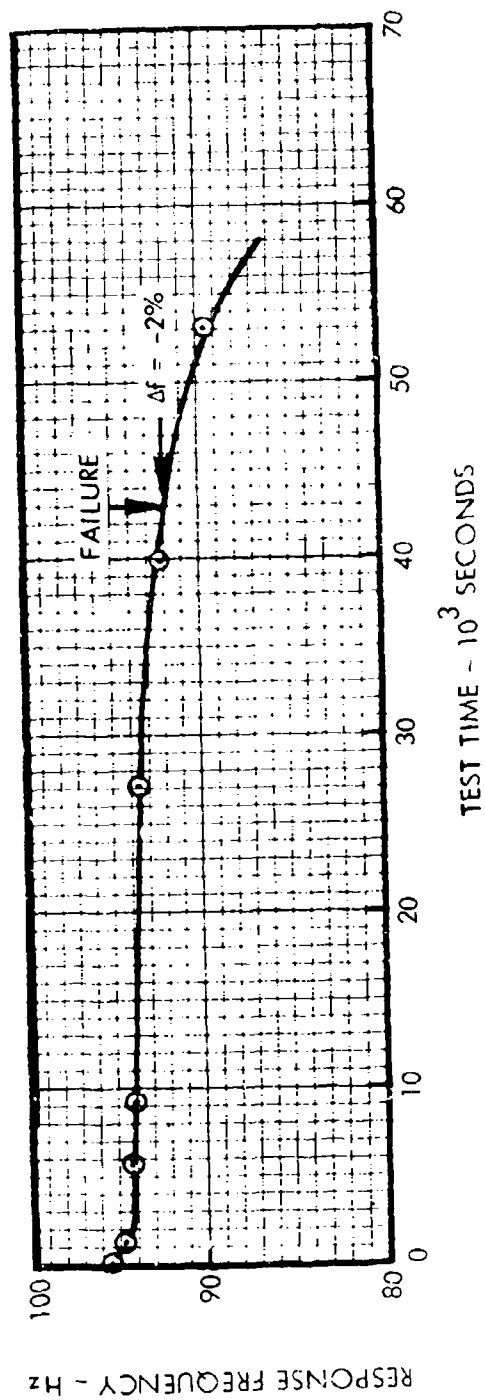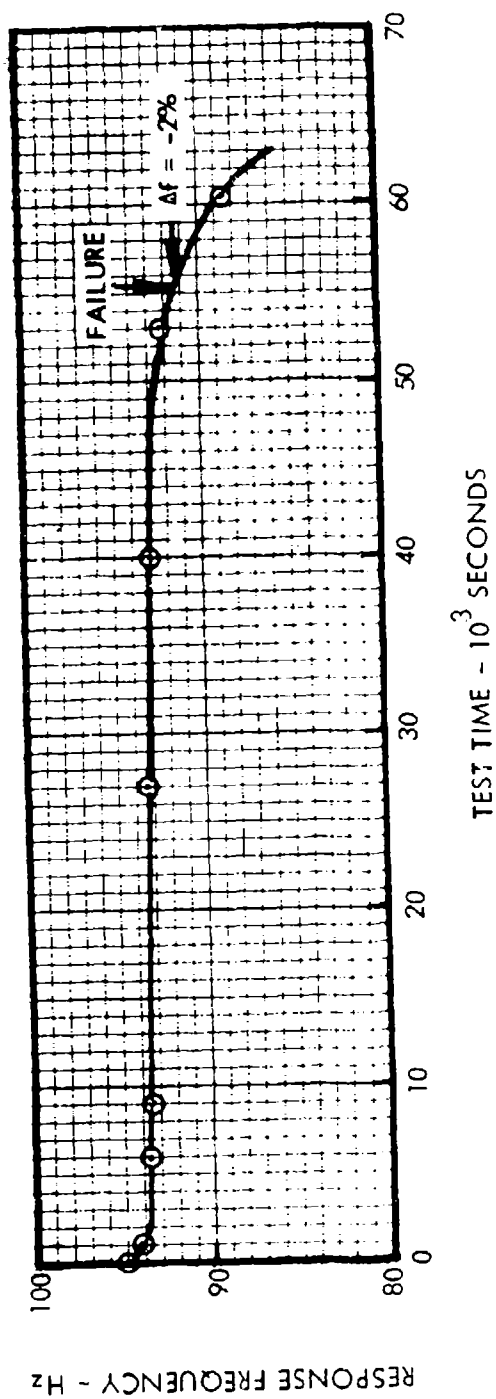
FIGURE 13. TYPICAL FREQUENCY TIME HISTORIES FOR COUPON SPECIMENS

33

Figures 14 and 15 are typical probability density analyses of the acceleration excitation and strain response signals for two response amplitudes. As indicated in the figures, these data approximate a Gaussian distribution.

3. Test Results

The coupon fatigue data are tabulated in Tables II and III while Figures 16 and 17 present the fatigue curves developed from these data. The median life is shown by a least squares regression line drawn through the data points for each configuration and test condition. The scatter present in the data is indicated by the 95% confidence bands shown on the plots. The regression line and confidence bands were computed by the methods delineated in Reference 4, Appendix II. The results of the statistical analyses conducted on these data are shown in Table IV for reference. The fatigue curve for riveted aluminum at room temperature was found to agree very closely with similar data published in Reference 4.

B. Stiffened Panel Fatigue Tests

1. Test Specimen Design

The fatigue data from the coupon tests were used to modify the stiffened structure skin design nomograph, Figure 73 of AFFDL-TR-67-156[4]. The stiffened-skin test panels were designed using this nomograph, with temperature effects included, and the following guidelines:

o   Overall size identical to the test panels described in AFFDL-TR-71-107[8] to use existing frames.

o   Range of structural and test parameters consistent with those of AFFDL-TR-67-156 and AFFDL-TR-71-107 to provide a logical transition from ambient to high temperature design criteria.

o   Total quantity of 27 aluminum and 21 titanium specimens.

Previous test programs[4,8] have shown that fatigue failures could be expected in the outer bays if all bays were of the same approximate size. Therefore, the center bays of all specimens were designed to have a greater surface area than that of any of the adjacent outer bays since the center bay was considered to be the primary test area.

Eight aluminum and four titanium specimens were designed to be tested at room temperature for direct comparison with the data of Reference 4. An identical number of these same specimen designs were to be tested at elevated temperatures. Another eight of the aluminum specimens were also designed with faying surface sealant to evaluate the effect of the sealant on fatigue endurance; these specimens were identical to eight of the specimens without sealant. The specimens with sealant were included in this program to ascertain the validity of previous empirical design criteria, which are based on tests conducted on specimens without sealant, for use on structures which use sealant.
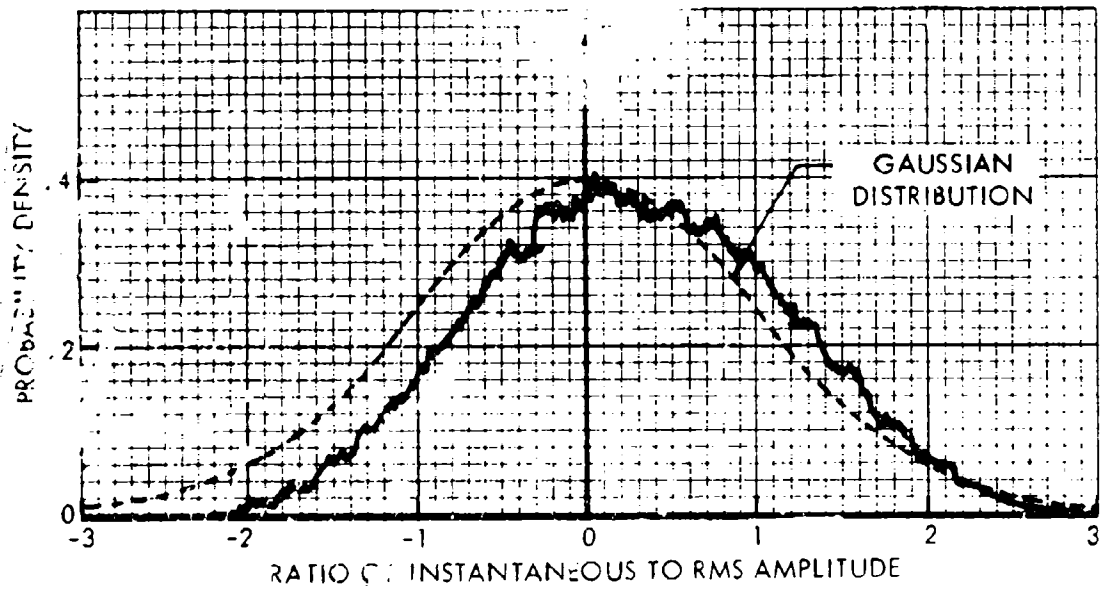
a) ACCELERATION LEVEL CORRESPONDING TO 820 µ IN/IN RMS
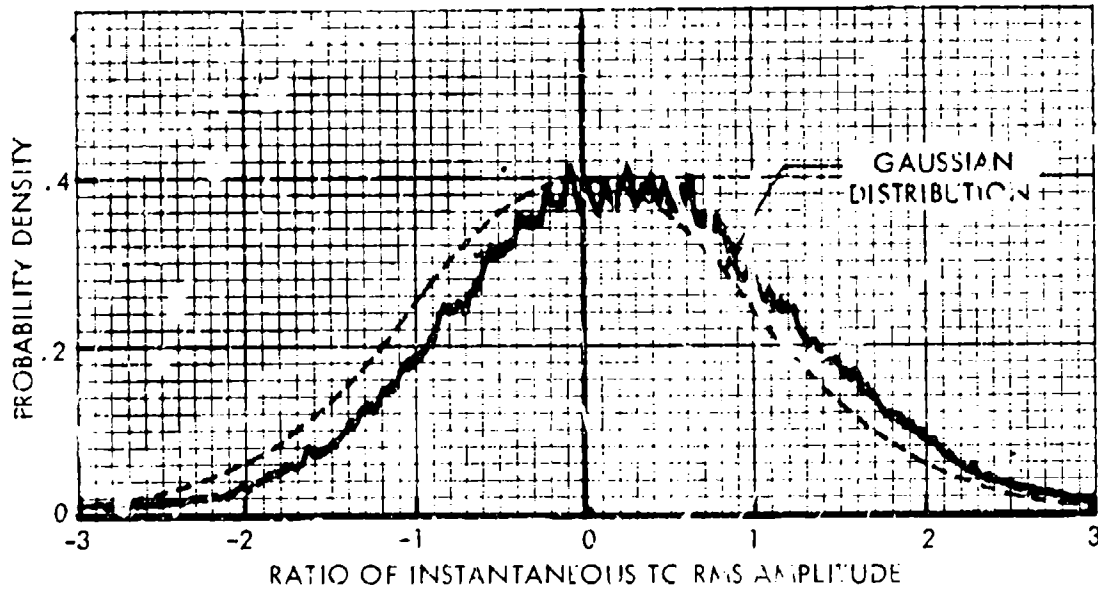
b) ACCELERATION LEVEL CORRESPONDING TO 480 µ IN/IN RMS

FIGURE 14. AMPLITUDE DISTRIBUTION OF EXCITATION
TITANIUM COUPON SPECIMEN (RIVETED)

35
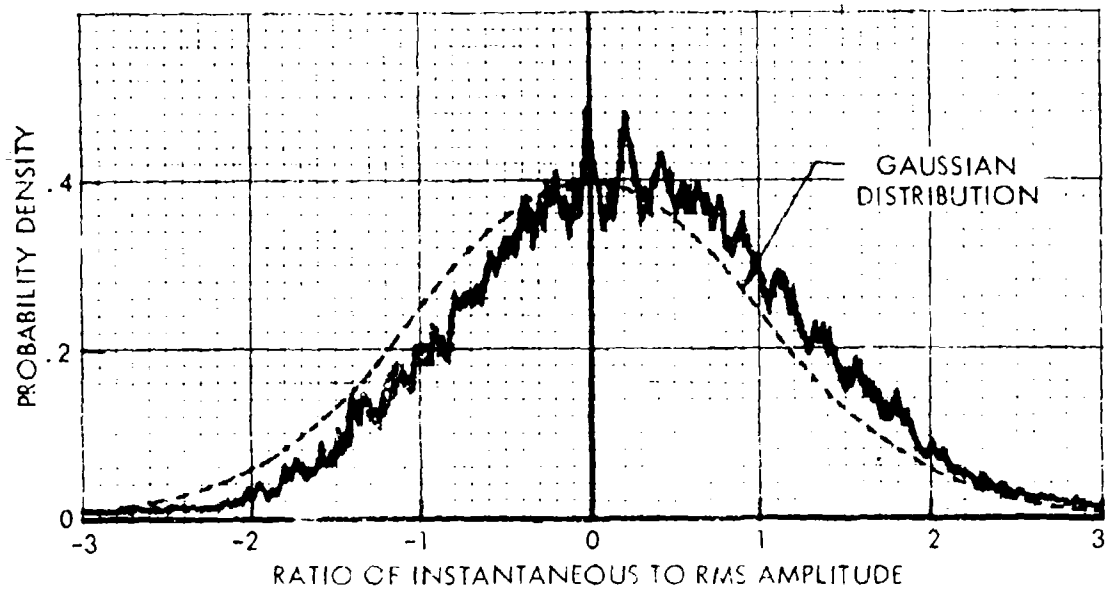
a) OVERALL STRAIN LEVEL: 820 μ IN/IN RMS
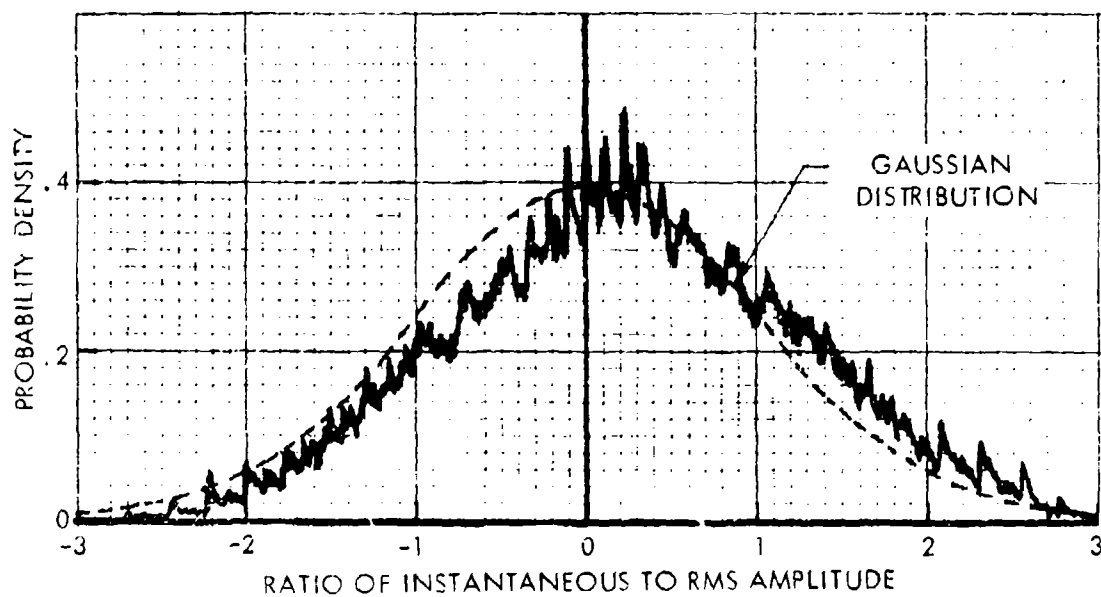
b) OVERALL STRAIN LEVEL: 480 μ IN/IN RMS

FIGURE 15. AMPLITUDE DISTRIBUTION OF SPECIMEN RESPONSE
TITANIUM COUPON SPECIMEN (RIVETED)

36

TABLE II
ALUMINUM COUPON SPECIMENS
SUMMARY OF FATIGUE TEST RESULTS

Plain Specimens

Room Temperature			300°F		
Specimen No.	Stress ksi rms	Life Cycles	Specimen No.	Stress ksi rms	Life Cycles
1	22.4*	1.08×10^4	1	18.5	1.14×10^5
2	22.4*	6.07×10^3	2	18.5	9.75×10^4
3	22.4*	9.00×10^3	3	18.5	7.42×10^4
4	17.6	2.96×10^5	4	17.0	2.87×10^5
5	16.8*	2.31×10^5	5	17.0	2.87×10^5
6	16.8*	1.43×10^5	6	17.0	2.88×10^5
7	16.8*	1.01×10^5	7	10.6	1.80×10^6
8	16.8	6.14×10^5	8	10.6	1.46×10^6
9	14.6	6.80×10^5	9	10.6	1.93×10^6
10	14.0	8.26×10^5	10	10.2	2.00×10^6
11	14.0	1.53×10^6	11	10.2	2.00×10^6
12	14.0	8.80×10^5	12	8.5	2.60×10^6

Riveted Specimens

Room Temperature			300°F		
Specimen No.	Stress ksi rms	Life Cycles	Specimen No.	Stress ksi rms	Life Cycles
1	14.0	1.27×10^5	1	14.7	4.40×10^4
2	14.0	1.31×10^5	2	14.7	4.30×10^4
3	14.0	1.30×10^5	3	14.7	4.08×10^4
4	12.0	4.97×10^5	4	9.2	2.55×10^5
5	12.0	5.12×10^5	5	9.2	3.00×10^5
6	12.0	1.15×10^5	6	9.2	2.90×10^5
7	10.5	8.20×10^5	7	6.2	1.22×10^6
8	10.5	7.92×10^5	8	6.2	1.51×10^6
9	10.5	7.20×10^5	9	6.2	1.52×10^6
10	6.6	6.75×10^6	10	4.1	4.44×10^6
11	5.9	4.11×10^6	11	4.1	5.22×10^6
12	5.7	2.70×10^6	12	4.1	7.82×10^6

* Invalid data - ends of beam weighted and response highly nonlinear. Not used in fatigue curve.

NOTE: Fatigue life (in cycles) is the product of resonant frequency and test time to failure.

TABLE III
TITANIUM COUPON SPECIMENS
SUMMARY OF FATIGUE TEST RESULTS

Plain Specimens

Room Temperature			600°F		
Specimen No.	Stress ksi rms	Life Cycles	Specimen No.	Stress ksi rms	Life Cycles
1	35.5	3.28×10^5	1	26.9	5.40×10^5
2	35.5	3.24×10^5	2	26.9	2.74×10^5
3	35.5	3.55×10^5	3	26.9	3.38×10^5
4	28.7	5.15×10^5	4	25.3	2.74×10^5
5	28.7	9.45×10^5	5	24.8	2.50×10^5
6	28.7	8.65×10^5	6	24.6	2.26×10^5
7	21.4	5.18×10^6	7	22.9	3.38×10^5
8	21.4	3.97×10^6	8	22.2	2.26×10^5
9	21.4	2.57×10^6	9	21.5	2.82×10^5
10	21.2	1.89×10^6	10	19.7	8.90×10^5
11	21.2	1.67×10^6	11	19.7	8.38×10^5
12	21.2	5.52×10^6	12	19.7	1.14×10^6
13	17.9	1.53×10^7	13	14.9	7.18×10^6
14	17.0	3.05×10^7	14	14.9	7.32×10^6
			15	14.9	5.00×10^6

Riveted Specimens

Room Temperature			600°F		
Specimen No.	Stress ksi rms	Life Cycles	Specimen No.	Stress ksi rms	Life Cycles
1	20.9	5.00×10^5	1	19.2	3.48×10^4
2	19.4	4.18×10^5	2	19.2	5.34×10^4
3	17.8	3.82×10^5	3	19.2	5.93×10^4
4	16.0	1.11×10^6	4	13.6	4.57×10^5
5	16.0	9.60×10^5	5	13.6	2.52×10^5
6	16.0	4.50×10^5	6	13.6	5.02×10^5
7	13.9	2.23×10^6	7	10.1	8.55×10^5
8	13.9	1.34×10^6	8	10.1	6.24×10^5
9	13.0	1.46×10^6	9	10.1	1.04×10^6
10	12.8	4.10×10^6	10	5.5	1.65×10^7
11	12.0	3.02×10^6	11	5.2	8.02×10^6
12	11.2	5.22×10^6	12	3.5*	1.87×10^7

*Did not fail.

NOTE: Fatigue life (in cycles) is the product of resonant frequency and test time to failure.

RANDOM AMPLITUDE REVERSED BENDING – ZERO MEAN STRESS

O PLAIN SPECIMENS — LEAST SQUARES REGRESSION LINE
△ RIVETED SPECIMENS —·—·— LIMITS OF 95% CONFIDENCE BAND
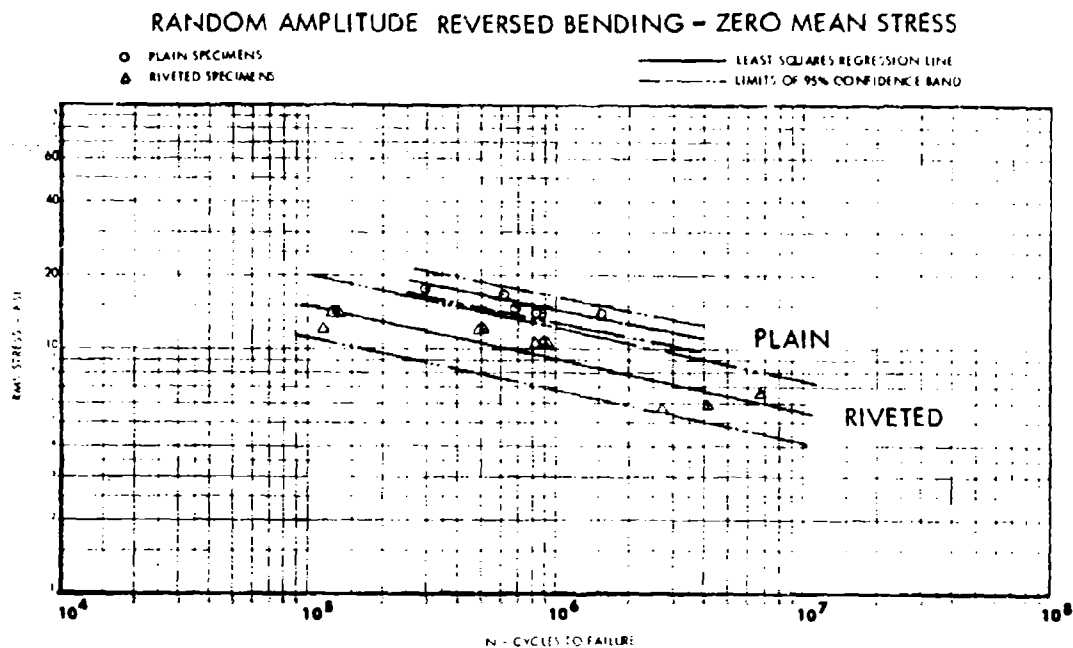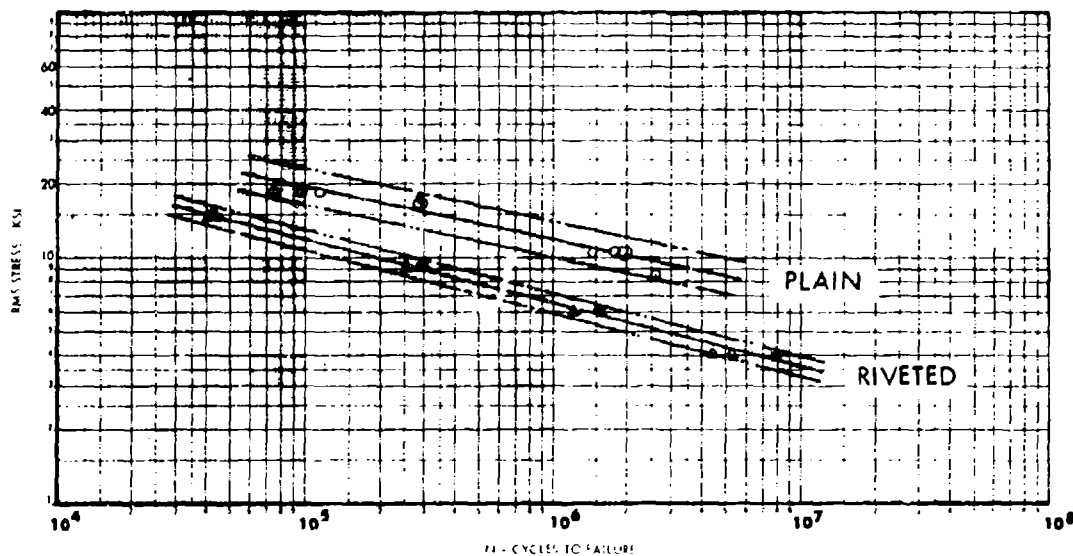
a) ROOM TEMPERATURE

b) 300°F TEMPERATURE

FIGURE 16. COUPON FATIGUE TEST RESULTS
ALUMINUM SPECIMENS

39

RANDOM AMPLITUDE REVERSED BENDING — ZERO MEAN STRESS

a) ROOM TEMPERATURE
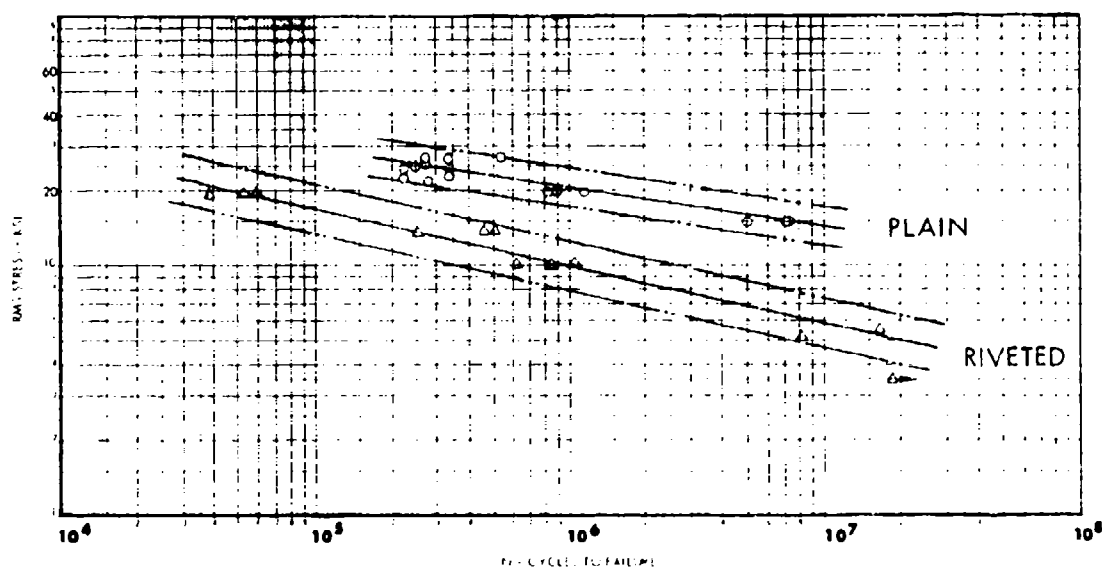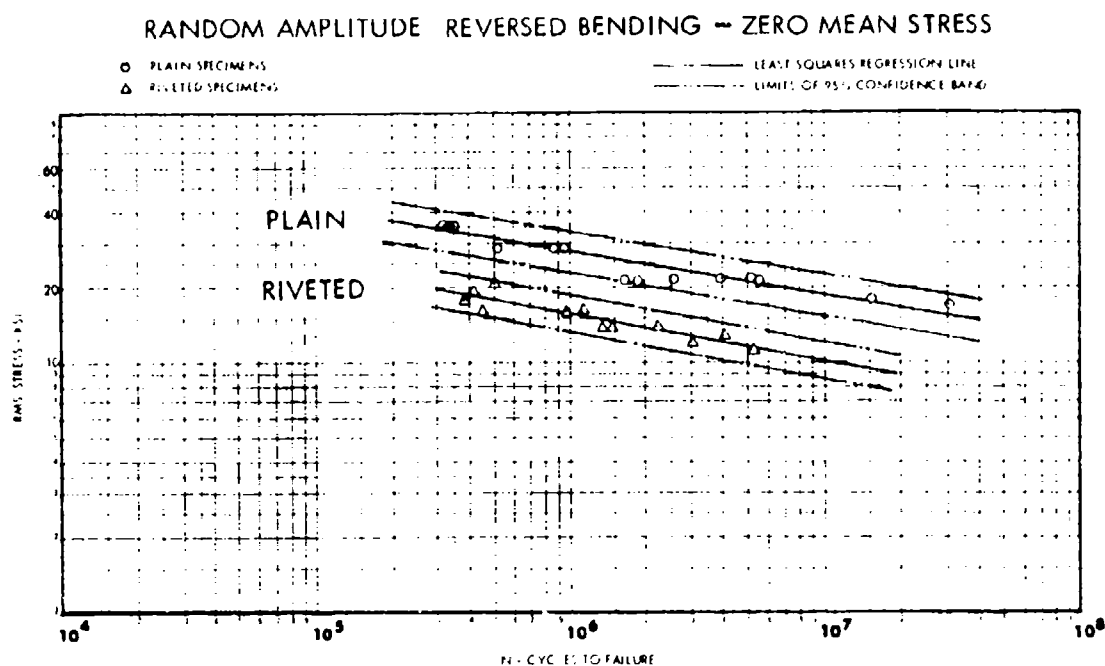
b) 600°F TEMPERATURE

FIGURE 17. COUPON FATIGUE TEST RESULTS
TITANIUM SPECIMENS

40

TABLE IV
SUMMARY OF STATISTICAL PROPERTIES
FOR COUPON FATIGUE DATA

Alloy	Test Temperature °F	Sample Size	Regression Line*		σ_c Standard Deviation	R_c Correlation Coefficient
			A Intercept	B Slope		
Aluminum-Plain	RT	6	2.424	-.215	**	**
Aluminum-Plain	300°F	12	2.362	-.215	0.034	-0.969
Aluminum-Riveted	RT	12	2.261	-.217	0.059	-0.921
Aluminum-Riveted	300°F	12	2.376	-.260	0.020	-0.996
Titanium-Plain	RT	14	2.438	-.167	0.039	-0.942
Titanium-Plain	600°F	15	2.234	-.155	0.039	-0.915
Titanium-Riveted	RT	12	2.335	-.190	0.035	-0.915
Titanium-Riveted	600°F	11	2.377	-.230	0.045	-0.976

NOTE: *Regression Line: $\text{Log } \tilde{\sigma} = A + B \text{ Log } N$ ($\bar{\sigma}$ in ksi)
   **Insufficient data points - regression line slope taken same as 300°F condition.

41

The general specimen configuration is shown in Figure 18, with the detailed dimensions for each of the panels listed in Tables V and VI for the aluminum and titanium alloys, respectively. More detailed drawings are presented in Appendix III. As noted in Table V, two of the aluminum specimen designs had 12 panel bays because of the small center bay in relation to the overall specimen size. All other specimens had nine panel bays. Two replicates of each specimen design were fabricated to provide statistical accuracy consistent with previous test programs. One additional titanium specimen was fabricated for an investigation of thermal buckling effects and was subsequently fatigue tested. An additional aluminum specimen was fabricated to evaluate the effect of intermediate temperature on life.

All specimen manufacturing was accomplished in conformance with standard aircraft manufacturing processes and procedures, with quality control surveillance at all steps. All aluminum zee-section stiffeners were hot formed from sheet stock, while extrusions were used for the frames and clips. All titanium parts were chemically cleaned during manufacture to prevent degradation by foreign materials. The titanium stiffeners and frames were fabricated from sheet stock by welding strips together to form the desired sections. An automatic Tungsten-Inert-Gas (TIG) welding process was used for these longitudinal welds. These parts were subsequently straightened by stress relieving. This approach was taken because of the prohibitive cost of procuring extrusions or hot-forming these titanium sections in small quantities. Cold-forming was deemed undesirable in most instances because of the large bend radii that would result (at least six times the thickness). Automatic riveting, with a Drivmatic riveting machine, was used whenever possible for uniformity. Monel countersunk rivets (MS20427M4) were used on the titanium specimen skins, while aluminum countersunk rivets (LS10795 MP4) were used on the skins of all aluminum specimens. Typical aluminum and titanium specimens are shown in Figure 19.

2. Test Set-up

The test panels were installed in a steel frame, with two identical specimens mounted side-by-side, as shown in Figure 20. Two steel frames were used to minimize down time between tests.

All tests were conducted in the high intensity, grazing incidence, acoustic test facility shown in Figure 21. The test frame was installed in the facility wall with the panel substructure exposed to the noise, opposite to the normal installation, to enable application of heat directly to the skin surface without subjecting the lamps to the noise environment (see figure 22). Response tests conducted at the beginning of the test program indicated no discernible difference in panel response due to panel orientation (i.e., substructure inside or outside the test chamber).

Elevated temperatures were attained with a bank of 2500 watt tungsten-filament quartz lamps mounted vertically in front of the test panels. The 3/8-inch diameter quartz lamp elements were encased in a 1-inch quartz tube, with the lamp ends isolated from the tube for protection from the noise environment. The lamp installation is shown in Figure 22. The lamps were powered by a multi-channel power supply, with two lamps per channel to provide uniform temperature control over the surface of the panel. Temperatures were controlled by varying power input through a silicone controlled rectifier on each channel.
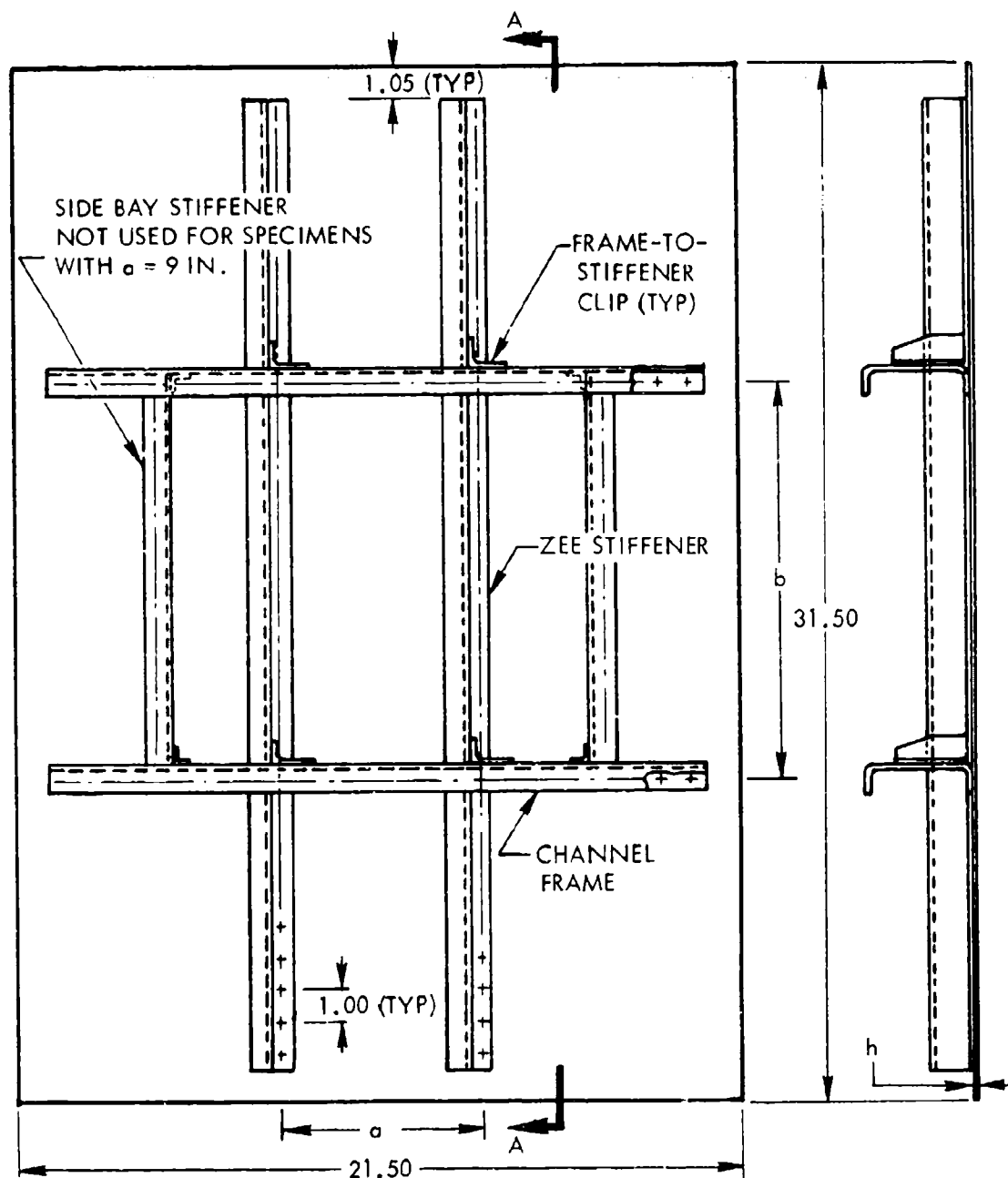
PLAN VIEW   SECTION A-A

NOTE: EDGE MEMBER OMITTED FOR CLARITY

FIGURE 18. STIFFENED-SKIN SPECIMEN CONFIGURATION

43

TABLE V
ALUMINUM STIFFENED-SKIN SPECIMEN DETAILS

Specimen No.	No. of Specimens	No. of Bays	Specimen Dimensions					Test Temperature
			a	b	b/a	h	h_r	
AL-1	2	12	6	9	1.5	0.032	0.040	300°F
-2	2	12	5	10	2.0	0.032	0.040	300°F
-3	2	9	6	12	2.0	0.032	0.040	RT
-4	2	9	6	12	2.0	0.032	0.040	300°F
-5	2	9	6	12	2.0	0.050	0.063	300°F
-6	2	9	9	18	2.0	0.040	0.050	RT
-7	2	9	9	18	2.0	0.040	0.050	300°F
-8	2	9	9	18	2.0	0.063	0.071	300°F
-9	2	9	6	18	3.0	0.032	0.040	300°F
-10 ⚠4	2	9	6	12	2.0	0.032	0.040	RT
-11 ⚠4	2	9	6	12	2.0	0.032	0.040	300°F
-12 ⚠4	2	9	9	18	2.0	0.040	0.050	RT
-13 ⚠4	2	9	9	18	2.0	0.040	0.050	300°F
-14	1	9	6	12	2.0	0.032	0.040	150°F

TOTAL: 27

NOTES:
1. h = skin thickness - inch
2. h_r = stiffener thickness - inch
3. Overall panel dimensions 21.5 x 31.5 inches.
4. Seal per LAC G230 using STM40-111 sealant.

TABLE VI
TITANIUM STIFFENED-SKIN SPECIMEN DETAILS

Specimen No.	No. of Specimens	Specimen Dimensions					Test Temperature
		a	b	b/a	h	h_r	
1	1	6	12	2.0	0.024	0.036	600°F
2	2	6	12	2.0	0.032	0.044	RT
3	2	6	12	2.0	0.032	0.044	400°F
4	2	6	12	2.0	0.032	0.044	600°F
5	2	6	18	3.0	0.032	0.044	400°F
6	2	6	18	3.0	0.044	0.056	RT
7	2	6	18	3.0	0.044	0.056	400°F
8	2	6	18	3.0	0.044	0.056	600°F
9	2	8	16	2.0	0.032	0.044	400°F
10	2	8	16	2.0	0.044	0.056	400°F
11	2	8	16	2.0	0.056	0.068	400°F

TOTAL: 21

NOTES:

1. h = skin thickness - inch
2. h_r = stiffener thickness - inch
3. Overall panel dimensions 21.5 x 31.5 inches.
4. All panels have nine bays.
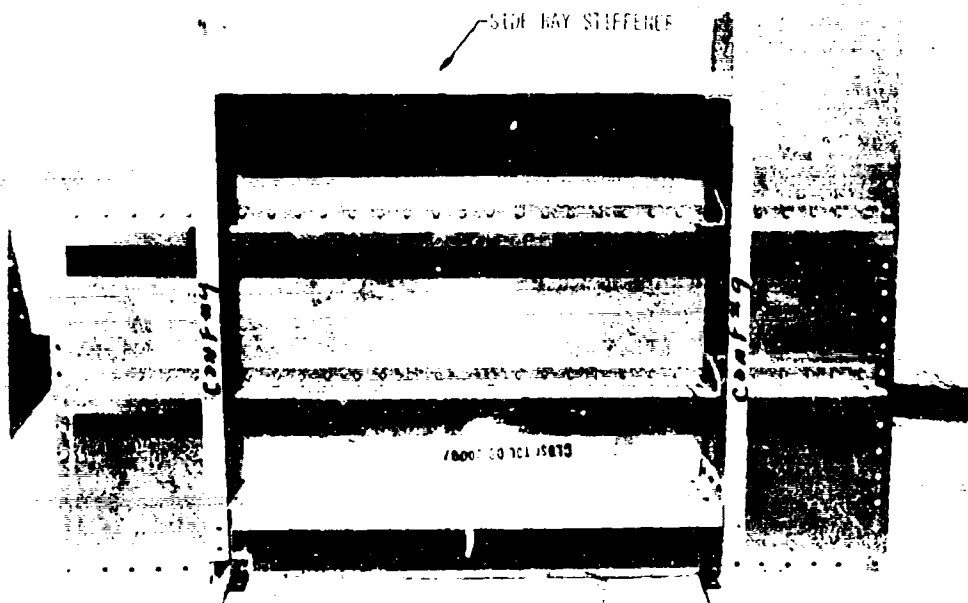
a) ALUMINUM SPECIMEN
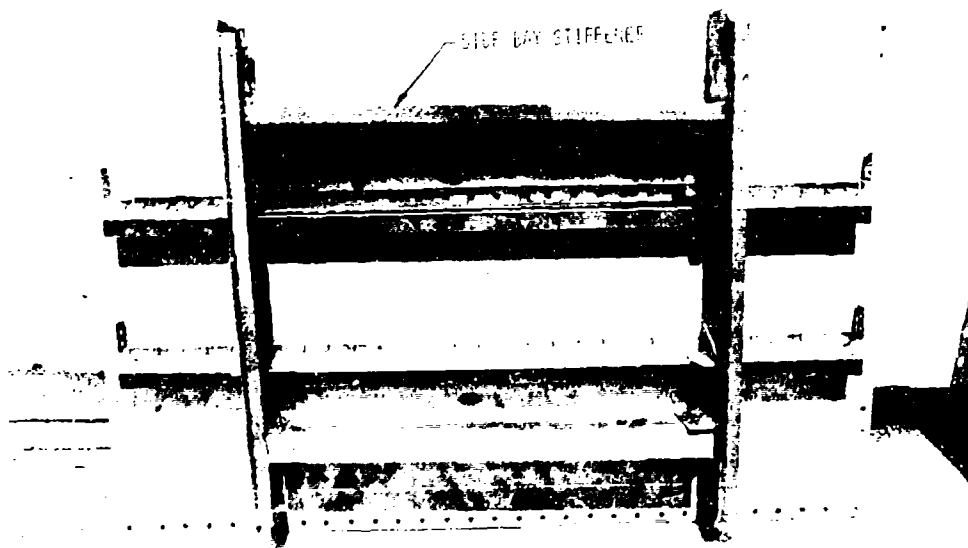
b) TITANIUM SPECIMEN

FIGURE 19. TYPICAL STIFFENED-SKIN TEST SPECIMENS

46
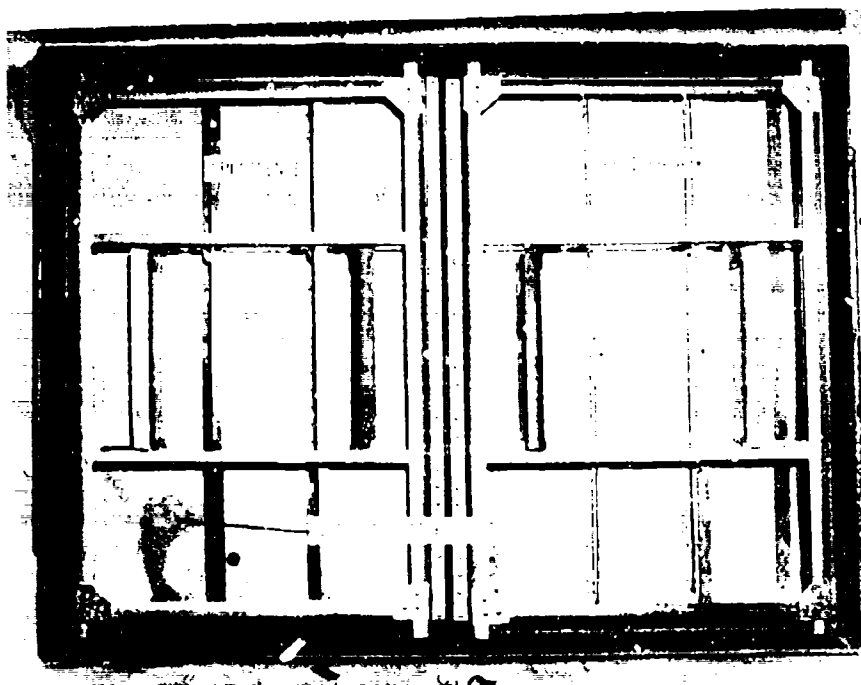
FIGURE 20. TEST SPECIMENS INSTALLED IN STEEL FRAME
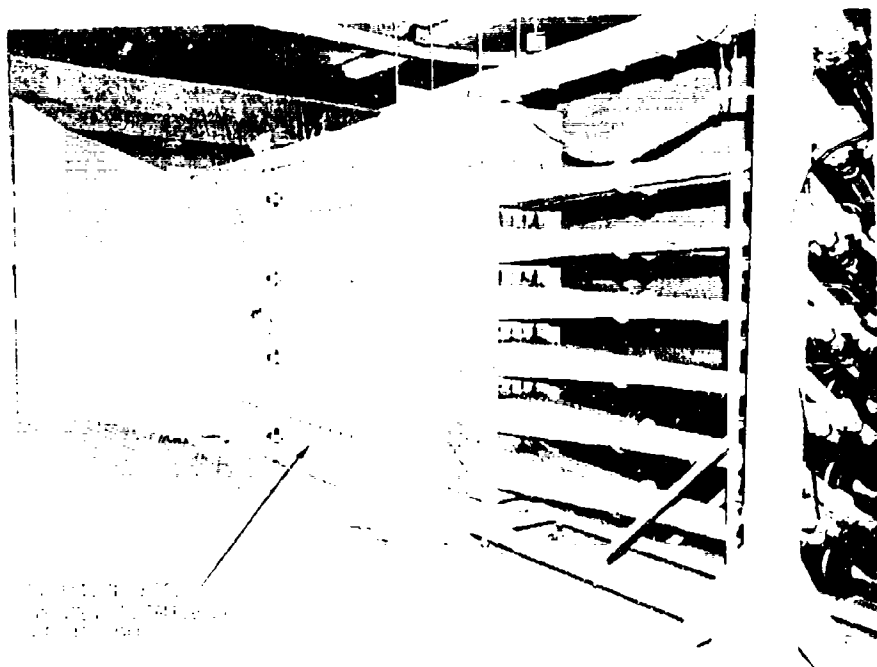
FIGURE 21. ACOUSTIC TEST FACILITY
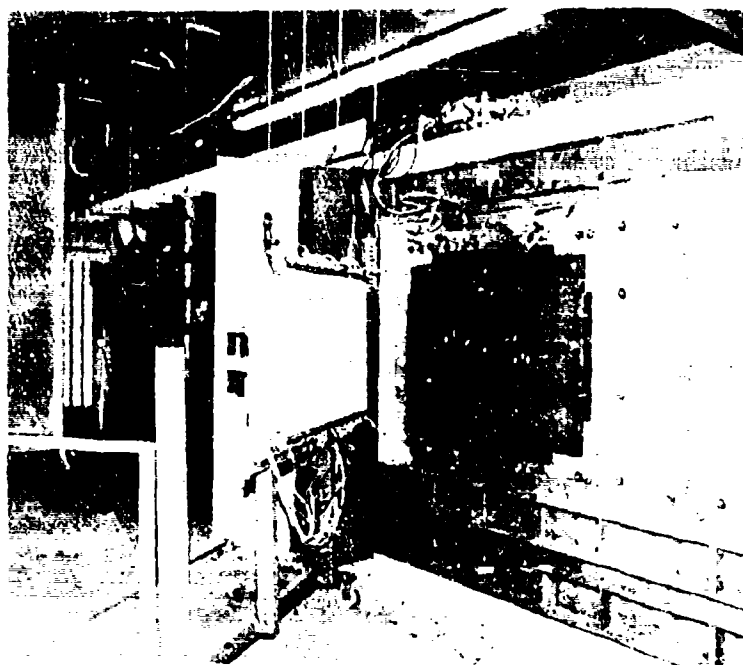
a) HEATING LAMPS ROTATED BACK FROM SPECIMENS
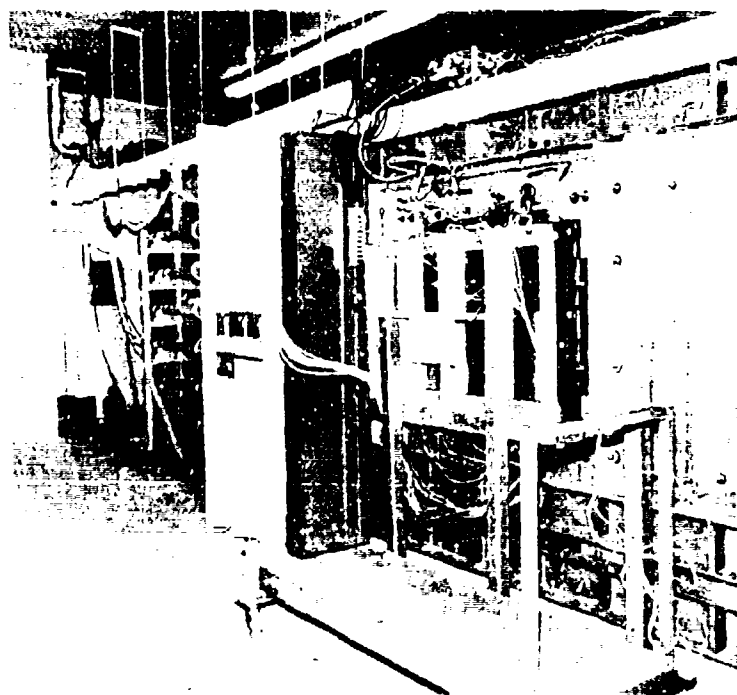
b) HEATING LAMPS IN PLACE

FIGURE 22. ACOUSTIC FATIGUE SET-UP FOR ELEVATED TEMPERATURE TESTS

A modal investigation at room and elevated temperature was conducted on the first titanium specimen to determine placement of the strain gages. Figure 23 shows the strain gage locations for the aluminum and titanium specimens. Micro-Measurements V/K-05-125AD-350 strain gages were bonded to the titanium specimens with BLH Electronic EPY 600 adhesive cured at 650°F. The 1-inch integral gage leads were silver soldered to teflon covered wires. BLH FAE-12-12S13ET strain gages were bonded to the aluminum panels using EPY 600 adhesive cured at 350°F. Lead wires for these gages were 30-gage enameled wire bonded to the panel surface. Teflon tape was used over the lead wires and gages to prevent motion of the wire. Solder tabs at the edge of the panel, where the response was greatly reduced, were used to connect the enameled wire to an insulated lead wire. A typical gage installation for the aluminum specimens is shown in Figure 24.

Chromel-Alumel foil thermocouples, RdF Corp. 20112, were bonded to the specimens with EPY 600 adhesive at the locations shown in Figure 23 and cured simultaneously with the strain gages. The thermocouples were located on the basis of an initial thermal survey on the first titanium specimen, using 14 thermocouples. The locations selected for each specimen provided skin temperatures in the vicinity of the strain gages. Typical thermocouple installations are also shown in Figure 24.

3. Test Procedure

Several tests were conducted on each test specimen prior to fatigue testing. The static and dynamic parameters measured were those indicated by the analysis to be requisite to derivation of useful empirical relations. Instrumentation schematics for these tests are detailed in Appendix III. The tests were generally conducted in the sequence described in following subsections.

a. Room Temperature Frequency - The test specimens, installed in the test frame, were mounted over duct electro-mechanical speakers as shown in Figure 25. Low level sinusoidal noise excitation was applied to the specimen and strain amplitude plotted versus frequency, at ambient temperature, for each strain gage. The frequency scale near the fundamental mode was then expanded to provide better resolution of this mode, and the sine sweep was repeated. The resultant strain-frequency plot was used to compute damping ratios by the half-power method[14].

b. Temperature Effects on Frequency - The test set-up described in the preceding subsection was also used to determine the changes in fundamental frequency with increasing temperature. Six heat lamps were mounted above the specimens as shown in Figure 26. The room temperature Chladni pattern for the fundamental mode was obtained using cork particles; the heat lamps were then turned on and the fundamental mode frequency was tracked by manually varying the speaker input frequency to maintain a fundamental mode response. Skin temperature and response frequency were recorded on data sheets for later analysis.

The critical buckling temperature of the center bay was also determined during this series of tests. The buckling temperature was defined as the temperature increase at which the frequency was a minimum; this was determined from a plot of frequency versus temperature for each specimen.

49
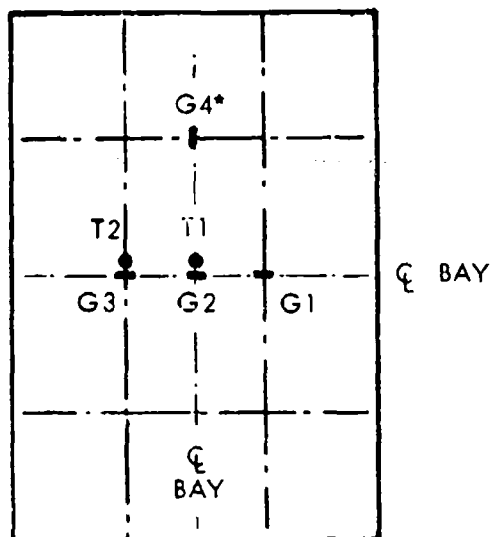
a) ALUMINUM SPECIMENS
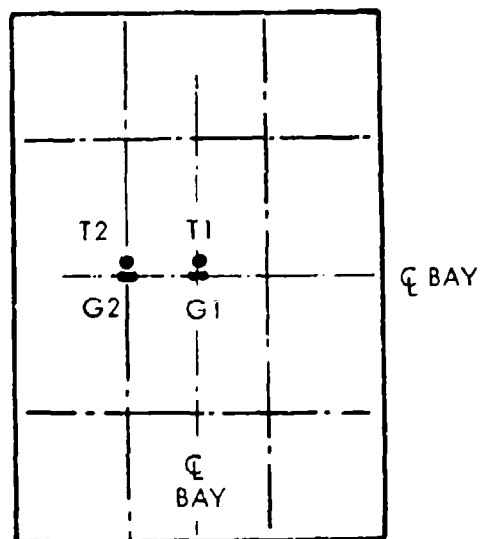
b) TITANIUM SPECIMENS

FIGURE 23. STRAIN GAGE AND THERMOCOUPLE LOCATIONS

50

VIEW OF UPPER HALF OF SPECIMEN

VIEW B
SOLDER TAB DETAIL

VIEW A
STRAIN GAGE/THERMOCOUPLE
DETAIL
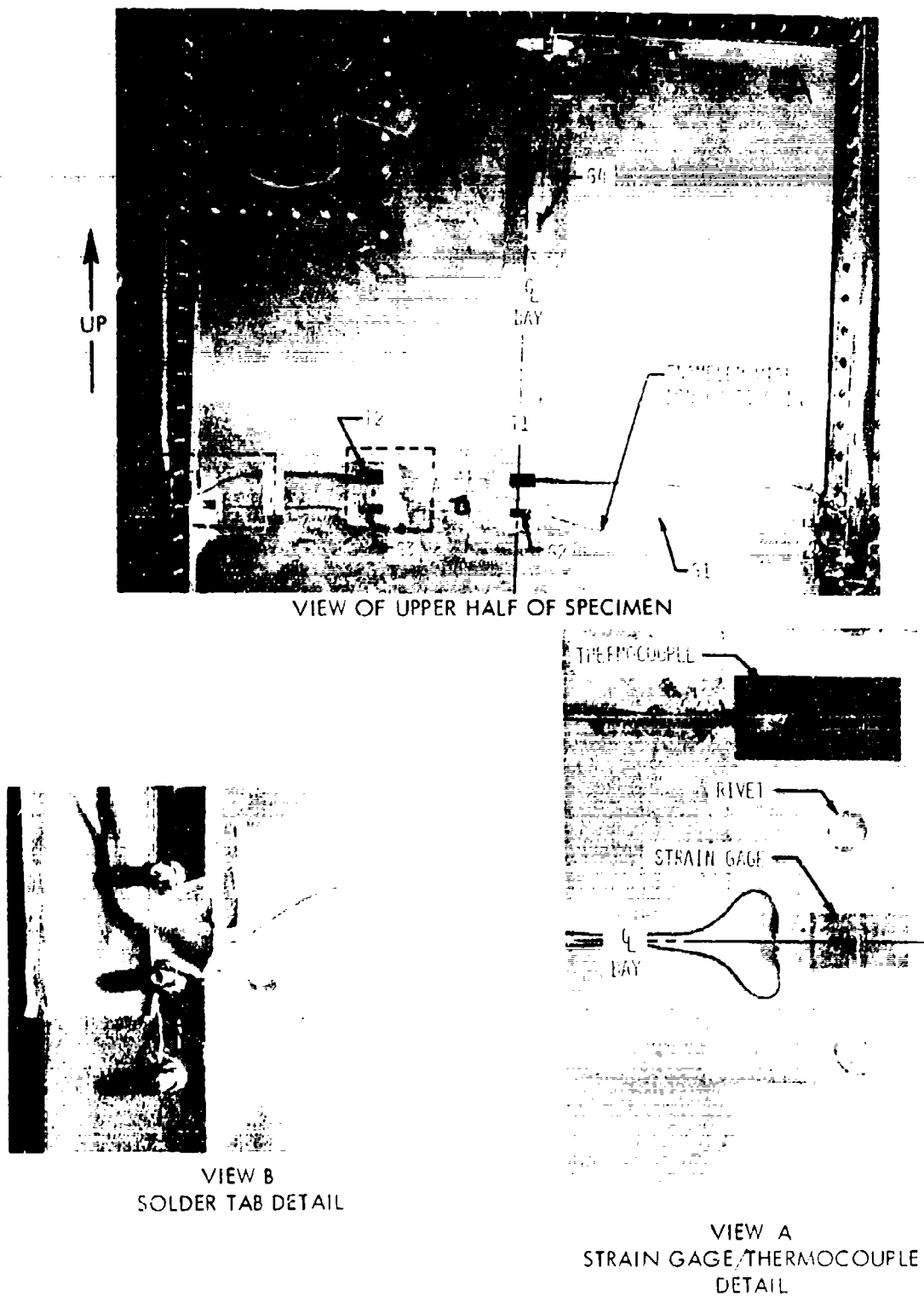
FIGURE 24. TYPICAL STRAIN GAGE INSTALLATION
ALUMINUM SPECIMENS

51
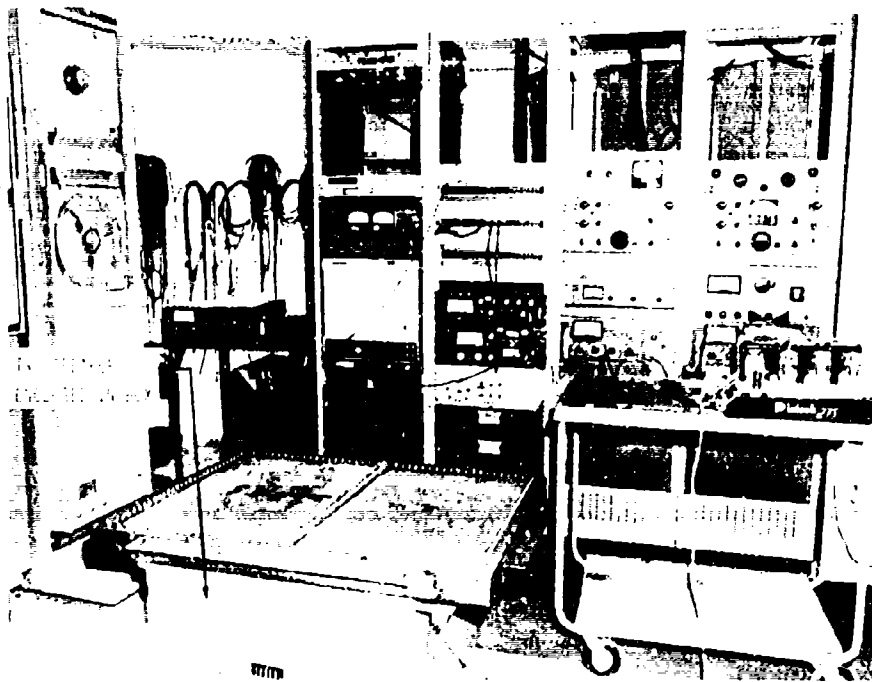
FIGURE 25. AMBIENT TEMPERATURE FREQUENCY TEST SET-UP

FIGURE 26. TEST SET-UP TO MEASURE FREQUENCY VARIATION WITH TEMPERATURE

c.   Thermal Strain and Deflection   - Thermal strain and deflection of the panel center bay were measured on all elevated temperature specimens in the absence of acoustic excitation. The test panels, in the test frame, were installed in the wall of the progressive wave test chamber with the heat lamps in place. Thermal strains were measured with a BLH SR4 Strain Indicator while slowly increasing the panel temperature; the set-up for these measurements is shown in Figure 27. A compensating strain gage, identical to the specimen gages, was bonded to a narrow strip of the specimen alloy and placed on the face of the panel near the edge. The compensating gage location was experimentally determined to maintain the same temperature as that at the panel gages.

The center bay displacement due to thermal buckling, at the midpoint of the bay, was measured concurrently with the thermal strains. A contacting displacement gage was temporarily clamped to the frames of the specimen as shown in Figure 28. The thermal strain and displacement data were recorded on data sheets versus increasing temperature for later analysis.

d.   Excitation Spectrum Shaping - With the specimens mounted in the test chamber, heat was gradually applied to bring the specimens to the desired test temperature. Sinusoidal strain response plots were then made of each strain gage at a constant sound pressure level. The fundamental response frequency at the test temperature, as determined from these plots, was used to locate the frequency limits for shaping of the input noise spectrum.

The input noise spectra were determined by the type of response obtained during these frequency scans. Where single mode response was obtained a narrow-band random input with a 100 Hz bandwidth was used; this did not usually require additional spectrum shaping. Where multi-mode response was obtained, a broader bandwidth was used (normally 300 Hz bandwidth) which was shaped to a flat response by using a 1/3 octave band spectrum shaper.

e.   Fatigue Tests - Fatigue testing was initiated following completion of spectrum shaping. The desired temperature was stabilized before application of the noise excitation. The test excitation level was established by using the modified design chart described previously (See Section III.B.1). Temperatures on the specimen were recorded on a multi-channel strip chart recorder, while noise and strain levels were recorded directly onto a 14-track FM magnetic tape recorder. Parallel outputs on a monitor panel allowed direct observation of the noise and strain signals. Test levels were controlled by maintaining a constant overall noise level at one of the microphone locations.

Visual inspection of each specimen was generally accomplished per the following schedule:

Test Time	Inspection Interval
0 to 1 Hr.	15 minutes
1 to 4 Hrs.	30 minutes
4 Hrs. to End	60 minutes

53
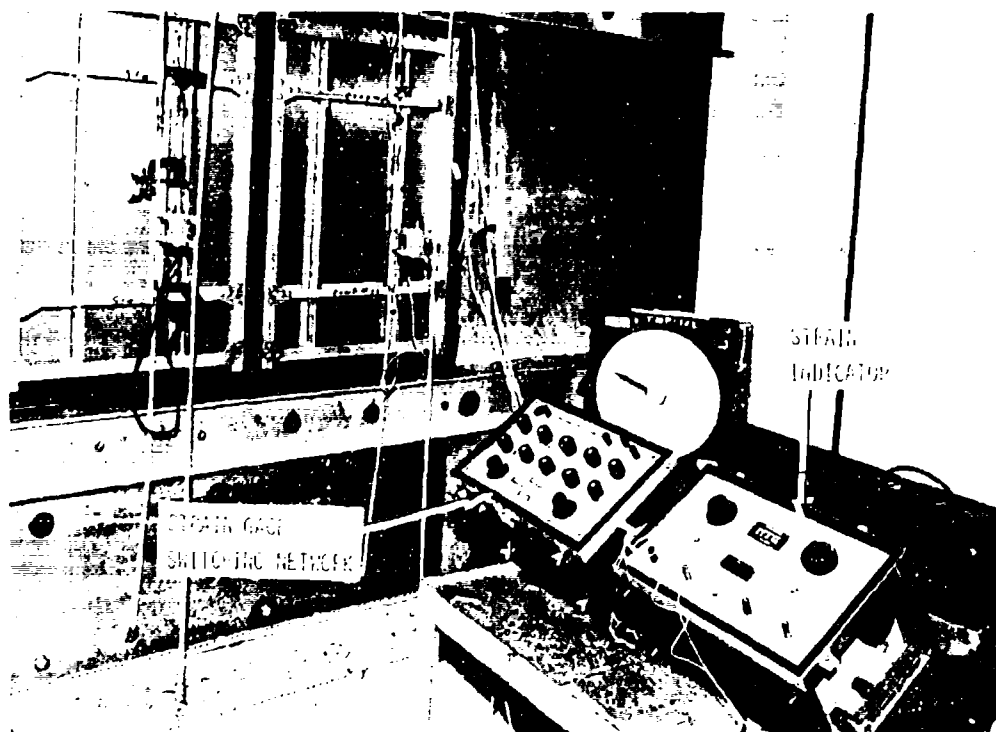
FIGURE 27. THERMAL STRAIN AND BUCKLING AMPLITUDE TEST SET-UP
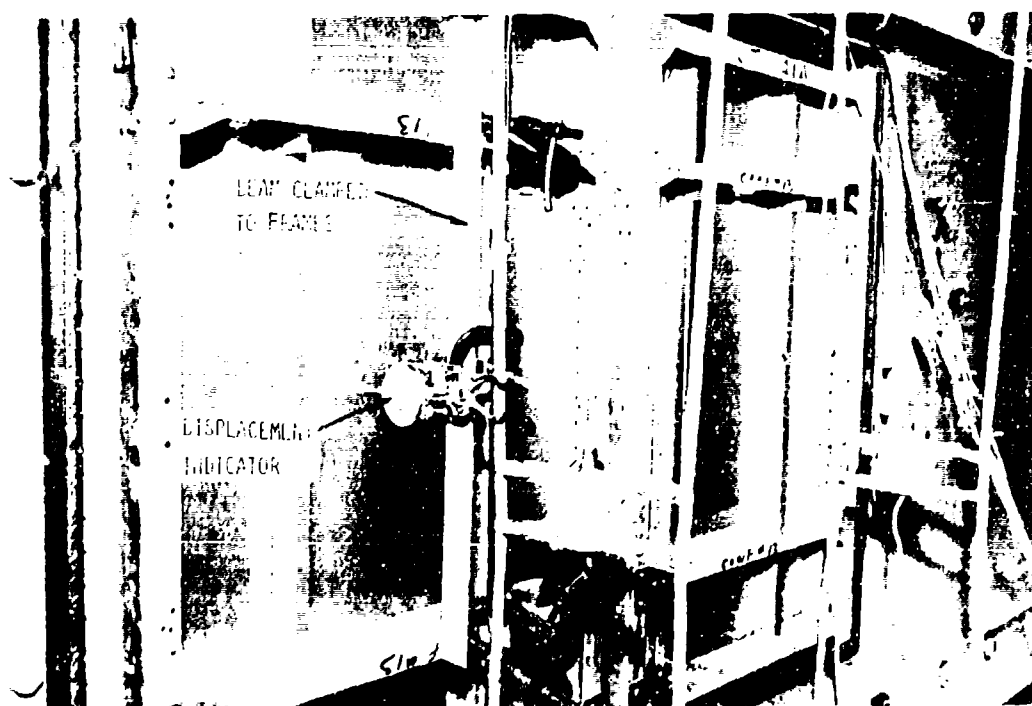
FIGURE 28. BUCKLING AMPLITUDE DISPLACEMENT GAGE SET-UP

These inspection intervals were selected to minimize down-time, while maintaining the maximum possible resolution on life (failure detection), since a cooling-heating cycle was necessary for each inspection. The actual inspection intervals varied from those shown above in some instances; the intervals were usually shorter (particularly at the beginning of the test) for light structure, while the intervals for the thickest panels started out at 30 minutes.

4.   Test Results

The data collected during the various tests conducted on each specimen are much too extensive to be included in their entirety; instead, typical examples and summaries of the test data are presented, in the same sequence as discussed in the preceding section.

a.   Room Temperature Frequency - Room temperature fundamental mode frequencies are tabulated in Tables VII and VIII for the aluminum and titanium specimens. The frequencies shown were recorded at the ambient temperature (generally 65-70°F). The specimens were allowed to stabilize at this temperature for at least 12 hours prior to measurement of these frequencies; hence, the panel skin and substructure, as well as the test frame, should have been in a near-equilibrium thermal state.

Typical examples of the panel strain response are shown in Figures 29 (a) and 30 (a). These show the dominant fundamental mode response for the selected strain gage locations, which is normal for room temperature response. Figure 31 presents the fundamental mode strain response curves for this specimen with an expanded frequency scale to illustrate the damping ratio measurement. As mentioned previously the damping ratios were determined by the half-power method, and the results are tabulated in Tables VII and VIII. The values listed are averages for all the strain gages on each specimen.

An indication of the damping variation between configurations is obtained from Figure 32, which shows the effect of frequency on damping ratio. Data from four other sources[4, 8, 15, 16] are also shown in this figure. All of the data, except for that from Reference 15, are for fundamental mode response. These data are typical of all damping data in the degree of scatter present; however, they may prove useful in establishing realistic limits of assumed damping ratios for structural design. A regression line was plotted through the data centroid, as shown in Figure 32, with a slope taken as an average of the Reference 15 and 16 curves. This regression line can be used to estimate damping for all modes, including the fundamental. As an alternative, the mean damping value of 0.016 (for all data points plotted) may be used for the fundamental mode.

b.   Temperature Effects on Frequency - The change in the fundamental frequency with increasing and decreasing temperature was measured for empirical correlation and for determination of the panel buckling temperature. Several sets of data were accumulated for most of the specimens, all in tabular form of temperature versus frequency. It was found that, after the initial heating and buckling, during cooling the unbuckling occurred at a higher temperature than the initial buckling, as shown in Figure 33. This hysteresis effect was attributed to the gradual heating of the panel substructure, causing the panel to reach its neutral position (unbuckling) at a higher skin temperature during the decreasing temperature test. Alternatively, holding the panel at a constant temperature, above buckling, will result in gradually decreasing buckling amplitudes due to expansion of

55

TABLE VII
ALUMINUM SPECIMENS
SUMMARY OF FUNDAMENTAL MODE FREQUENCY AND DAMPING
PANEL CENTER BAY - ROOM TEMPERATURE

Specimen Number	f_o Fundamental Mode Frequency - Hz	ζ Fundamental Mode Damping
AL-1A	217	0.0145
-1B	225	0.0080
-2A	233	0.0055
-2B	244	0.0097
-3A	166	0.0135
-3B	184	0.0160
-4A	194	0.0188
-4B	171	0.0193
-5A	295	0.0109
-5B	282	0.0125
-6A	94	0.0153
-6B	105	0.0155
-7A	76	0.0203
-7B	80	0.0187
-8A	144	0.0095
-8B	141	0.0192
-9A	146	0.0167
-9B	163	0.0252
-10A	215	0.0139
-10B	187	0.0186
-11A	173	0.0152
-11B	148	0.0192
-12A	94	0.0177
-12B	78	0.0179
-13A	86	0.0195
-13B	95	0.0153
-14A	192	0.0212

TABLE VIII
TITANIUM SPECIMENS

SUMMARY OF FUNDAMENTAL MODE FREQUENCY AND DAMPING
PANEL CENTER BAY - ROOM TEMPERATURE

Specimen Number	f_o Fundamental Mode Frequency - Hz	ζ Fundamental Mode Damping
TI-1A	172	0.0084
-2A	210	0.0176
-2B	227	0.0275
-3A	211	0.0094
-3B	191	0.0156
-4A	201	0.0167
-4B	200	0.0125
-5A	171	0.0172
-5B	166	0.0204
-6A	205	0.0169
-6B	178	0.0154
-7A	205	0.0155
-7B	200	0.0115
-8A	195	0.0114
-8B	203	0.0217
-9A	141	0.0238
-9B	116	0.0234
-10A	169	0.0152
-10B	153	0.0123
-11A	190	0.0213
-11B	191	0.0184
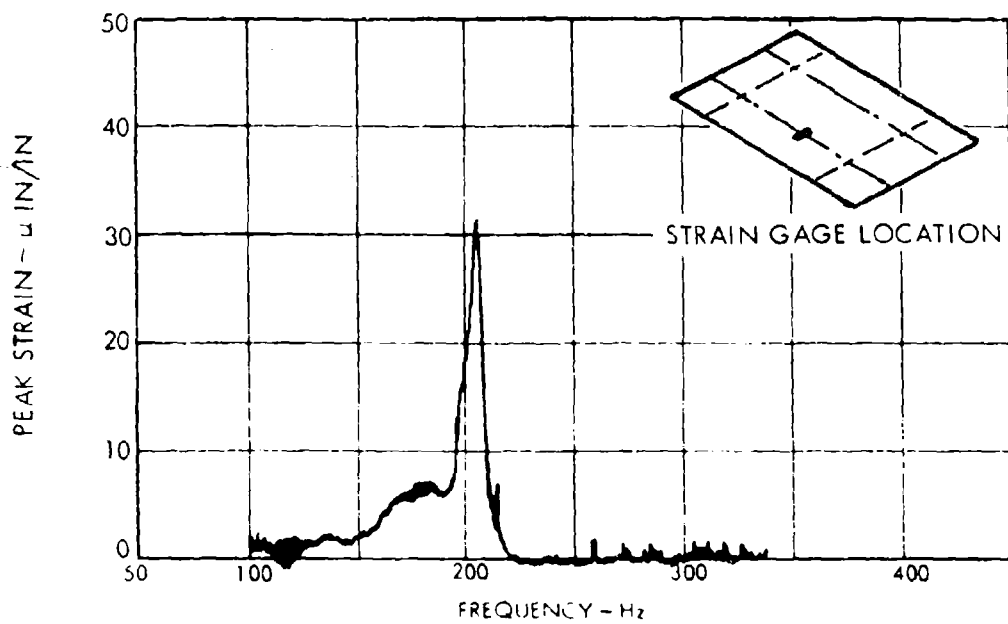
57

a) LOW LEVEL NOISE SINE SWEEP: ROOM TEMPERATURE
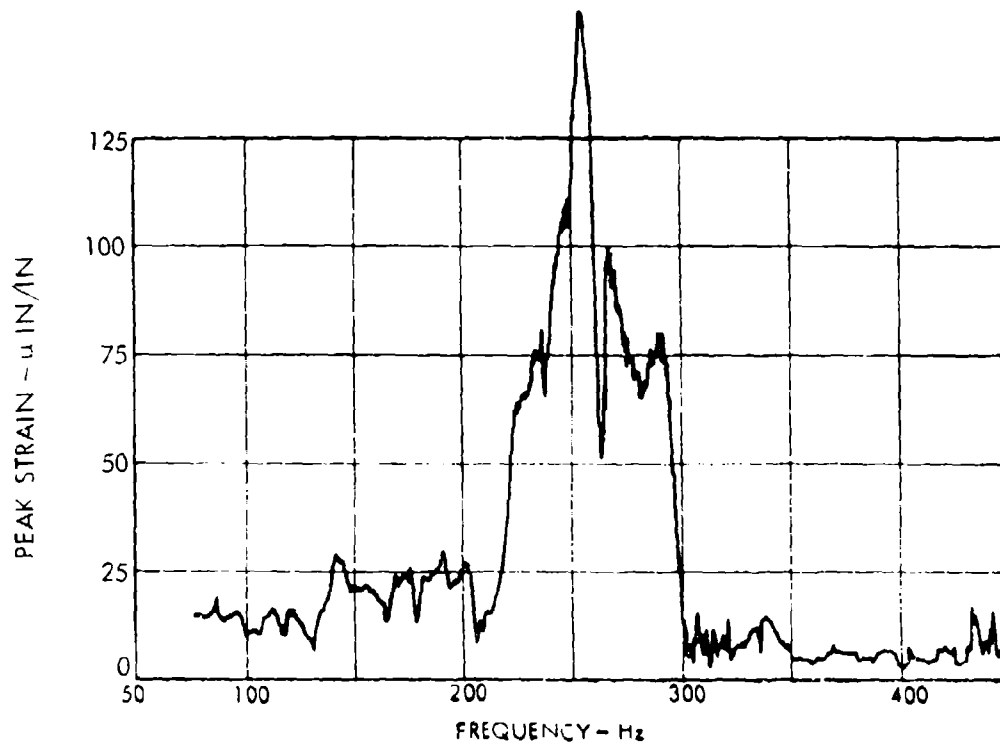
b) HIGH INTENSITY SINE SWEEP: 140 dB @ 300°F

FIGURE 29. SINUSOIDAL STRAIN RESPONSE
ALUMINUM SPECIMEN AL-1A
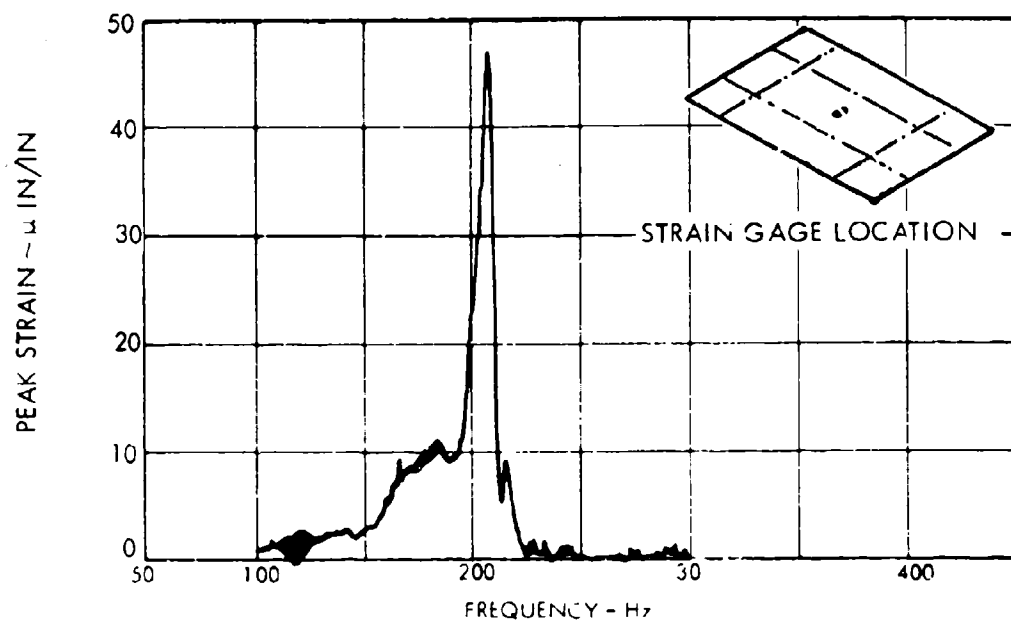
58

a) LOW LEVEL NOISE SINE SWEEP: ROOM TEMPERATURE
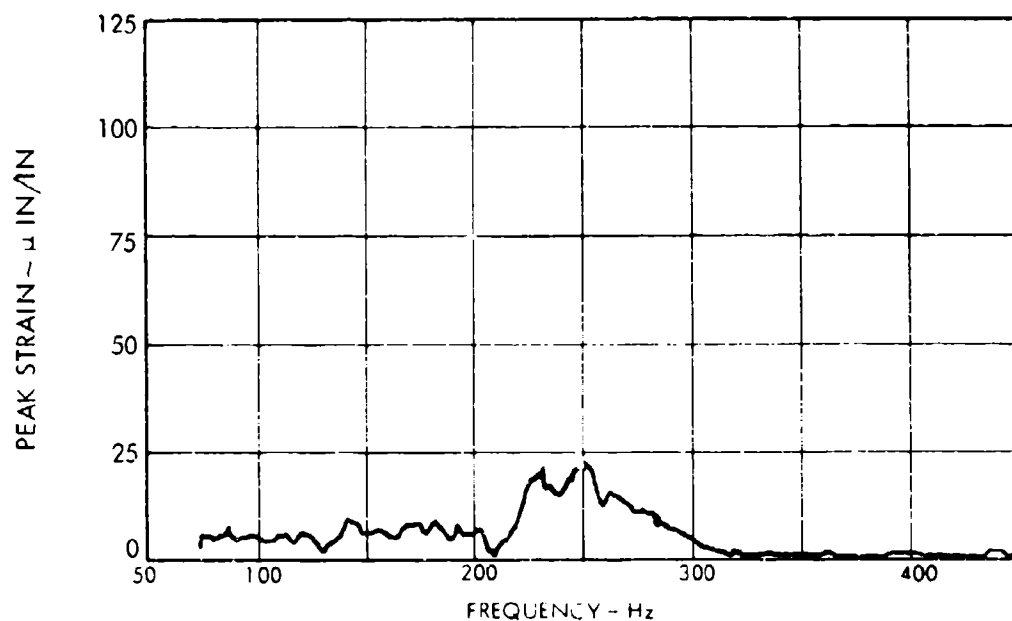
b) HIGH INTENSITY SINE SWEEP: 140 dB @ 300°F

FIGURE 30. SINUSOIDAL STRAIN RESPONSE
ALUMINUM SPECIMEN AL-1A
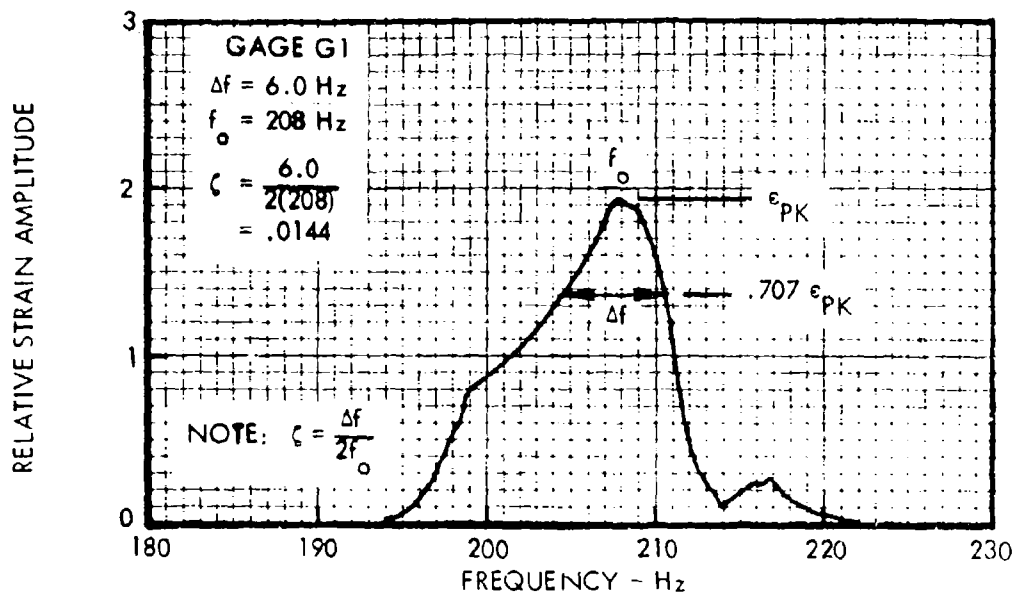
a) STRAIN GAGE ON RIVET ROW
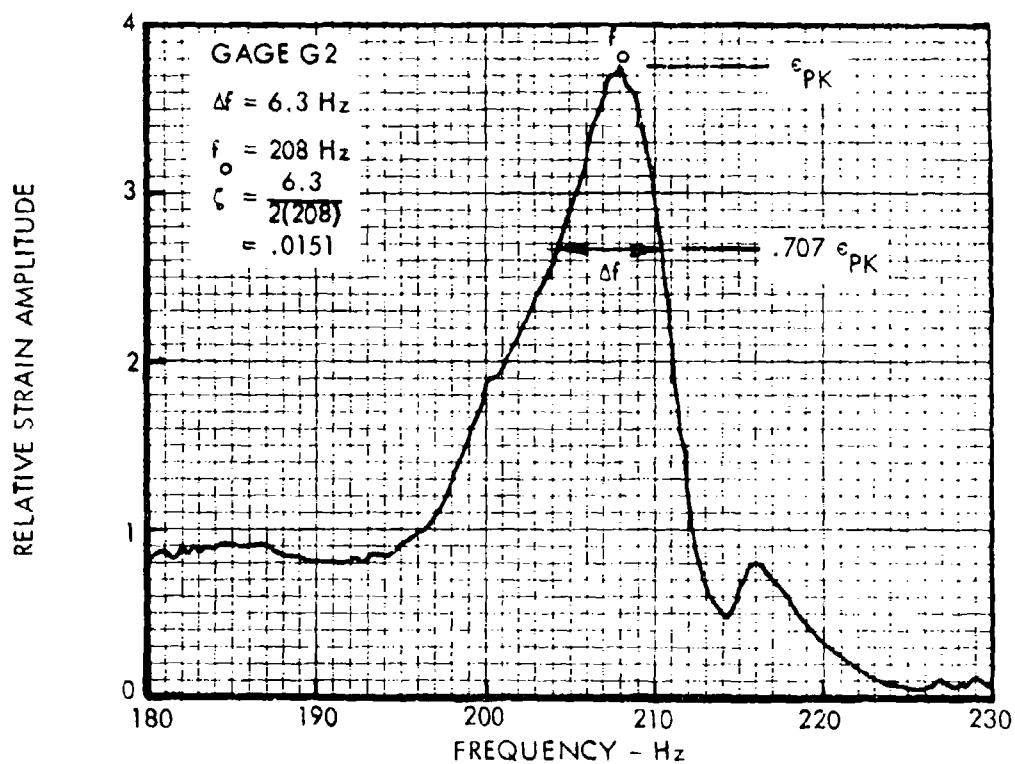
b) STRAIN GAGE AT CENTER OF BAY

FIGURE 31. EXPANDED SCALE FREQUENCY RESPONSE USED TO
MEASURE DAMPING, ALUMINUM SPECIMEN AL-1A
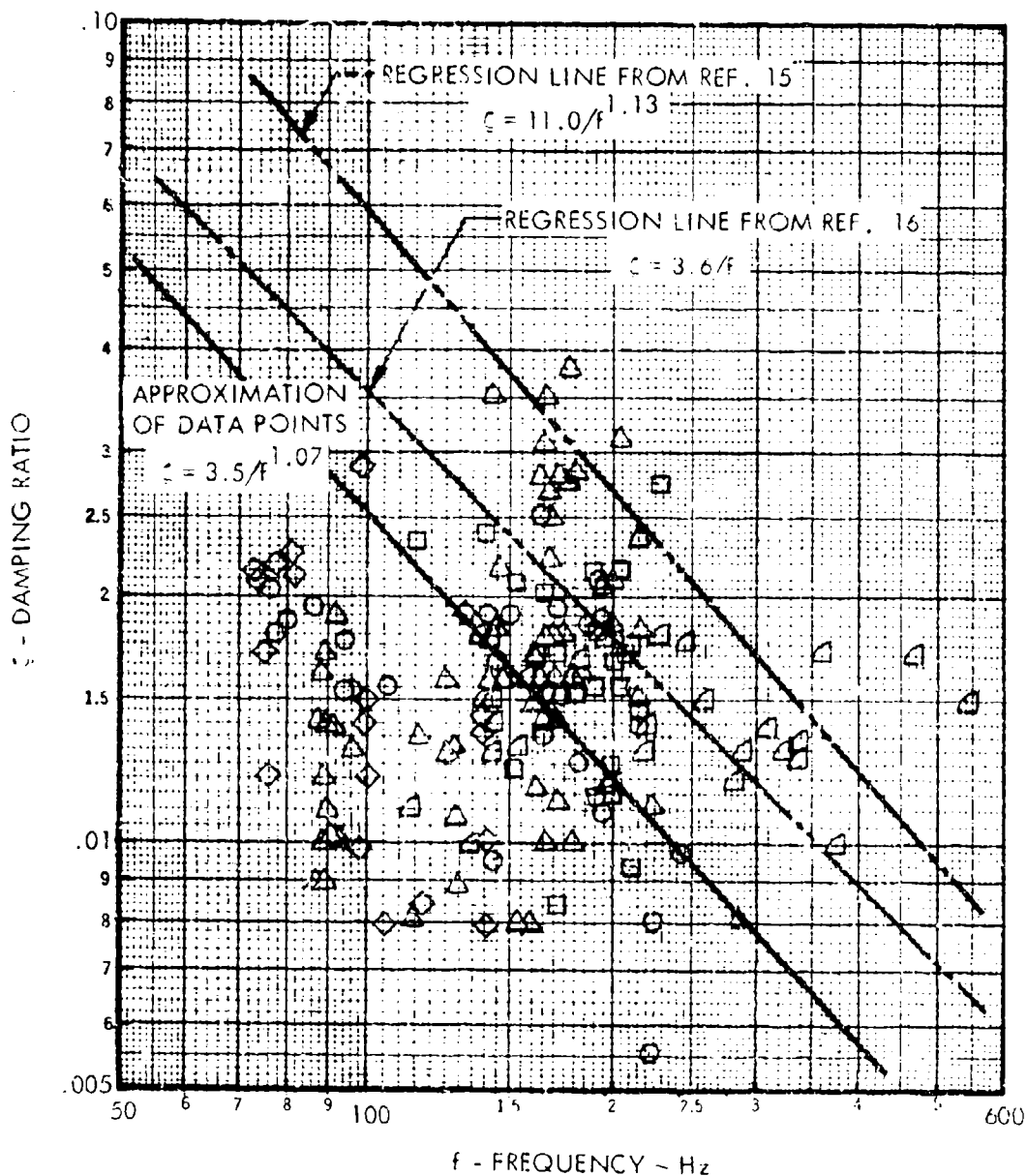
FIGURE 32. DAMPING VARIATION WITH FREQUENCY
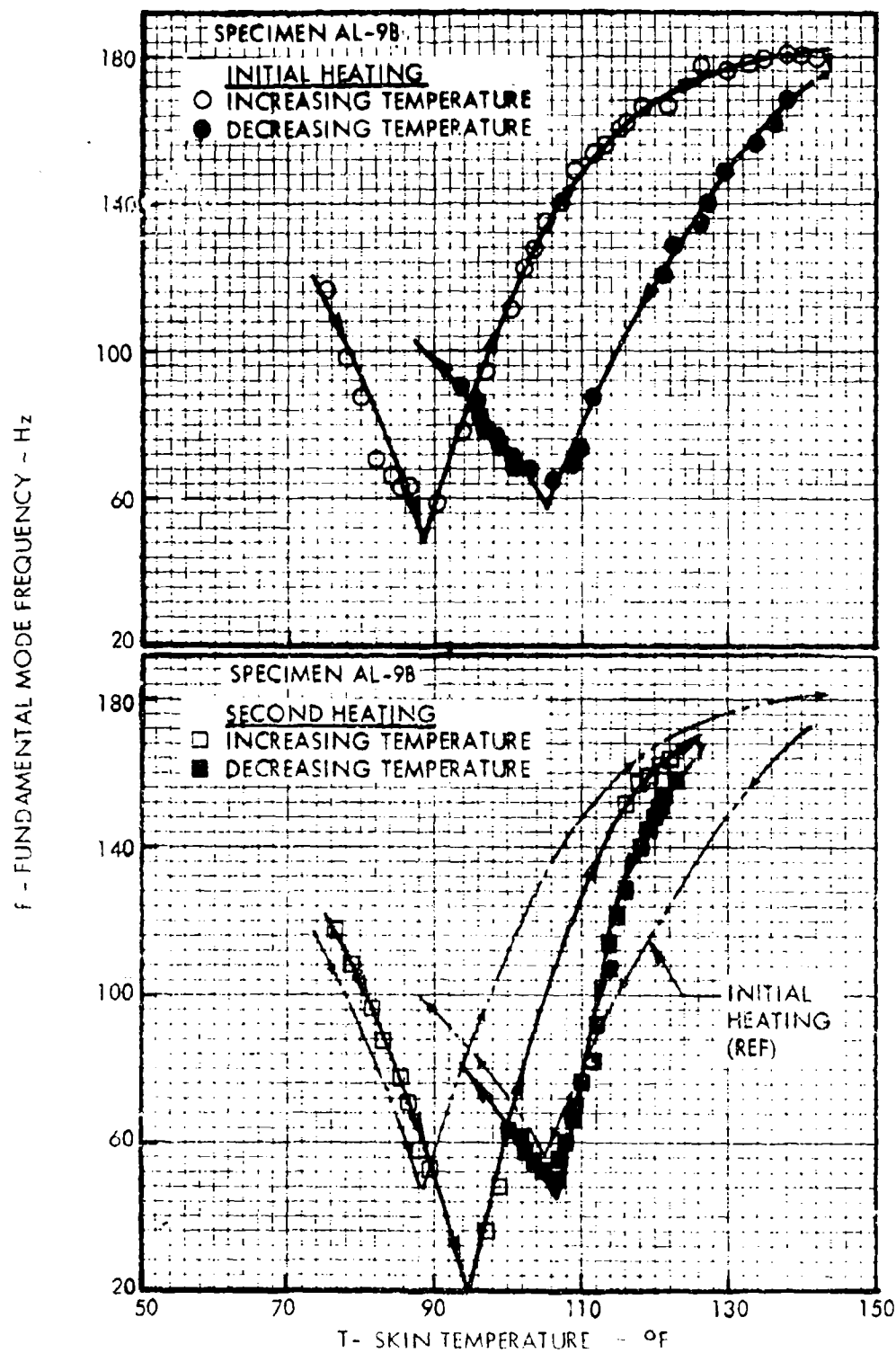
FIGURE 33. EFFECT OF TEMPERATURE ON FUNDAMENTAL MODE FREQUENCY

the substructure. It should be noted that, if the entire structure (skin and stiffeners) were heated uniformly with no external restraints at the structure boundaries, the skin would not buckle because the in-plane residual stresses would be avoided.

Panel skin buckling temperatures were determined from the above frequency temperature plots as the temperature at which the frequency was a minimum (see figure 33). Because of the hysteresis effect, only the initial heating cycle was used to determine the buckling temperatures since heating rates and substructure temperatures were not controlled Since the analytical buckling temperatures are defined as a temperature increase relative to ambient, the measured initial temperature was subtracted from the buckling temperature. The critical buckling temperatures for each of the aluminum and titanium specimens are listed in Table IX.

c.   Thermal Strain and Deflection - Thermal strains and center bay buckling ampli-tude were measured only on the elevated temperature specimens, since room temperature curing adhesives were used for the strain gages on the room temperature specimens. The thermal strains were recorded for two purposes: (1) Determination of the thermal (mean) stress at the test temperature, and (2) correlation with analytical data to provide em-pirical equations for predicting thermal strain. Figure 34 depicts typical thermal strain variation with temperature; the entire thermal strain data set is not included because of its size and the fact that the pertinent information is contained in the later empirical correlation, Section IV.

Center bay buckling amplitudes were measured solely for correlation with the analy-tical results, to provide an interim correlation in the thermal stress calculation. Maxi-mum buckling amplitudes at the individual specimen test temperatures are itemized in Table X.

4.   Excitation Spectrum Shaping - The results of the sinusoidal, high intensity, noise frequency sweeps are typified by Figures 29 (b) and 30 (b). These response plots, made at the individual specimen test temperatures. served to locate the significant panel response for shaping of the excitation spectrum.

The response frequencies obtained during these frequency sweeps at room temperature were always different from those obtained in the low level noise frequency sweeps. The low level sweeps were conducted in a room with a controlled temperature and humidity environment, whereas the high intensity sweeps were made in the grazing incidence test facility, with a significant air flow over the panel, where no temperature control was possible. Aside from the obvious temperature difference, which has been noted in past programs[4, 8], the panel response nonlinearities served to drastically alter the response frequency. Many of the specimens, particularly those tested at room temper-ature, exhibited highly nonlinear response where increasing sound pressure levels caused the response frequencies to increase; only slight increases occurred in the strain amplitudes. The combinations of these two events were in some cases offset: the frequency decrease due to a decrease in the ambient temperature was counteracted by an increase in the panel response frequency due to nonlinearity.

63

TABLE IX

ALUMINUM AND TITANIUM SPECIMENS
SUMMARY OF SKIN BUCKLING TEMPERATURES
PANEL CENTER BAY

Aluminum Specimens		Titanium Specimens	
Specimen Number	Buckling* Temperature - °F	Specimen Number	Buckling* Temperature - °F
AL-1A	8	TI-1A	38
-1B	8	-2A	--**
-2A	10	-2B	--**
-2B	11	-3A	57
-3A	12	-3B	44
-3B	8	-4A	40
-4A	14	-4B	59
-4B	8	-5A	28
-5A	34	-5B	28
-5B	24	-6A	--**
-6A	7	-6B	--**
-6B	11	-7A	51
-7A	6	-7B	50
-7B	8	-8A	12
-8A	18	-8B	16
-8B	15	-9A	19
-9A	7	-9B	17
-9B	6	-10A	31
-10A	10	-10B	19
-· · ·	10	-11A	39
-11.	9	-11B	49
-11B	6		
-12A	6		
-12B	5		
-13A	4		
-13B	4		
-14A	18		

NOTES: *Buckling Temperature in °F above room temperature.

**Room temperature specimens.

64
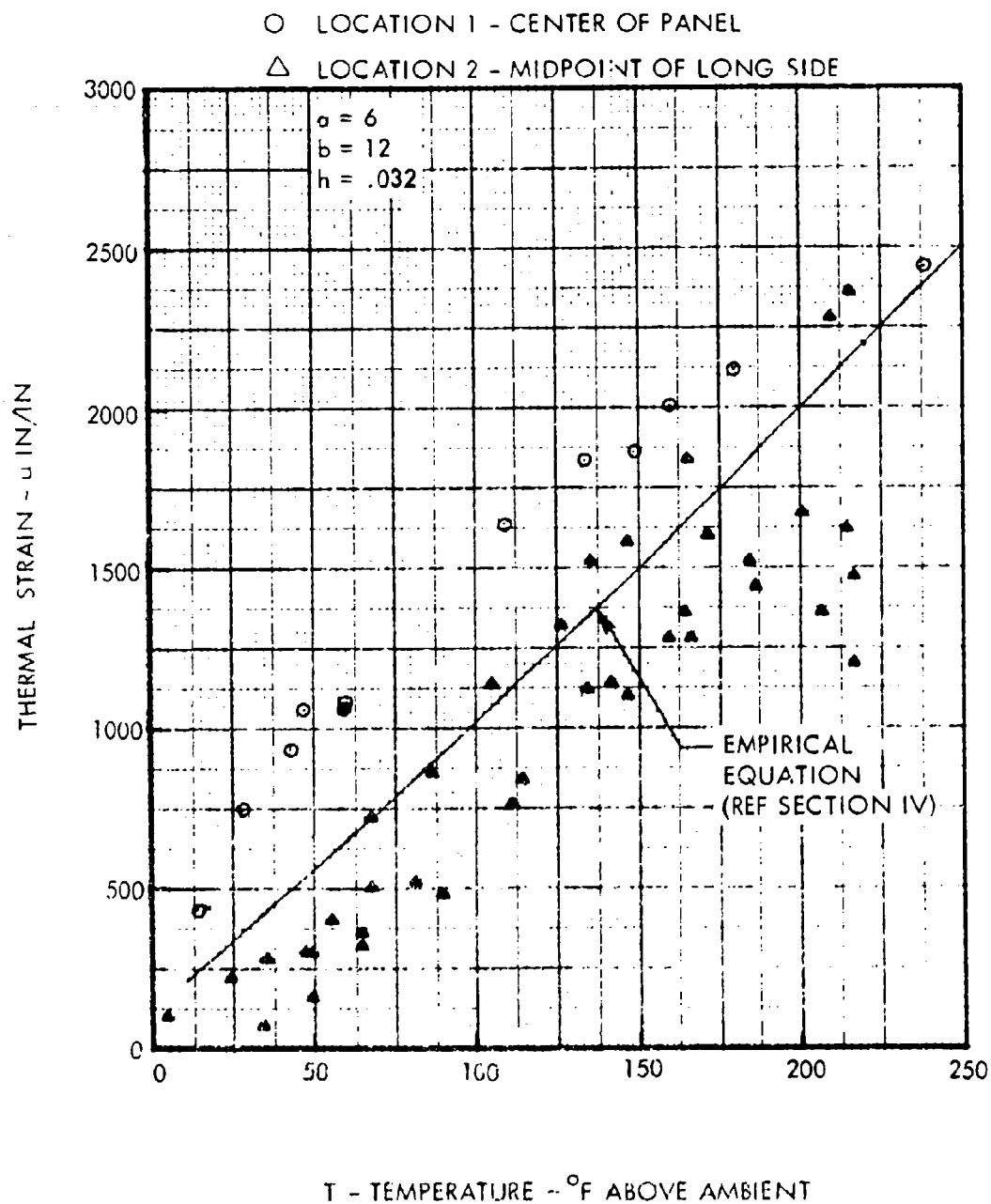
FIGURE 34. THERMAL STRAIN RESPONSE
ALUMINUM SPECIMEN AL-4

65

TABLE X

ALUMINUM AND TITANIUM SPECIMENS
SUMMARY OF THERMAL BUCKLING AMPLITUDES

Aluminum Specimens			Titanium Specimens		
Specimen No.	Test Temperature °F	Maximum Displacement In.	Specimen No.	Test Temperature °F	Maximum Displacement In.
AL-1A	300	0.17	TI-1A	400	-
-1B	300	0.17	-2A	RT	0
-2A	300	0.16	-2B	RT	0
-2B	300	0.20	-3A	600	0.24
-3A	RT	0	-3B	600	0.24
-3B	RT	0	-4A	400	0.17
-4A	300	0.24	-4B	400	0.17
-4B	300	0.24	-5A	400	0.26
-5A	300	0.25	-5B	400	0.23
-5B	300	0.25	-6A	RT	0
-6A	RT	0	-6B	RT	0
-6B	RT	0	-7A	400	0.16
-7A	300	0.35	-7B	400	0.20
-7B	300	0.31	-8A	600	0.27
-8A	300	0.35	-8B	600	0.30
-8B	300	0.36	-9A	400	0.12
-9A	300	0.26	-9B	400	0.27
-9B	300	0.25	-10A	400	0.12
-10A	RT	0	-10B	400	0.26
-10B	RT	0	-11A	400	0.23
-11A	300	0.20	-11B	400	0.23
-11B	300	0.24			
-12A	RT	0			
-12B	RT	0			
-13A	300	0.26	NOTE: Maximum buckling amplitude measured at midpoint of center bay.		
-13B	300	0.35			
-14A	150	0.12			

66

The excitation spectrum for the majority of the specimens had a relatively narrow bandwidth, usually 100 Hz, to concentrate the available acoustic energy at the specimen response frequency. Typical narrow-band excitation spectra are shown in Figure 35. Several of the elevated temperature specimens, especially the 600°F titanium panels, exhibited a relatively flat response, with no single significant mode. In these cases, broad-band excitation was used to envelope the first two or three response peaks. The bandwidth in this case was typically 200 to 300 Hz, as shown in Figure 36. Although a band-pass filter was used to cut out the unwanted low and high frequencies, the roll-off of the noise signal in most cases was very gradual, due to harmonic distortion generated in the electropneumatic transducers.

Probability density analyses were made of the input spectra shown in Figures 35 and 36 to determine the distribution of instantaneous peaks. These analyses, presented in Figures 37 and 38, closely approximate a Gaussian distribution as noted on the figures.

e.   Fatigue Tests – The noise and strain signals, recorded on FM magnetic tape, were re-recorded onto a loop recorder (10-Second sample) for narrow-band spectrum analyses. Spectrum analyses, with a 5 Hz nominal bandwidth, of each strain gage response were made at the beginning of the test and periodically throughout the test. Sample strain response spectra are shown in Figures 39 through 44. The strain response spectra provided the specimen response frequency, while the response strain level was taken as the overall rms strain. Representative excitation spectra were discussed in the preceding section, and presented in Figures 35 and 36.

Probability density analyses were made of the strain response spectra shown in Figures 39 through 44 to determine the distribution of response peaks. These analyses are shown in Figures 45 through 50 and approximate a Gaussian distribution.

Table XI summarizes the fatigue test results for the 27 aluminum specimens while Table XII summarizes the test results for the 21 titanium specimens. These data are plotted in the form of fatigue curves in Figures 51 and 52 for the aluminum and titanium specimens, respectively. The data points were plotted and a least squares regression analysis was performed on the data for each test temperature. Since most of the test conditions did not contain sufficient data points on which to base a valid statistical analysis, only the centroid of the data set was used from these analyses. The slope of the appropriate coupon fatigue curve (from Figure 16 or 17) was then plotted through the data centroid to establish the curves shown. The applicable statistical properties are itemized in Table XIII for reference. The fatigue curves of Figures 51 and 52 show the decrease in fatigue life due to the combined effect of thermal stress and degradation of alloy properties caused by the elevated temperatures. The room temperature curves are lower (stresswise for equal life) than the comparable coupon fatigue curve; this is attributed to the difference in response between the two configurations. The stiffened panel response was very highly nonlinear in most cases, with relatively high damping, while the coupon response was linear with low damping.

Fatigue failures generally occurred in the rivet row at the midpoints of the long and short sides of the center bay. The distribution of failures at these locations is shown in Table XIV.

FILTER BANDWIDTH: 5 Hz
SCAN RATE: 1.0 Hz/SEC
SAMPLE TIME: 10 SEC
TIME CONSTANT: 3 SEC
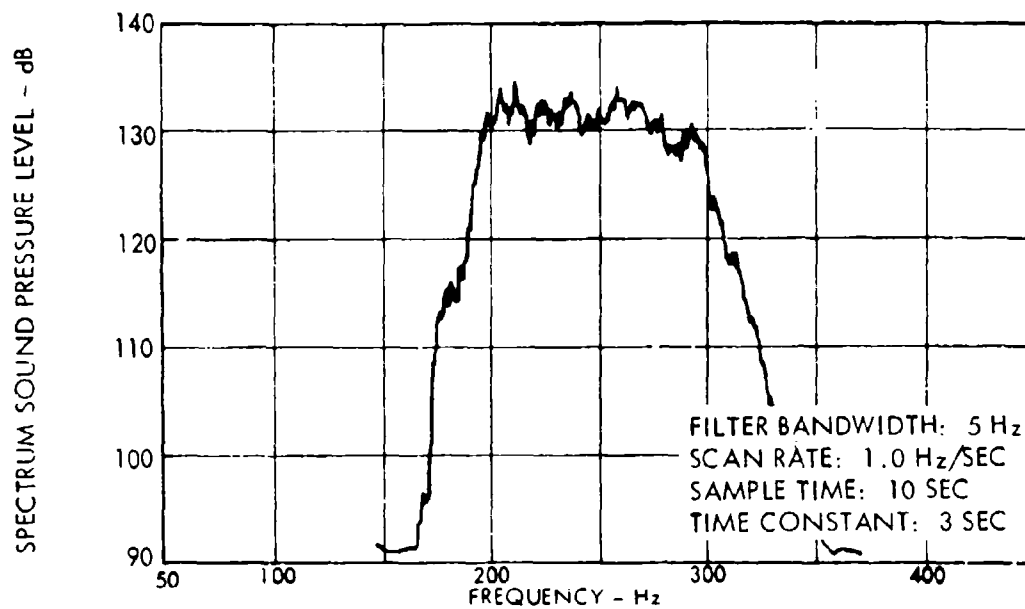
FIGURE 35. TYPICAL NARROW-BAND TEST SPECTRUM

FILTER BANDWIDTH: 5Hz
SCAN RATE: 1.0 Hz/SEC
SAMPLE TIME: 10 SEC
TIME CONSTANT: 3 SEC
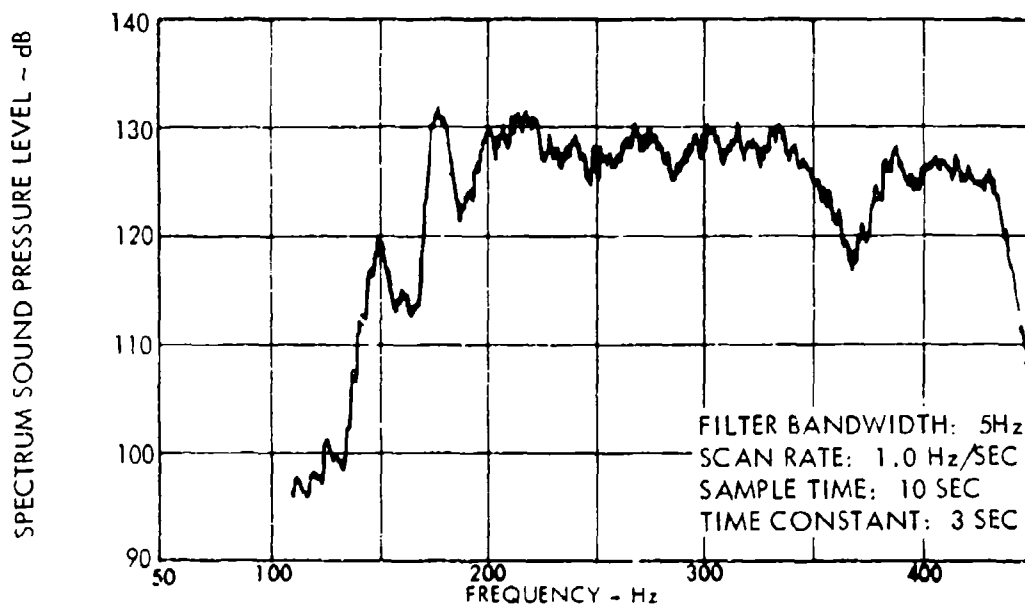
FIGURE 36. TYPICAL BROAD-BAND TEST SPECTRUM
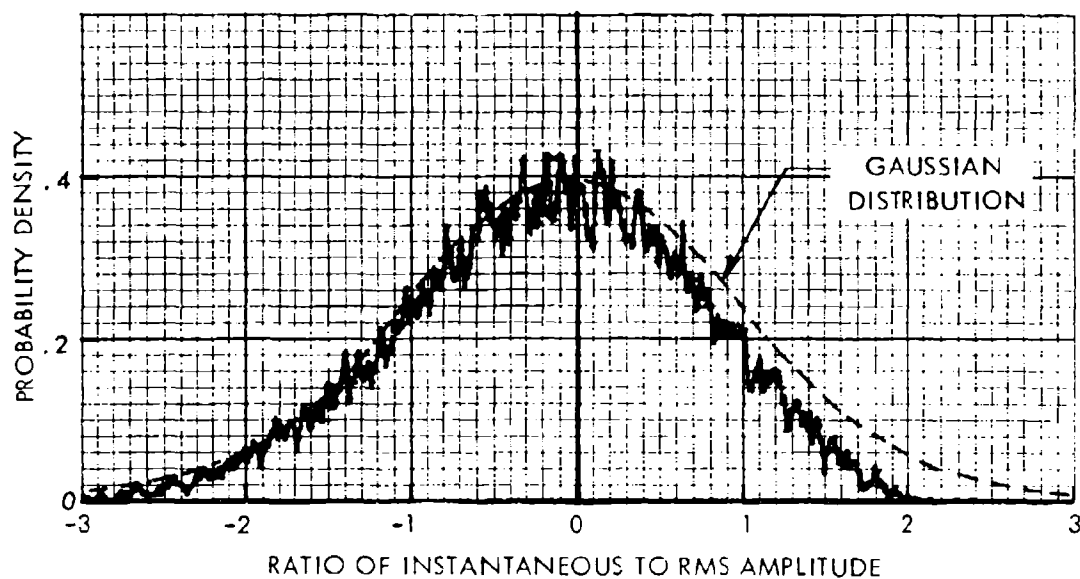
FIGURE 37. AMPLITUDE DISTRIBUTION - NARROW-BAND
NOISE SPECTRUM OF FIGURE 35.
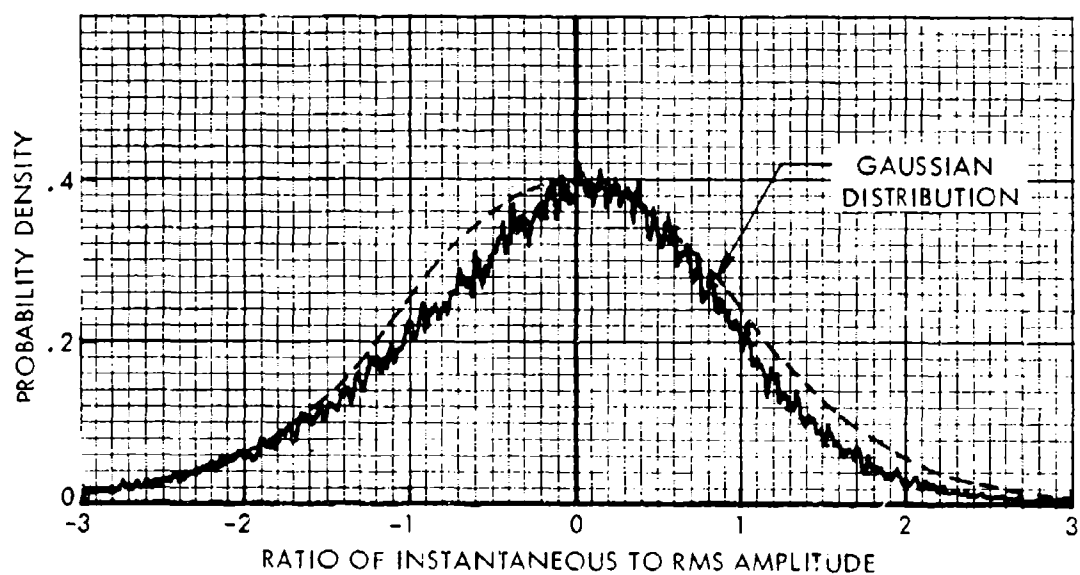
FIGURE 38. AMPLITUDE DISTRIBUTION - BROAD-BAND
NOISE SPECTRUM OF FIGURE 36.
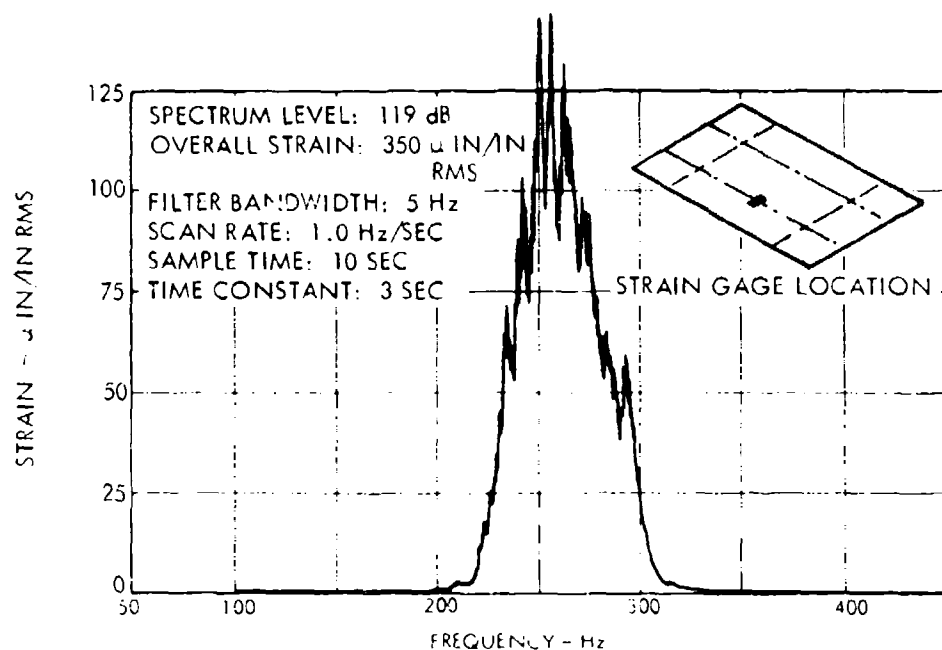
FIGURE 39. NARROW-BAND ANALYSIS
ALUMINUM SPECIMEN AL-1A
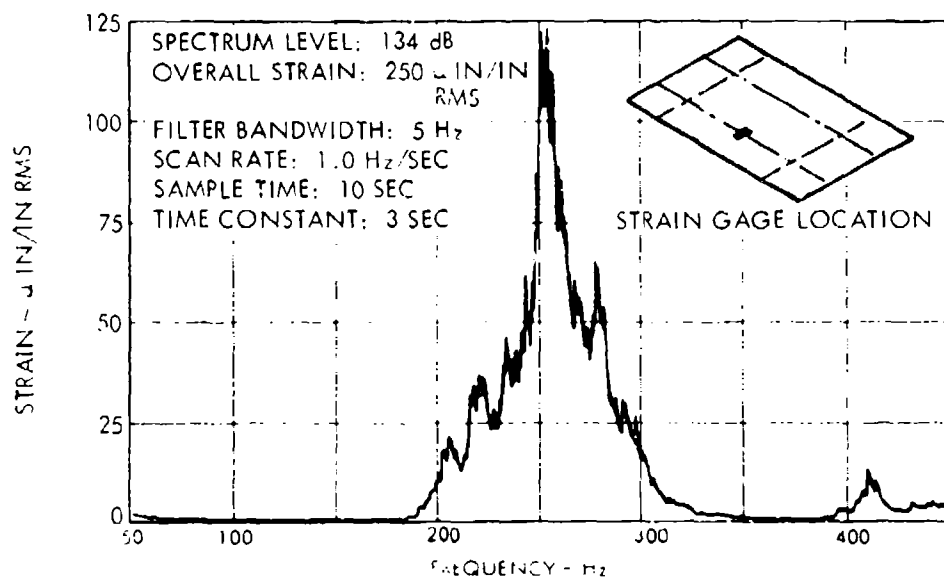
FIGURE 40. NARROW-BAND ANALYSIS
ALUMINUM SPECIMEN AL-3A

70
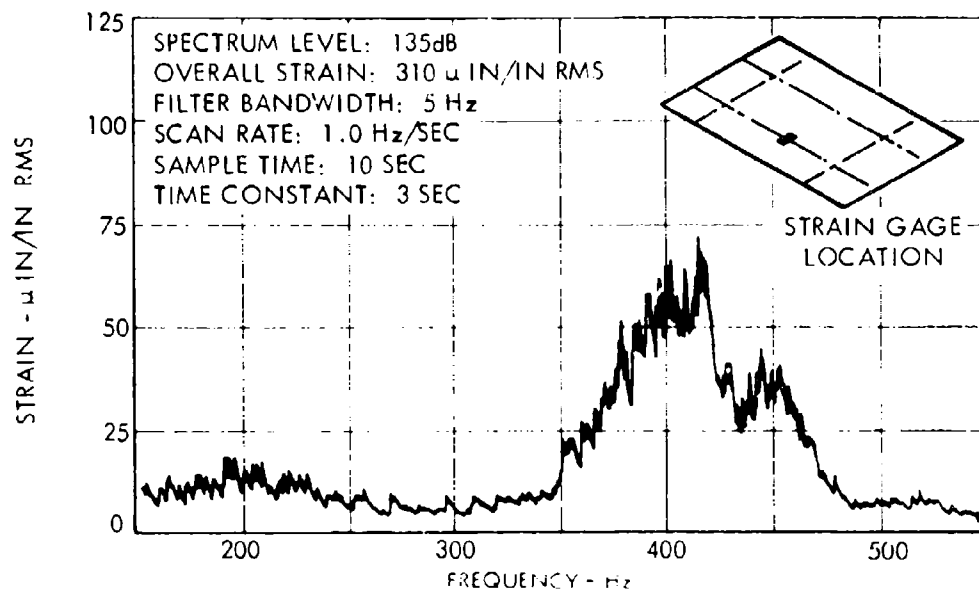
FIGURE 41. NARROW-BAND ANALYSIS
ALUMINUM SPECIMEN AL-4A
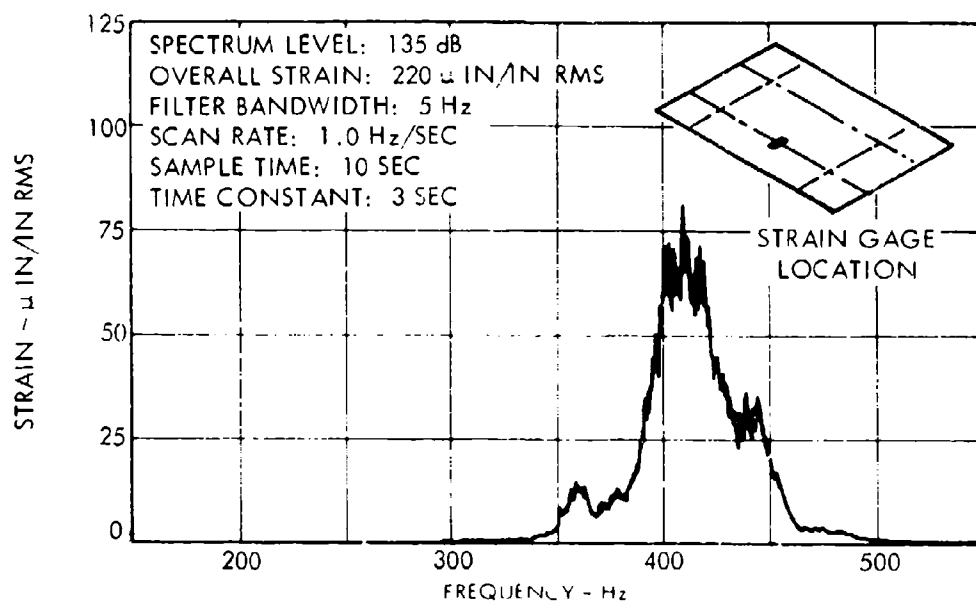
FIGURE 42. NARROW-BAND ANALYSIS
ALUMINUM SPECIMEN AL-4B

71
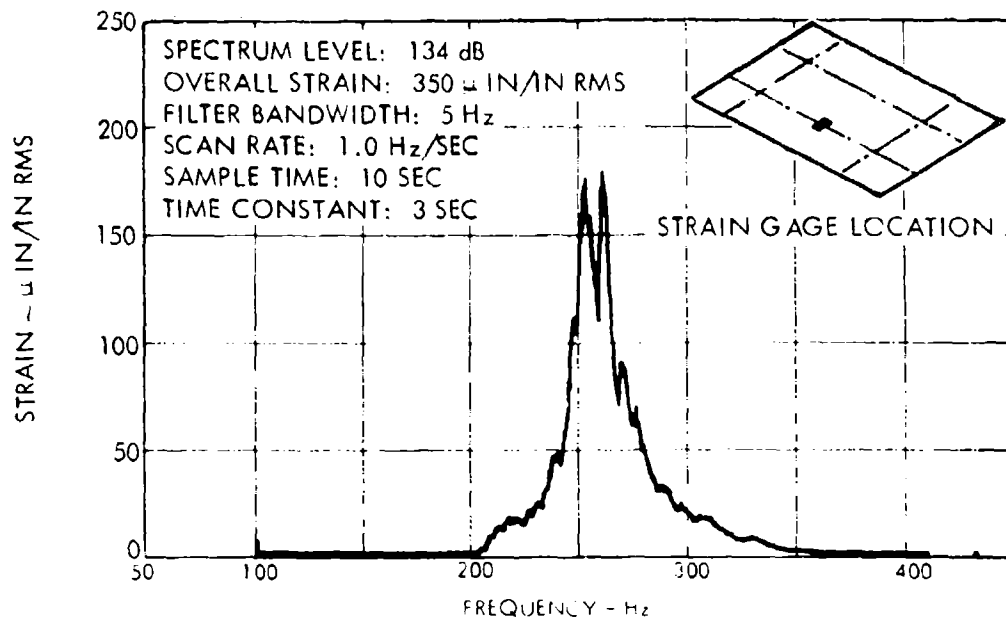
FIGURE 43. NARROW-BAND ANALYSIS
TITANIUM SPECIMEN TI-3B
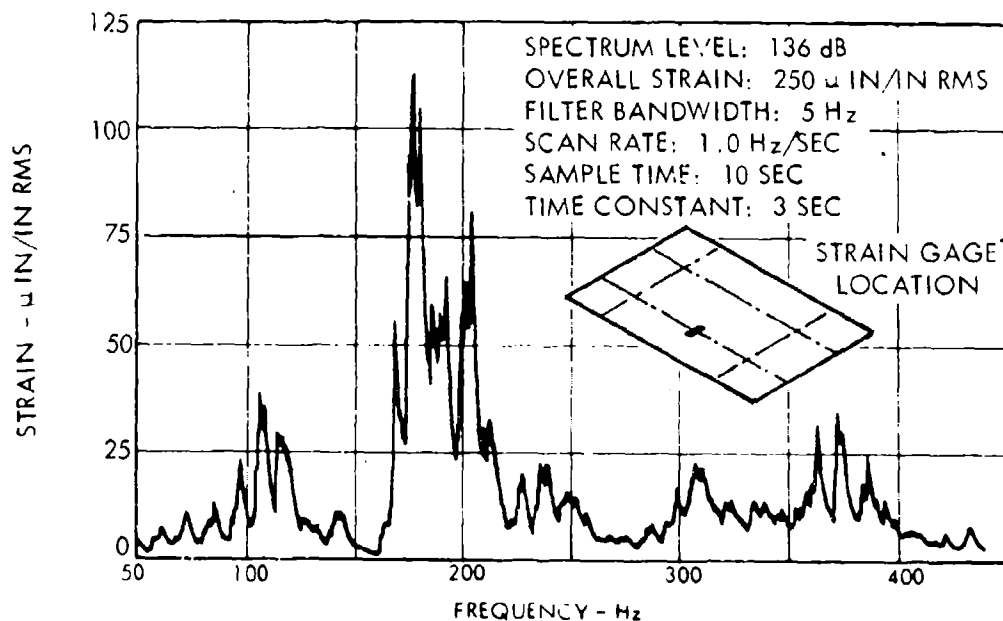
FIGURE 44. NARROW-BAND ANALYSIS
TITANIUM SPECIMEN TI-10A

72
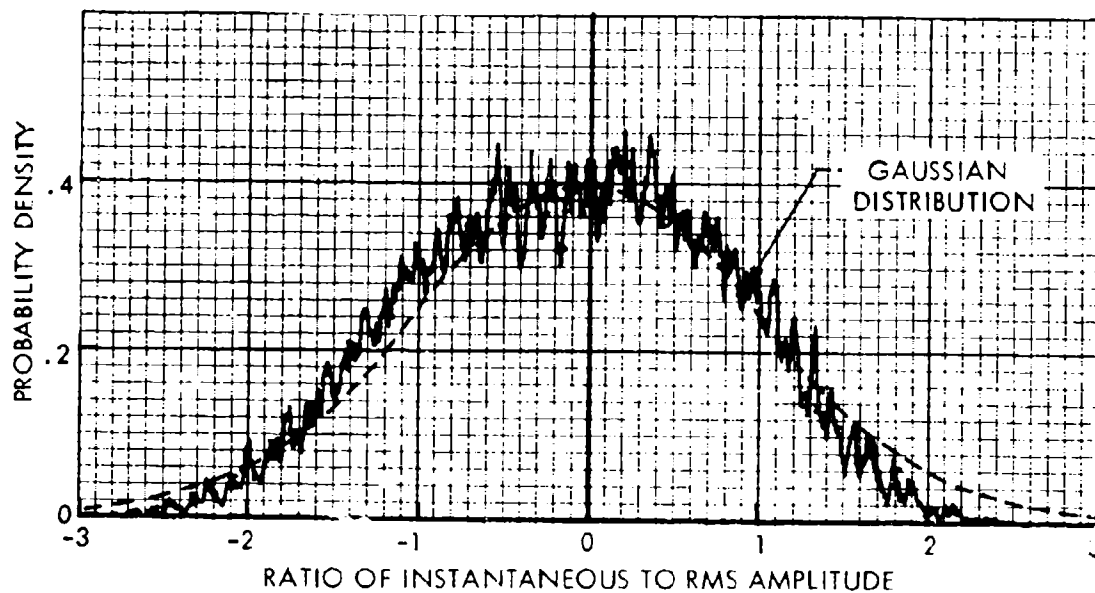
FIGURE 45.   AMPLITUDE DISTRIBUTION OF STRAIN RESPONSE
SPECIMEN AL-1A (REF. FIGURE 39)
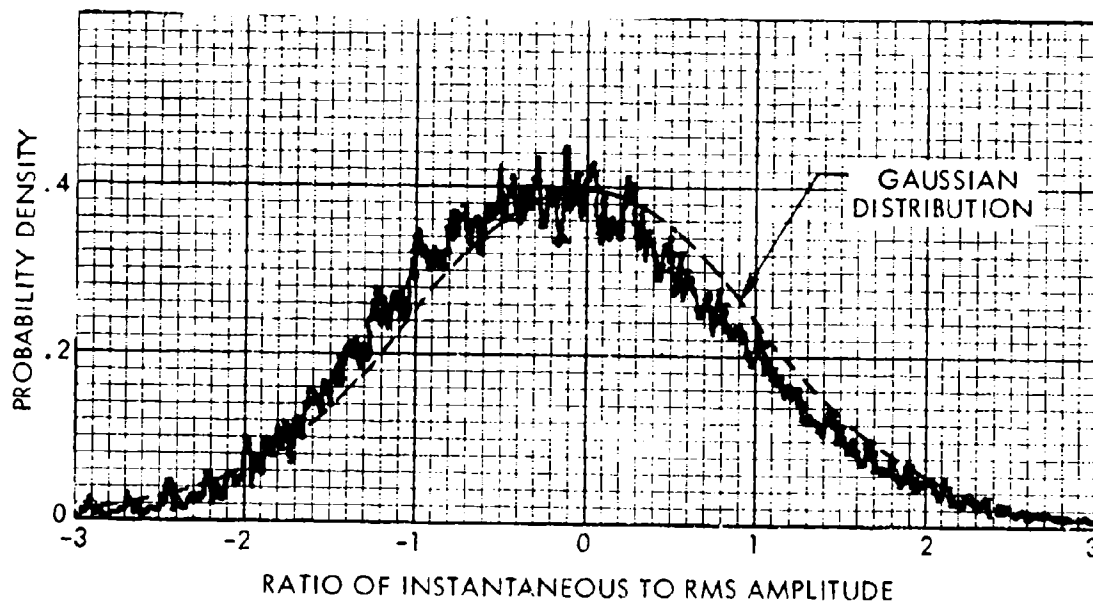
FIGURE 46.   AMPLITUDE DISTRIBUTION OF STRAIN RESPONSE
SPECIMEN AL-3A (REF. FIGURE 40)
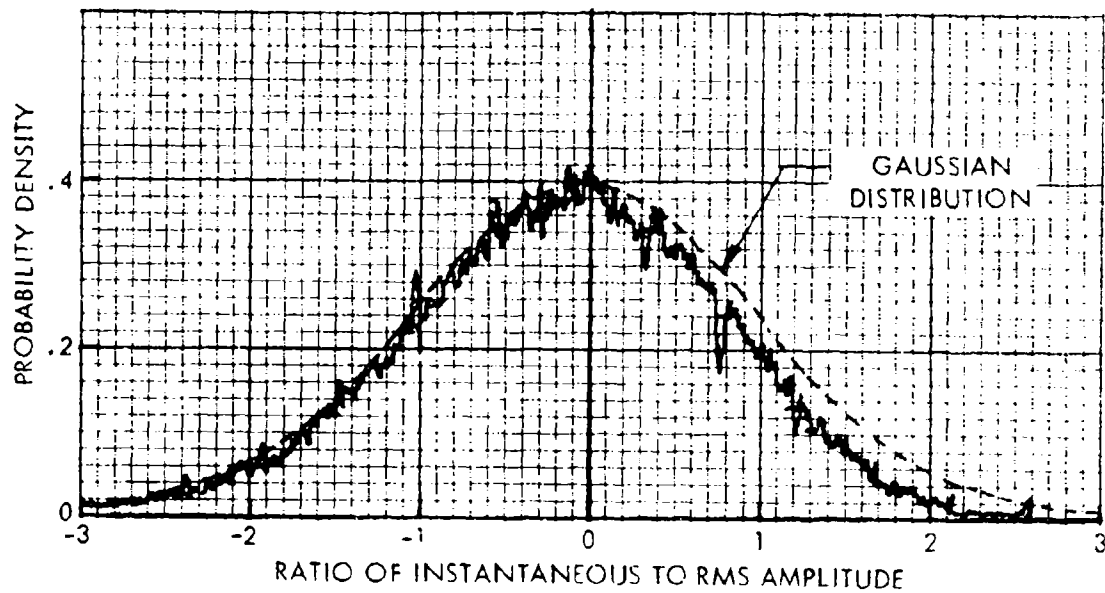
FIGURE 47. AMPLITUDE DISTRIBUTION OF STRAIN RESPONSE
SPECIMEN AL-4A (REF. FIGURE 41)
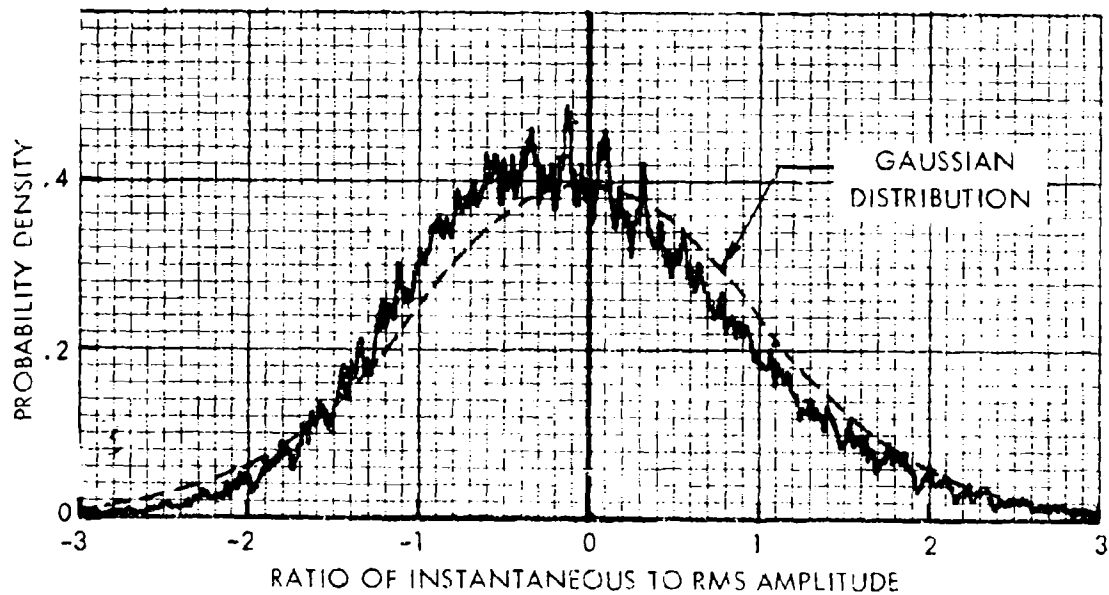
FIGURE 48. AMPLITUDE DISTRIBUTION OF STRAIN RESPONSE
SPECIMEN AL -4B (REF. FIGURE 42)
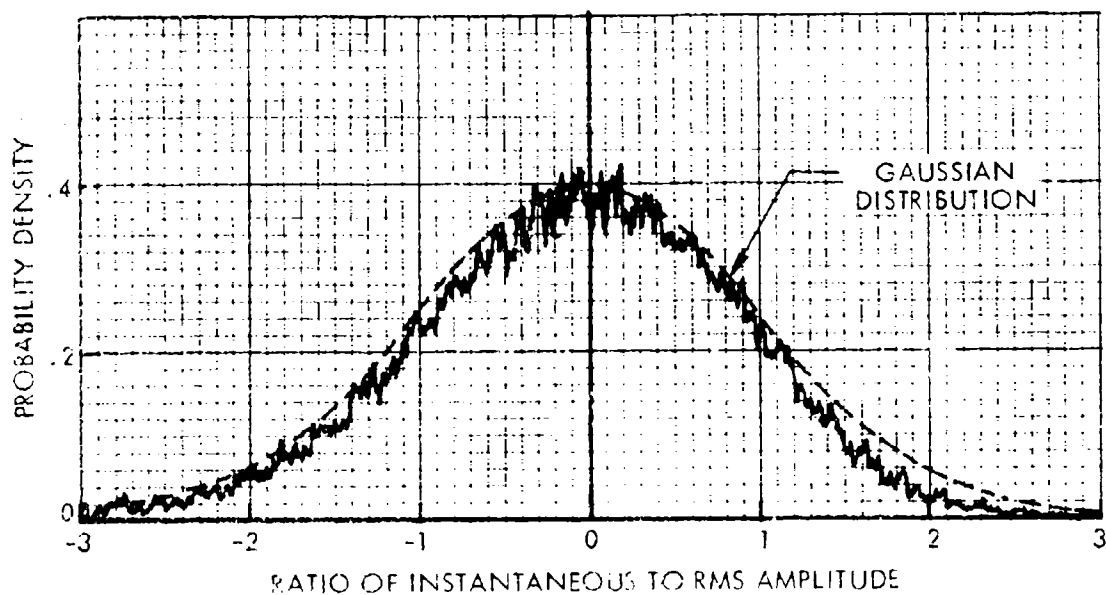
FIGURE 49. AMPLITUDE DISTRIBUTION OF STRAIN RESPONSE
SPECIMEN TI-3B (REF. FIGURE 43)
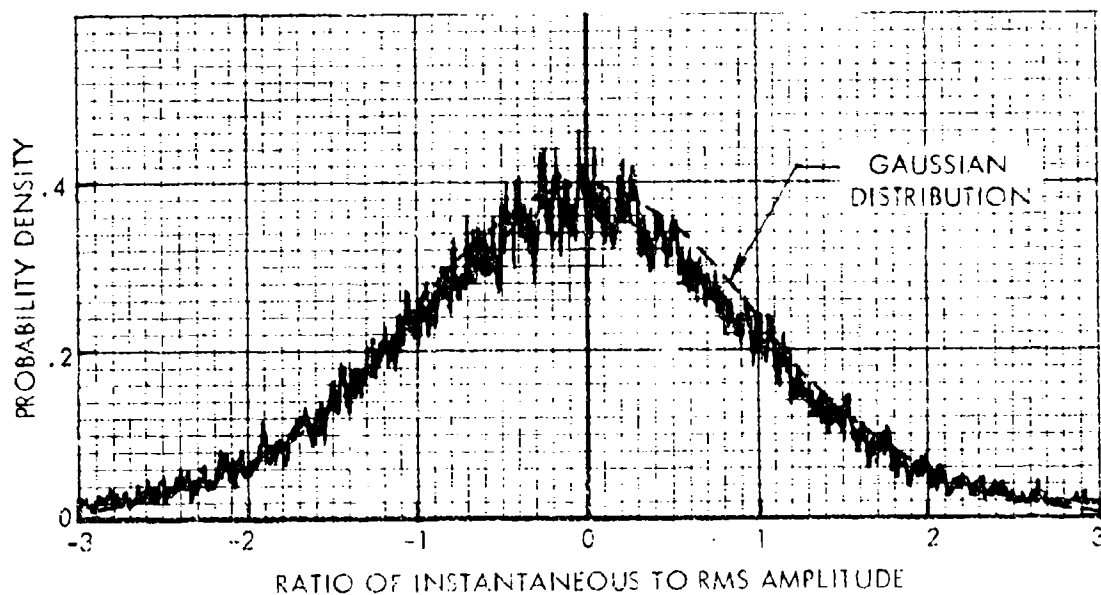
FIGURE 50. AMPLITUDE DISTRIBUTION OF STRAIN RESPONSE
SPECIMEN TI-10A (REF. FIGURE 44)

TABLE XI
ALUMINUM SPECIMENS
SUMMARY OF FATIGUE TEST RESULTS

Specimen No.	Test Temperature °F	Strain Thermal μin/in	Strain Dynamic μin/in rms	Spectrum Level dB	Response Frequency Hz	Life Cycles
AL-1A	300	2400	210	119	300	1.08×10^6
-1B	300	2400	150	122	270	4.68×10^6
-2A	300	2250	530	135	220	3.95×10^5
-2B	300	2250	390	131	490	1.32×10^6
-3A	RT	0	270	134	255	3.67×10^6
-3B	RT	0	300	131	275	4.46×10^6
-4A	300	2600	230	135	405	8.46×10^5
-4B	300	2600	220	135	428	1.16×10^6
-5A	300	2750	140	128	258	2.55×10^6
-5B	300	2750	90	126	280	3.30×10^6
-6A	RT	0	230	132	200	$2.36 \times 10^{7*}$
-6B	RT	0	230	130	132	1.01×10^7
-7A	300	2600	250	128	235	8.63×10^5
-7B	300	2600	380	130	110	4.03×10^5
-8A	300	2700	200	134	255	3.44×10^6
-8B	300	2700	120	132	250	2.70×10^6
-9A	300	2600	290	127	370	6.66×10^5
-9B	300	2600	200	127	345	9.32×10^5
-10A	RT	0	390	137	205	3.51×10^6
-10B	RT	0	400	132	215	2.40×10^6
-11A	300	2600	140	133	295	7.12×10^5
-11B	300	2600	140	131	280	9.27×10^5
-12A	RT	0	350	132	135	3.53×10^6
-12B	RT	0	310	134	135	5.70×10^6
-13A	300	2600	100	102	185	1.78×10^6
-13B	300	2200	360	122	220	1.21×10^6
-14A	150	750	370	123	325	9.71×10^5

*No skin failure.

NOTE: Fatigue life (in cycles) is the product of response frequency and test time to failure.

76

TABLE XII
TITANIUM SPECIMENS
SUMMARY OF FATIGUE TEST RESULTS

Specimen No.	Test Temperature °F	Strain		Spectrum Level dB	Response Frequency Hz	Life Cycles
		Thermal μin/in	Dynamic μin$_{rms}$			
TI-1A	400	1750	190	134	355	4.48×10^6
-2A	RT	0	600	137	290	2.14×10^6
-2B	RT	0	465	139	270	1.29×10^6
-3A	600	2500	160	135	255	2.52×10^6
-3B	600	2500	180	134	260	2.57×10^6
-4A	400	1600	270	129	440	1.58×10^6
-4B	400	1600	230	128	460	2.07×10^6
-5A	400	1000	200	126	390	3.18×10^6
-5B	400	1000	260	113	495	6.71×10^6
-6A	RT	0	180	133	200	$1.76 \times 10^{7*}$
-6B	RT	0	230	132	195	$1.69 \times 10^{7*}$
-7A	400	2000	80	129	440	1.11×10^7
-7B	400	1150	130	127	460	2.16×10^7
-8A	600	2900	100	136	400	2.16×10^6
-8B	600	2900	60	130	500	3.60×10^6
-9A	400	1000	340	135	180	1.94×10^6
-9B	400	1550	340	134	180	4.21×10^6
-10A	400	1600	190	136	225	7.92×10^6
-10B	400	1600	200	140	200	1.01×10^7
-11A	400	1680	260	137	230	1.05×10^7
-11B	400	1680	230	136	300	1.17×10^7

* No skin failure.

NOTE: Fatigue life (in cycles) is the product of response frequency and test time to failure.
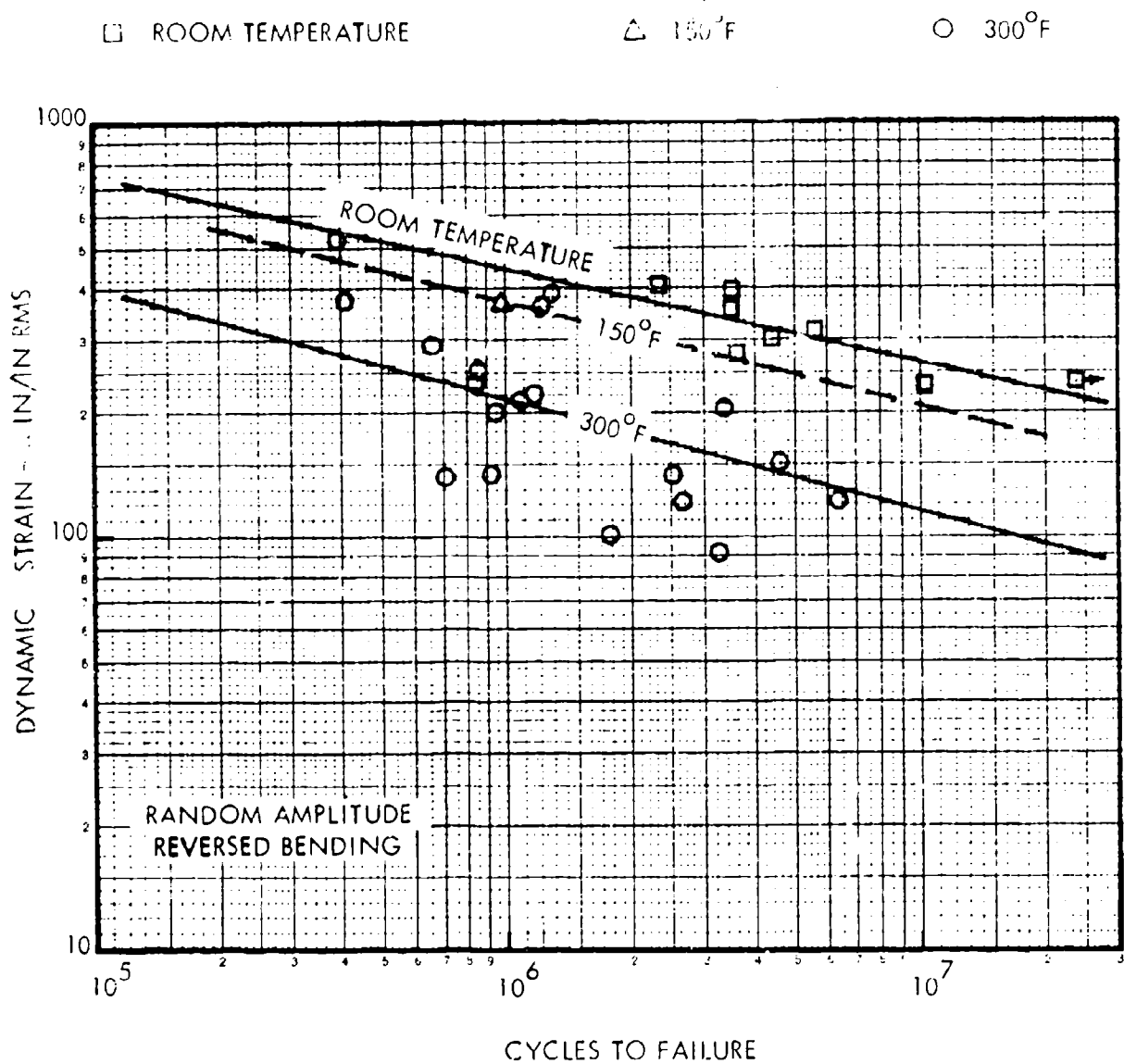
FIGURE 51. FATIGUE TEST DATA
ALUMINUM SPECIMENS

78
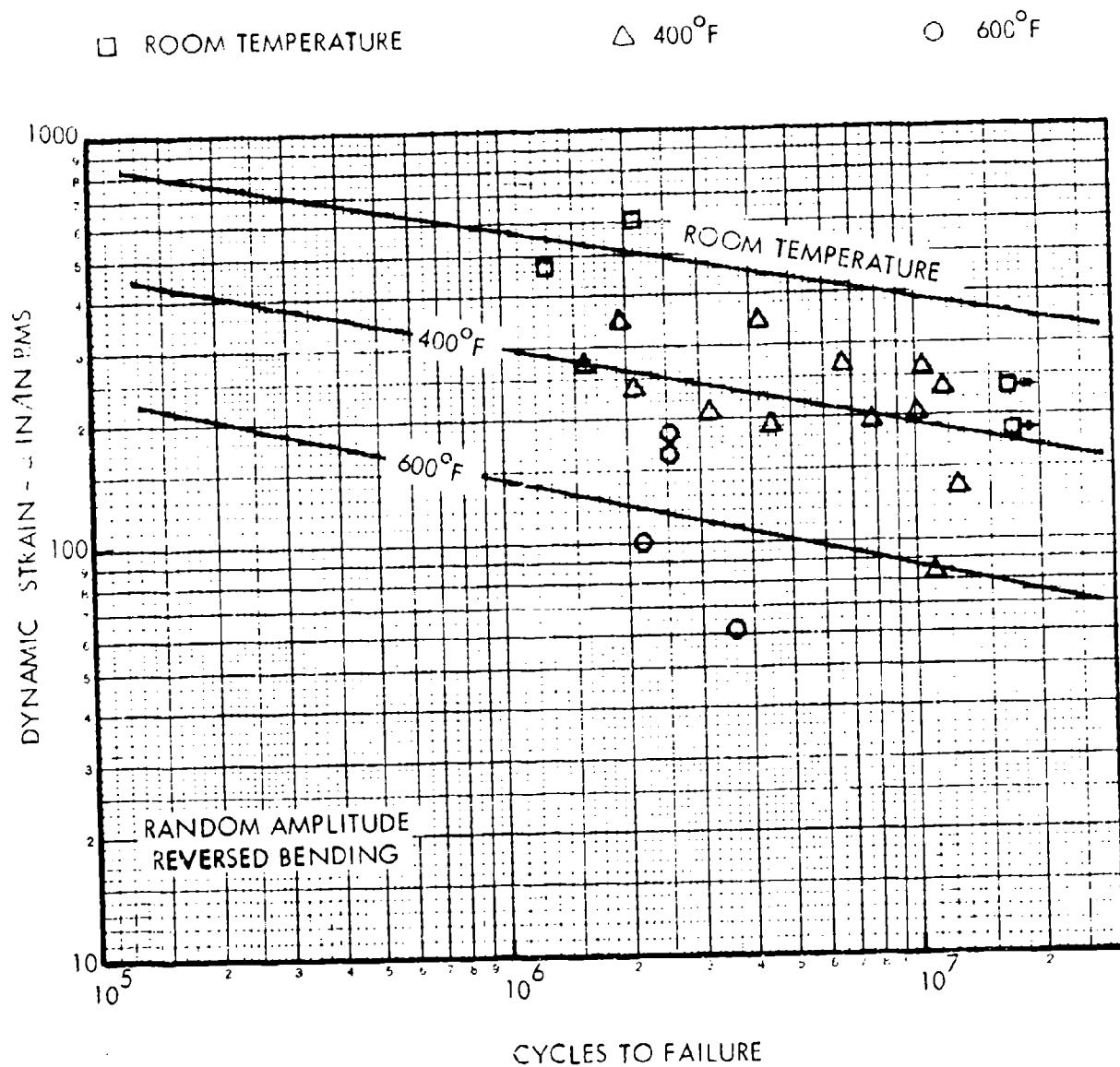
FIGURE 52. FATIGUE TEST DATA
TITANIUM SPECIMENS

79

TABLE XIII
SUMMARY OF STATISTICAL PROPERTIES
FOR STIFFENED PANEL FATIGUE DATA

Alloy	Test Temperature OF	No. Data Points	σ_c Standard Deviation	R_c Correlation Coefficient
Aluminum	RT	8	0.056	-0.833
Aluminum	150	1	-	-
Aluminum	300	18	0.165	-0.673
Titanium	RT	4	0.111	-0.931
Titanium	400	13	0.146	-0.564
Titanium	600	4	0.209	-0.622

TABLE XIV
STIFFENED PANEL FAILURE DISTRIBUTION

Test Condition	Alloy	Stiffener Rivet Row % of Total Failures	Frame Rivet Row % of Total Failures
Room Temperature:	Aluminum	100	0
	Titanium	100	0
Elevated Temperature:	Aluminum	21	79
	Titanium	77	23

Figures 53 and 54 show some of the failures obtained for each of these locations on the aluminum and titanium specimens. The room temperature failures were, in all cases, identical to those obtained on previous test programs[4, 8] in that failure occurred at the location of highest dynamic stress (i.e. at the midpoint of the long side of the panel bay).

It is not clear what caused the failures during the elevated temperature tests to occur at the frame rivet row, on the short side of the panel, because of the difference of the failure distribution between the aluminum and titanium panels. It is apparent from the measured thermal strains that the highest thermal strains occur at the short side of the panel, whereas the highest dynamic strains occur at the midpoint of the long side (for a fundamental mode response). The combination of thermal and dynamic strains at the midpoint of the short side may, in some cases, prove more damaging than those at the other side. The frame rivet row failures may in some cases be attributed to dynamic response in a higher order mode, most probably the (1,2) mode. It was not possible to visually observe the specimen response during the elevated temperature tests because of the close proximity of the lamp fixture to the skin surface.

Regardless of the failure location, the desired end product (a fatigue curve at the various test temperatures) is achievable by using only the dynamic strain component at the failure location. These curves were discussed previously and shown in Figures 51 and 52.

Three other types of failure were observed during these tests: rivet failure, skin failures in the outer bays, and substructure failures. All of these occurred predominately in the titanium specimens, with only two rivet failures, two outer bay skin failures, and three substructure failures noted during the aluminum panel tests.

The rivet failures generally were evidenced as fatigue of the rivet heads at the beginning of the countersink taper. Only one rivet failure, prior to skin failure, was experienced during the aluminum panel test program. This occurred in the 0.063 skin AL-8A specimen at the stiffener-to-frame intersection. The rivets on the stiffener-to-frame clip of Specimen AL-5B failed at approximately the same time that a skin crack occurred over the frame.

Fifteen of the titanium panels experienced rivet failures. The rivet failures occurred as fatigue of the heads, identical to that described for the aluminum specimens, and as deformation of the rivet heads. This deformation, shown in Figure 55, was extreme enough in some instances to allow the rivet head to pass through the hole in the skin. These failures were usually randomly scattered over the surface of the panel. In a few instances, the rivet failures occurred in adjoining rivets, allowing the skin to work loose from the substructure; however, this occurred after the initial skin failure in the center bay on all specimens but TI-11A and B. These specimens, with the thickest skins (0.056), proved stronger than the rivets and substructure. (The rivets and rivet spacing remained constant for all specimens). It was concluded that the rivet size and substructure thickness should have been increased in this case.

81
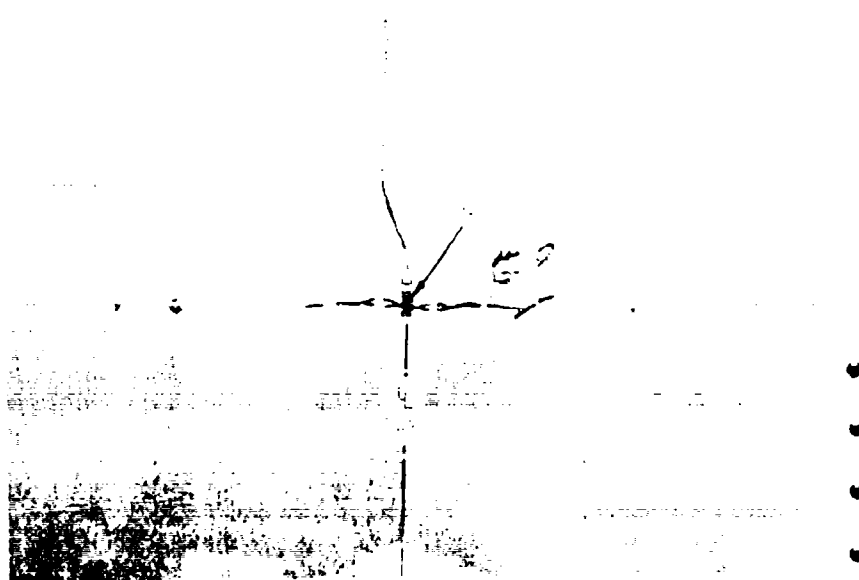
FRAME RIVET ROW — SPECIMEN AL-5A
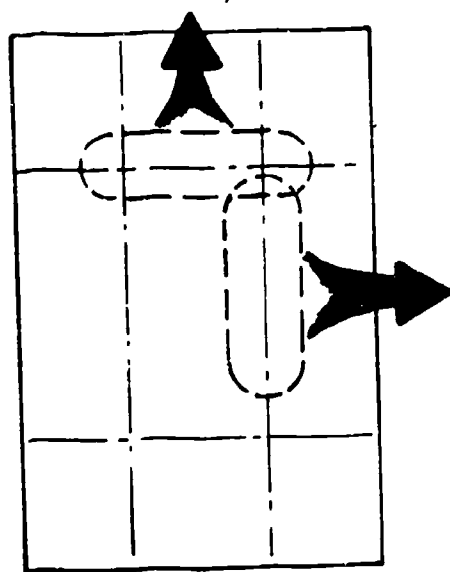
PLAN VIEW OF SPECIMEN
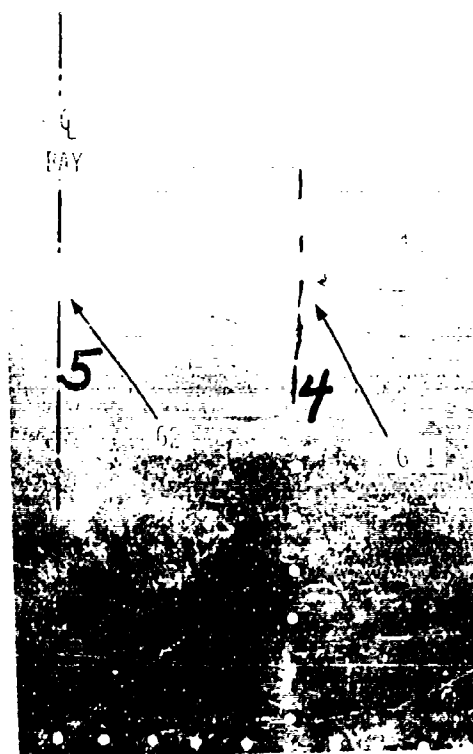
STIFFENER RIVET ROW
SPECIMEN AL-12A

FIGURE 53. TYPICAL SKIN FAILURES
ALUMINUM SPECIMENS
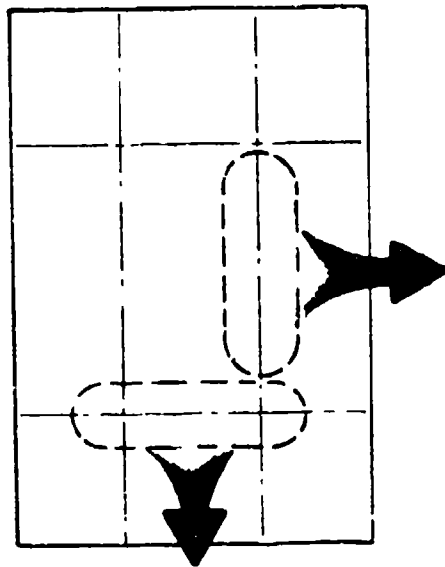
PLAN VIEW OF SPECIMEN
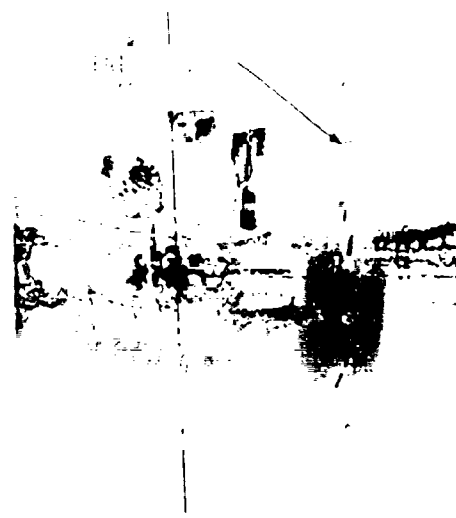
STIFFENER RIVET ROW
SPECIMEN TI-4A
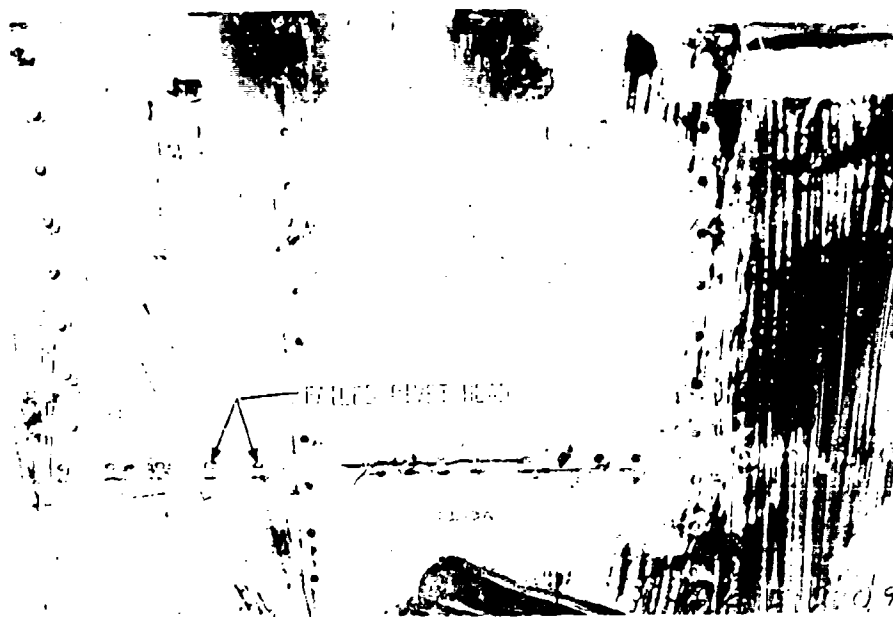
FRAME RIVET ROW - SPECIMEN TI-9A

FIGURE 54. TYPICAL SKIN FAILURES
TITANIUM SPECIMENS

83

EDGE OF RIVET
HEAD CRACKED
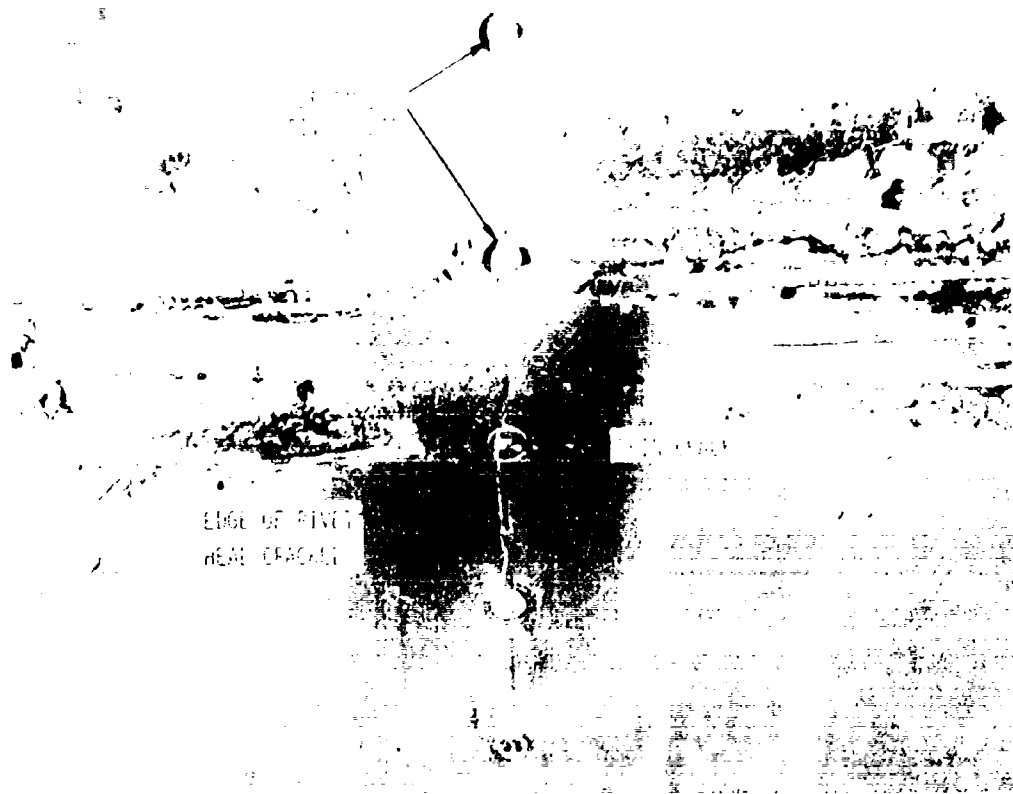
FIGURE 55. TYPICAL RIVET FAILURES
TITANIUM SPECIMENS

84

The only aluminum specimens to incur cracks in the outer bay skins were AL-5A and B.
These failures were judged to be small enough and sufficiently far removed from the
initial outer bay crack so as to have negligible effect on the center bay response and
thermal strain. Approximately 50% of the titanium specimens experienced skin cracks
in the outer bay skins prior to or concurrent with the center bay skin cracks. In all
cases, these were either sufficiently far removed from the center bay (i.e., at the end
rivet on a frame) or small enough that their presence did not significantly affect the
center bay response.

f.   Effect of Sealant on Fatigue - As mentioned previously, eight of the aluminum
specimens, of two different designs, were fabricated using faying surface sealant at all
joints where metal-to-metal contact occurred. These specimens were identical in all
respects, except for the sealant, to eight of the other specimens, as identified in
Table XV.

TABLE XV
SPECIMEN DESIGNATION FOR SEALANT EVALUATION

| Specimen Size | Test Temperature | Specimen Identification | |
		Without Sealant	With Sealant
6 x 12 x 0.032	RT	AL-3	AL-10
6 x 12 x 0.032	300°F	AL-4	AL-11
9 x 18 x 0.040	RT	AL-6	AL-12
9 x 18 x 0.040	300°F	AL-7	AL-13

The measured dynamic data for these specimens formed the basis for comparison
of the effects of sealant on response and life. Room temperature fundamental mode fre-
quencies and damping ratios were tabulated in Table VII for these specimens.

A comparison of both of these parameters, individually, shows that any effect that the
sealant has is lost in the scatter in the data. Figure 56, which shows the damping
ratios plotted versus the fundamental frequency, clearly shows that faying surface sealant
produces no discernable difference on the dynamic response. A further evaluation of the
fatigue data of Table XI and Figure 51 reinforced this conclusion. The results of both
designs are intermingled in the scatter band of the data.

Since faying surface sealant has no net effect on dynamic response or fatigue life for
the type of structures considered, it can be concluded that the design criteria generated
on previous programs, without sealant, are valid for structures where sealant is used. (This
includes most of the secondary structure on current generation aircraft.)
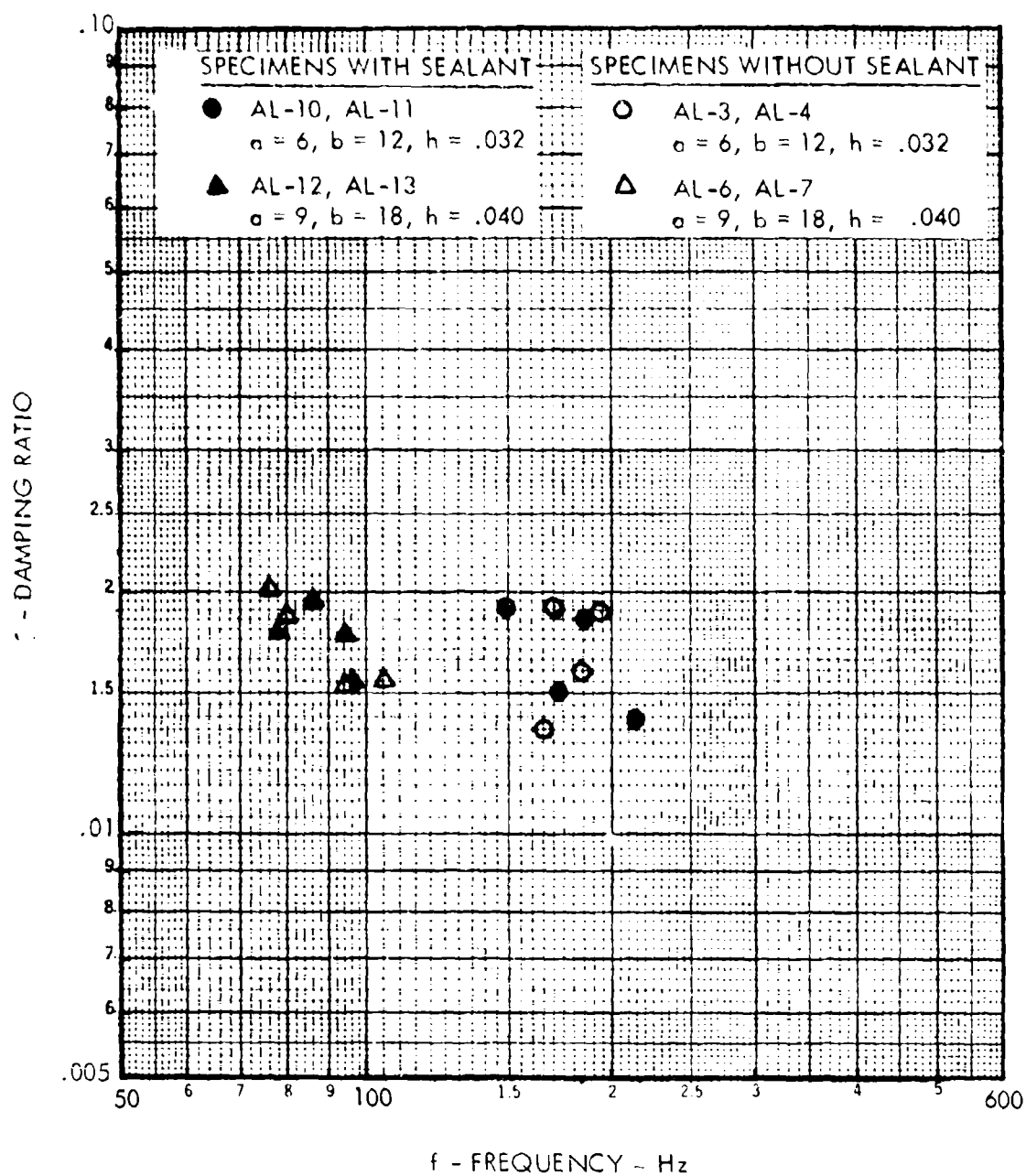
FIGURE 56. EFFECT OF SEALANT ON DYNAMIC RESPONSE

86

IV – CORRELATION OF ANALYTICAL AND EXPERIMENTAL RESULTS

The principal objective of this program was the establishment of empirical design criteria for aircraft structures subjected to combined acoustic and thermal environments. The analytical development provided the interrelation among the applicable parameters, while the experimental program provided measured values of the individual parameters. Correlation of these data then can provide the necessary empirical constants, or factors, for derivation of the design methods.

The derivation of empirical parameters follows the sequence in which each parameter is required in the thermal and dynamic stress relations, respectively. Generally, the measured data were plotted versus calculated values (using the results of the simple panel analysis), and a least squares linear regression analysis was performed to determine empirical constants. The least squares regression analysis follows the method of Reference 4, Appendix II. In some instances an exponential regression analysis was performed to determine whether exponential factors should be considered; however, in each case the linear relationship was judged to provide the best correlation. Most of the correlation plots exhibited an off-set in the y-intercept (measured data axis), because of non-linearities and other variations in the measured data. In all instances this off-set was judged to be small, in relation to the variance in the data, so that the final equation could be established by the approximate relation

$$(\ )_e = \bar{m}(\ )_c$$

where $()_e$ = empirical value

$()_c$ = calculated value, from analytical results

$\bar{m}$ = slope of approximate regression line through the origin and the data centroid $(\bar{x}, \bar{y})$.

The nine-bay analysis results were also correlated with the test data to establish empirical relations for use in a digital computer program. This correlation effort is described in Appendix IV.

A. Thermal Stress

As the thermal stress is dependent on the skin buckling temperature and buckling amplitude, these parameters must be established first.

1. Skin Buckling Temperature

Skin critical buckling temperatures were listed in Table X and were found to be consistently higher than the values calculated from the analysis by Equation (5a). The correlation plot of the buckling temperature, Figure 57, shows that considerable scatter was present in the measured data, as evidenced by a correlation coefficient, R_c, of 0.718. (Note that the correlation coefficient between two variables is zero when no correlation exists, and

87
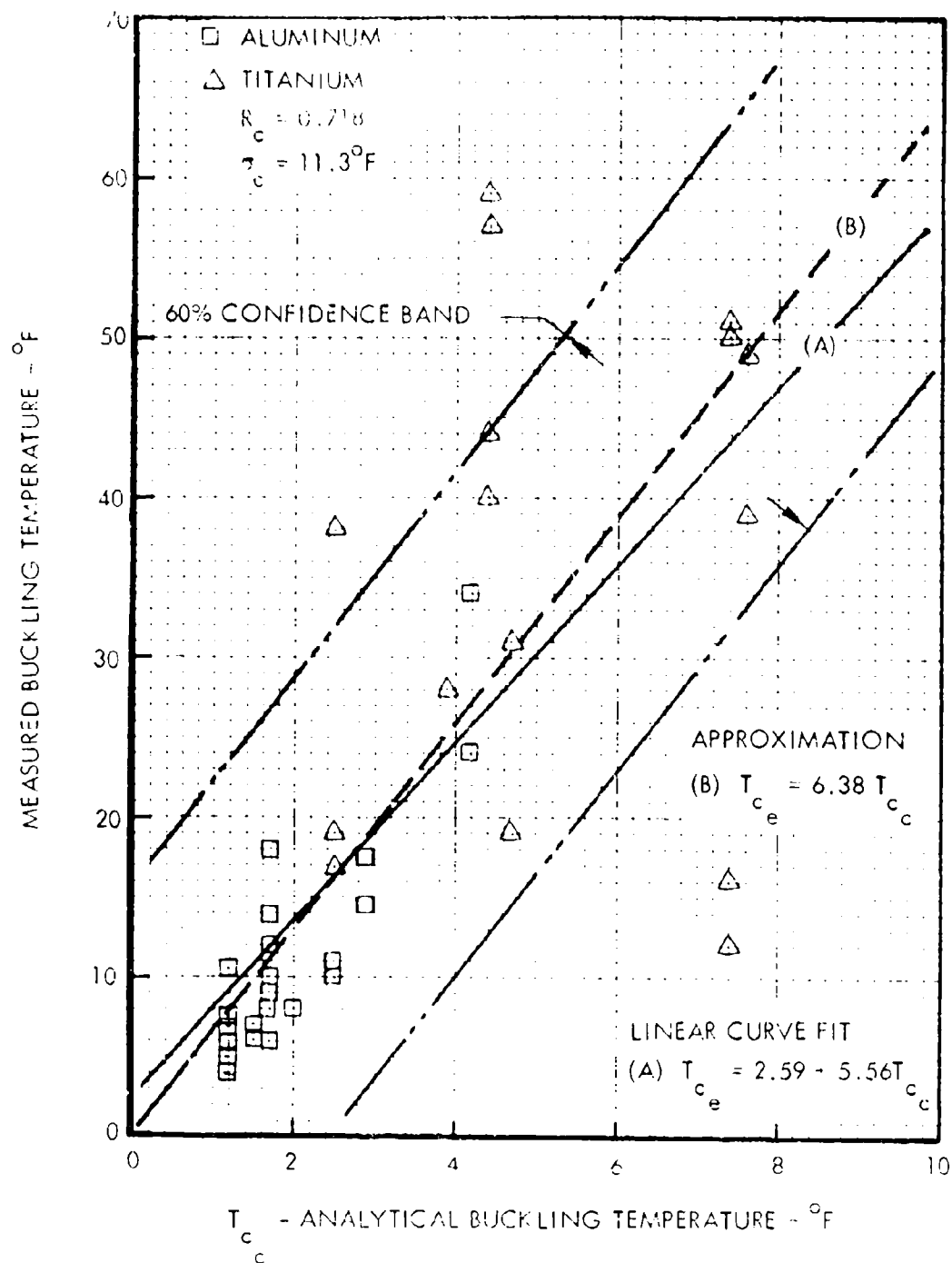
FIGURE 57. BUCKLING TEMPERATURE CORRELATION

88

unity when their relationship can be represented exactly by a straight line.) Repeated measurements on the same specimen revealed that the critical buckling temperature could vary significantly, depending on the heating rate and the temperature differential between the skin and substructure. Pre-stresses introduced during specimen fabrication (i.e., misalignment of frames and stiffeners, and other factors) also influence the buckling temperature.

The equation of the regression line, (A), through the data points of Figure 57 has a 2.59°F off-set on the measured buckling temperature axis. A line, (B), plotted through the origin and the centroid $(\bar{x}, \bar{y})$ of the data set is also shown on the figure. Comparison of the two equations shows very little difference in the results, particularily in view of the scatter present in the data. Hence, the simpler approximation, Equation (B), was selected to represent the correlation between measured and analytical values, which results in the following empirical relation for multi-bay structures:

$$T_{c_e} = \frac{5.25\, h^2\, F_{11}}{a\, ab(1 + v)} \tag{60}$$

where T_{c_e} is the temperature increment above ambient. The temperature ratio, r, remains identical to the analytical definition, or

$$r = T/T_{c_e}$$

It should again be pointed out that the skin temperature, T, is the temperature increase above ambient.

2. Buckling Amplitude

The panel skin buckling amplitude, W_o, is related to the critical buckling temperature by Equation (22). For a specific configuration, the buckling amplitude varies directly with the square root of the temperature increase, T. Therefore, the measured temperature increase, corresponding to a measured buckling amplitude, was used to compute analytical buckling amplitudes by Equation (22).

Because of the multitude of data points (temperature-displacement data at approximately 25°F increments for each elevated temperature specimen to the maximum test temperature), a digital computer program was written to accomplish the individual computations. The empirical buckling temperature relation, (60), was used instead of the measured buckling temperatures to minimize the effects of cumulative errors. The specimen dimensions and temperature-displacement data were entered into the program individually for each specimen and then grouped into equal aspect ratios. The data were then plotted on a digital plotter in one of the following forms:

o   Measured versus calculated displacement ratio

o   Displacement ratio versus temperature ratio.

89

The first of these plot formats is illustrated in Figures 58 through 60 for aspect ratios of 1.5, 2 and 3, respectively. As on the buckling temperature correlation plot, two lines are shown on each figure. The first, line (A), represents the least squares regression line while line (B) represents the zero-origin approximation. Because of the slight difference, the approximate regression line was used in all cases. The slopes of these lines are tabulated in Table XVI to illustrate the variation in slope with aspect ratio.

TABLE XVI

SLOPE OF BUCKLING AMPLITUDE CORRELATION PLOTS

ASPECT RATIO		SLOPE
b/a	F_{11}	
1.5	2.17	2.167
2.0	2.50	2.571
3.0	3.33	3.046

A simple average of these slopes, when used to derive an empirical relation, yields empirical displacements higher than measured for aspect ratios less than 2, while the reverse is true for aspect ratios greater than 2. The effect of aspect ratio on the slope is shown in Figure 61. Variation of the power of F_{11} resulted in the conclusion that an additional power of 0.75 provided the minimum error in the slopes for each of the aspect ratios. This gives an empirical buckling amplitude relation of

$$W_{o_e} = 2.50 hF_{11}^{1.75} \left[(r-1)/R \right]^{1/2} \tag{61}$$

where R remains as defined in Equation (19a). This equation shows a greater dependency on aspect ratio than that indicated by the analytical equation. This additional dependence on aspect ratio results in a reversal of the trends given by the analysis and shown in Figure 3. The effect of this aspect ratio correction will be more clearly defined in the later Design Method Section.

The measured displacement data were plotted versus temperature ratio as shown in Figures 62 through 64 for the three aspect ratios. The empirical equation is also shown for each aspect ratio, and illustrates the agreement between the empirical trend and the data with varying aspect ratio. Since most of the test specimens had an aspect ratio of 2, the corresponding displacement plot of Figure 63 shows the magnitude of scatter that can be expected in any given set of buckling amplitude measurements. To quantify the variance, all data were plotted in the correlation plot of Figure 65, using Equation (61). The correlation coefficient and standard deviation from the mean are indicated in the figure, as are the limits of the 60% confidence bands. Hence, for any given displacement estimate, the maximum error expected, for a confidence level of 60%, should be less than ± 0.59 times the skin thickness.
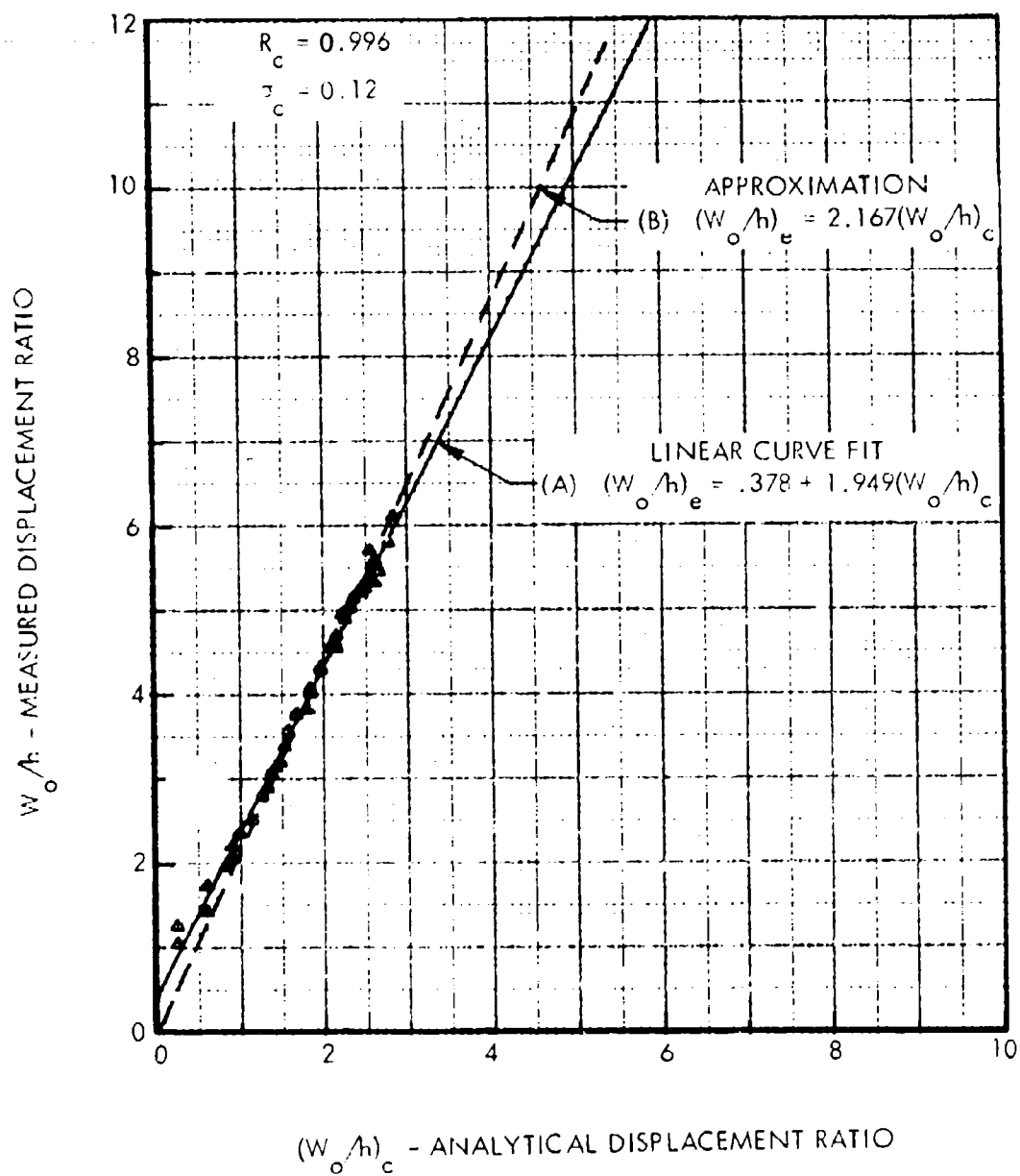
FIGURE 58. BUCKLING AMPLITUDE CORRELATION
ASPECT RATIO = 1.5

91
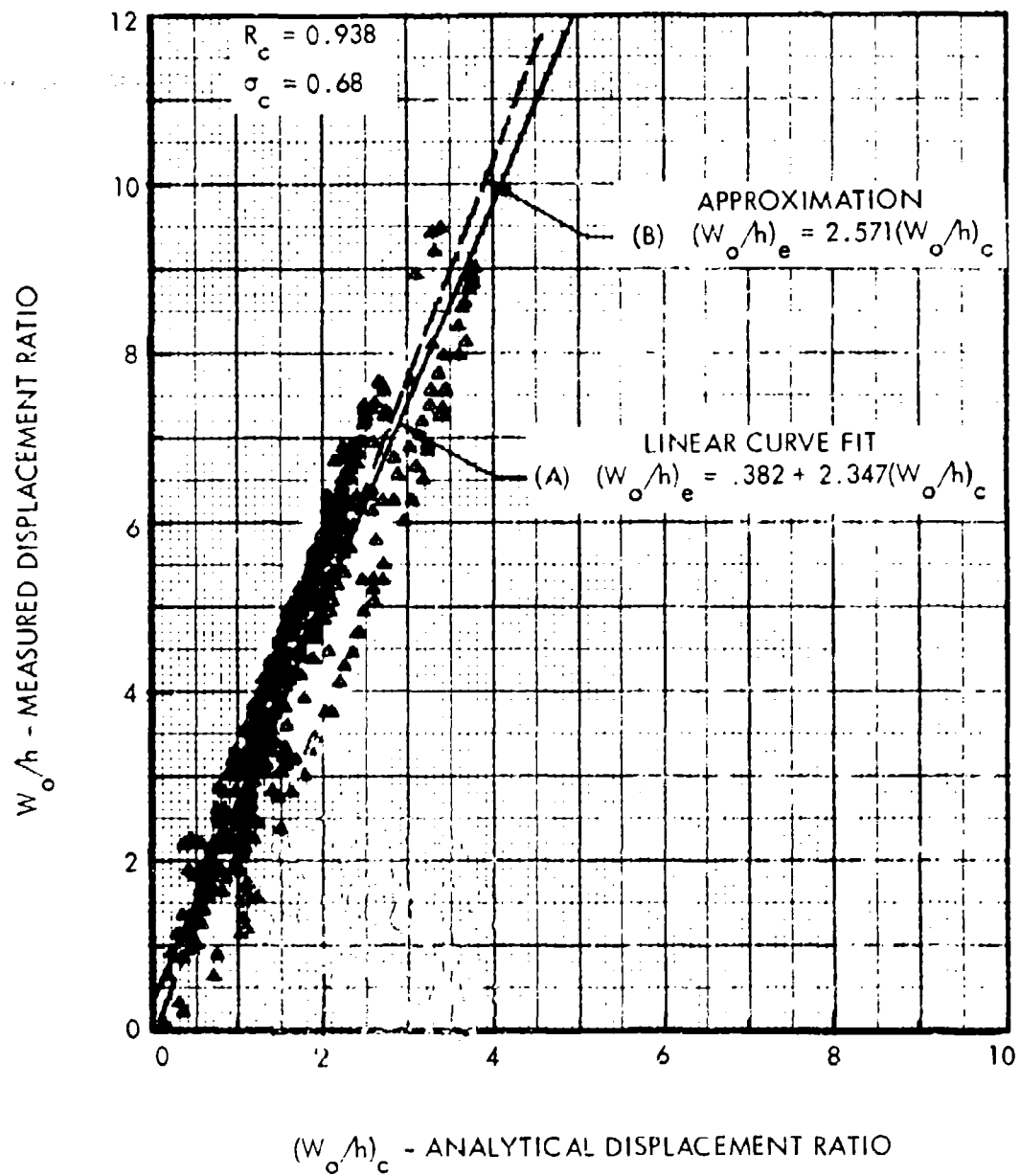
FIGURE 59. BUCKLING AMPLITUDE CORRELATION
ASPECT RATIO = 2
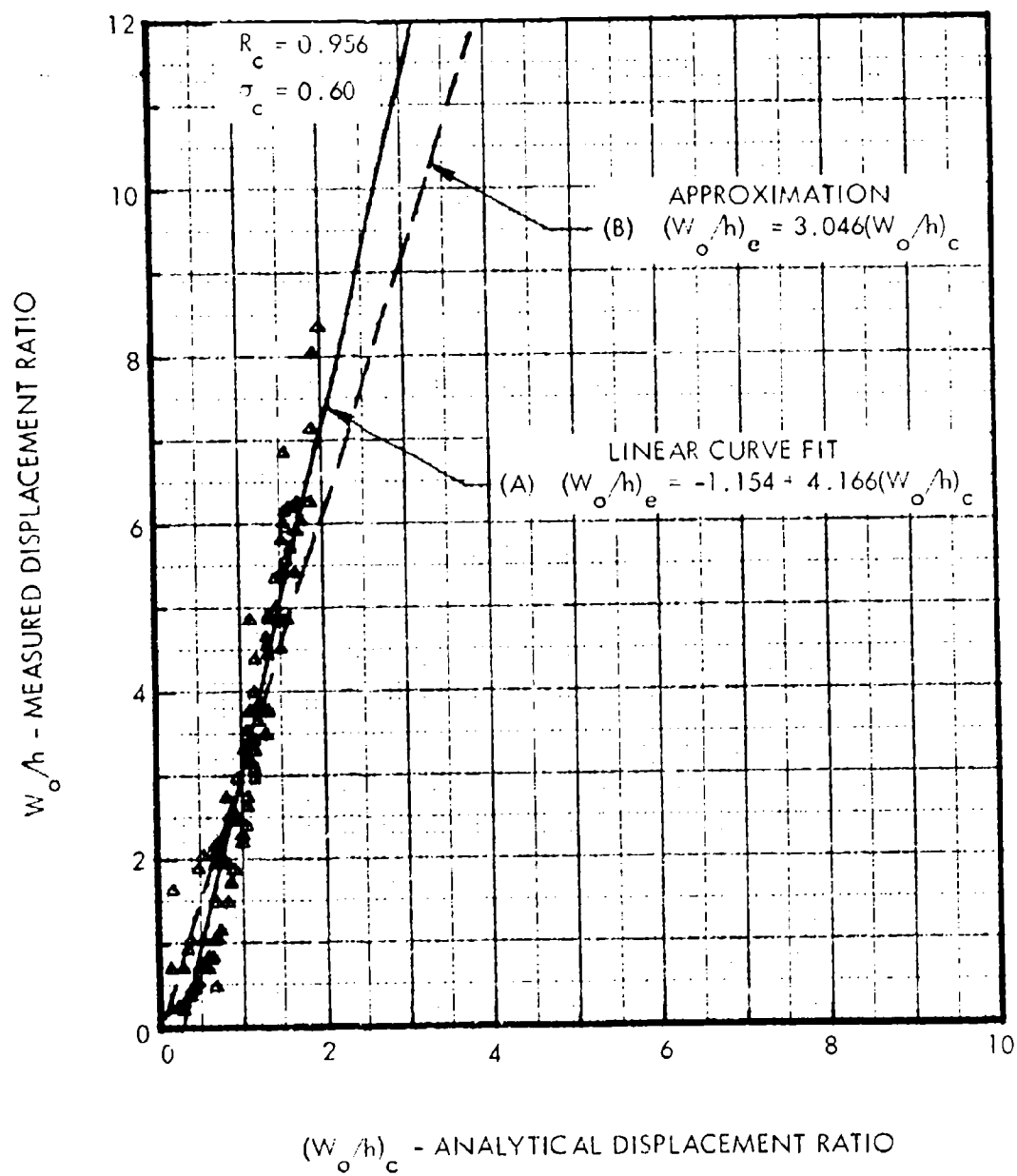
FIGURE 60. BUCKLING AMPLITUDE CORRELATION
ASPECT RATIO = 3

93

The vertical axis is labeled "m̃ – SLOPE OF APROXIMATE REGRESSION LINE" with values 0, 1, 2, 3, 4.

The horizontal axis is labeled F_{11} – ASPECT RATIO with values 0, 1, 2, 3, 4, 5.

$$\tilde{m} = 1.248 \, F_{11}^{.75}$$
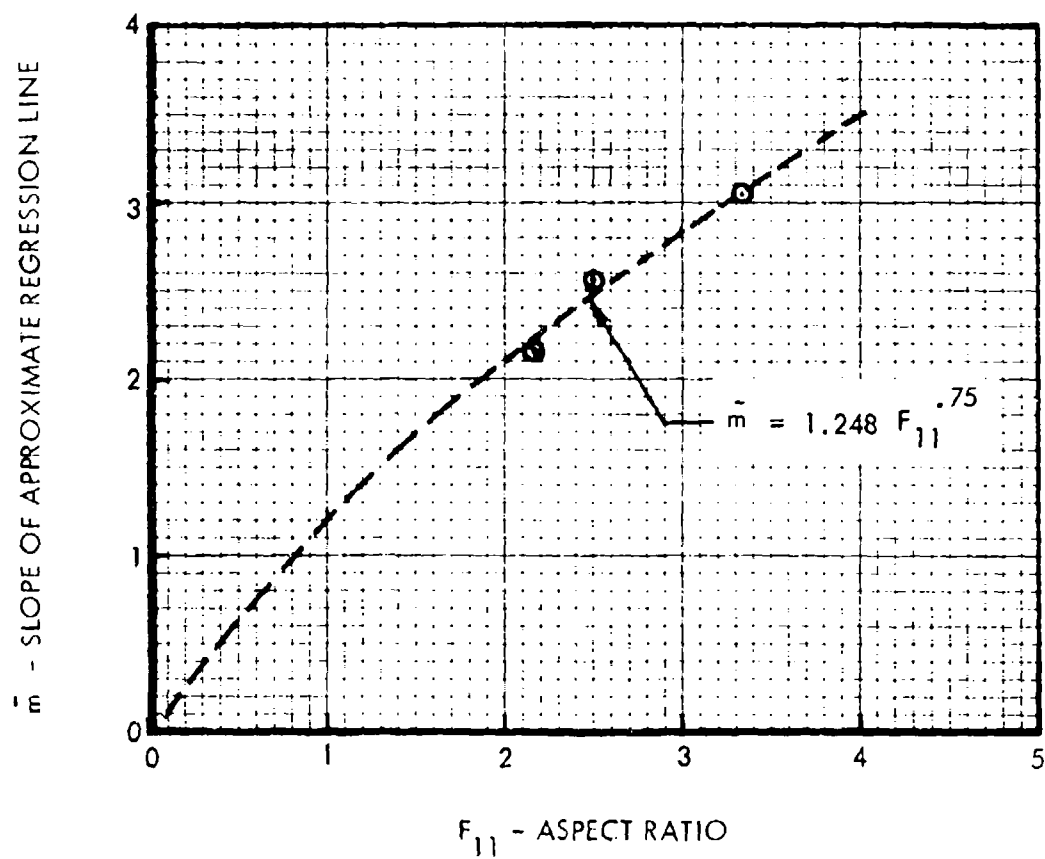
FIGURE 61. EFFECT OF ASPECT RATIO ON REGRESSION LINE SLOPE

94
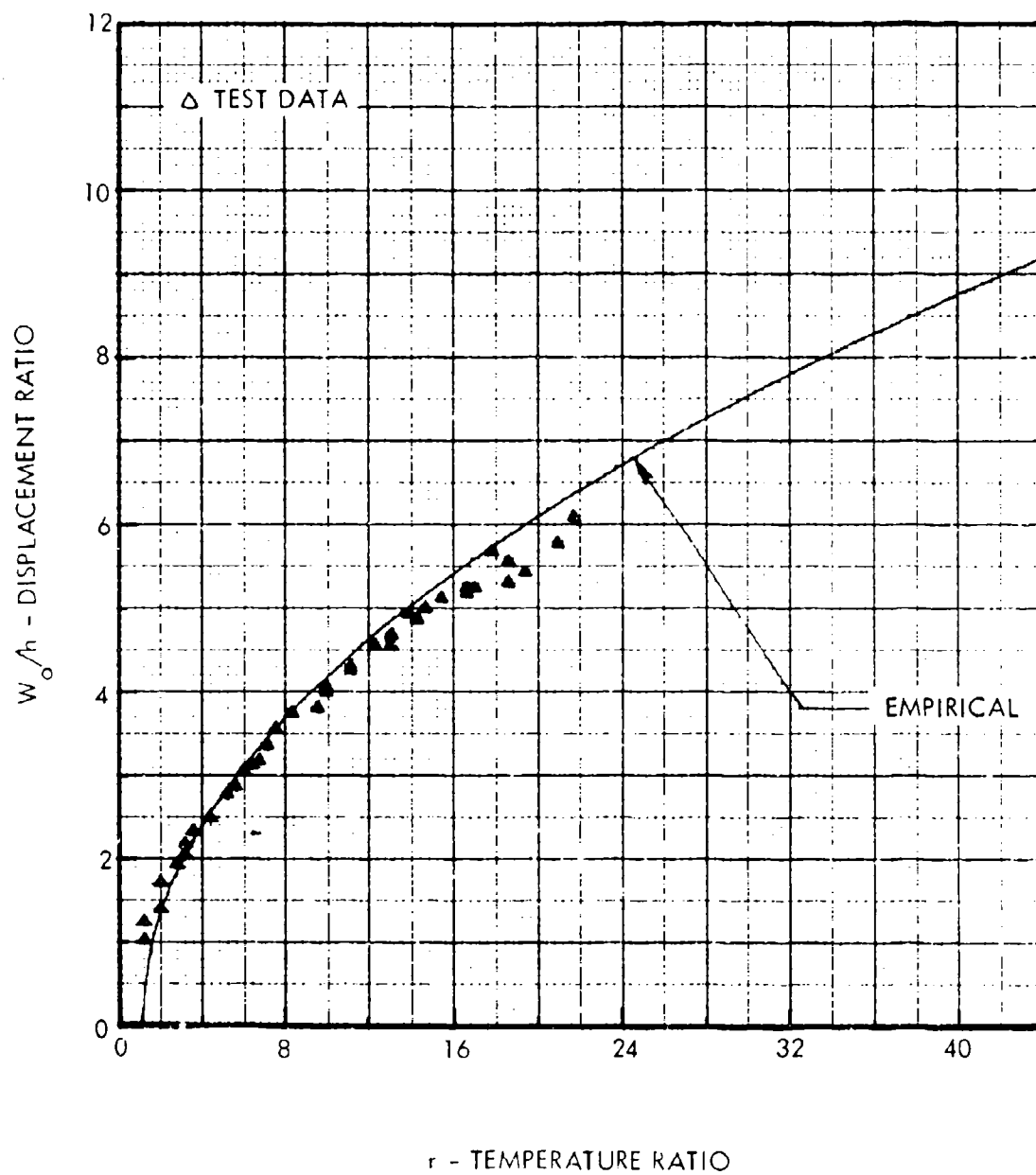
FIGURE 62. COMPARISON OF MEASURED AND EMPIRICAL BUCKLING AMPLITUDE
ASPECT RATIO = 1.5
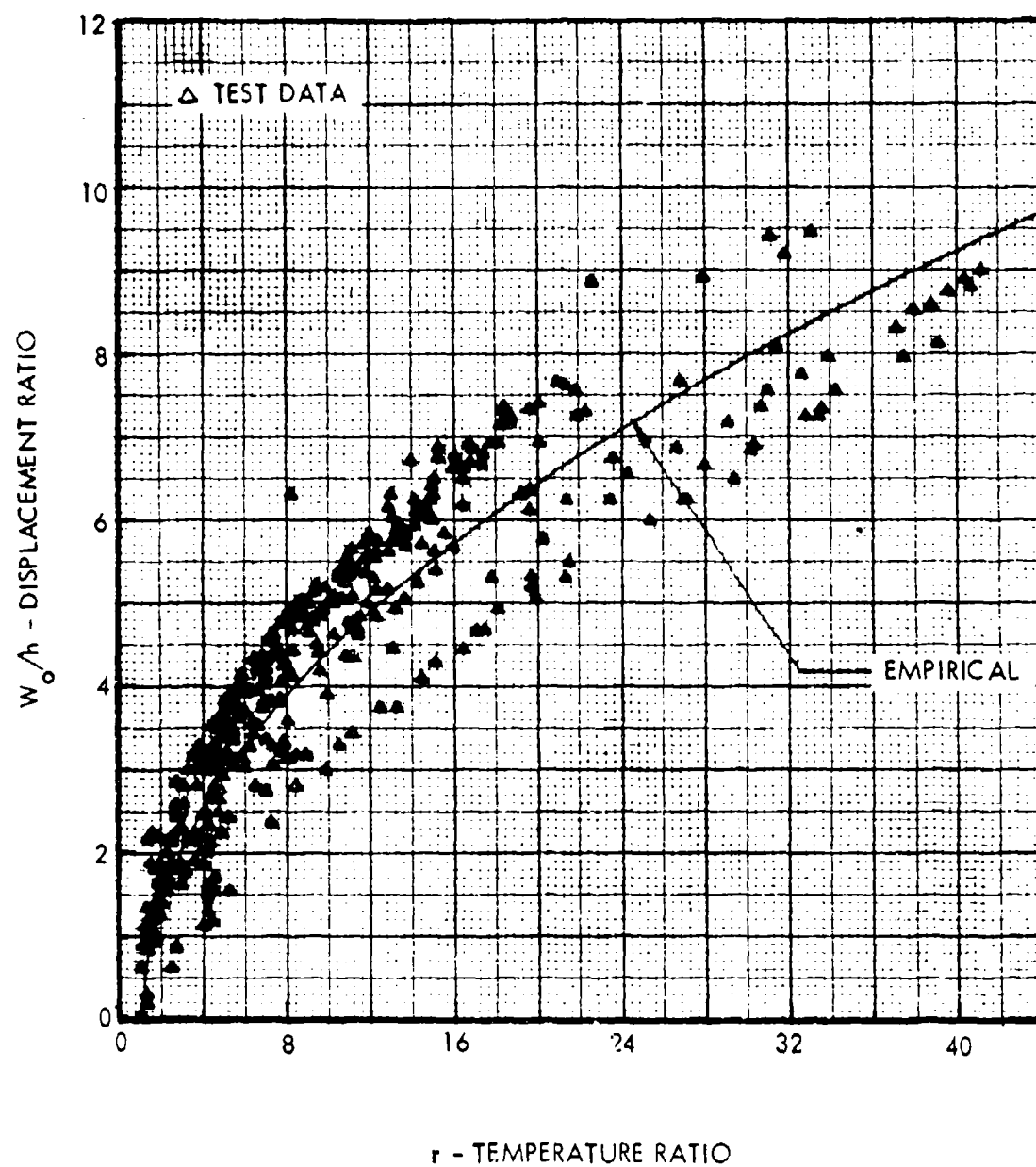
FIGURE 63. COMPARISON OF MEASURED AND EMPIRICAL BUCKLING AMPLITUDE
ASPECT RATIO = 2
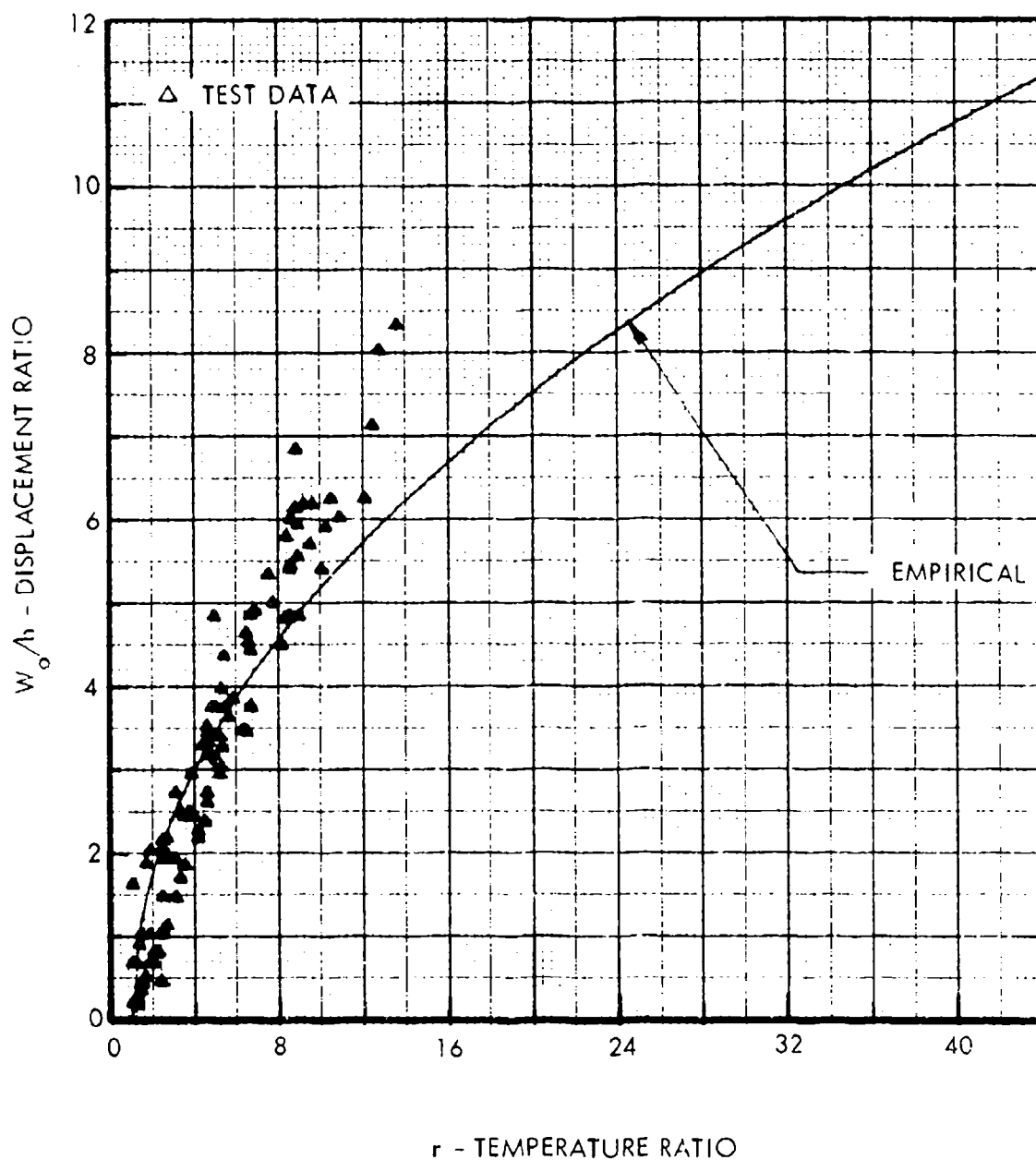
FIGURE 64. COMPARISON OF MEASURED AND EMPIRICAL BUCKLING AMPLITUDE
ASPECT RATIO = 3

97
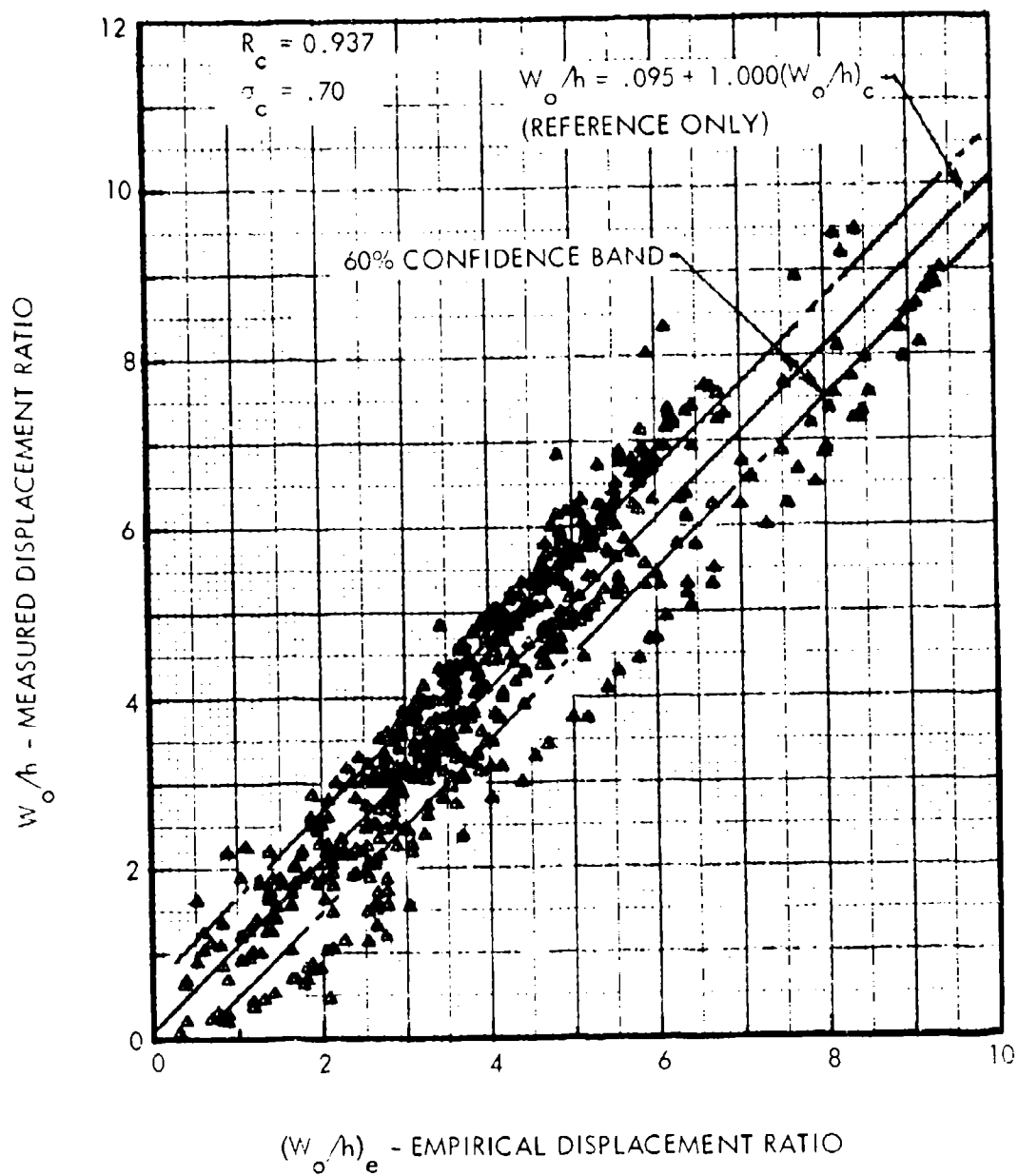
FIGURE 65. BUCKLING AMPLITUDE CORRELATION
ALL ASPECT RATIOS

3. Thermal Strain

Thermal strains were measured during the test program on each of the elevated temperature specimens at increasing temperature increments of approximately 25°F. The buckling amplitude computer program was adapted to accept the thermal strain input and compute analytical strains, as well as to plot the data. The analytical stresses at the midpoints of the sides were converted to strains for direct comparison with the measured data and to simplify the computation, since the elastic modulus is temperature-dependent.

The analytical buckled panel strain is thus given by:

$$\epsilon_x(x, b/2) = -\left[\frac{\alpha T}{1-\nu}\right] + \frac{\pi^2 W_o^2}{8ab(1-\nu^2)}\left[\frac{b}{a}(2-\nu^2) + \nu\frac{a}{b}\right] \tag{62a}$$

$$\epsilon_y(a/2, y) = -\left[\frac{\alpha T}{1-\nu}\right] + \frac{\pi^2 W_o^2}{8ab(1-\nu^2)}\left[\frac{a}{b}(2-\nu^2) + \nu\frac{b}{a}\right] \tag{62b}$$

The first component of these stresses is the expansion strain $\alpha T/(1-\nu)$, which is linear and applies for all values of r. It was, therefore, advantageous to delete this strain component from both the analytical value and the measured strains. This was accomplished by reducing the magnitude of the measured strains by the value of the expansion strain at the temperature for which the data were taken. The remaining strain components, due only to the panel buckling, were correlated directly against one of the following calculated strains due to buckling:

$$\epsilon_{x_c} = \frac{\pi^2 W_o^2}{8ab(1-\nu^2)}\left[\frac{b}{a}(2-\nu^2) + \nu\frac{a}{b}\right] \tag{63a}$$

$$\epsilon_{y_c} = \frac{\pi^2 W_o^2}{8ab(1-\nu^2)}\left[\frac{a}{b}(2-\nu^2) + \nu\frac{b}{a}\right] \tag{63b}$$

The empirical equation for buckling amplitude, (61), was used in these computations to reduce the cumulative error.

The test data were measured at three locations, in the direction indicated below:

      1. Center of panel $(x = a/2, y = b/2) \sim \epsilon_x$

      2. Midpoint of panel long side $(x = 0 \text{ or } a, y = b/2) \sim \epsilon_x$

      3. Midpoint of panel short side $(x = a/2, y = 0 \text{ or } b) \sim \epsilon_y$

Measured strains at the three locations were then plotted versus calculated strains, with the result shown in Figures 66 and 67. Absolute values of both measured and calculated data were used, even though the sign of the buckling stress is positive. The negative measured
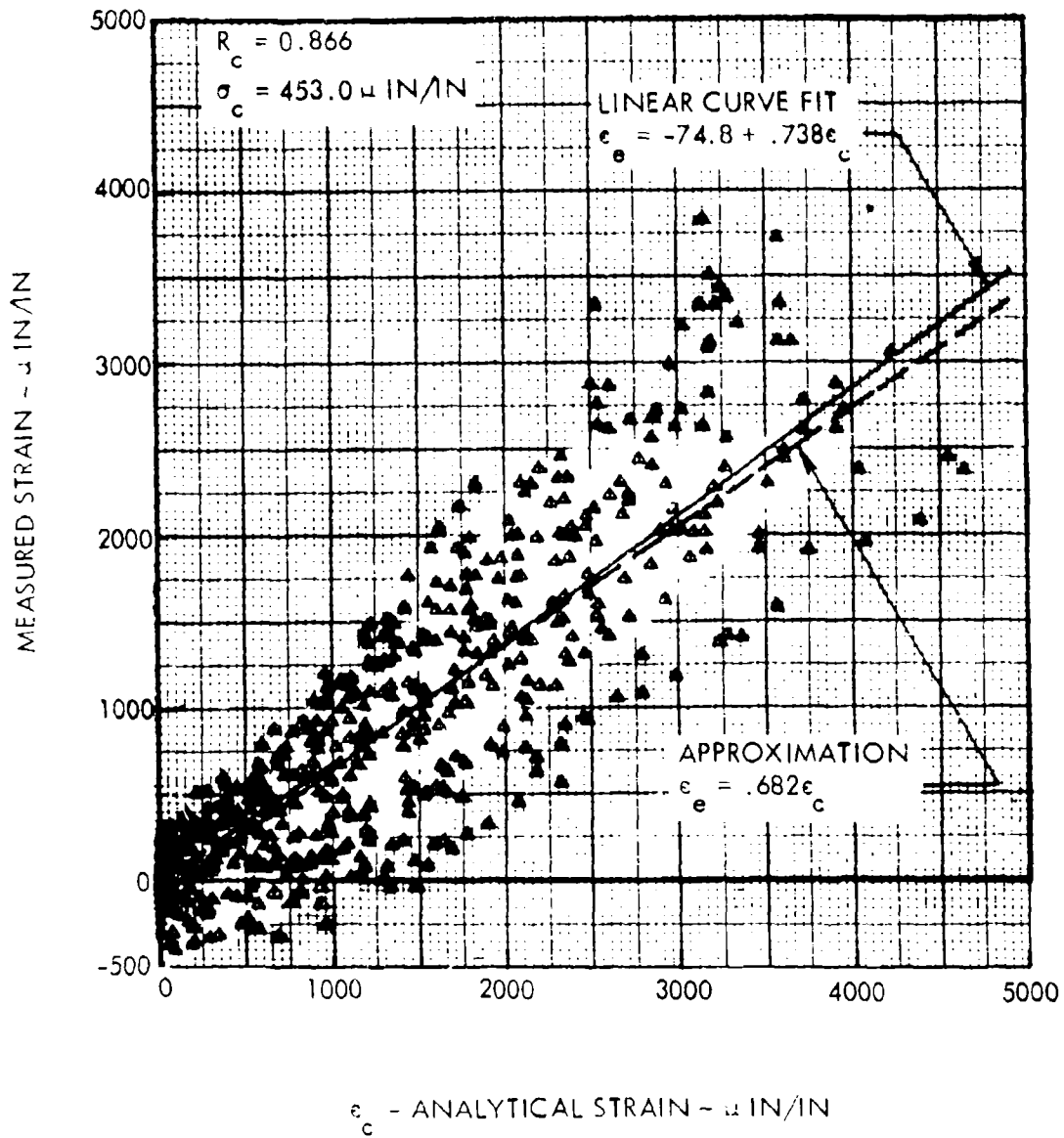
FIGURE 66. THERMAL BUCKLING STRAIN CORRELATION
LOCATION 1 & 2 - PANEL LONG LENGTH MIDPOINT

100
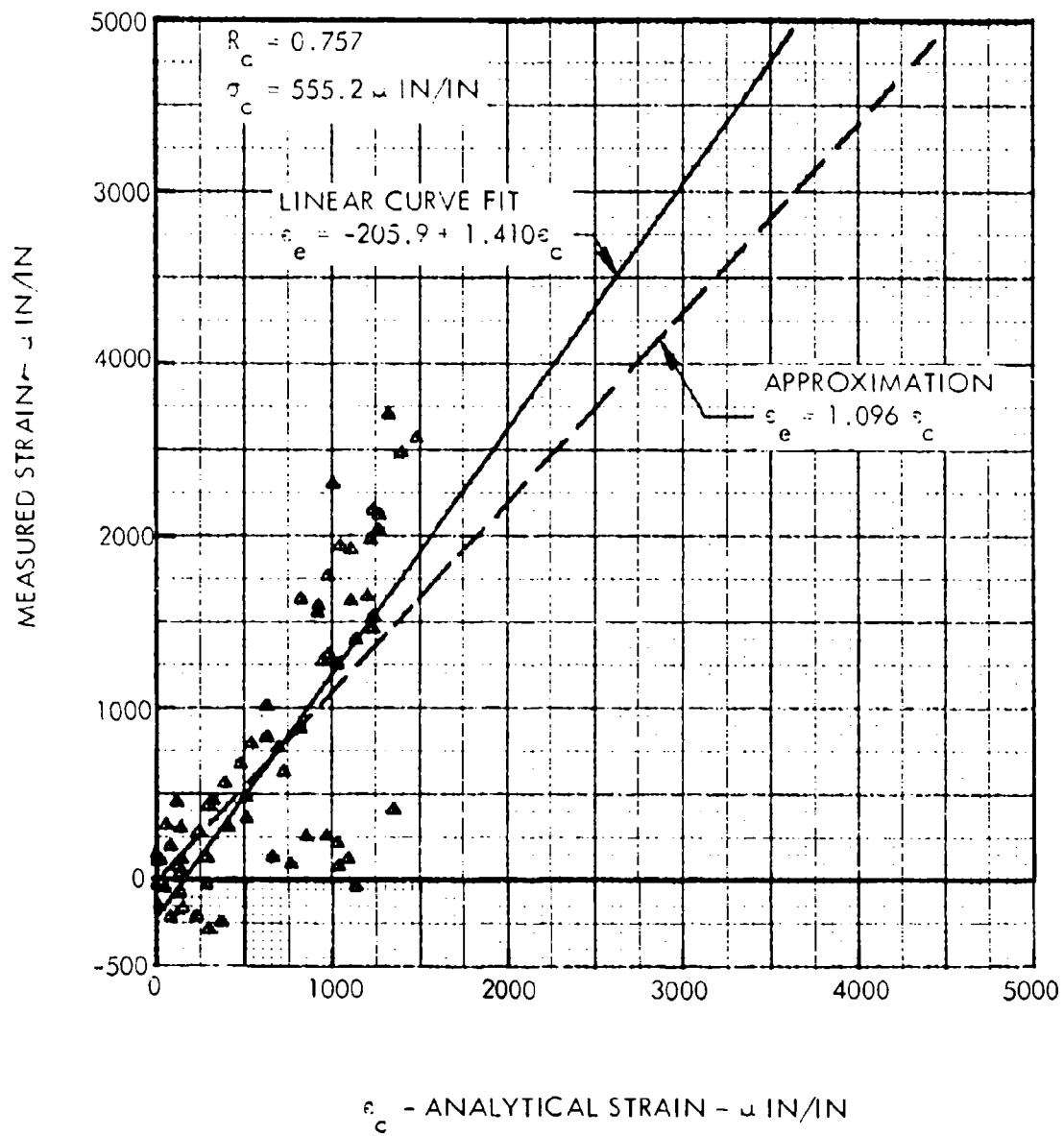
FIGURE 67. THERMAL BUCKLING STRAIN CORRELATION
LOCATION 3 - PANEL SHORT LENGTH MIDPOINT

strains on the plots are the result of subtraction of the expansion strain. The least squares regression lines and the simpler zero-origin approximation are again indicated, with the difference between the two negligible in comparison to the scatter in the data. Therefore, the simpler approximation was selected in each case, resulting in the following empirical relations for thermal stress:

o Midpoint of panel long side

$$\sigma_{x_e} = -\left[\frac{E\alpha T}{1-\nu}\right] + \frac{0.82 EW_o^2}{ab(1-\nu^2)} \left[\frac{b}{a}(2-\nu^2) + \nu\frac{a}{b}\right] \tag{64a}$$

o Midpoint of panel short side

$$\sigma_{y_e} = -\left[\frac{E\alpha T}{1-\nu}\right] + \frac{1.66 EW_o^2}{ab(1-\nu^2)} \left[\frac{a}{b}(2-\nu^2) + \nu\frac{b}{a}\right] \tag{64b}$$

These equations are applicable only for the mid-plane of the panel in the direction indicated. Strains for other locations can be readily derived from these relations by use of the analytical equations involving spatial location.

The results of the strain correlation are illustrated in Figures 68 through 70, which show the measured data and the empirical equation plotted versus temperature ratio for several of the test specimens. The agreement in the trends of the empirical relation and the measured data is considered good in view of the considerable scatter which exist in the data.

The influence of temperature on the coefficient of thermal expansion, α, is reflected in the empirical curves of Figures 68 through 70 by the curvature in the empirical line. The value of α for aluminum increases (with increasing temperature) for all temperatures below 300°F, while α for titanium reaches an upper limit at a temperature of 400°F.

B. Dynamic Stress

Computation of the dynamic stress involves the frequency and sound pressure spectrum level in addition to certain specimen dimensions. The frequency response at a specific temperature above ambient is, in turn, dependent on the room temperature fundamental frequency. Hence, the derivation of the empirical dynamic parameters will be discussed in the order in which they will be used.

1. Ambient Temperature Fundamental Frequency

Measured room temperature fundamental frequencies, from Tables VII and VIII, were plotted versus values calculated by Equation (30). The results are shown in Figure 71 for all aluminum and titanium specimens, with the two forms of regression line indicated. Since there was very little difference in the two slopes, the approximation was selected, and the following empirical relation resulted for room temperature fundamental mode frequency:

102
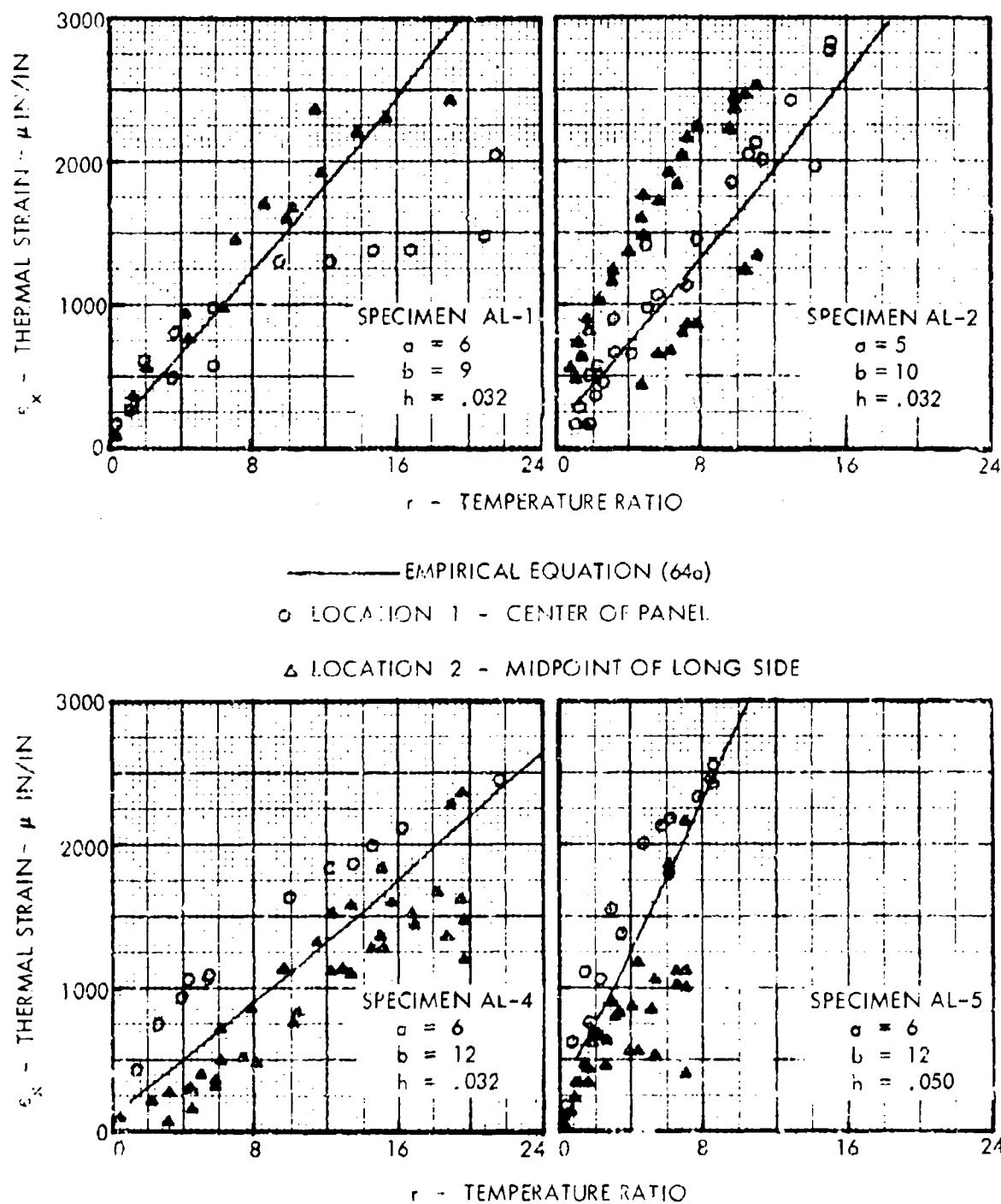
FIGURE 68. COMPARISON OF EMPIRICAL AND MEASURED THERMAL STRAINS

103
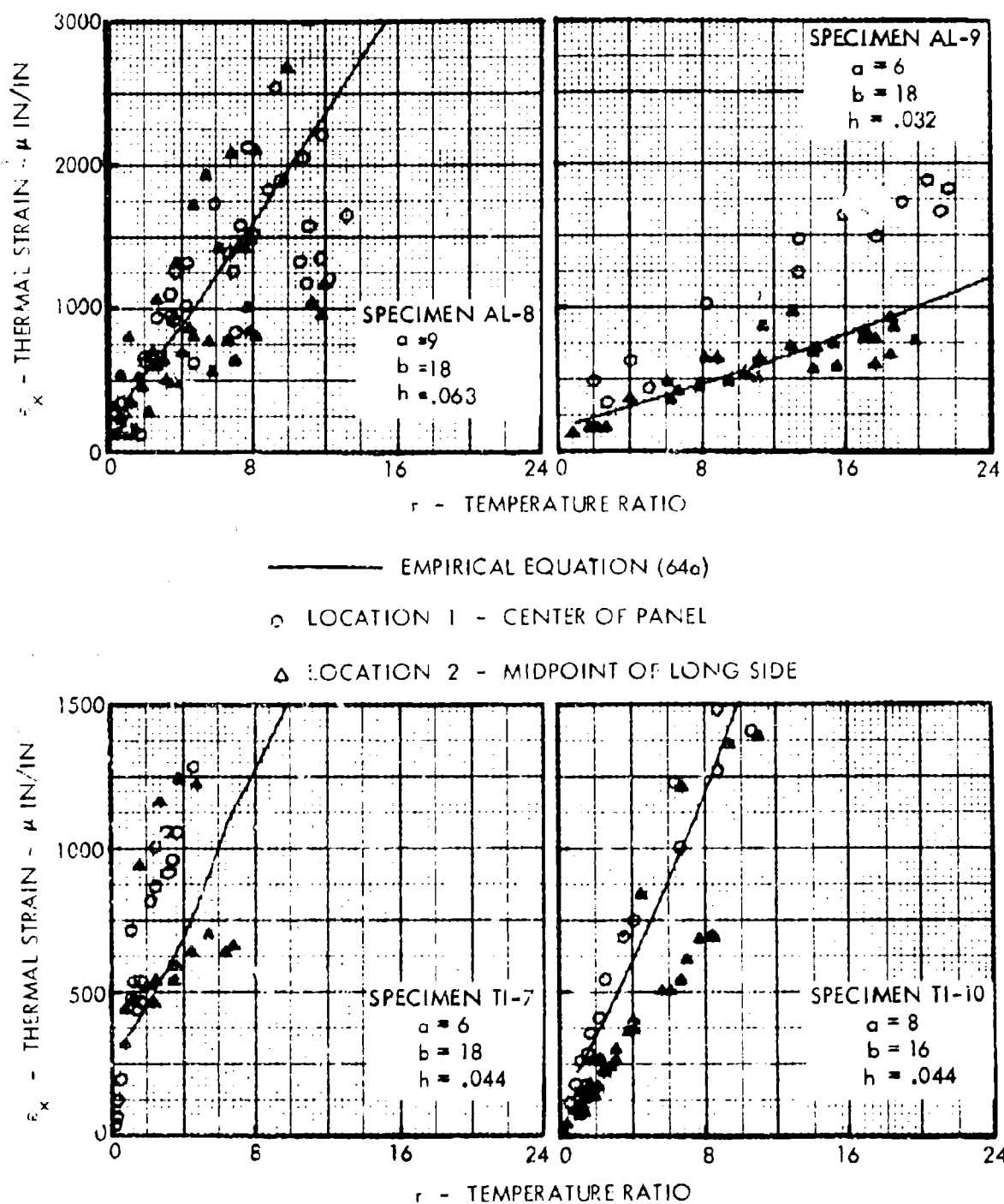
FIGURE 69. COMPARISON OF EMPIRICAL AND MEASURED THERMAL STRAINS

104
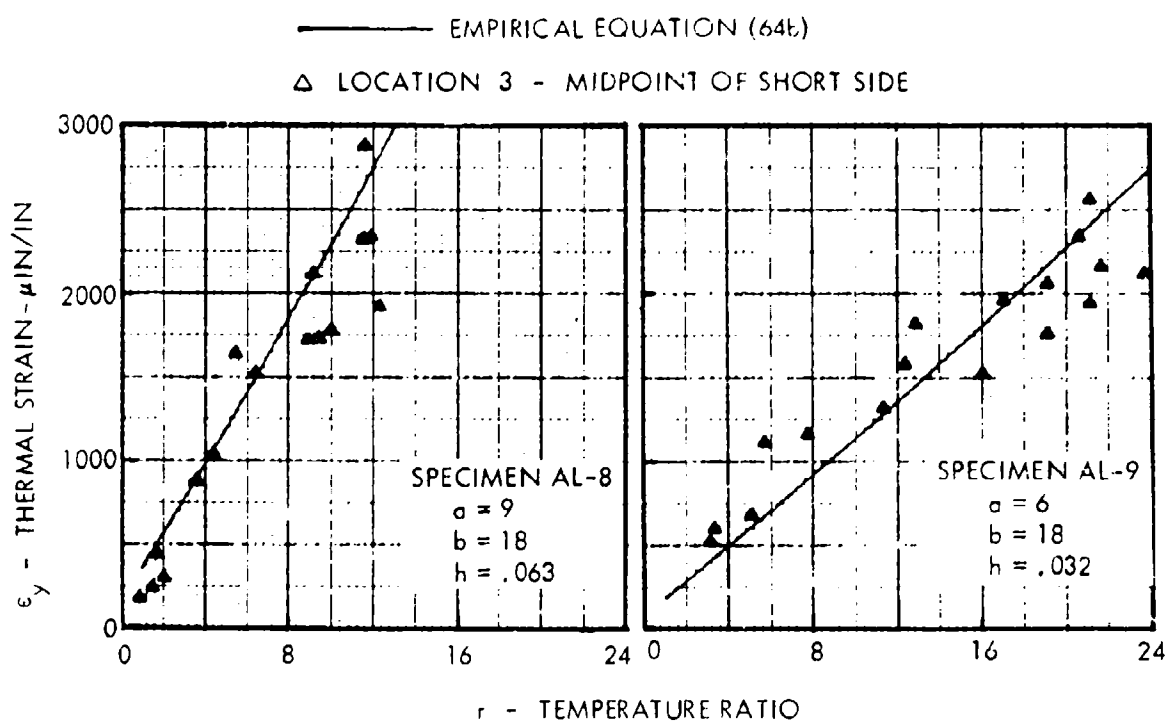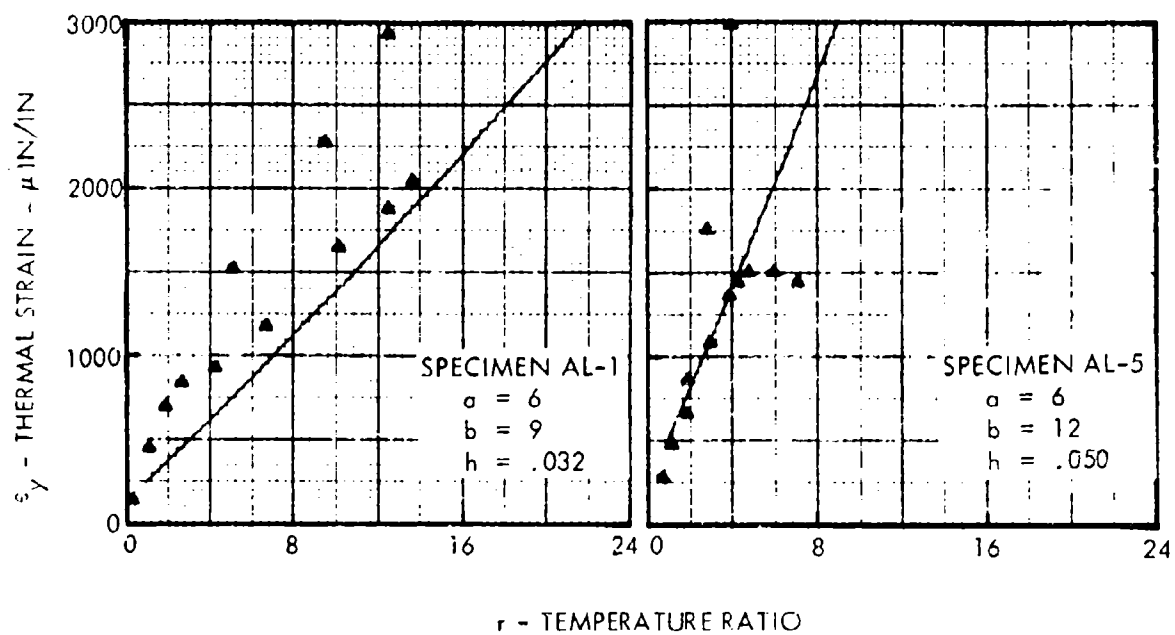
FIGURE 70. COMPARISON OF EMPIRICAL AND MEASURED THERMAL STRAINS

105
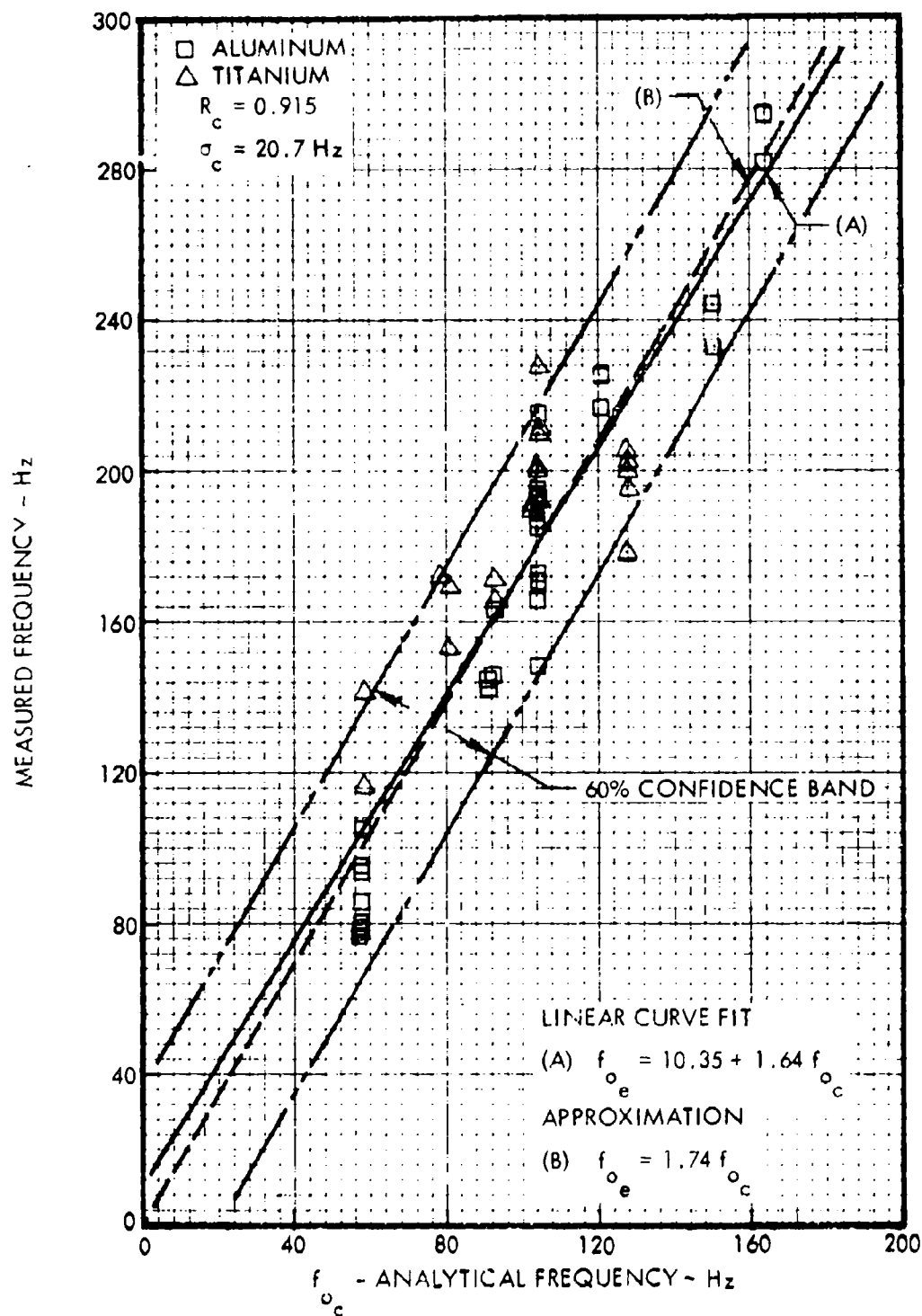
FIGURE 71. FUNDAMENTAL MODE FREQUENCY CORRELATION
AMBIENT TEMPERATURE

106

$$f_{o_e} = \frac{2.73}{ab} F_{11} \left[\frac{D}{\gamma h} \right]^{1/2} \qquad (65a)$$

or, alternatively,

$$f_{o_e} = 0.79 \frac{F_{11} h}{ab} \left[\frac{E}{\gamma (1-\nu^2)} \right]^{1/2} \qquad (65b)$$

This equation is based on a simply supported plate analytical model. Use of more realistic boundaries for the analytical model is not justified because, like the buckling temperature, a certain amount of scatter is present in the measured data for a particular specimen configuration. This scatter is attributable to the same factors that create the scatter in the buckling temperature, as discussed previously.

The correlation coefficient for the plot of Figure 71 is $R_c = 0.915$, hence the probability of accurately estimating the fundamental mode frequency for a specific design configuration is considered good. For instance, the error in the estimated frequency should be less than ± 18 Hz for a confidence level of 60%.

2. Elevated Temperature Fundamental Frequency

The fundamental frequency response of a heated panel is given by Equation (30) as a function of temperature ratio and the room temperature frequency. At the critical buckling temperature, $r = 1$, the analytical frequency decreases to zero, as shown in Figure 4. However, as shown in Figure 33, the measured data did not exhibit this tendency. Measured frequency ratios, $f(r)/f_o$, were plotted against the measured temperature ratio, r, with the data from all specimens plotted on the same graph. The data distribution is indicated by the shaded area of Figure 72; the data points were distributed uniformly within the limits of the scatter band. The data were separated into two groups, above and below the critical temperature, and measured frequency ratios plotted against calculated frequency ratios. A least squares regression line was computed for each group and then slightly modified to provide identical values at $r = 1$ so that a continuous curve would result. The empirical equations are thus

$$f(r)_e = f_o \left[0.60 + 0.40 \, (1-r)^{1/2} \right] \qquad (0 \leq r \leq 1)$$

$$\qquad\qquad\qquad\qquad\qquad\qquad\qquad\qquad\qquad\qquad (66)$$

$$f(r)_e = f_o \left[0.60 + 0.44 \, (r-1)^{1/2} \right] \qquad (r \geq 1)$$

The curve produced by this equation is also shown in Figure 72. No means were available to reduce the scatter in the frequency ratio data since, for identical configurations, the frequency ratios varied from the minimum to the maximum shown in Figure 72. Much of this scatter is directly related to errors accumulated in the room temperature fundamental frequency and the buckling temperature measurements.
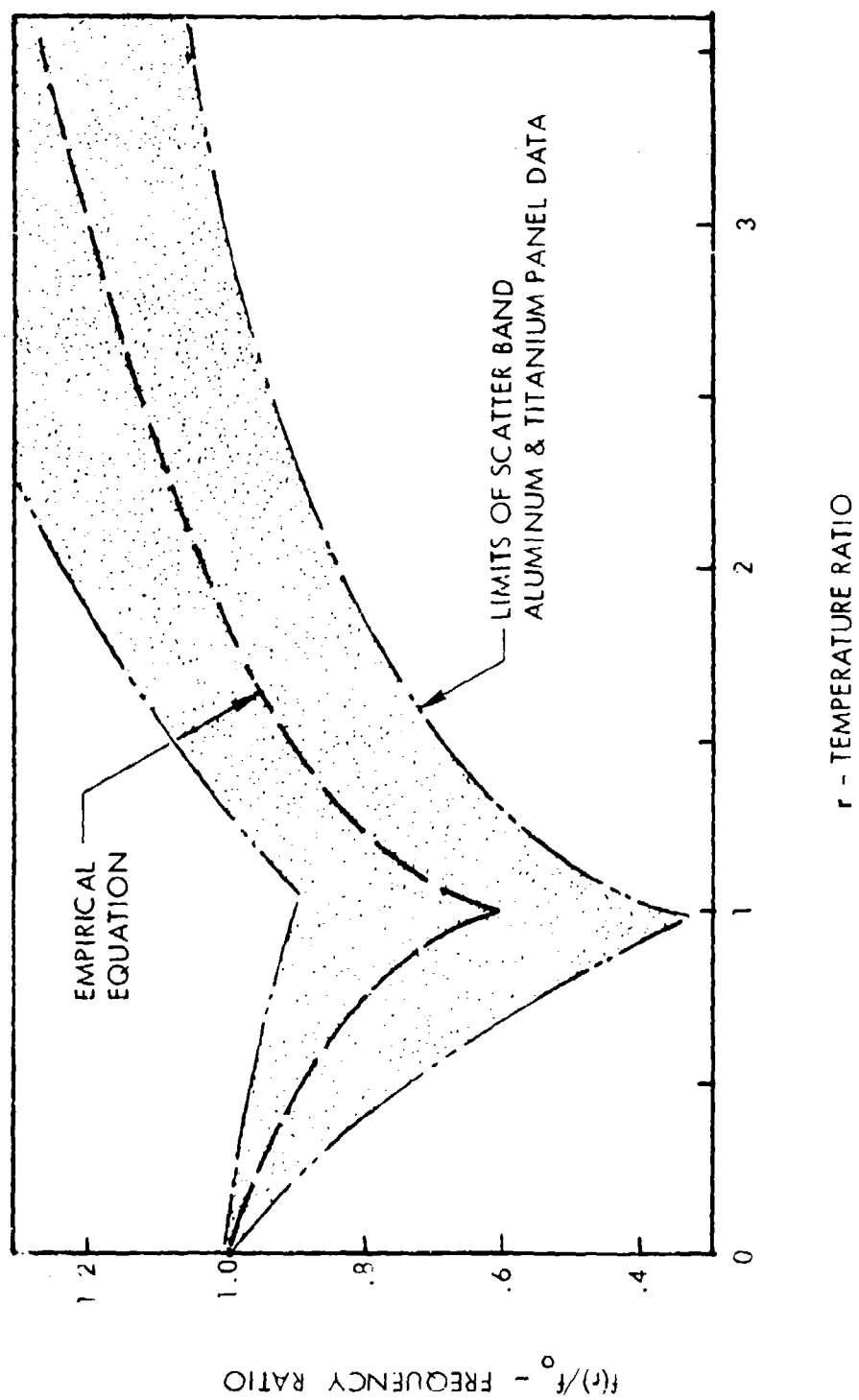
FIGURE 72. MEASURED FREQUENCY VARIATION WITH TEMPERATURE

108

3. Dynamic Strain

Dynamic stresses were calculated using the following equations from Reference 4 for clamped edge conditions:

o   Rivet row at midpoint of long side ($x = 0$, $y = b/2$)

$$\tilde{\sigma}_x = \frac{6}{\pi^{3/2}} \left(\frac{b}{h}\right)^2 \frac{\Phi(f)}{AR} \left[\frac{f(r)}{\zeta}\right]^{1/2} \tag{67a}$$

o   Rivet row at midpoint of short side ($x = a/2$, $y = 0$)

$$\tilde{\sigma}_y = \frac{6}{\pi^{3/2}} \left(\frac{a}{h}\right)^2 \frac{\Phi(f)}{AR} \left[\frac{f(r)}{\zeta}\right]^{1/2} \tag{67b}$$

The aspect ratio parameter, AR, is defined as

$$AR = 3 \, (b/a)^2 + 3 \, (a/b)^2 + 2$$

Dynamic strain analyses were made several times during each test, in the form of a narrow-band analysis, as discussed previously. The response frequencies, sound pressure levels, and overall strain levels from these analyses were used in the dynamic strain correlation for the two locations given above. These locations correspond to locations 2 and 3 for the thermal strain correlation.

The calculated strains for each measurement location were plotted versus the corresponding measured strains as shown in Figure 73, and the least squares regression lines were computed. As noted in the figures, the least squares curve fit has a very gradual slope, with residual values of 176 and 137 μin/in at zero calculated strain. The approximate zero-origin curve fit is also shown for each case. From a practical viewpoint, the strain without noise excitation should be zero, which is not the case for the least squares curve fit. Since a large variance is present in the data (correlation coefficients of less than 0.30 for both plots) either line can be used without loss of accuracy. Because of this lack of correlation, a conservatism factor of 2 was applied to the approximate relations to produce the following empirical dynamic stress relations:

o   Rivet row at midpoint of long side ($x = 0$, $y = b/2$)

$$\tilde{\sigma}'_{x_e} = 0.36 \left(\frac{b}{h}\right)^2 \frac{\Phi(f)}{AR} \left[\frac{f(r)}{\zeta}\right]^{1/2} \tag{68a}$$

o   Rivet row at midpoint of short side ($x = a/2$, $y = 0$)

$$\tilde{\sigma}_{y_e} = 1.30 \left(\frac{a}{h}\right)^2 \frac{\Phi(f)}{AR} \left[\frac{f(r)}{\zeta}\right]^{1/2} \tag{68b}$$

The probability of accurately predicting dynamic stresses for a particular application is low because of the scatter in the data; hence, these relations should only be used to provide
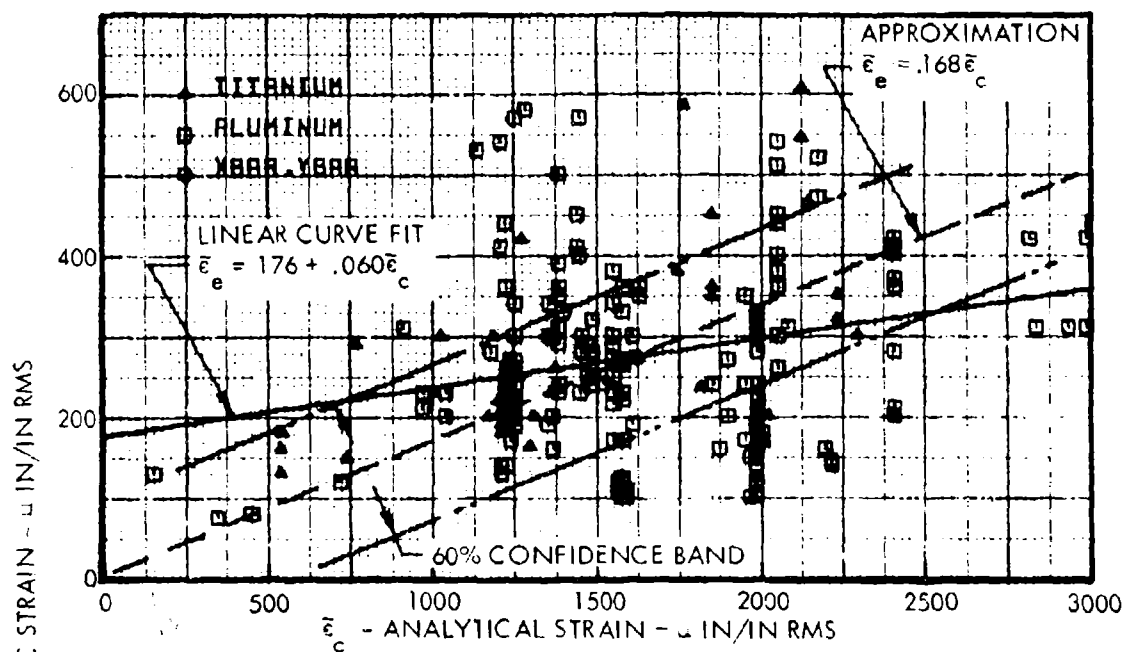
a) LOCATION 2 - PANEL LONG SIDE RIVET ROW AT MIDPOINT
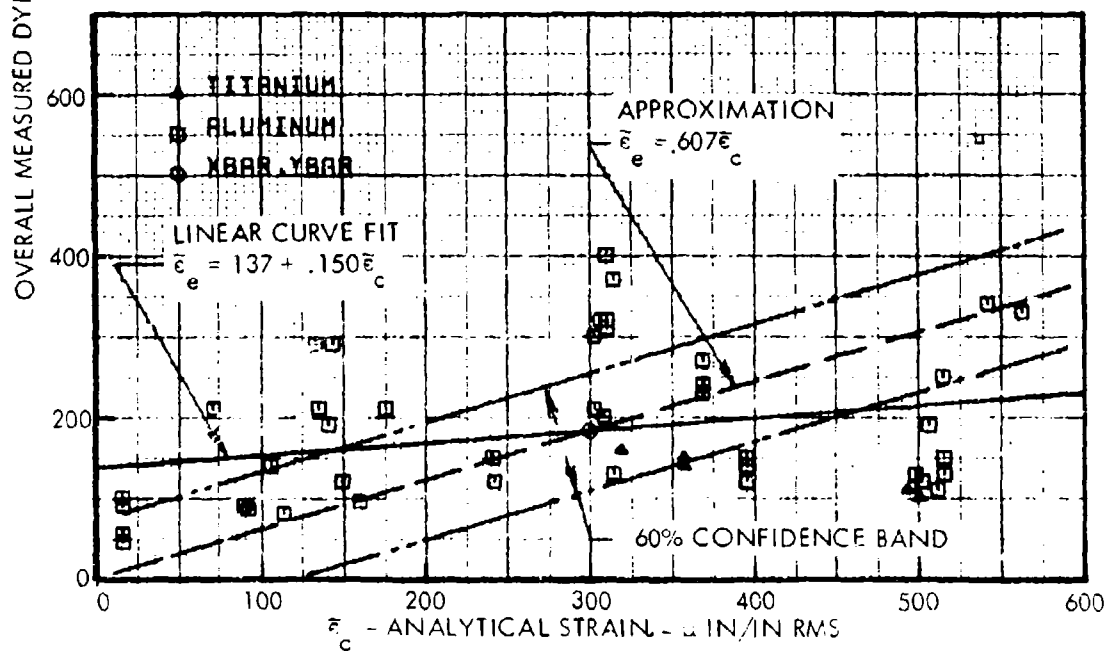
b) LOCATION 3 - PANEL SHORT SIDE RIVET ROW AT MIDPOINT

FIGURE 73. DYNAMIC STRAIN CORRELATION - ALL TEMPERATURES

110

gross estimates of the stress magnitude. Assuming a 60% confidence level, errors in the estimated stresses can be expected to be on the order of ±95 and ±70 μin/in (rms) from the mean value for locations 2 and 3, respectively.

The above results have been derived using measured strain data, regardless of the test temperature. This was done because separation of the data by test temperature produced no significant difference in empirical stress. Figure 74 shows the room and elevated temperature data separately for strain location 2, and shows approximately 4% difference in the slopes of the approximate regression line. Such a small difference, in comparison with the data variation, does not justify establishment of separate relations for room and elevated temperature dynamic strains.
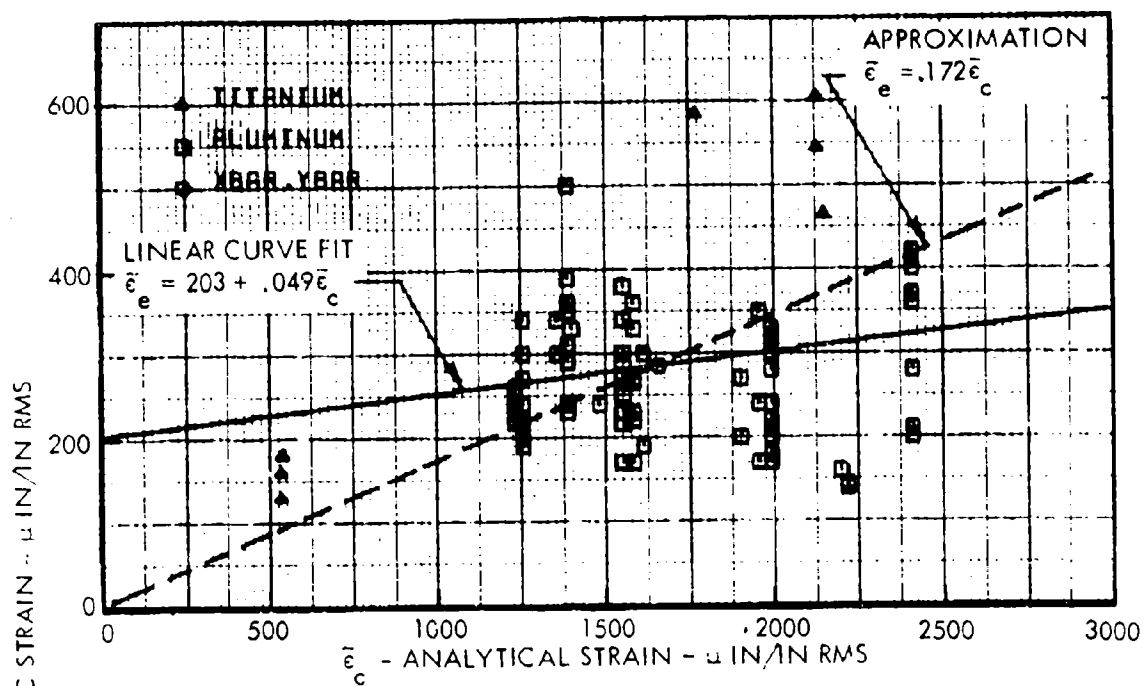
a) ROOM TEMPERATURE DATA
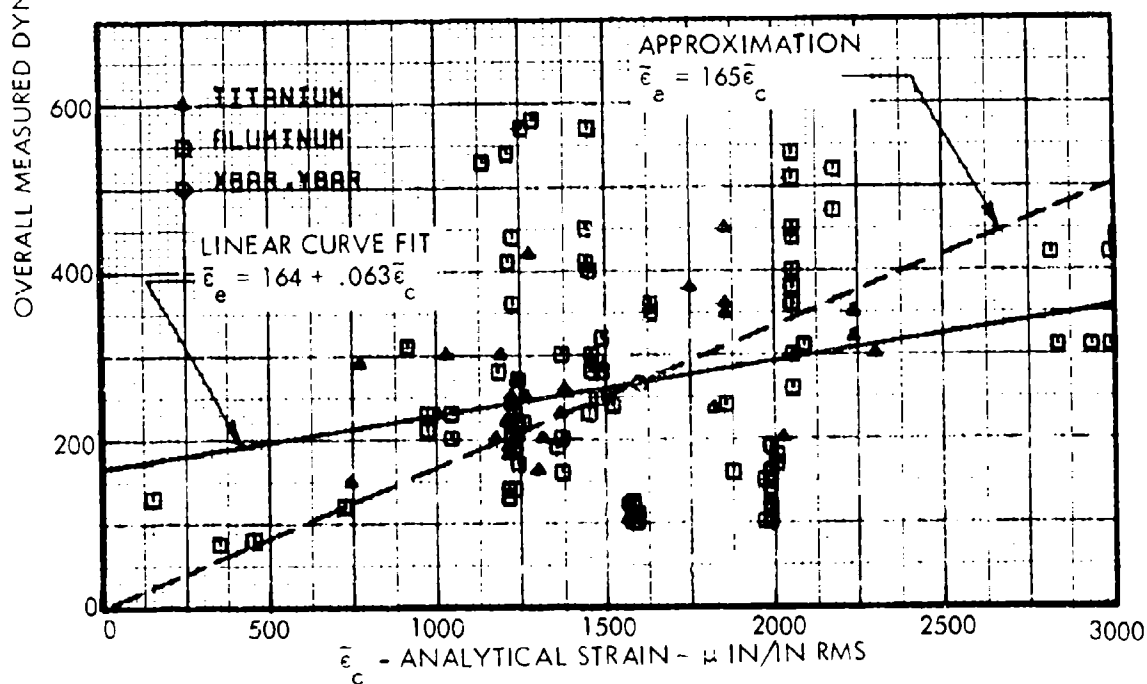
b) ELEVATED TEMPERATURE DATA

FIGURE 74. DYNAMIC STRAIN CORRELATION AT LOCATION 2

112

V - DESIGN METHODS

A useful tool for the design engineer is the design nomograph, which graphically displays an equation for rapid solution. The empirical equations of the preceding section were formulated into such nomographs and are presented in the following subsections. The results of the empirical derivation, together with existing room temperature criteria, are summarized here to clarify application of the design technique. The empirical subscript, e, has been dropped from all equations presented here to simplify the results.

A. Ambient Temperature Design Criteria

The design criteria at ambient temperatures are unchanged from existing criteria. Only the dynamic response of the structure is involved in the design as long as the ambient temperature state does not cause buckling of the skin.

1. Skin Design

The skin design criteria of AFFDL-TR-67-156[4] are valid for aluminum structures at ambient temperatures. Figure 75 depicts the nomenclature for a simple flat panel which is representative of a single bay of a stiffened-skin structure. The dynamic stress at the midpoint of the long side is given by Equation (36c), Reference 4, as

$$\widetilde{\sigma} = 1.62 \times 10^{-4} \left[\frac{E}{\gamma} \right]^{1/4} \frac{a^{1.25}}{h^{1.75}} \frac{\Phi(f)}{\varsigma^{.56}} \frac{(b/a)^{1.75}}{(AR)^{.84}} \sim ksi_{rms} \qquad (69a)$$

Dynamic stresses at this point are also given by Equation (68a), or

$$\widetilde{\sigma} = 3.60 \times 10^{-4} \left[\frac{b}{h} \right]^2 \frac{\Phi(f)}{AR} \left[\frac{f_o}{\zeta} \right]^{1/2} \sim ksi_{rms} \qquad (69b)$$

where f_o is given by Equation (65), or

$$f_o = 0.79 \frac{F_{11} h}{ab} \left[\frac{E}{\gamma(1-\nu^2)} \right]^{1/2} \sim Hz$$

The aspect ratio parameter is defined as

$$AR = 3(b/a)^2 + 3(a/b)^2 + 2$$

while the pressure density is defined by

$$\Phi(f) = 2.91 \times 10^{\left[(S_L/20) - 9\right]} \sim psi$$

113
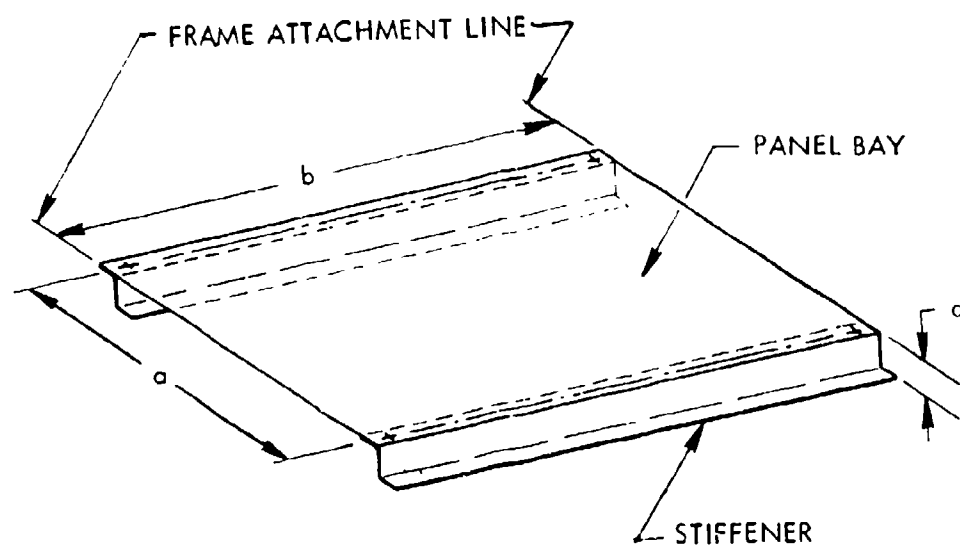
FIGURE 75. STIFFENED PANEL BAY

Comparison of these stress equations shows that, for identical configurations, Equation (69a) gives higher stresses than (69b). Since both are based on the same analytical model, the difference is in the data on which these empirical relations are based. These empirical relations can then be considered as bounds for predicting dynamic stresses. The form of the latter equation lends itself to much easier solution.

Figure 76 presents a nomograph, based on Equation (69a) from Reference 4, for stiffened-skin plating design. This nomograph was adapted for titanium structures by using the data of Section III.

EXAMPLE: A flat, aluminum alloy, stiffened structure is to be designed to withstand an estimated spectrum level of 120 dB for 5×10^8 cycles. The skin design is determined by the following:

Assume: o Damping ratio: $\zeta = 0.012$

o Stiffener spacing: $a = 4.75$ inches

o Aspect ratio: $b/a = 1.5$

Enter the nomograph, Figure 76, with the design life and follow through the nomograph, as indicated by the arrows, to obtain a skin thickness $h = 0.032$ inch.

The fundamental frequency is calculated by Equation (65) as $f_o = 340$ Hz. At this frequency, the service environment spectrum level is checked with the spectrum level used above. If necessary, an iteration can be made to obtain agreement.

2. Stiffener Flange Design

The acoustic loading on the surface of a stiffened panel is transferred to the substructure predominately by a transverse shear loading, causing the open section stiffeners to bend and twist. The stiffener loading is reacted along the skin-stiffener attachment (rivet) line and at the clip attachments to the frames. The resulting stresses at the stiffener flange are given by Equation (67), Reference 8, as

$$\tilde{\sigma}_f = 0.9 \left[\frac{0.0121 \, b^3 d}{I^* F_{11}} \; \Phi(f) \left(\frac{f_o}{\zeta} \right)^{1/2} \right]^{1/5} \sim ksi_{rms} \tag{70}$$

where $I^* = (I_{xx} I_{zz} - I_{xz}^2)/I_{zz}$.

This relation is valid only for the fundamental mode of the panel. The above flange stress is used in conjunction with a fatigue curve developed for flange failures; this curve is presented in Figure 77 (Reference 8, Figure 44).

EXAMPLE: A flat, aluminum alloy, stiffened structure is to be designed to withstand an estimated spectrum level of 120 dB for 5×10^8 cycles. The stiffener design is determined by the following:

115
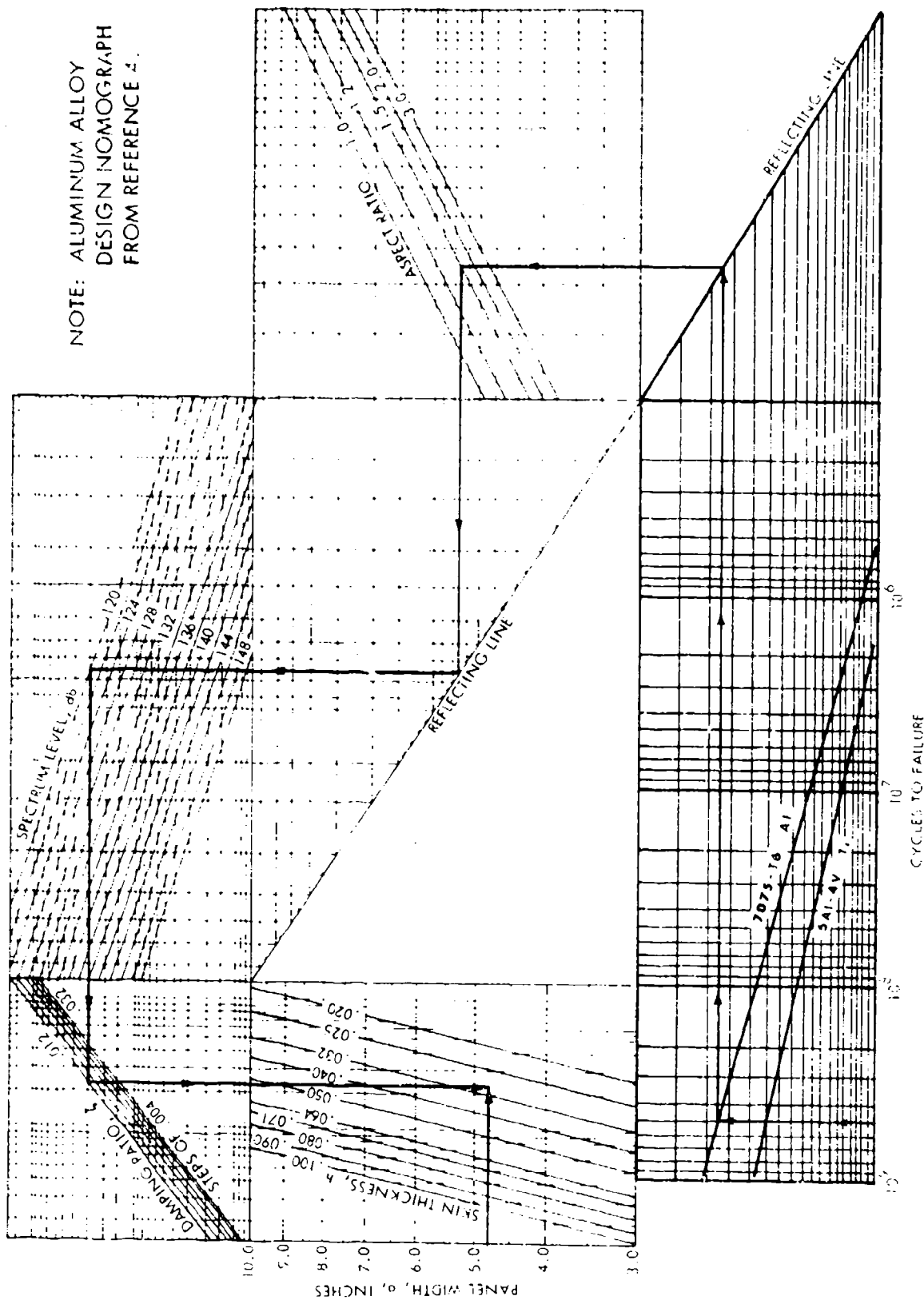
FIGURE 76. STIFFENED PANEL SKIN DESIGN NOMOGRAPH
AMBIENT TEMPERATURE

116
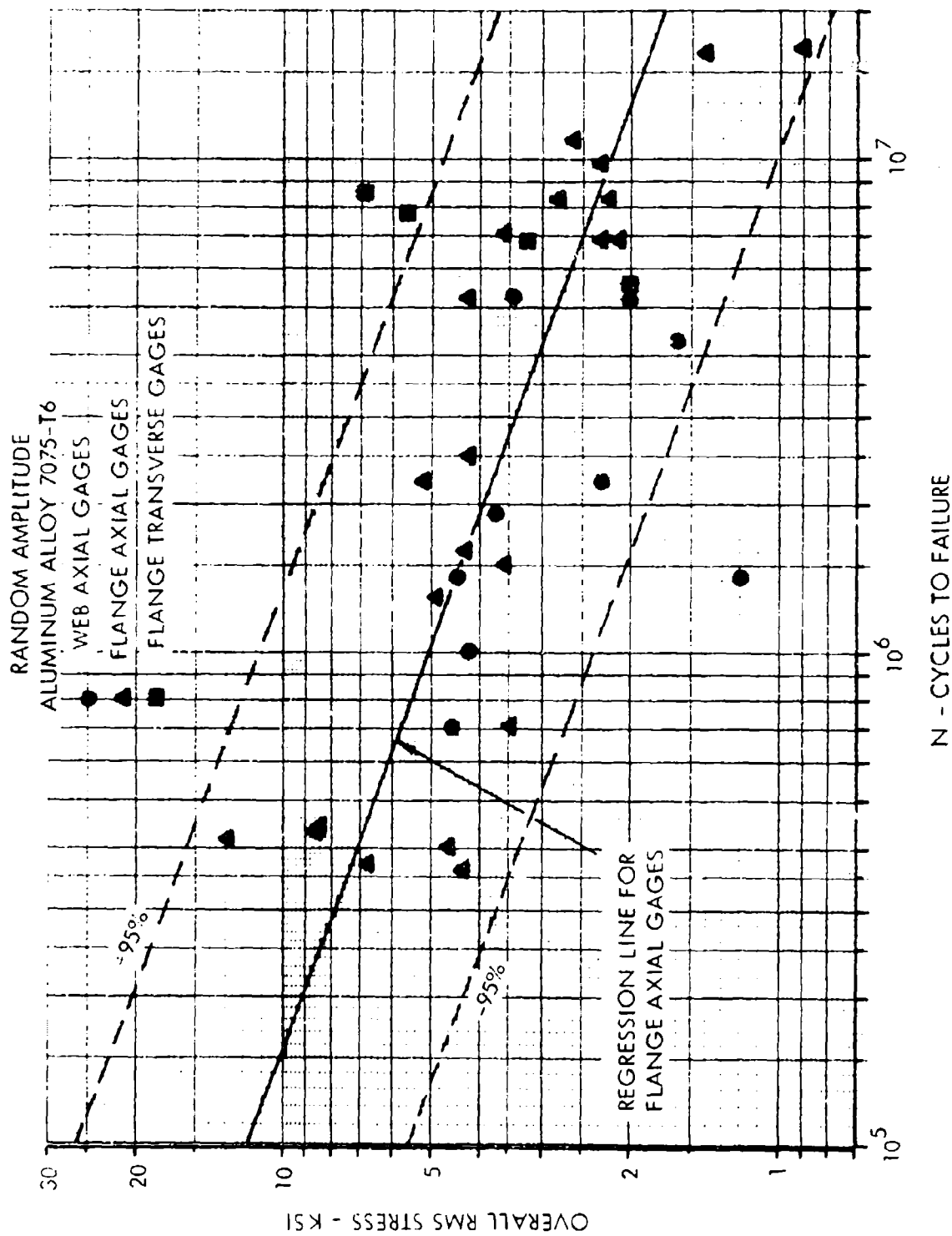
FIGURE 77. STIFFENED PANEL STIFFENER FATIGUE CURVE
AMBIENT TEMPERATURE (FROM REFERENCE 8)

117

Assume: o   Damping ratio: $\zeta = 0.012$

       o   Stiffener spacing: $a = 4.75$ inches

       o   Aspect ratio: $h/a = 1.5$ $(F_{11} = 2.17)$

From the previous example,

$$h = 0.032 \text{ inch}$$
$$f_o = 340 \text{ Hz}$$

The stiffener is a zee-section 0.040 inch thick with a flange width of 0.75 inch and height of 1.25 inch; the section properties give a value of $I^* = 0.01255$ inch^4.

From Equation (70), the attachment stress is

$$\widetilde{\sigma}_f = 0.9 \left[\frac{0.0121 \, (7.125)^3 \, (1.25) \, (2.9 \times 10^{-3})}{(0.01255) \, (2.17)} \left(\frac{340}{0.012} \right)^{1/2} \right]^{1/5}$$

$$= 2.25 \text{ ksi}_{rms}$$

From Figure 77, the life is estimated to be $N = 9 \times 10^6$ cycles, or considerably less than the design requirement.

The above procedure should then be repeated using a thicker or deeper zee stiffener until the desired life is achieved. It is also possible to reduce the stiffener spacing, thereby reducing the fundamental frequency and perhaps altering the excitation (dependent on the spectrum shape).

B. Elevated Temperature Design Criteria

The elevated temperature design criteria are used in essentially the same sequence in which they were discussed in Section IV. Since more than one method of application is available, all the criteria will be summarized and then followed by examples of usage.

1. Skin Buckling Temperature

The critical buckling temperature of a single panel, such as that shown in Figure 75, is given by Equation (60), or

$$T_c = \frac{5.25 \, h^2 \, F_{11}}{\alpha \, ab(1 + \nu)} \quad \sim \text{°F above ambient}$$

118

The temperature ratio is then defined as

$$r = T/T_c$$

where T is the temperature rise of the structure above ambient. Figure 78 is a nomograph of the above equation for a constant value of Poisson's ratio. The value of $\nu = 0.32$ was selected as representative of the most commonly used aircraft alloys.

2. Skin Buckling Amplitude

The empirical skin buckling amplitude is given by Equation (61), or

$$W_o = 2.50hF_{11}^{1.75} \left[\frac{r-1}{R} \right]^{1/2} \quad \sim \quad \text{inches}$$

where R is defined by Equation (19a) as

$$R = 3 \left[(5-\nu^2)F_{11}^2 - 2(5 + \nu)(1-\nu) \right]$$

A nomograph to predict buckling amplitudes is shown in Figure 79; this nomograph was also developed for a constant value of $\nu = 0.32$.

3. Thermal Stress

Thermal stresses due to in-plane expansion and skin buckling are given by Equations (64), for the midpoint of each side, or:

o Midpoint of panel long side

$$\sigma_x = \left\{ -\frac{E\alpha T}{1-\nu} + \frac{0.82 \, EW_o^2}{ab(1-\nu^2)} \left[\frac{b}{a}(2-\nu^2) + \nu \frac{a}{b} \right] \right\} \times 10^{-3} \sim \text{ksi}$$

o Midpoint of panel short side

$$\sigma_y = \left\{ -\frac{E\alpha T}{1-\nu} + \frac{1.66 \, EW_o^2}{ab(1-\nu^2)} \left[\frac{a}{b}(2-\nu^2) + \nu \frac{b}{a} \right] \right\} \times 10^{-3} \sim \text{ksi}$$

Thermal stresses must be computed at the midpoint of both sides, since the short side stress is greater than that at the center of the long side. This is opposite to the magitudes of the dynamic stresses at the two locations.

The above relations were simplified to

$$\sigma_x = \sigma_T + \sigma_{x_b} \quad ; \quad \sigma_y = \sigma_T + \sigma_{y_b}$$

119
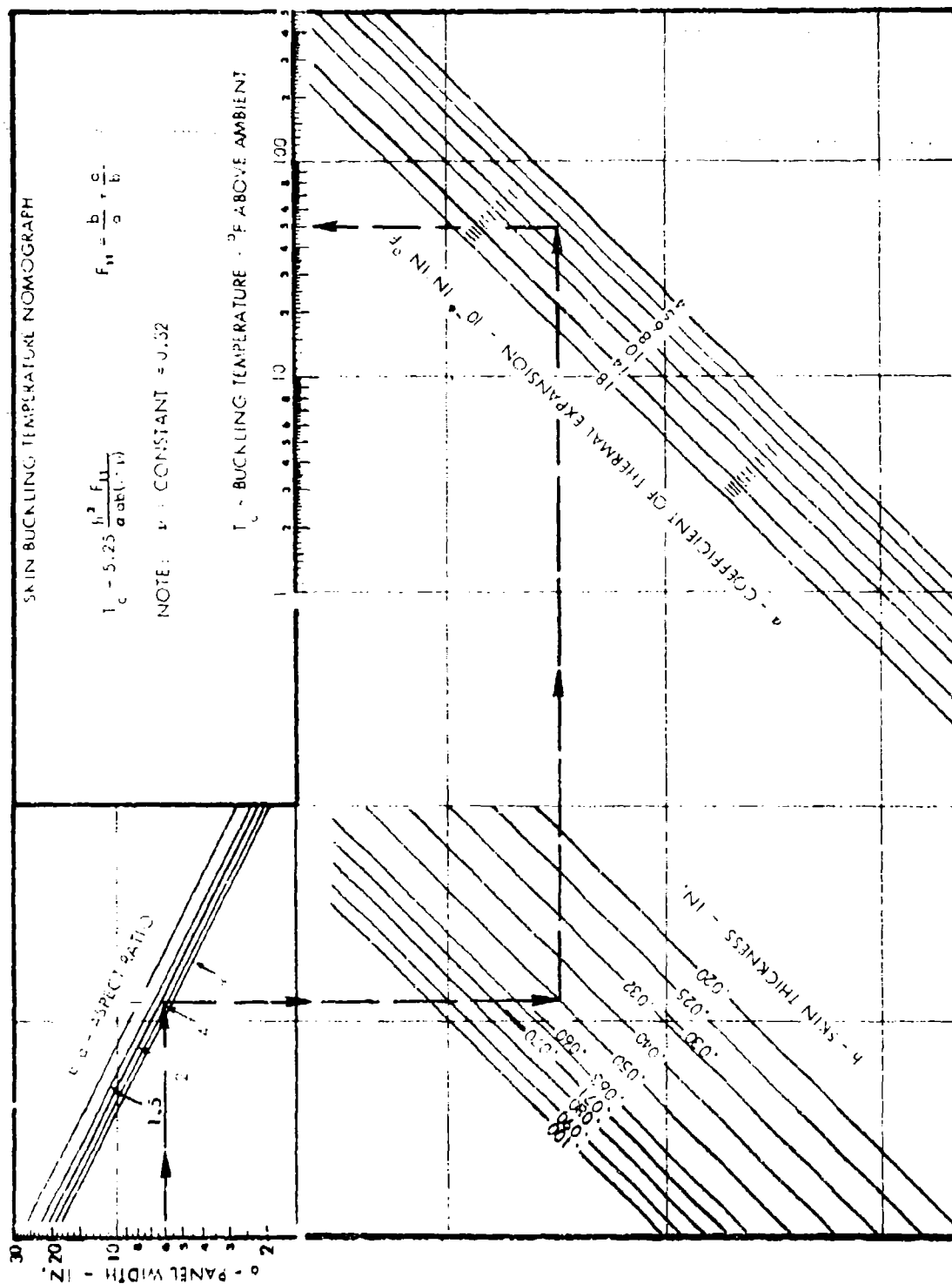
FIGURE 78. SKIN BUCKLING TEMPERATURE NOMOGRAPH

120
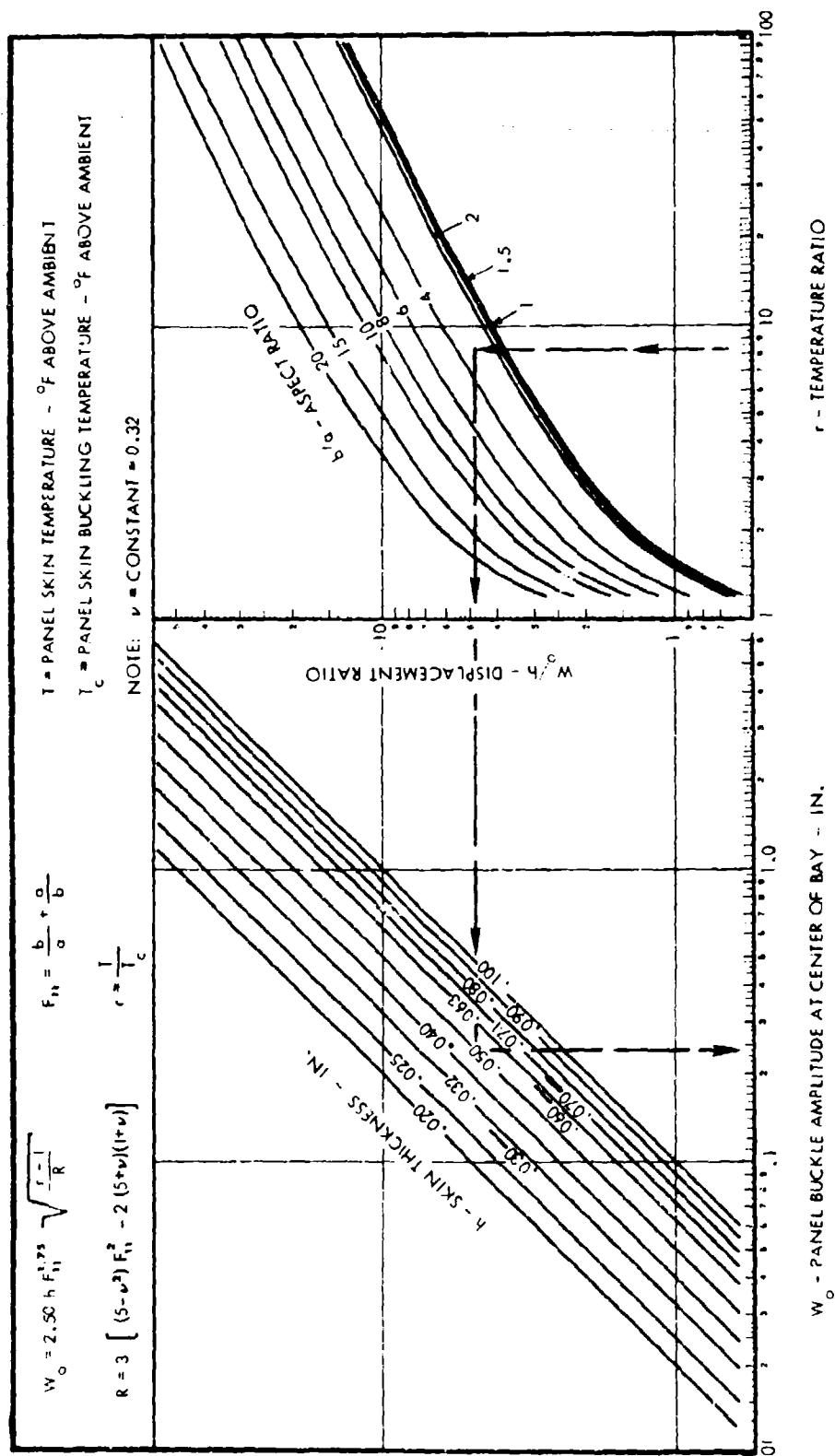
FIGURE 79. SKIN BUCKLING AMPLITUDE NOMOGRAPH

121

for development of design nomographs. These respective stresses are the in-plane expansion and buckling stresses as inferred from the preceding equations. Figure 80 is a nomograph of the thermal expansion stress, σ_T, while Figures 81 and 82 represent nomographs of the thermal buckling stresses in the x and y-directions, respectively. Again, the parameter $\nu = 0.32$ was used to develop these nomographs.

4. Ambient Temperature Fundamental Mode Frequency

The fundamental mode frequency for a single bay of a multi-bay structure is given by Equation (65b), or

$$f_o = \frac{0.79 \, F_{11}}{ab} \, h \left[\frac{E}{\gamma(1-\nu^2)} \right]^{1/2} \quad \sim \text{Hz}$$

The nomograph corresponding to this equation is presented in Figure 83, for $\nu = 0.32$. The chart was simplified by taking advantage of the essentially constant ratio of E/γ for most aircraft structural alloys. An average ratio of $E/\gamma = 3.98 \times 10^{10}$ in^2/sec^2 was used; this is an average of the ratios for aluminum, titanium, stainless steel, and Inconel alloys.

5. Elevated Temperature Frequency Response

The fundamental mode frequency at a temperature increase, T, is given by Equation (66), or

$$f(r) = f_o \left[0.60 + 0.40 \, (1-r)^{1/2} \right] \quad \sim \text{Hz} \qquad (o \leq r \leq 1)$$

$$= f_o \left[0.60 + 0.44 \, (r-1)^{1/2} \right] \quad \sim \text{Hz} \qquad (r \geq 1)$$

Figure 84 is a nomograph of this relationship to simplify the computation.

6. Dynamic Stress

Dynamic stresses at any temperature can be computed by Equation (68):

o   Rivet row at midpoint of long side

$$\tilde{\sigma}_x = 3.60 \times 10^{-4} \left[\frac{b}{h} \right]^2 \frac{\phi(f)}{AR} \left[\frac{f(r)}{f_o} \right]^{1/2} \quad \sim \text{ksi}_{rms}$$

o   Rivet row at midpoint of short side

$$\tilde{\sigma}_y = 13.0 \times 10^{-4} \left[\frac{a}{h} \right]^2 \frac{\phi(f)}{AR} \left[\frac{f(r)}{\zeta} \right]^{1/2} \quad \sim \text{ksi}_{rms}$$

122
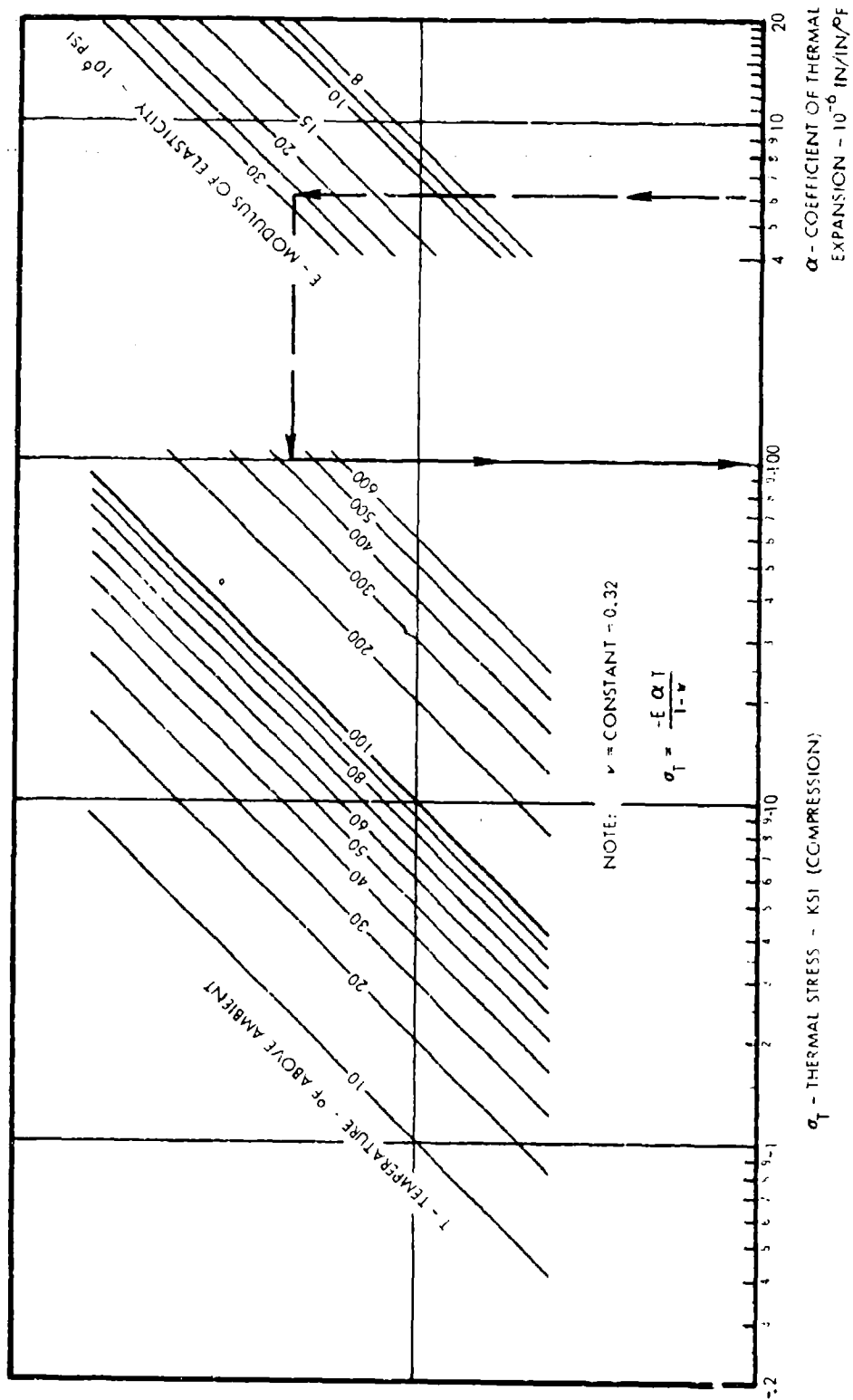
FIGURE 80. THERMAL EXPANSION STRESS NOMOGRAPH

123
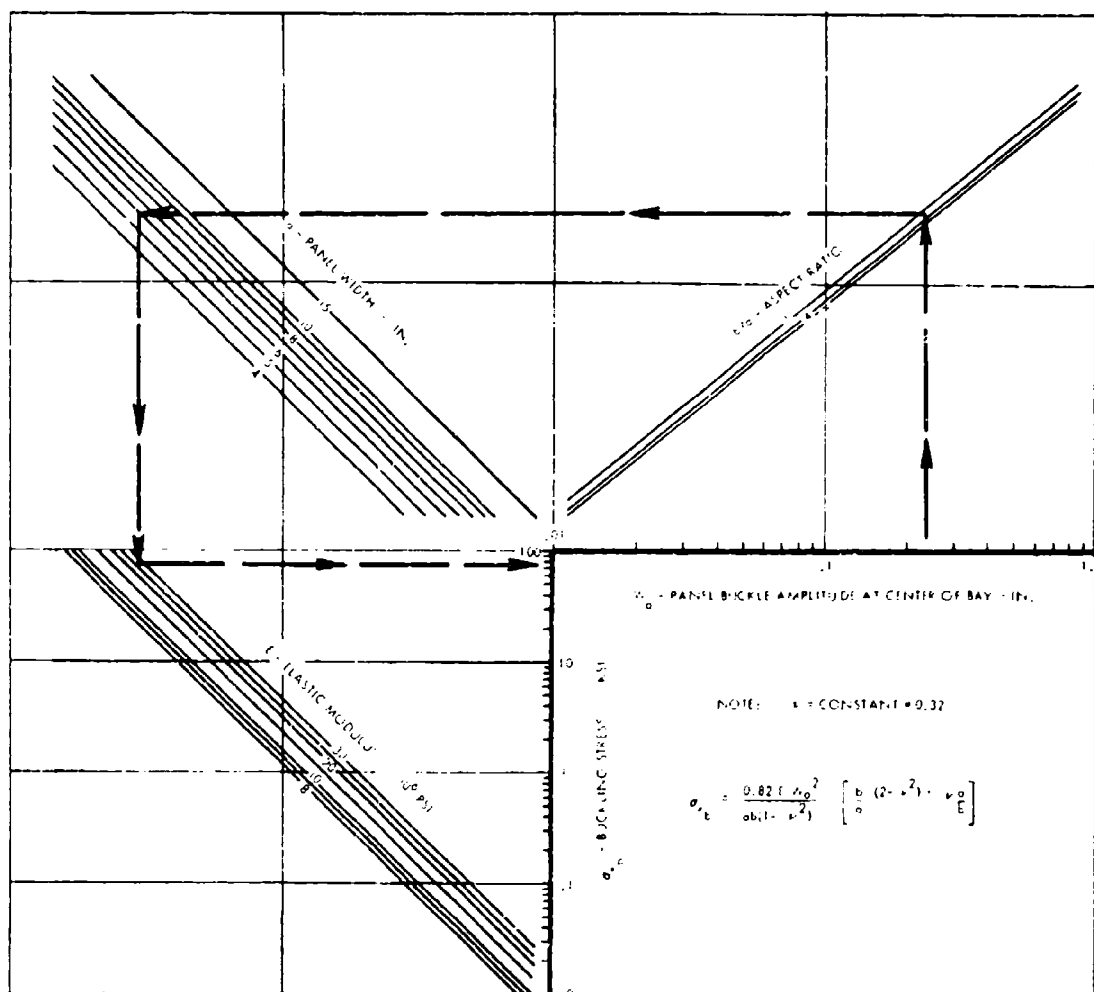
FIGURE 81. THERMAL BUCKLING STRESS NOMOGRAPH
X - DIRECTION STRESS
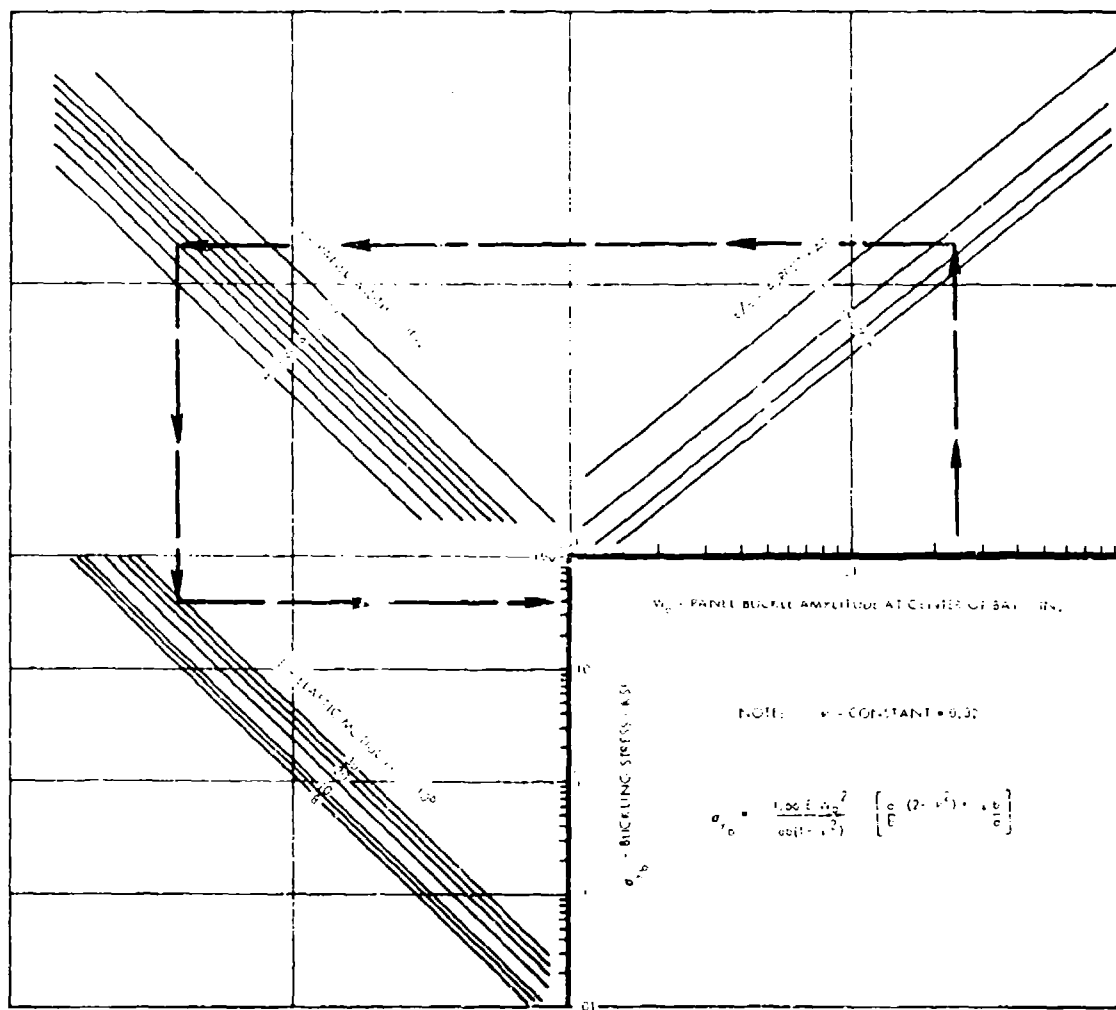
FIGURE 82. THERMAL BUCKLING STRESS NOMOGRAPH
Y - DIRECTION STRESS

125

b/a – ASPECT RATIO

1.5
2
4
8

$$f_o = 0.79 \, \frac{F_{11} h}{ab} \sqrt{\frac{E}{\gamma(1 - \nu^2)}}$$

$$F_{11} = \frac{b}{a} + \frac{a}{b}$$

NOTE: (1) ν = CONSTANT = 0.32
(2) E/γ = CONSTANT = 3.98×10^{10} IN^2/SEC^2

h – SKIN THICKNESS – IN

.030
.060
.100
.090
.080
.063
.050
.040
.025
.020

f_o – FUNDAMENTAL FREQUENCY – Hz

a – PANEL WIDTH – IN
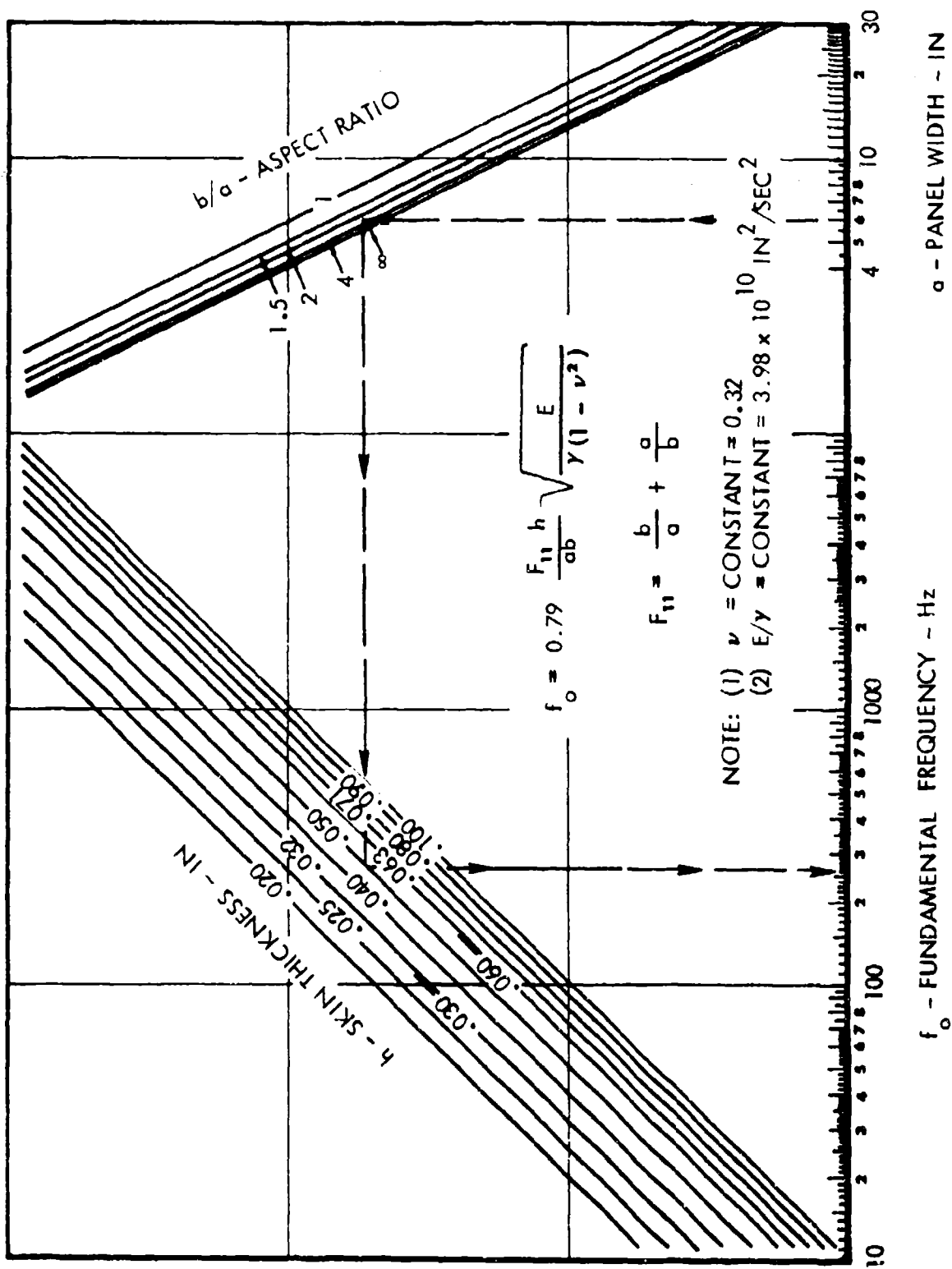
FIGURE 83. AMBIENT TEMPERATURE FUNDAMENTAL FREQUENCY NOMOGRAPH

126
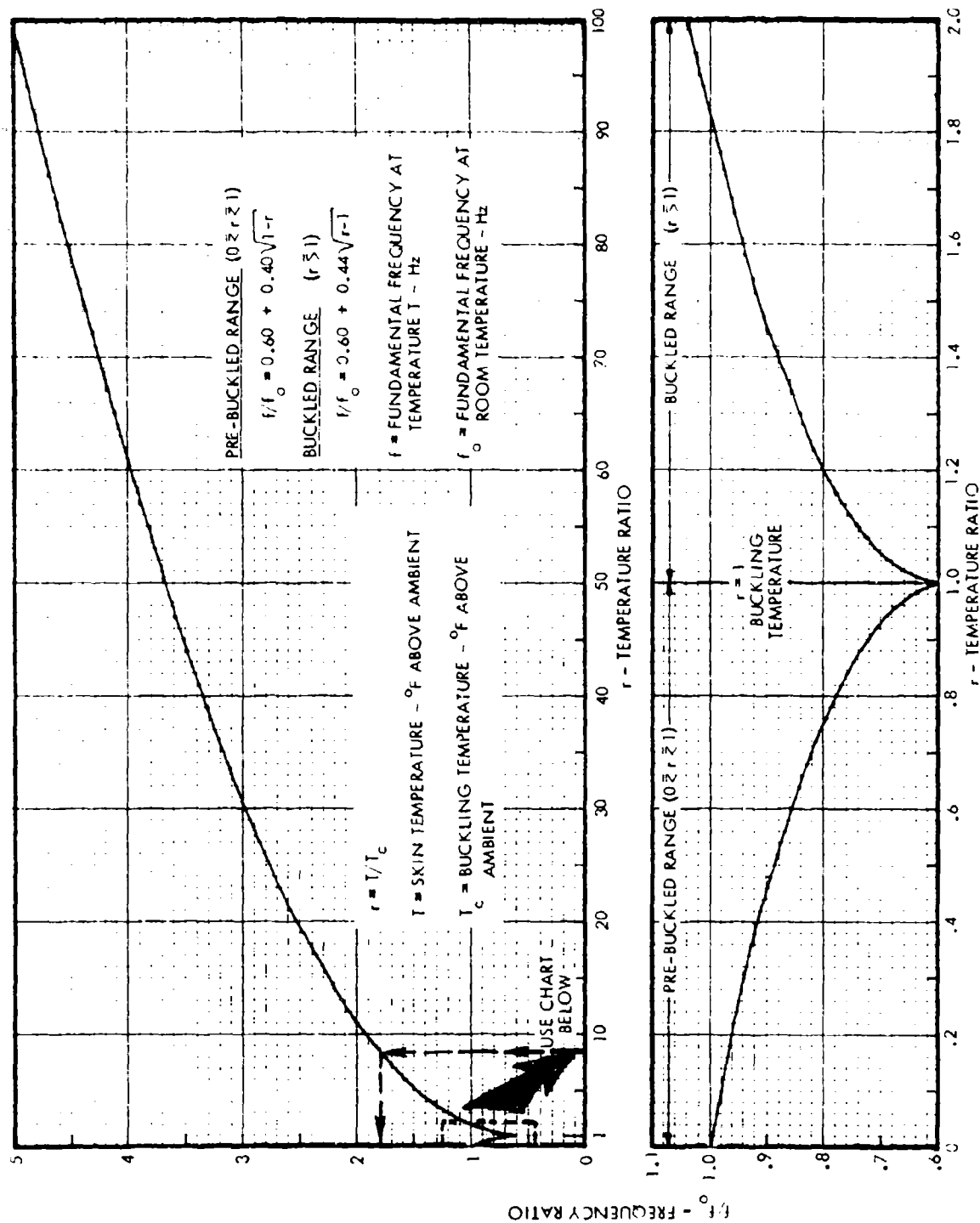
FIGURE 84. ELEVATED TEMPERATURE FUNDAMENTAL FREQUENCY NOMOGRAPH

127

The elevated temperature response frequency, $f(r)$, must be used for these computations. The stresses at both locations must generally be calculated for elevated temperature applications because of the interaction of the thermal and dynamic stresses.

The stiffened panel fatigue test data of Tables XI and XII were used to establish the design life nomograph of Figure 85 for elevated temperature applications. This nomograph is applicable for 7075-T6 aluminum at temperatures of 150° and 300°F, and 6Al-4V titanium at temperatures of 400° and 600°F.

7. Application of the Design Procedure

At least two alternative methods of application are possible using the criteria developed on this program. These alternatives are described in the following subsections in the form of sample applications.

a. Design Life Nomograph — The most direct method involves the use of the design nomograph for life, Figure 85. The alloys and structural temperatures must agree with those for which the nomograph was developed. This nomograph includes thermal mean stress effects in the data, thereby negating the need to compute these parameters.

EXAMPLE: A flat aluminum structure is to be designed for a service life of 100 hours at a sound pressure spectrum level of 120 dB and a service temperature of 300°F.

Assume: o Aspect ratio: $b/a = 3.0$ ($F_{11} = 3.33$)

      o Damping ratio: $\zeta = 0.016$

      o Ambient temperature: $80°F$

As a first step, assume a frequency, at the service temperature, of 300 Hz. Then, the life in cycles is

$$N = (300 \text{ Hz})(100 \text{ hr})(3600 \text{ sec/Hr}) = 1.08 \times 10^8 \text{ cycles}$$

Enter the nomograph of Figure 85 with this life and follow through the parameters to the skin thickness chart. Several spacing/skin thickness ratios are now possible, all of which will meet the design life goal. Assuming a skin thickness of 0.050 inch, the panel width is found to be 5.0 inches.

At this point a structural configuration is defined; however, the assumed frequency must be checked. Compute the fundamental mode frequency at the ambient temperature using Figure 83, ($f_0 = 390$ Hz) then compute the skin buckling temperature increase using Figure 77, where $\alpha = 13.5 \times 10^{-6}$ in/in/°F from Figure V-2, Appendix V. ($T_c = 33°F$) The temperature ratio is then

$$r = T/T_c = 220/33 = 6.7$$
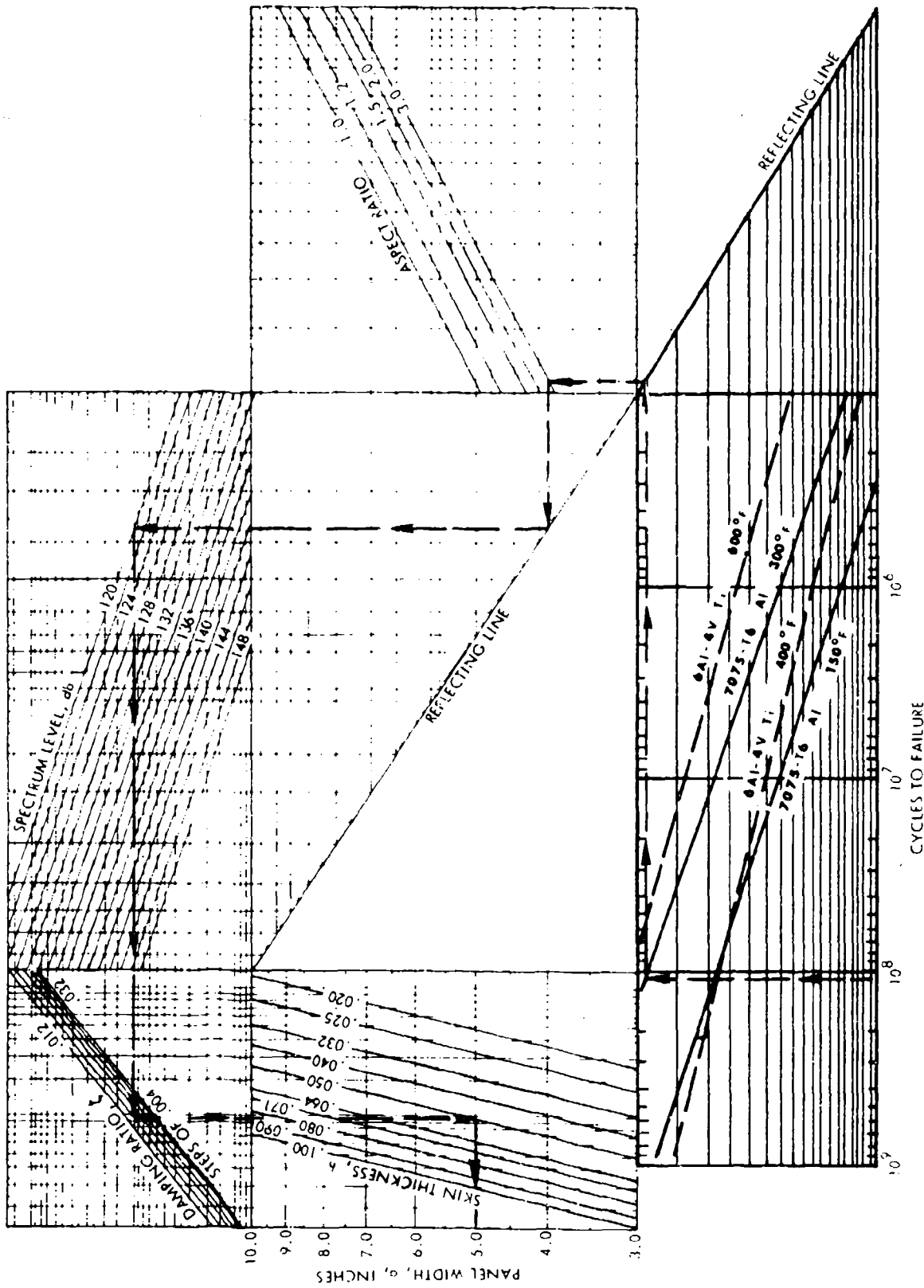
FIGURE 85. STIFFENED PANEL SKIN DESIGN NOMOGRAPH
ELEVATED TEMPERATURES

129

621

Figure 84 then yields the frequency ratio $f(r)/f_o = 1.65$, and the elevated temperature frequency is

$$f(r) = 1.65 f_o = 645 \text{ Hz}$$

Since this frequency is greater than the assumed frequency, the anticipated life will be less than the design goal, and an iteration is necessary. The above procedure is repeated using the calculated frequency of 645 Hz. One or more iterations may be necessary to obtain agreement between the initial and final frequency (or design life).

Several spacing/skin thickness ratio combinations may be derived using this method, and the weight of each calculated to obtain a minimum weight design.

This method may also be used for structural temperatures different than those indicated on the nomograph by assuming a linear relationship between the temperatures shown and interpolating.

b. Mean Stress Fatigue Curves - An alternate design method involves the use of fatigue curves where the mean stress effects are known (i.e., Figure V-4, Appendix V). This method can be used where the alloy or temperature does not coincide with those of the Figure 85 nomograph.

EXAMPLE: A flat structure is to be designed for a service life of 100 hours at a spectrum sound pressure level of 140 dB, and a service temperature of 500°F. Stainless steel PH15-7Mo is selected as the alloy to be used for this structure.

Assume: o Aspect ratio: $b/a = 3.0$ ($F_{11} = 3.33$)

o Damping ratio: $\zeta = 0.016$

o Ambient temperature: 80°F

A fatigue curve for the selected alloy was obtained from MIL-HDBK-5B[17] to give the effects of mean stress on fatigue life. This axial loading, constant amplitude fatigue curve was converted to an equivalent random amplitude fatigue curve (Figure 86) using the method of Reference 1.

Assume a stiffener spacing of $a = 6$ inch and a skin thickness of $h = 0.050$ inch. From MIL-HDBK-5B,

$$\gamma = (.277/386) = 7.17 \times 10^{-4} \text{ lb}-\text{sec}^2/\text{in}^4$$
$$\alpha = 6.1 \times 10^{-6} \text{ in/in/°F @ } 500°F$$
$$E_o = 29.0 \times 10^6 \text{ psi @ RT}$$
$$E = 26.97 \times 10^6 \text{ psi @ } 500°F$$

130

REF. 17, FIGURE 2.5.7.1.8(b)
CONVERTED TO EQUIVALENT RANDOM AMPLITUDE
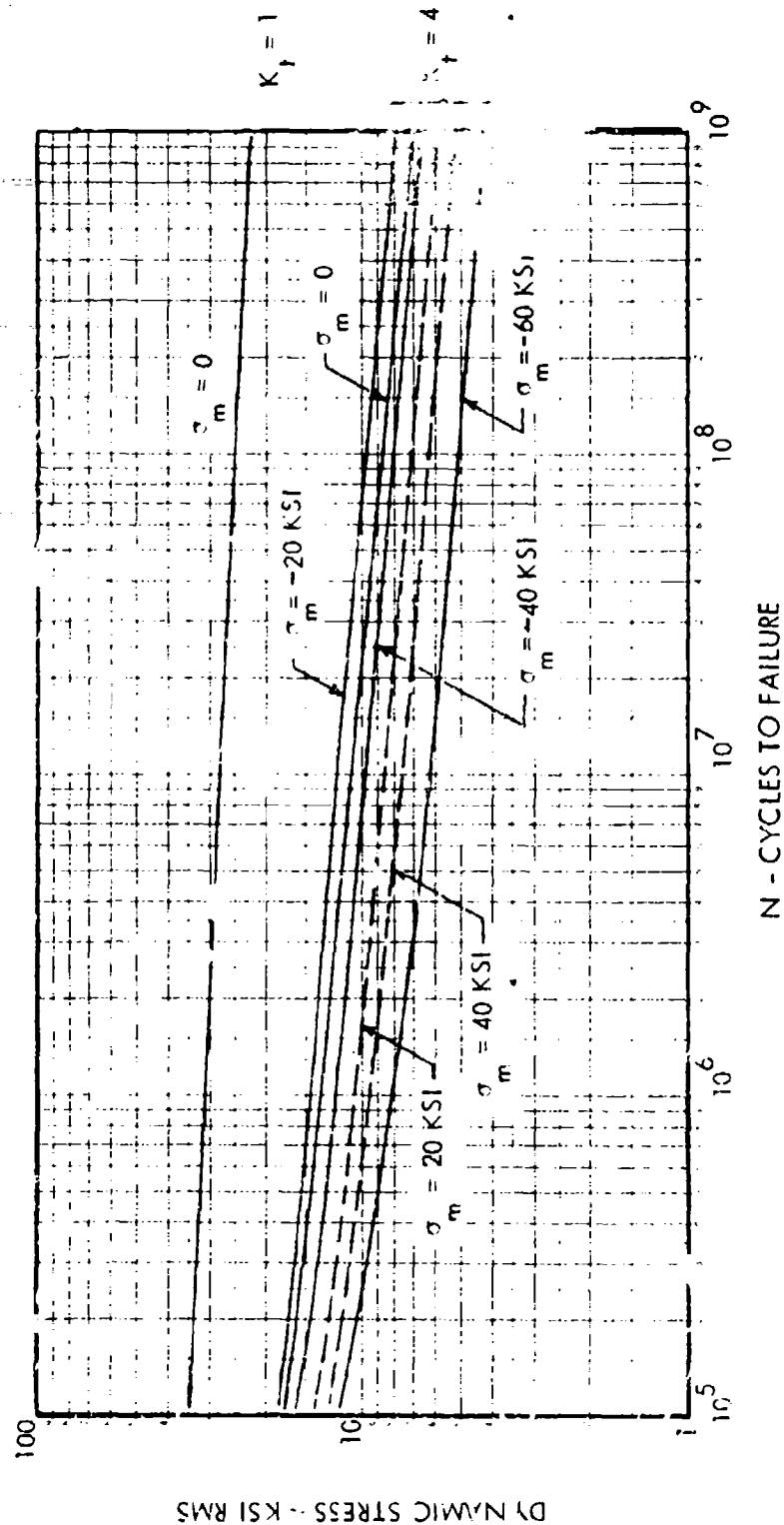
FIGURE 86. RANDOM LOADING FATIGUE CURVE FOR PH15-7Mo STAINLESS STEEL AT 500°F

131

The skin critical buckling temperature is found from Figure 78 as $T_c = 50°F$. Then $r = 420/50 = 8.4$ and the buckling amplitude i $W_o = 0.240$ inch, from Figure 79.

The thermal stresses at the midpoints of the two sides are found from Figures 80 through 82, or

$$\sigma_T = -100 \text{ ksi}$$

$$\sigma_{x_b} = 75 \text{ ksi}; \quad \sigma_{y_b} = 40 \text{ ksi}$$

then

$$\sigma_x = \sigma_T + \sigma_{x_b} = -100 + 75 = -25 \text{ ksi}$$

$$\sigma_y = \sigma_T + \sigma_{y_b} = -100 + 40 = -60 \text{ ksi}$$

The ambient temperature fundamental frequency is $f_o = 260$ Hz from Figure 83. From Figure 84 the frequency ratio corresponding to a temperature ratio of 8.4 is 1.8. Then

$$f(r) = 1.8 f_o = 468 \text{ Hz}$$

The dynamic stresses are then

$$\tilde{\sigma}_x = 3.60 \times 10^{-4} \left[\frac{18}{.05}\right]^2 \left[\frac{2.9 \times 10^{-2}}{29.33}\right] \left[\frac{468}{.016}\right]^{1/2} = 7.89 \text{ ksi}_{rms}$$

$$\tilde{\sigma}_y = 13.0 \times 10^{-4} \left[\frac{6}{.05}\right]^2 \left[\frac{2.9 \times 10^{-2}}{29.33}\right] \left[\frac{468}{.016}\right]^{1/2} = 3.17 \text{ ksi}_{rms}$$

The value of $\Phi(f) = 2.9 \times 10^{-2}$ is the acoustic pressure density corresponding to 140 dB, while AR = 29.33 is the aspect ratio parameter.

Enter the fatigue curve of Figure 86 ($K_t = 4$) with the dynamic stress $\tilde{\sigma}_x = 7.89$ ksi$_{rms}$ and thermal mean stress $\sigma_x = -25$ ksi. This combination gives a life of approximately 4.5×10^8 cycles. Using the y-direction stresses, $\tilde{\sigma}_y = 3.17$ ksi$_{rms}$ and $\sigma_y = -60$ ksi, gives a life greater than 10^{10} cycles.

At a frequency of 468 Hz the life is

$$\text{LIFE} = \frac{N}{3600f} = \frac{4.5 \times 10^8}{(3600)(468)} = 267 \text{ Hours}$$

which is greater than the 100 hour design requirement. The design can be optimized by iteration on the above procedure to decrease the skin gage or increase the stiffener spacing such that the predicted life is equal to or greater than the 100-hour design life.

8. Limitations in the Design Procedure

Application of these design procedures should be tempered with a thorough understanding of their limitations. Certain of the initial assumptions stated during the analytical development were negated by derivation of the empirical relations. However, the limits of the physical and environmental parameters tested in the experimental program then apply to these design criteria. These limitations are itemized below.

a. Physical Constraints - The bounds of the test specimen dimensions were used to establish these limitations. These should be treated only as a guide as the equations and nomographs are normally valid beyond these limits. Individual judgment must be applied in unusual cases where the constraints are drastically exceeded, particularily in the case of the design charts. The guidelines on size are:

o Panel bay width: $a = 5$ to 9 inches

o Panel bay aspect ratio: $b/a = 1.5$ to 3

o Panel skin thickness: $h = 0.024$ to 0.063 inch

b. Environmental Constraints - The acoustic environment generally has no restrictions as regards applicability of the design criteria. Spectrum levels below 120 dB will normally result in low dynamic stresses and a long fatigue life. The higher noise levels will generally result in nonlinear response, but these effects are included in the design criteria, since many of the test specimens exhibited a high degree of nonlinearity.

The thermal environment must be nearly uniform over the surface of a panel bay. The skin temperature is limited to the maximum temperature for which the alloy retains significant structural properties. The limiting temperatures are, for the alloys considered:

o 7075-T6 aluminum: 300°F maximum

o 6Al-4V annealed titanium: 600°F maximum.

The design life criteria are based only on specific nominal temperatures, requiring the use of interpolation for intermediate temperatures. Extrapolation beyond the temperature limits may be permissible to some extent if care is exercised and the further temperature degradation effects are included.

Probably the most important restriction on the design method is in the estimation of the ambient temperature and the state of the structure at this temperature. All thermal response relations are referenced to the ambient temperature and the assumption that a state of stress equilibrium exists (i.e., no mean stresses). It is impractical at this stage to give guidelines for estimating the ambient temperature state, because it is dependent on the length of time at a uniform temperature, external constraints, and other influences. It will be noted that a change in ambient temperature over a short time interval constitutes a temperature change as far as the analytical relations are concerned.

c. __External Constraints__ - The external constraints imposed on the test panels precluded significant thermal expansion of the substructure. This is considered representative of structural applications in the direct flow path of engine exhausts or other heat sources, where only localized areas of the structure are heated. The criteria can also be applied to design applications involving gradual heating of an entire structural area, where all structure expands at about the same rate. This corresponds to a relaxation of the external constraints from those considered here. In this case, the thermal buckling amplitudes and stresses given by the relations delineated herein will result in a conservative design.

It should be noted that the empirical results presented herein are applicable only for the case of simultaneously application of heat and noise. Alternate application of these environments, wherein significant thermal stress cycles are incurred, were not considered in this program.

VI - CONCLUSIONS

Design methods were developed to estimate the acoustic fatigue life of aircraft structure exposed to simultaneous noise and elevated temperatures. These design methods are applicable to flat, stiffened-skin structures fabricated of aluminum or titanium alloys. The methodology was derived through a combined analytical/experimental program, wherein the analysis served to identify parameters important to the experimental effort. Analytical results are presented for a single panel and for a multi-bay panel subjected to a spatially uniform temperature rise. This analysis covers the pre- and post-buckled states for each structural model. Coupon fatigue tests were conducted to isolate temperature degradation effects on the fatigue life of each alloy. A total of 27 aluminum and 21 titanium stiffened panels were subjected to a thermal environment and tested to failure under high intensity random noise. The data from the test program were used to modify the analytical results and to provide design equations, nomographs, and a computer program for predicting acoustic fatigue life. The following conclusions were drawn from the results of this investigation:

a.   The analytical and experimental investigation results indicate that the overall rms stress response of stiffened structure skins to acoustic excitation, at ambient or elevated temperatures, can be estimated using empirical relations based on thin plate and Miles' response theories. However, significant variance between estimated and measured stresses can be expected because of cumulative errors in predicting the excitation and response characteristics.

b.   Existing substructure design criteria[8] for ambient temperature structures are considered valid for elevated temperature applications, where the skin gages are determined from the design criteria of this report.

c.   The assumption that the substructure was thermally isolated from the skin proved adequate for establishing empirical criteria for skin thermal buckling effects. However, the analytical development should be extended to include heating of the substructure to refine the elevated temperature response characteristics.

d.   The thermal buckles experienced on certain structural designs may prove excessive for operational use; hence buckling amplitude should be a significant consideration in the design of elevated temperature structures.

e.   Structural buckling temperatures, amplitudes, and stresses can be estimated using the empirical results of this program. Since each of these parameters is based on a temperature increase relative to ambient, the confidence in the estimated thermal and dynamic response will be directly related to the accuracy of the ambient temperature predictions.

f.   The use of faying surface sealant between the skin and substructure has no discernable effect on acoustic fatigue life, at ambient or at elevated temperatures.

g.   The analyses presented for the elevated temperature dynamic response of box and curved structures in Appendices I and II are preliminary and should be used with caution until further development and verification by experimental data.

REFERENCES

1. McGowan, P. R., et. al, "Structural Design for Acoustic Fatigue," ASD-TDR-63-820, October 1963.

2. Miles, J. W., "On Structural Fatigue Under Random Loading," Journal of Aeronautical Sciences, Vol. 21, November 1954.

3. Miner, M. A., "Cumulative Damage in Fatigue," Journal of Applied Mechanics, Vol. 12, 1954.

4. Ballentine, J. R., Rudder, F. F. Mathis, J. T., and Plumblee, H. E., "Refinement of Sonic Fatigue Structural Design Criteria," AFFDL-TR-67-156, January 1968.

5. Clarkson, B. L., "Stresses in Skin Panels Subjected to Random Acoustic Loading," AFML-TR-67-199, June 1967.

6. Ballentine, J. R., Plumblee, H. E., and Schneider, C. W., "Sonic Fatigue in Combined Environment," AFFDL-TDR-66-7, May 1966.

7. Rudder, F. F., Jr., "A Study of Effects of Design Details on Structural Response to Acoustic Excitation," NASA CR-1959, 1971.

8. Rudder, F. F., "Acoustic Fatigue of Aircraft Structural Component Assemblies," AFFDL-TR-71-107, September 1971.

9. Nelson, T. F., "An Investigation of the Effects of Surrounding Structure on Sonic Fatigue," NASA CR-1536, May 1970.

10. Timoshenko, S. P. and Gere, J. M., Theory of Elastic Stability, McGraw-Hill Book Company, Second Edition, 1961, pp 394-408.

11. Shulman, Y., "On the Vibration of Thermally Stressed Plates in the Pre-Buckling and Post-Buckling States," M.I.T. Tech Report 25-25, January 1958.

12. Timoshenko, S. P., and Woinowsky-Krieger, S., Theory of Plates and Shells, McGraw-Hill Book Company, Second Edition, 1958, pp 415-428.

13. Langhaar, H. L., Energy Methods in Applied Mechanics, John Wiley and Sons, Inc., 1962, pp 159-164.

14. Thompson, W. T., Vibration Theory and Applications, Prentice-Hall, Inc., 1965, p. 74.

15. Schneider, C. W., "Development of an Empirical Method for Calculating Dynamic Stresses in Flat Elastic Panels," Lockheed-Georgia Company Report ER-9702, Dec. 1967.

16.   Jacobs, L. D., and Lagerquist, D. R., "Finite-Element Analysis of Complex Panel Response to Random Loads," AFFDL-TR-68-44, April 1968.

17.   Anon., "Metallic Materials and Elements for Aerospace Vehicle Structures," MIL-HDBK-5B, September 1971.

18.   Szechenyi, E., "Approximate Methods for the Determination of the Natural Frequencies of Stiffened and Curved Plates," J. Sound Vib., 14, No. 3, 8 February 1971, pp. 401-418.

19.   Petyt, M., "Vibration of Curved Plates," J. Sound Vib., Vol. 15, No. 3, 8 April 1971, pp. 381-396.

20.   Anon., "Aerospace Structural Metals Handbook," AFFML-TR-68-115.

APPENDIX I

VIBRATION ANALYSIS OF NINE-CELL BOX STRUCTURE AT ELEVATED TEMPERATURES

The simple panel analysis described in Section II is based on the assumption that the temperature distribution over the panel is uniform and in a steady state. Based on these assumptions, the application of the simple panel theory to a flat, stiffened, nine-bay panel structure was presented. For the nine-bay stiffened panel, the assumption of a uniform temperature distribution may not be too restrictive, but if the same assumption is applied to a box structure configuration, the results may be considered unrealistic.

As was shown in the nine-bay panel analysis, this assumption of a uniform temperature distribution implies that thermal equilibrium exists at each temperature considered. That is, either the stiffeners experience the same temperature rise as the cover sheet, or the stiffeners are insulated from the cover sheet so that no heat conduction can occur. Since this analysis did not consider a thermal stress in the stiffeners, the assumption of a uniform temperature distribution in the cover sheet for the nine-bay stiffened panel, as applied in Section II, implies that the stiffeners are insulated from the cover sheet and that thermal radiation from the cover sheet to the stiffeners can be ignored in the analysis. Since the stiffeners do not present a large surface area when compared to the cover sheet area, and since the temperature range considered is rather low (less than $600^\circ F$), neglecting the thermal radiation effects for the stiffened nine-bay panel may be justified. The effect of these assumptions as applied to the nine-cell box structure will now be briefly discussed. This analysis is presented only as a beginning point for this complex structure; no experimental effort has been devoted to elevated temperature fatigue testing of nine-cell box structures.

Consider the nine-cell box structure configuration as illustrated in Figure I-1. For this configuration, the two cover sheets (located in the planes $z = 0$ and $z = h_1$) are of equal surface area, and the surface areas of the ribs are of the same order of magnitude as the areas of the cover sheets. It can thus be supposed that thermal radiation from one element to another will be significant in determining the temperature of the element. Also, it is evident that if the two cover sheets are maintained at different temperatures the ribs will not experience a uniform temperature distribution unless the ribs are insulated from the cover sheets.

The analysis of the uniformly heated, simply supported panel will now be used to obtain an estimate of the response frequency of the box structure when subjected to a temperature distribution such that the cover sheets and the ribs are each maintained at a specified uniform temperature. The assumed temperature distribution and the dimensions of the components are illustrated in Figure I-1.

As discussed in Reference 8, three mode numbers are required to describe the vibration of a box structure. The mode numbers are denoted by the nomenclature (m, n, p), where (m,n) are the mode numbers for the cover sheets in the x and y directions, respectively, and p denotes the mode number of the rib across the depth of the structure.
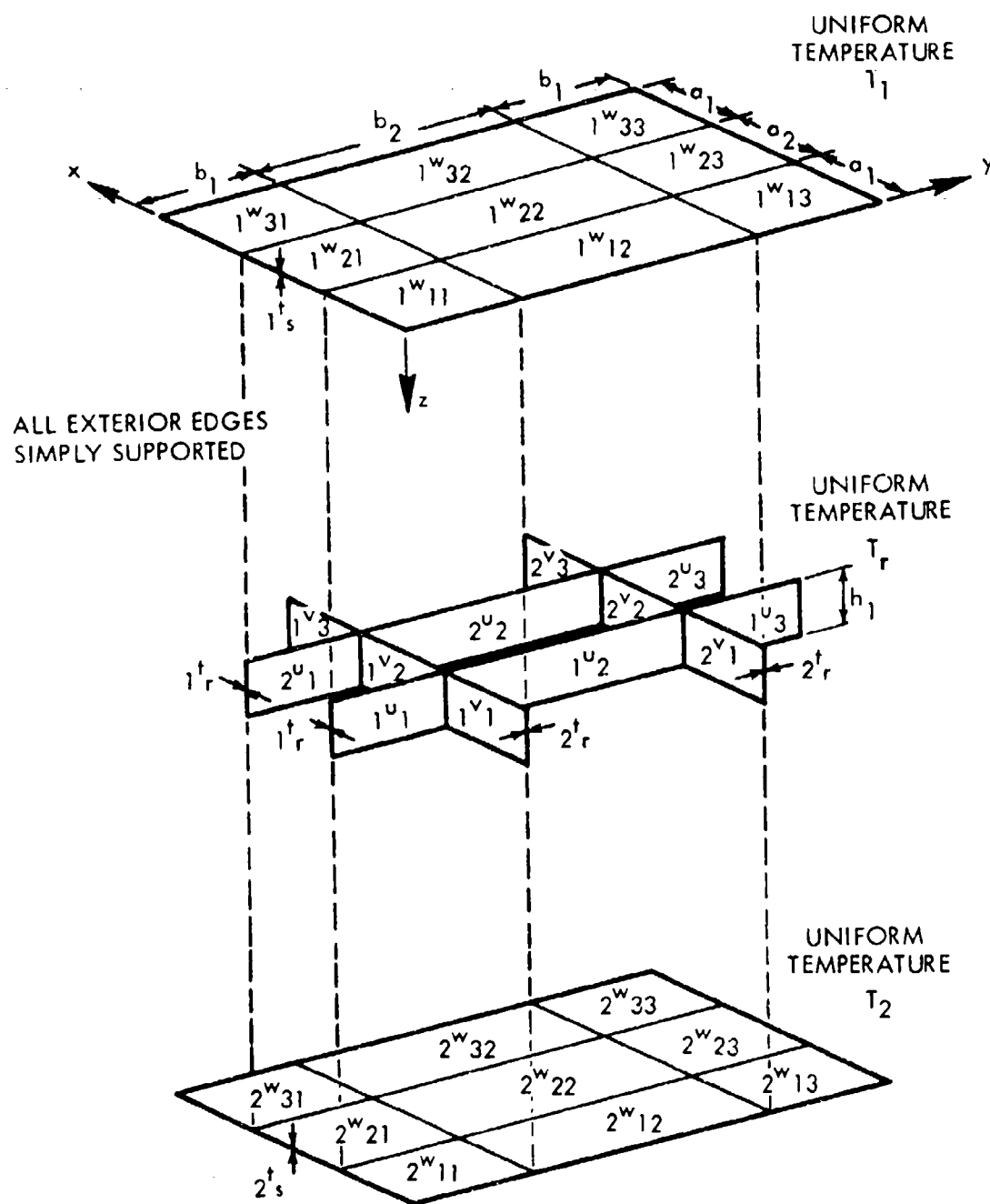
FIGURE I-1. NINE-CELL BOX STRUCTURE CONFIGURATION

Using the results of Equation (3), imposing the slope compatibility relations (Equations 43, Reference 8), and neglecting the detailed algebra, the modal mass the box structure for the (1,1,1) mode is

$$M_{111} = \gamma_1 t_s a_2 b_2 \left\{ \left[1 + \frac{2 t_s}{1 t_s} \right] M_s + 2 \left[\frac{1 t_r}{1 t_s} \right] \left[\frac{h_1}{b_2} \right]^3 M_r \right\} \qquad (1-1)$$

where

$$M_s = 1 + 2 \left(\frac{a_1}{a_2} \right)^3 + 2 \left(\frac{b_1}{b_2} \right)^3 + 4 \left(\frac{a_1 b_1}{a_2 b_2} \right)^3$$

$$M_r = 1 + 2 \left(\frac{a_1}{a_2} \right)^3 + 2 \left(\frac{2 t_r}{1 t_r} \right) \left(\frac{b_2}{a_2} \right)^3 \left[1 + 2 \left(\frac{b_1}{b_2} \right) \right]$$

Equation (1-1) represents the modal mass both below and above the critical temperature, since the mass is not dependent on temperature.

A. Pre-Buckled Frequency Response

The modal stiffness of the nine-cell structure below the critical temperature is obtained by using Equation (34a) and the slope compatibility relationships between the cover sheet bays and the rib bays. It is first assumed that all components are manufactured from the same material. As discussed previously, the uniform temperature of the cover sheet located in the plane $z = 0$ is denoted by T_1, the uniform temperature of all ribs is denoted by T_r, and the uniform temperature of the cover sheet located in the plane $z = h_1$ is denoted by T_2.

For these assumptions, the modal stiffness for the (1,1,1) mode is given as

$$K_{111} = \frac{\pi^4 \, _1 D_s}{a_2 b_2} \left\{ {}_1 K_s + \left(\frac{2 t_s}{1 t_s} \right)^3 \, {}_2 K_s + 2 \left(\frac{1 t_r}{1 t_s} \right)^3 \left[{}_1 K_r + \left(\frac{2 t_r}{1 t_r} \right)^3 \, {}_2 K_r \right] \right\} \qquad (0 \le r \le r_0) \quad (1-2)$$

where the terms are defined in Table I-I. It should be noted that the temperature rise, r, as defined in Equation (1-2) and Table I-I, is the ratio of the temperature rise of an individual component to the critical temperature of the center bay of the cover sheet located in the plane $z = 0$. That is, the critical temperature for the entire structure is defined by the buckling temperature of the center bay of the cover sheet located in the plane $z = 0$, whether or not this happens to be the lowest buckling temperature of all of the panel bays of the structure.

140

TABLE 1-1

TERMS APPEARING IN THE MODAL STIFFNESS EXPRESSION
EQUATION (1-2)

$$_1K_s = F_{11}^2(b_2,a_2)(1-r) + 2\left(\frac{a_1}{a_2}\right)F_{11}^2(b_2,a_1)(1-\,_2d_{12}r)$$

$$+ 2\left(\frac{b_1}{b_2}\right)F_{11}^2(b_1,a_2)(1-\,_2d_{21}r) + 4\left(\frac{a_1b_1}{a_2b_2}\right)F_{11}^2(b_1,a_1)(1-\,_2d_{11}r)$$

$$_2K_s = F_{11}^2(b_2,a_2)(1-\,_1d_{22}r) + 2\left(\frac{a_1}{a_2}\right)F_{11}^2(b_2,a_1)(1-\,_1d_{12}r)$$

$$+ 2\left(\frac{b_1}{b_2}\right)F_{11}^2(b_1,a_2)(1-\,_1d_{21}r) + 4\left(\frac{a_1b_1}{a_2b_2}\right)F_{11}^2(b_1,a_1)(1-\,_1d_{11}r)$$

$$_1K_r = \left(\frac{h}{a_2}\right)\left[F_{11}^2(h_1,b_2)(1-\,_1e_2r) + 2\left(\frac{b_1}{b_2}\right)F_{11}^2(h_1,b_1)(1-\,_1e_1r)\right]$$

$$_2K_r = \left(\frac{h}{b_2}\right)\left[F_{11}^2(h_1,a_2)(1-\,_2e_2r) + 2\left(\frac{a_1}{a_2}\right)F_{11}^2(h_1,a_1)(1-\,_2e_1r)\right]$$

$$F_{11}(b,a) = (b/a) + (a/b) \qquad\qquad _1e_i = \frac{h_1b_iF_{11}(b_2,a_2)}{a_2b_2F_{11}(h_1,b_i)}\left(\frac{_1t_s}{_1t_r}\right)^2\left(\frac{T_1}{T_r}\right)$$

$$_kd_{ij} = \frac{a_ib_jF_{11}(b_2,a_2)}{a_2b_2F_{11}(b_i,a_i)}\left(\frac{_kt_s}{_2t_s}\right)^2\left(\frac{T_k}{T_2}\right) \qquad\qquad _2e_i = \frac{h_1a_iF_{11}(b_2,a_2)}{a_2b_2F_{11}(h_1,a_i)}\left(\frac{_1t_s}{_2t_r}\right)^2\left(\frac{T_1}{T_r}\right)$$

$$r = T/T_c \qquad\qquad T_c = \frac{\pi^2\,_1t_s^2F_{11}(b_2,a_2)}{12\alpha(1+\nu)a_2b_2}$$

B. Post-Buckled Frequency Response

The analysis developed in Section II for a heated, simply supported panel above the critical temperature will now be used to derive the expression for the modal stiffness of a nine-cell box structure above the critical temperature. As for the nine-bay panel, the critical temperature, r_0, is defined as the temperature rise, r, necessary to cause the modal stiffness expression, Equation (I-2), to vanish.

For a rectangular flat panel with dimensions $a_i \times b_i$, and thickness, t, exposed to a uniform temperature distribution, T, the strain energy of the panel is expressed as

$$U_{ij} = \frac{\pi^4 D}{8 a_i b_i} \left| K^*(b_i, a_i, t, T,) q_{ij}^2(t) + R^*(b_i, a_i, t, T)_{ij} W_0 \right| \tag{I-3}$$

where

$$K^*(b_i, a_i, t, T) = F_{11}^2(b_i, a_i) \left[1 - d(a_i, b_i, t, T) r \right] + \frac{3}{4} R(b_i, a_i) \left(\frac{1 t_s}{t} \right)^2 \left(\frac{ij W_0}{1 t_s} \right)^2 \tag{I-4}$$

$$R^*(b_i, a_i, t, T) = F_{11}^2(b_i, a_i) \left[1 - d(a_i, b_i, t, T) r \right] + \frac{1}{8} R(b_i, a_i) \left(\frac{1 t_s}{t} \right)^2 \left(\frac{ij W_0}{1 t_s} \right)^2 \tag{I-5}$$

$$R(b_i, a_i) = 3 \left[(5 - \nu^2) F_{11}(b_i, a_i) - 2(5 + \nu)(1 - \nu) \right] \tag{I-6}$$

$$d(a_i, b_i, t, T) = \frac{a_i b_i F_{11}(b_2, a_2)}{a_2 b_2 F_{11}(b_i, a_i)} \left(\frac{1 t_s}{t} \right)^2 \left(\frac{T}{T_1} \right) \tag{I-7}$$

In these equations, the temperature parameter, r, is referenced to a panel with dimensions $a_2 \times b_2$ and thickness $1 t_s$ which is exposed to a uniform temperature increase T_1. Also, $ij W_0$ is the static buckled amplitude of the panel and $q_{ij}(t)$ is the dynamic amplitude of the panel ($|q_{ij}| \ll ij W_0$). In the derivation that follows, the analysis is limited to the box structure fundamental mode $(m, n, p) = (1, 1, 1)$.

Following the analysis developed in Reference 8 for box structure at ambient temperature, it is assumed that all components of the box structure are manufactured from the same material and that the structural geometry is as illustrated in Figure I-1. Using the above equations and again imposing the slope compatibility relations, the strain energy expression for the box structure for the $(1, 1, 1)$ mode is

$$U = \frac{\pi^4 D_s}{8 a_2 b_2} \left[K^{**} q^2(t) + R^{**} W_0^2 \right] \tag{I-8}$$

142

where K^{**} and R^{**} are defined in Table 1-II. In Equation (1-8), W_o is the static buckled panel amplitude and $q(t)$ is the dynamic panel amplitude of the center panel bay of the cover sheet located in the plane $z = 0$.

It is seen from Table 1-II and Equation (1-4) that the stiffness is a function of the ratio $(W_o/{}_1t_s)^2$. To determine this parameter as a function of the temperature increase T_1, or $r = T_1/T_c$, (where T_c is the critical temperature of the center bay of the cover sheet located in the plane $z = 0$) set $q(t) = 0$ in Equation (1-8) and obtain the strain energy as a function of W_o. Minimizing this result with respect to W_o gives the result

$$\frac{\partial U}{\partial W_o}\bigg|_{q_{11}(t) = 0} = \frac{\pi^4 {}_1 D_s}{8a_2 b_2} W_o \left[2R^{**} + \frac{\partial R^{**}}{\partial W_o} W_o \right] = 0 \qquad (1-9)$$

Solving Equation 1-9 for $(W_o/{}_1t_s)$ as a function of $r = T_1/T_c$, and then substituting the result into the expressions for K^{**} and R^{**} gives the strain energy expression in terms of the temperature parameter, r.

The modal stiffness is then derived by minimizing Equation 1-8 with respect to $q(t)$ so that the expression for the modal stiffness of the fundamental mode is

$$K_{111} = \frac{\pi^4 {}_1 D_s}{a_2 b_2} K^{**} \qquad (1-10)$$

where the terms $(W_o/{}_1t_s)$ appearing in K^{**} have been determined from Equation (1-9).

TABLE I-II

TERMS APPEARING IN THE STRAIN ENERGY EXPRESSION
EQUATION (I-8)

$$K^{**} = {_1}K_s^* + \left(\frac{2^t_s}{1^t_s}\right)^3 {_2}K_s^* + 2\left(\frac{1^t_r}{1^t_s}\right)^3 \left(\frac{h_1}{a_2}\right)\left[{_1}K_r^* + \left(\frac{2^t_r}{1^t_r}\right)^3 \left(\frac{a_2}{b_2}\right){_2}K_r^*\right]$$

$$R^{**} = {_1}R_s^* + \left(\frac{2^t_s}{1^t_s}\right)^3 {_2}R_s^* + 2\left(\frac{2^t_r}{1^t_s}\right)^3 \left(\frac{h_1}{a_2}\right)\left[{_1}R_r^* + \left(\frac{2^t_r}{1^t_r}\right)^3 \left(\frac{a_2}{b_2}\right){_2}R_r^*\right]$$

$$_iK_s^* = K^*(b_2, a_2, {_i}t_s, T_i) + 2\left(\frac{a_1}{a_2}\right)K^*(b_2, a_1, {_i}t_s, T_i)$$

$$+ 2\left(\frac{b_1}{b_2}\right)K^*(b_1, a_2, {_i}t_s, T_i) + 4\left(\frac{a_1 b_1}{a_2 b_2}\right)K^*(b_1, a_1, {_i}t_s, T_i)$$

$$_iR_s^* = R^*(b_2, a_1, {_i}t_s, T_i) + 2\left(\frac{a_1}{a_2}\right)R^*(b_2, a_1, {_i}t_s, T_i)$$

$$+ 2\left(\frac{b_1}{b_2}\right)R^*(b_1, a_2, {_i}t_s, T_i) + 4\left(\frac{a_1 b_1}{a_2 b_2}\right)R^*(b_1, a_1, {_i}t_s, T_i)$$

$$_1K_r^* = K^*(h_1, b_2, {_1}t_r, T_r) + 2\left(\frac{b_1}{b_2}\right)K^*(h_1, b_1, {_1}t_r, T_r)$$

$$_2K_r^* = K^*(h_1, a_2, {_2}t_r, T_r) + 2\left(\frac{a_1}{a_2}\right)K^*(h_1, a_1, {_2}t_r, T_r)$$

$$_1R_r^* = R^*(h_1, b_2, {_1}t_r, T_r) + 2\left(\frac{b_1}{b_2}\right)R^*(h_1, b_1, {_1}t_r, T_r)$$

$$_2R_r^* = R^*(h_1, a_2, {_2}t_r, T_r) + 2\left(\frac{a_1}{a_2}\right)R^*(h_1, a_1, {_2}t_r, T_r)$$

APPENDIX II

APPROXIMATE FREQUENCIES OF HEATED CYLINDRICAL PANELS

Szechenyi [18] presents an approximate technique for estimating the natural frequencies of curved panels. Szechenyi's result has been checked against analytical and experimental data presented by Petyt [19] with good agreement. The following development is based on the Reference 18 technique.

For either simply supported or clamped boundaries of the rectangular cylindrical shell illustrated in Figure II-1, Szechenyi obtains the expression for the frequency of the (m, n) mode as

$$f_{mn} = \frac{1}{2\pi} \left\{ \frac{D}{\gamma h} \left[(k_m^2 + k_n^2)^2 + \frac{h}{D} \sigma_x k_m^2 + \frac{h}{D} \sigma_y k_n^2 + \frac{12}{h^2} \frac{G^*}{r_c^2} \right] \right\}^{1/2} \quad (II-1)$$

where m is the mode number in the longitudinal direction and n is the mode number in the circumferential direction. The stresses σ_x and σ_y are the longitudinal panel edge stress and the circumferential panel edge stress, respectively.

The terms k_m, k_n and G^* depend upon the boundary conditions of the panel and are defined for simply supported edges as

$$k_m = M\pi/a \quad ; \quad G^* = \frac{(1 - \nu^2) k_m^4}{(k_m^2 + k_n^2)^2} \quad (II-2)$$

$$k_n = n\pi/b$$

For clamped edges, the factors k_m and k_n are

$$k_m = m\pi/\delta_m a \quad ; \quad k_n = n\pi/\delta_n b \quad (II-3)$$

Values of G^* can be obtained from Figure II-2, and values of δ_m and δ_n can be obtained from Figure II-3.

In terms of an internal pressure, P, and a uniform temperature rise, T, the edge stress components are

$$\sigma_x = -\frac{E\alpha T}{1-\nu}$$

$$\sigma_y = -\frac{E\alpha T}{1-\nu} + \frac{P \cdot r_c}{h} \quad (II-4)$$

145
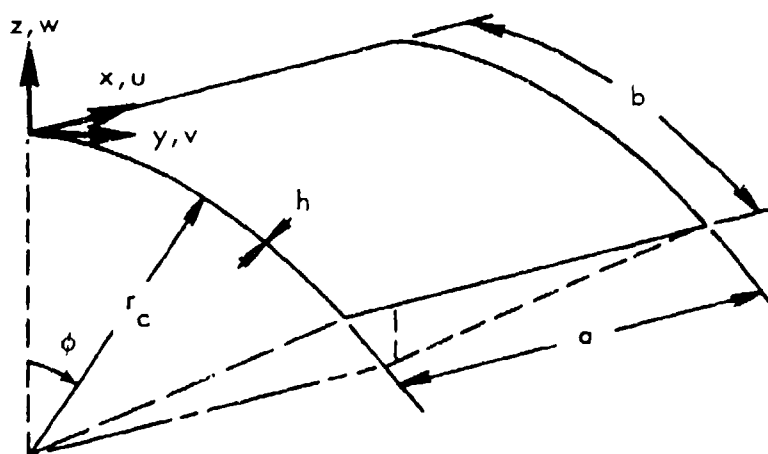
FIGURE 11-1. CYLINDRICALLY CURVED RECTANGULAR PANEL
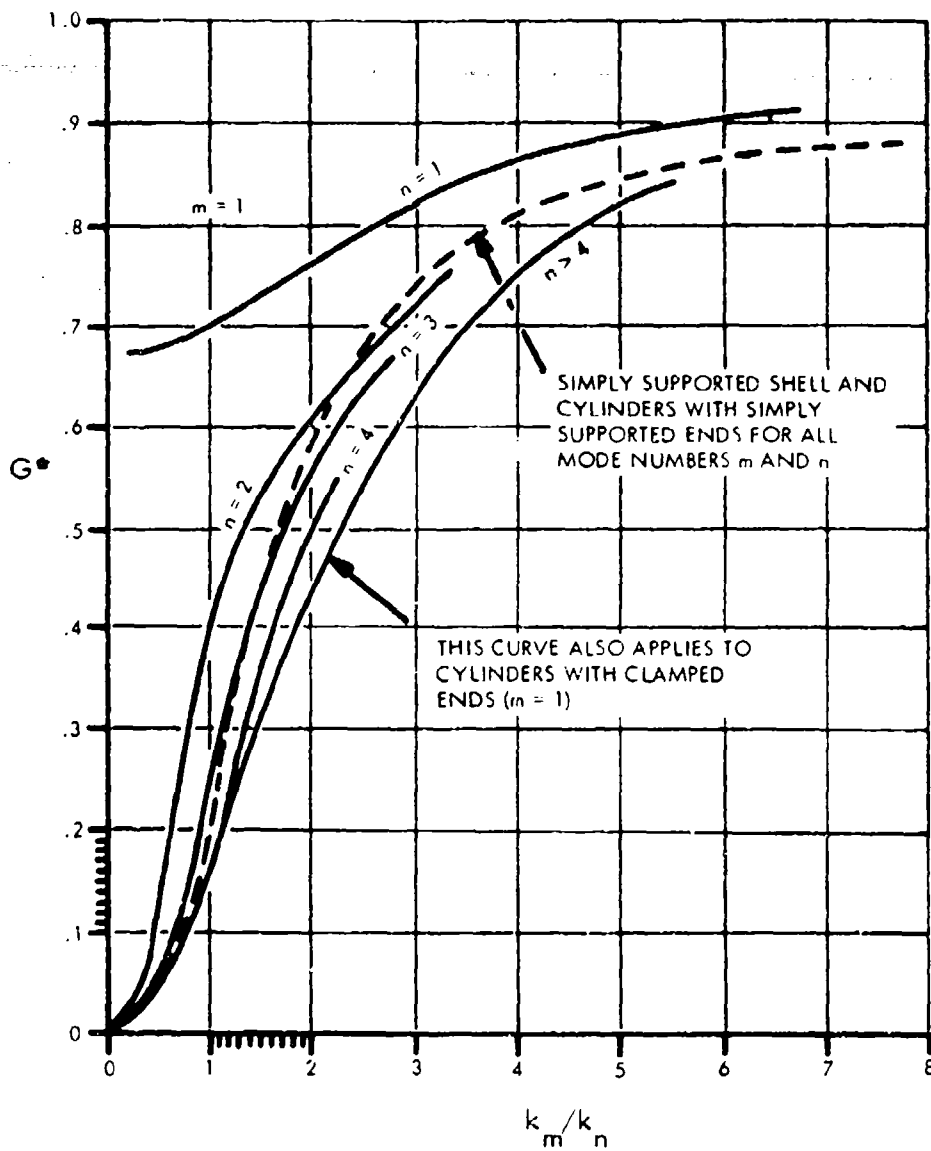
FIGURE II-2. VARIATION OF PARAMETER G* WITH RATIO k_m/k_n

δ_m
or
δ_n

1.0

.95

.90

.85

.80

.75

.70

4

3

2

MODE NUMBER = 1

0   5   10   15   20   25

$(a^2 \sigma h/D) \times 10^{-2}$
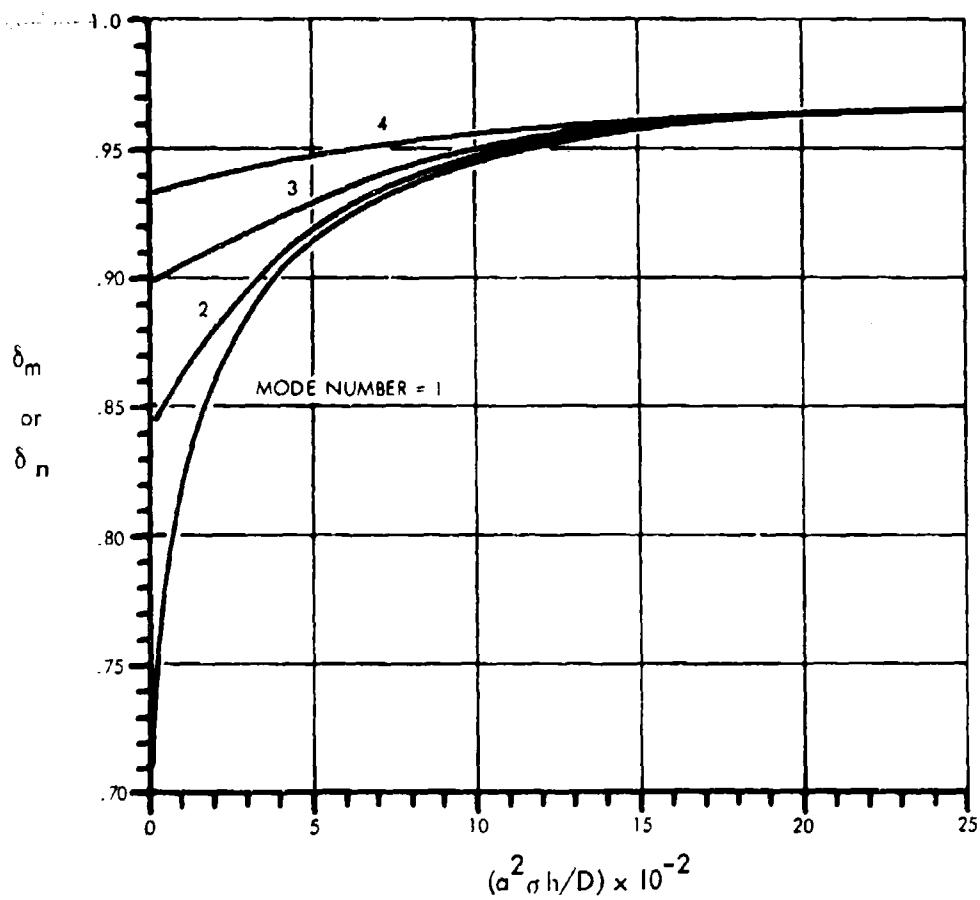
FIGURE II-3. VARIATION OF δ_m, δ_n WITH RATIO $a^2 \sigma h/D$

substituting Equations (I-4) into Equations (II-1) gives the result

$$f_{mn} = \frac{1}{2\pi} \left\{ \frac{D}{\gamma h} \left[(k_m^2 + k_n^2)^2 - \frac{E\alpha Th}{D(1-\nu)} (k_m^2 + k_n^2)^2 + \frac{Pr_c k_n^2}{D} + \frac{12G^*}{h^2 r_c^2} \right] \right\}^{1/2} \quad (II-5)$$

Setting the frequency expression given by Equation (II-5) to zero, the expression for the critical buckling temperature is then

$$T_c = \frac{12\alpha(1+\nu)}{h^2(k_m^2 + k_n^2)} \left[\frac{(Pr_c k_n^2/D) + (12\, G^*/h^2 r_c^2)}{(k_m^2 + k_n^2)^2} - 1 \right] \quad (II-6)$$

Hence, Equations (II-6) and (II-5) may be used to estimate the buckling temperature and frequency response, respectively, for curved stiffened structure. It should be emphasized that these results are tentative, since no experimental verification has yet been attempted.

APPENDIX III

TEST SPECIMEN DETAILS AND TEST INSTRUMENTATION

The stiffened panels used for the second phase of the experimental program are briefly described in Section III. That section also describes the test set-up and procedures used for each test. This appendix contains a more detailed description of the test specimens, together with schematic diagrams of the instrumentation used for each test. It supplements (rather than duplicates) the discussion in Section III.

A.   Stiffened Panel Specimens

The aluminum and titanium test panels were very similar in design, the only significant difference being in the substructure. The channel frames and zee stiffeners on the aluminum specimens were hot-rolled to a bend radius of approximately three times the thickness, whereas the titanium substructure was welded at the longitudinal corners. The general plan and edge view of the stiffened panels is presented in Figure III-1. Figures III-2 and III-3 show details of the frame and stiffener members for the aluminum and titanium specimens, respectively. The edge member used to support the test specimens in the steel test fixture is detailed in Figure III-4. The edge member shown is for the titanium specimens and was fabricated of 6Al-4V; the aluminum edge member was similar but made of 7075-T6. Only four edge members of each alloy were fabricated. They were removed from the specimens at the completion of testing and were installed on the next set of panels to be tested. Use of two sets of two edge members each allowed installation and checkout of specimens to proceed concurrent with testing.

B. Coupon Specimen Tests

The coupon fatigue testing described in Section III was accomplished using fixed end, cantilever beam test specimens. The specimen support was provided by the clamp blocks shown in Figure 8 and detailed in Figure III-5. Room temperature testing was accomplished using phenolic inserts between the specimen and the steel blocks. Elevated temperature testing used stainless steel inserts in place of the phenolic with asbestos insulation between the steel and the specimen to minimize heat flow into the clamp blocks from the test specimen.

The instrumentation set-up used for the coupon fatigue testing is shown schematically in Figure III-6. This depicts both the sinusoidal frequency input as well as the random amplitude input used for fatigue testing.

C. Stiffened Panel Tests

The test instrumentation discussed in the following subsections parallel the discussion of Section III.

150
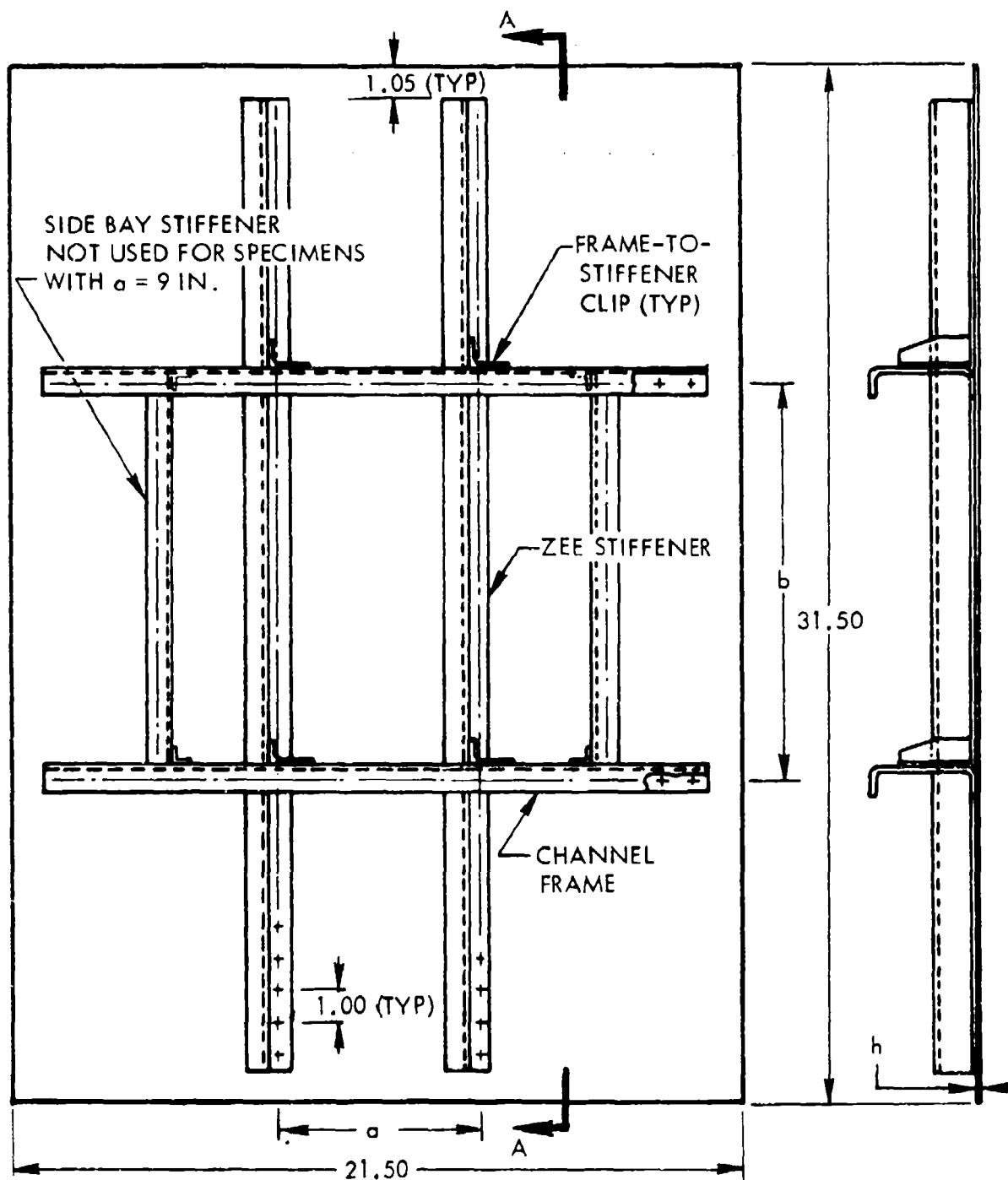
PLAN VIEW

SECTION A-A

NOTE: EDGE MEMBER OMITTED FOR CLARITY

FIGURE III-1 STIFFENED SKIN SPECIMEN CONFIGURATION

151

h_r	R
.040	.09
.050	.12
.063	.16
.071	.19
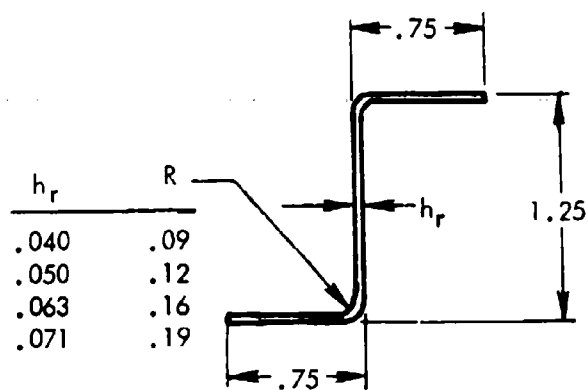
STIFFENER CROSS SECTION
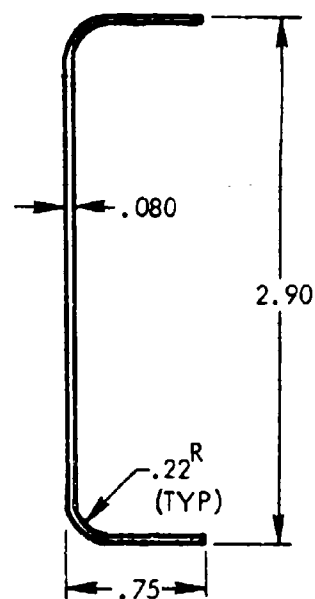
FRAME CROSS SECTION
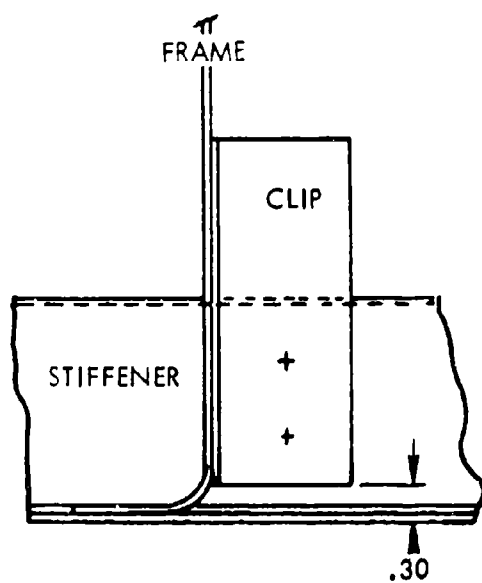
SECTION A-A
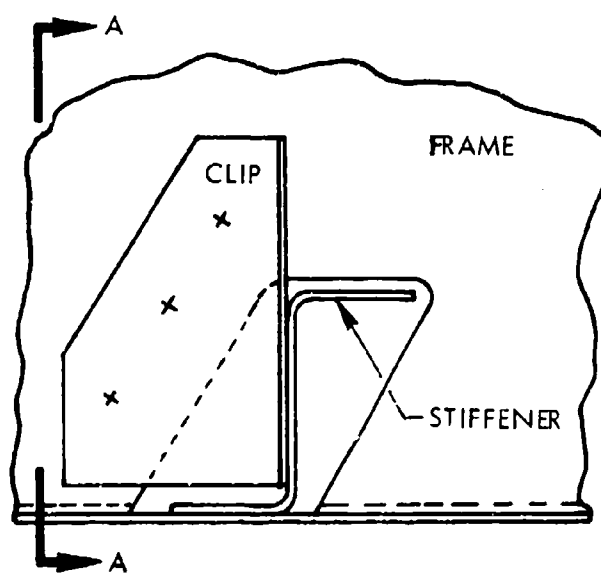
TYPICAL FRAME-STIFFENER INTERSECTION

FIGURE III-2. FRAME AND STIFFENER DETAILS
ALUMINUM SPECIMENS

152

SEAM TIG WELD (TYP)

h_r

1.25

0.75

STIFFENER CROSS SECTION

0.076

3.00

0.75

FRAME CROSS SECTION

FRAME

CLIP

STIFFENER

+

+

SECTION A-A

A

CLIP

×

×

×

FRAME

STIFFENER

A
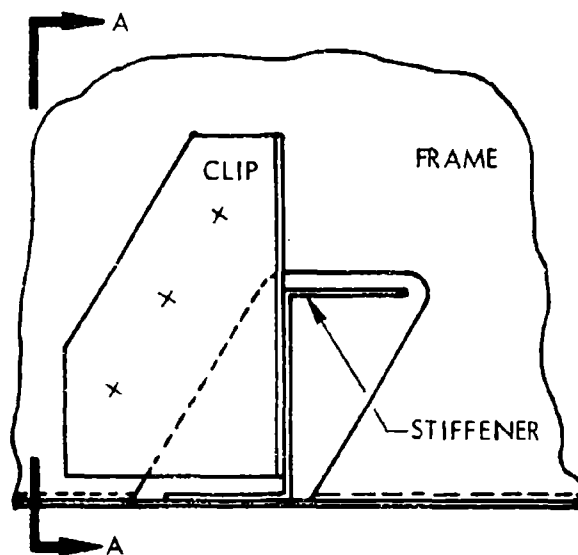
TYPICAL FRAME-STIFFENER INTERSECTION

FIGURE III-3. FRAME AND STIFFENER DETAILS
TITANIUM SPECIMENS

153
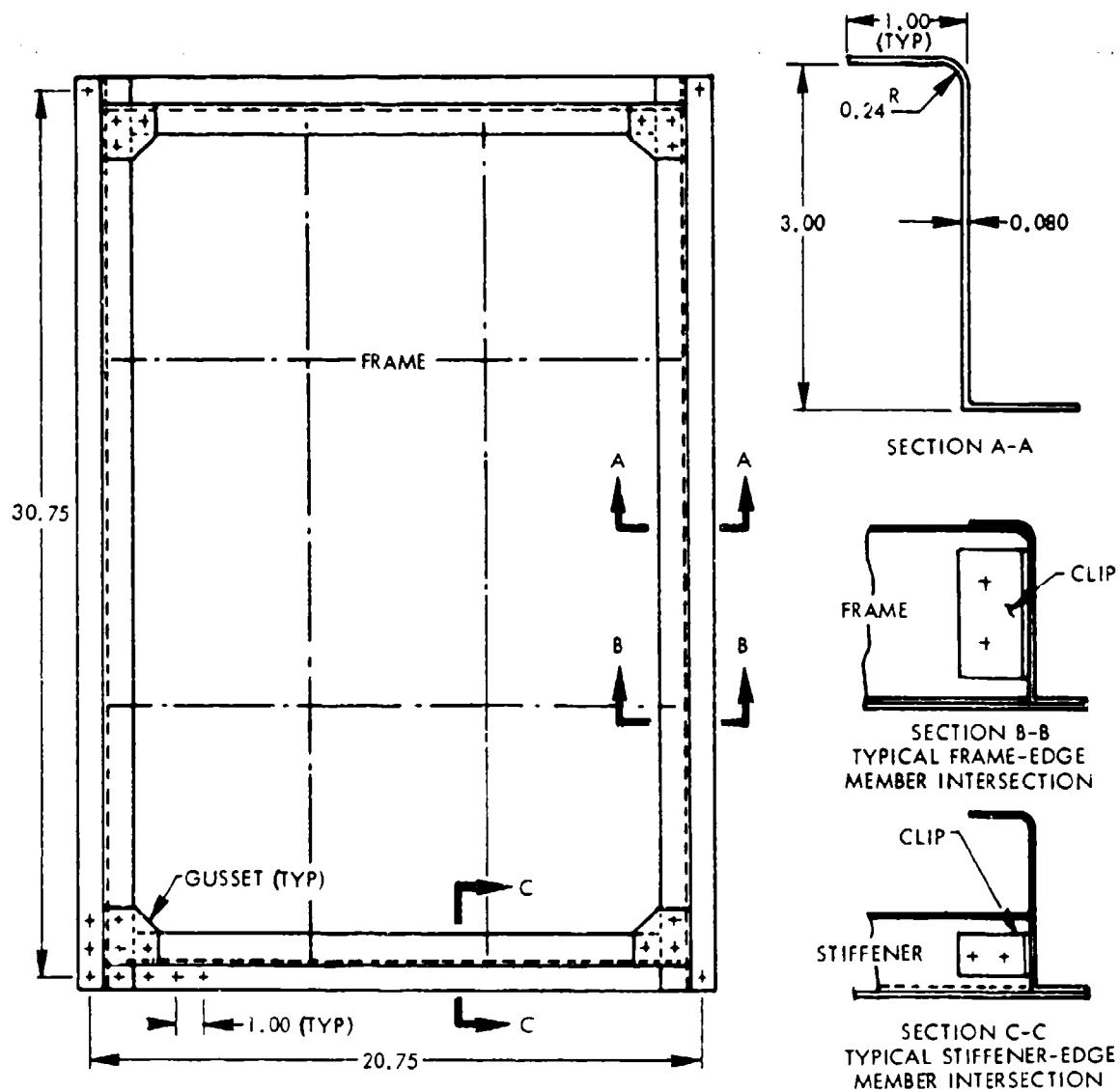
FIGURE III-4. STIFFENED PANEL EDGE MEMBER
TITANIUM SPECIMENS

154
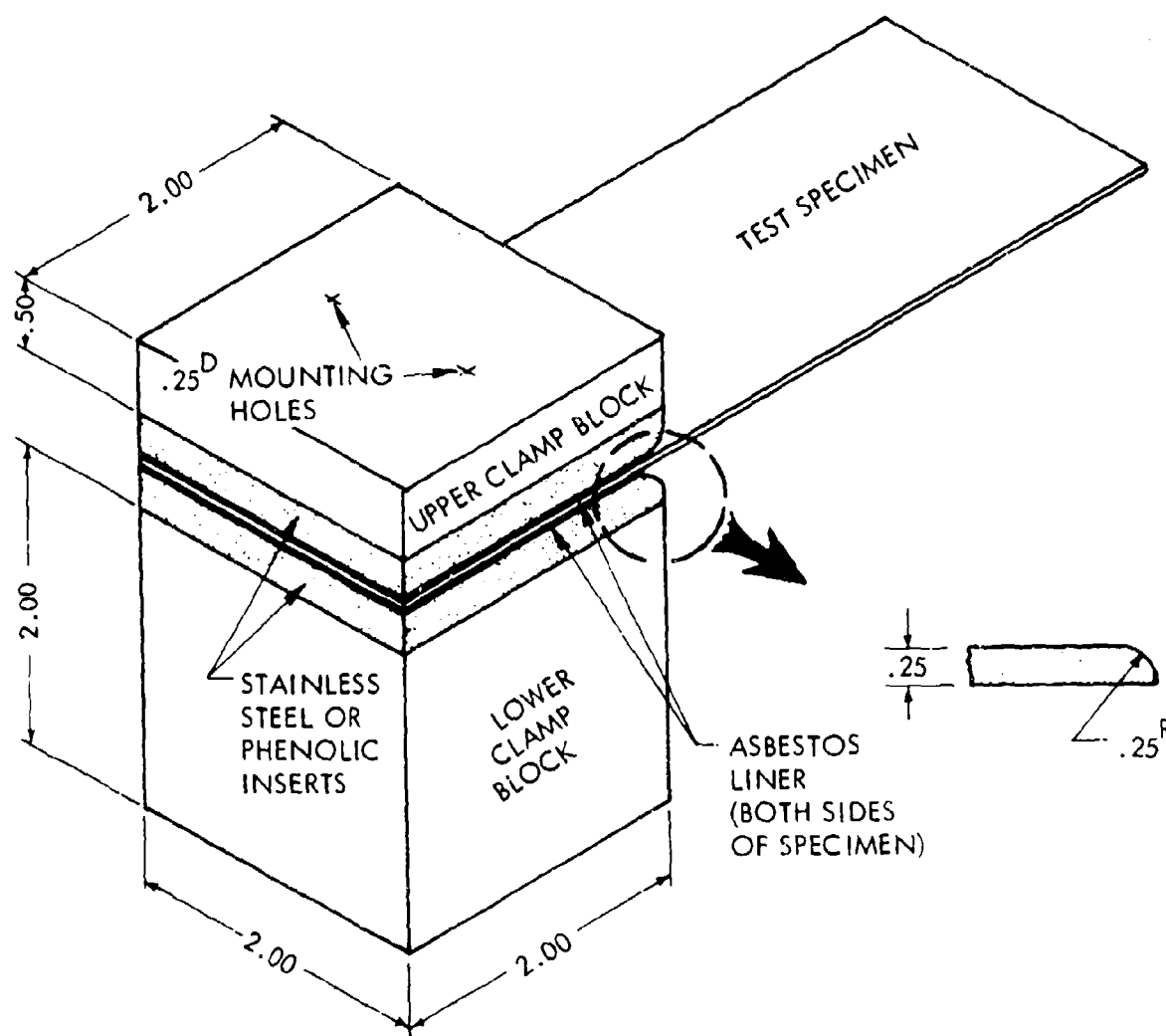
FIGURE III-5. COUPON SPECIMEN CLAMP BLOCK
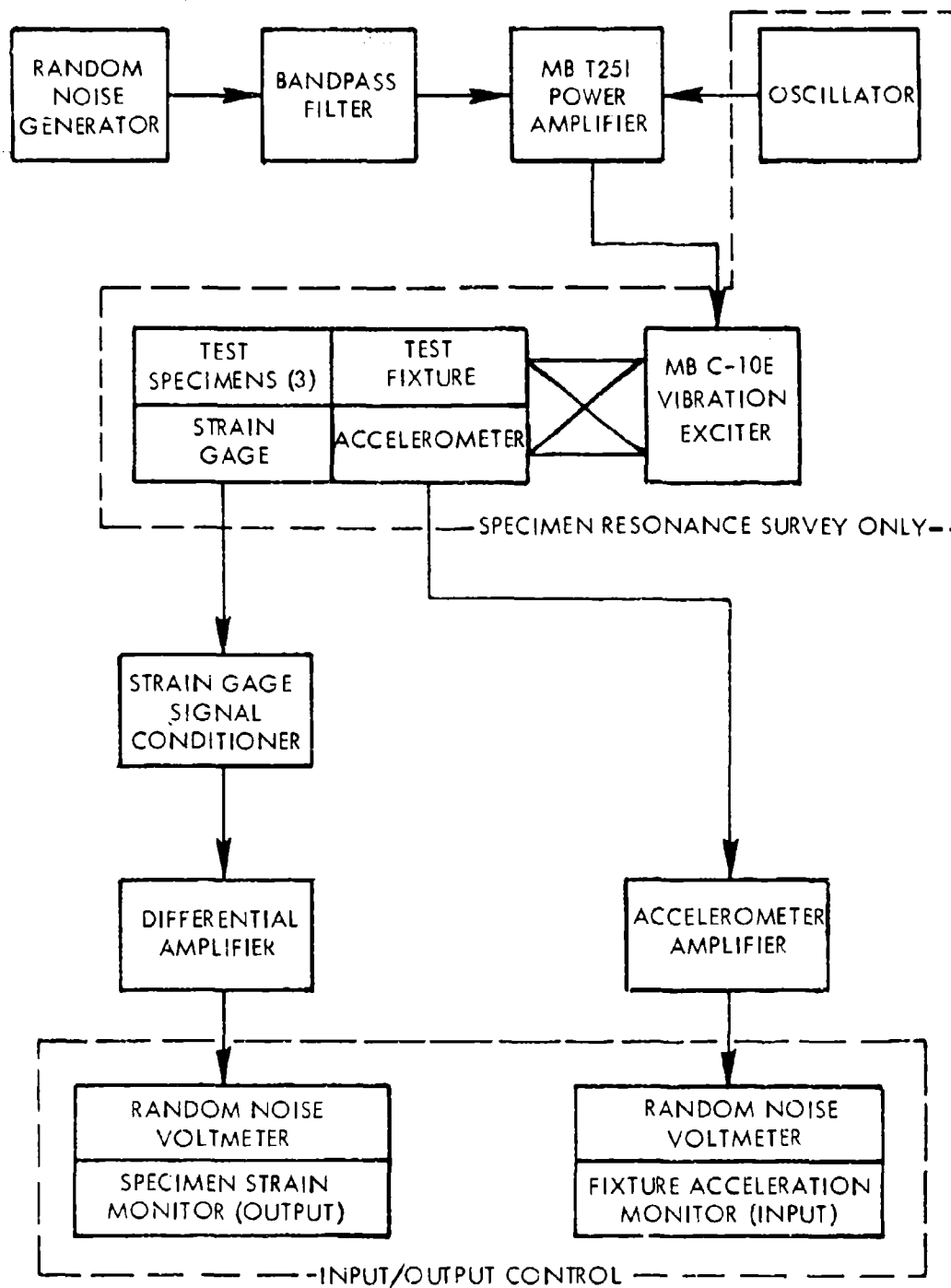
FIGURE III-6. SCHEMATIC DIAGRAM OF COUPON FATIGUE TEST

156

1.   Room Temperature Frequency

The room temperature fundamental mode frequency test set-up was shown in Figure 25.
Frequencies were determined by making sinusoidal frequency sweeps, at constant
input, and plotting the strain response. The instrumentation schematic diagram for this
is shown in Figure III-7.

2.   Temperature Effects on Frequency

The test set-up described above was also used to determine the elevated temperature
frequency response. Six heat lamps were positioned above the specimens as shown in
Figure 26 and the frequency was then manually varied to maintain a fundamental mode
response. The schematic diagram of the set-up is identical to that of Figure III-7,
except that strain response plots were not produced. Skin temperatures were manually
read from a single channel indicator.

3.   Thermal Strain and Deflection

The test set-up for these measurements is shown in Figures 27 and 28 and shown
schematically in Figure III-8. Temperatures were controlled manually and read from
a multi-channel recorder. Displacements and thermal strains corresponding to these
temperatures were manually read and recorded on data sheets.

4.   Excitation Spectrum Shaping and Fatigue Tests

The specimens were subjected to high intensity noise, and strain response plots were
produced at the desired test temperature. The schematic diagram for this test is shown
in Figure III-9. After determining the significant panel response modes, the desired
random spectrum shape was obtained using the equipment shown in the schematic diagram of
Figure III-10. This also shows the instrumentation used to record noise and strain on
magnetic tape for later analysis.

Three types of data analyses were accomplished: (a) narrow-band analyses of the noise
spectrum, (b) narrow-band analyses of the strain response, and (c) probability density
analyses of the noise and strain. The schematic diagram of the equipment necessary to
accomplish the first of those is shown in Figure III-11, while Figure III-12 shows the strain
narrow-band analysis instrumentation. The only difference in the two types of analysis
was in the log converter used for the noise analysis to obtain a dB scale. The probability
density analysis schematic diagram is shown in Figure III-13; noise and strain signals
were analyzed with the same instrumentation.
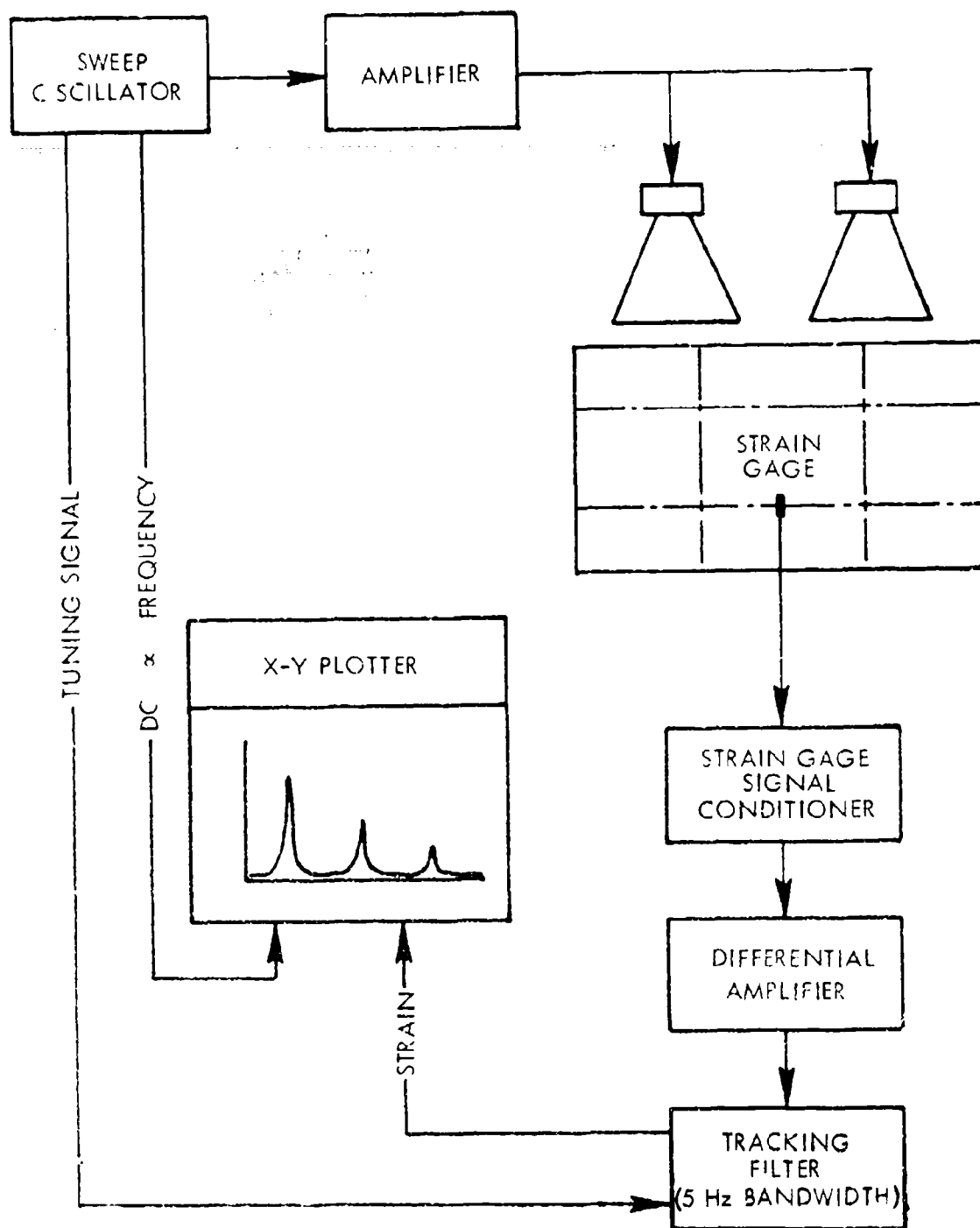
FIGURE III-7. SCHEMATIC DIAGRAM FOR STRAIN RESPONSE
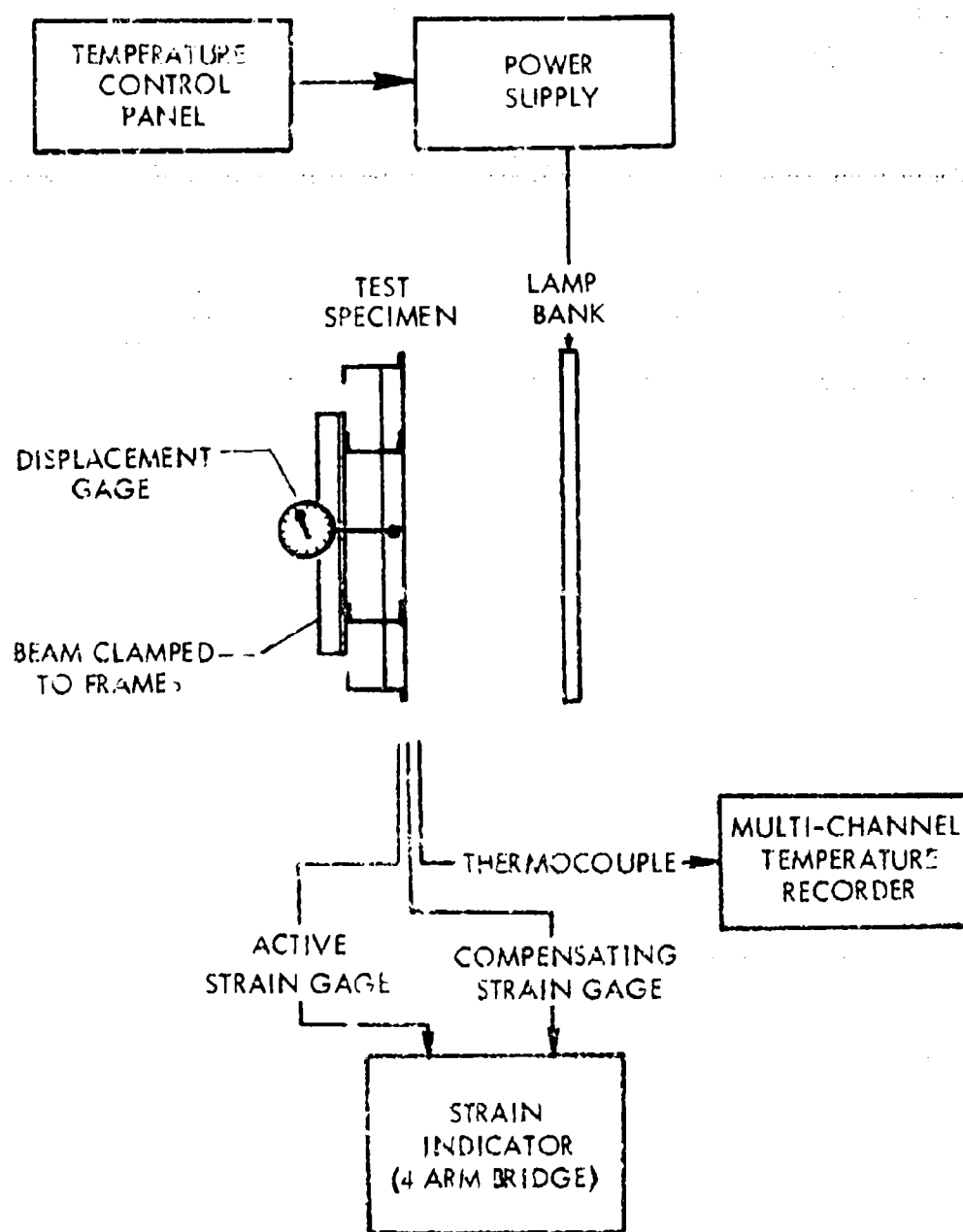
FIGURE III-8. SCHEMATIC DIAGRAM FOR THERMAL STRAIN
AND BUCKLING AMPLITUDE
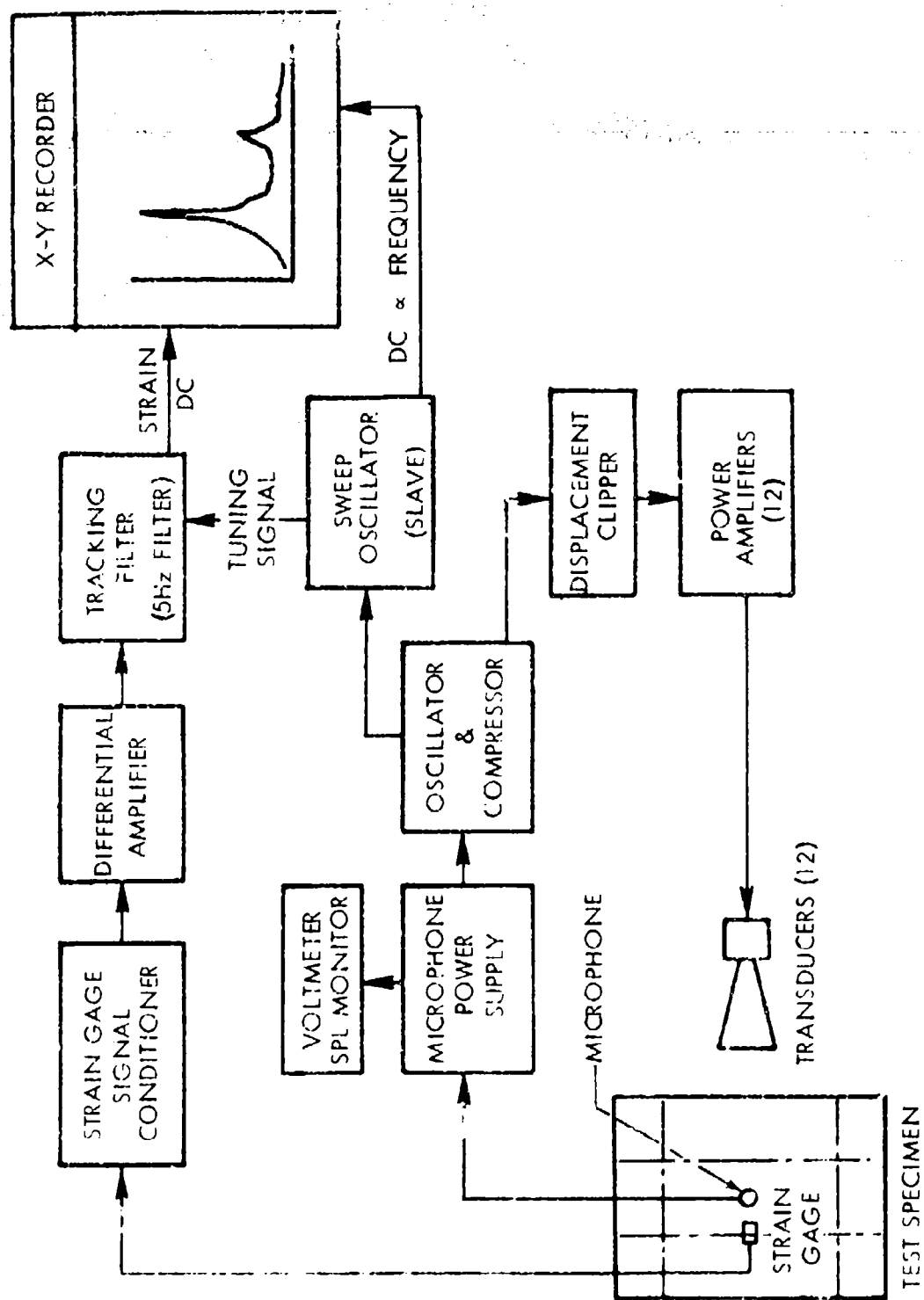
FIGURE III-9. SCHEMATIC DIAGRAM FOR HIGH INTENSITY NOISE FREQUENCY SWEEP STRAIN RESPONSE
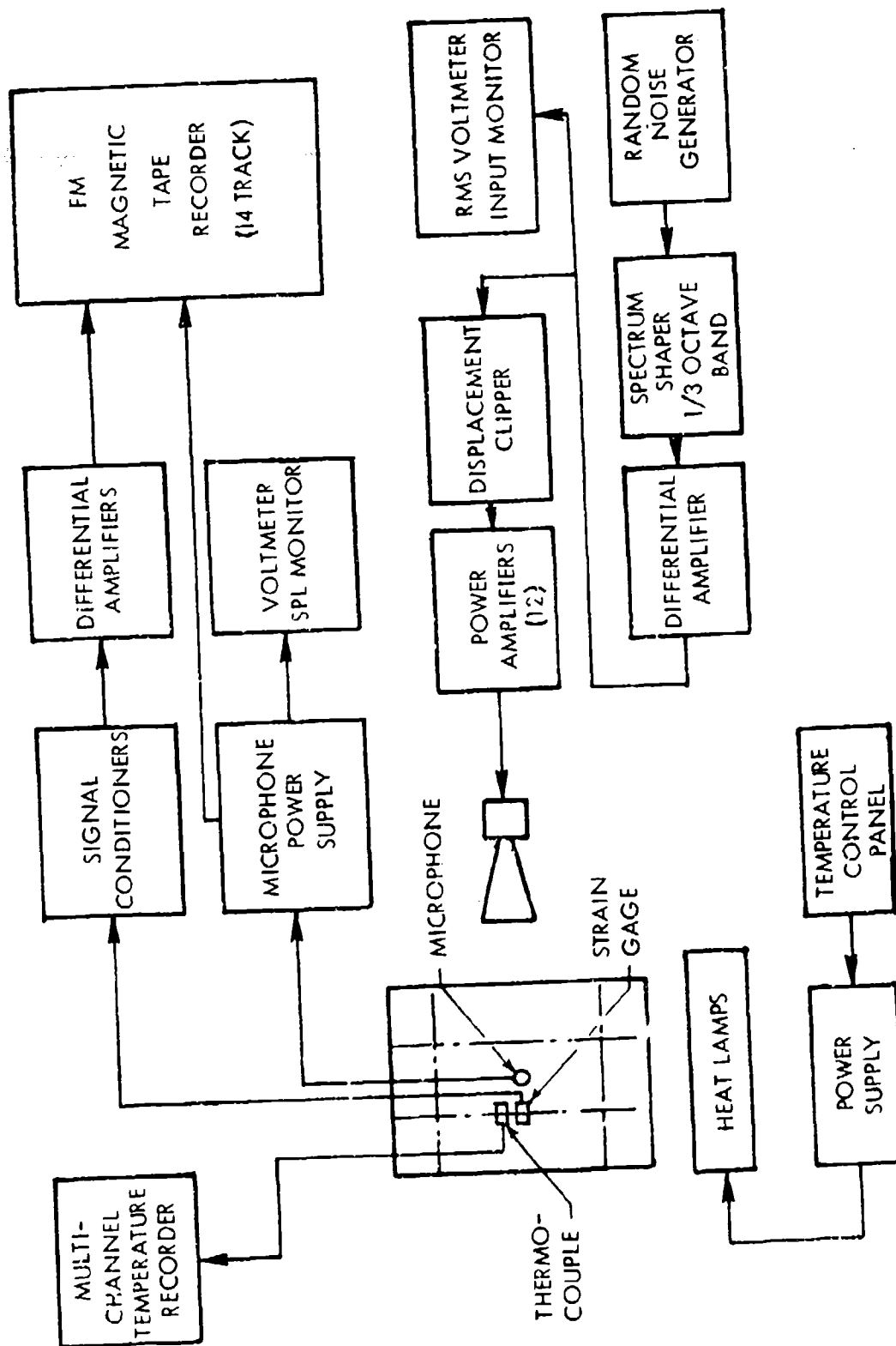
FIGURE III-10. SCHEMATIC DIAGRAM FOR RANDOM FATIGUE TEST AND DATA RECORDING
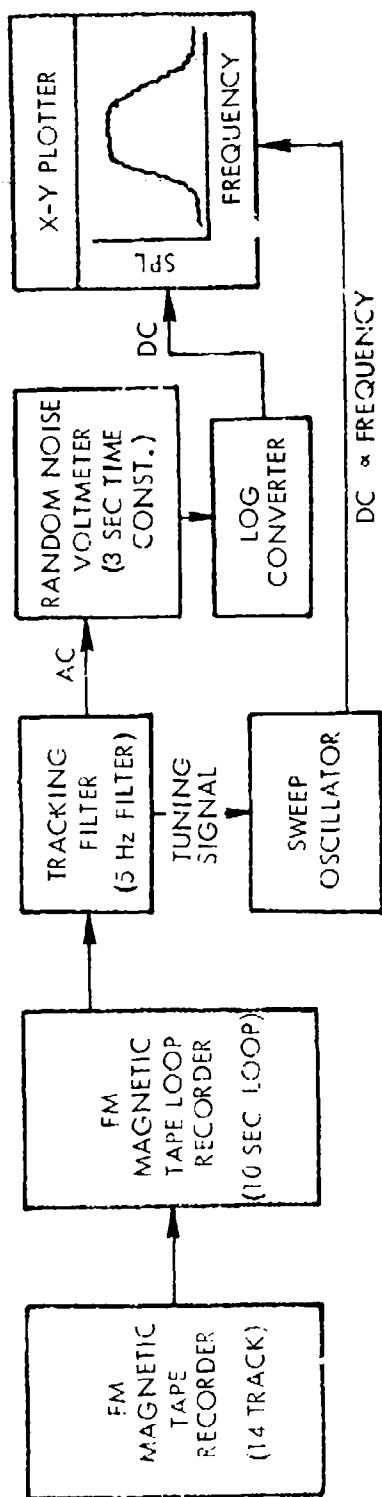
FIGURE III-11. SCHEMATIC DIAGRAM FOR NARROW-BAND ANALYSIS OF NOISE
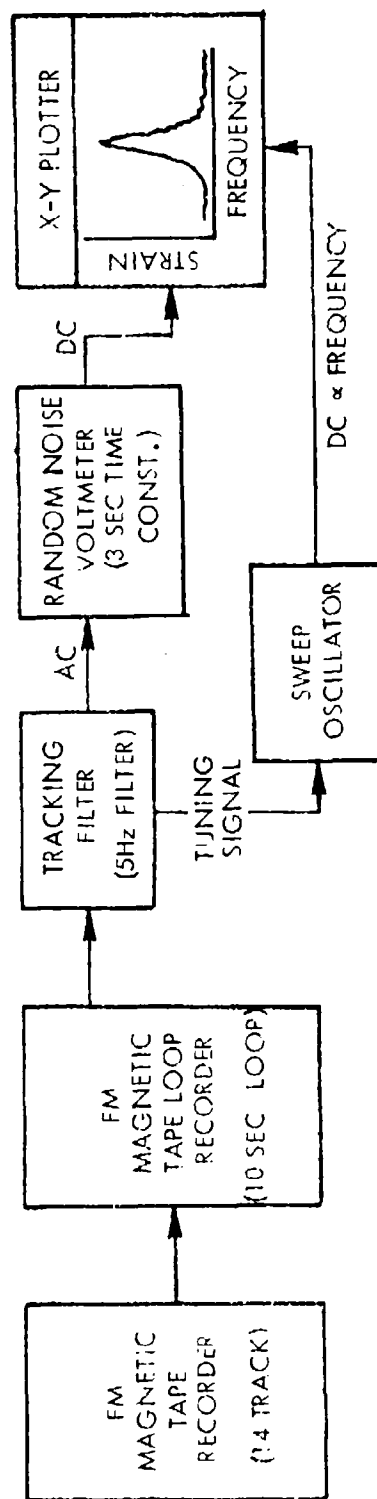
FIGURE III-12. SCHEMATIC DIAGRAM FOR NARROW-BAND ANALYSIS OF STRAIN
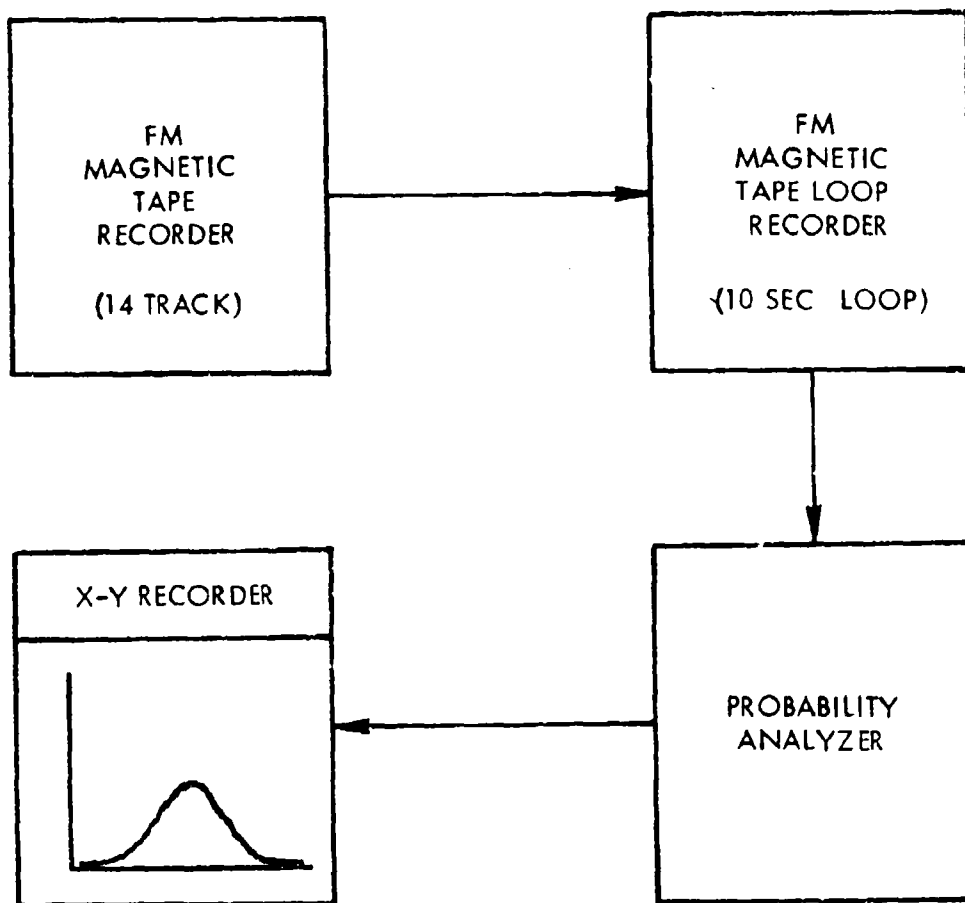
FIGURE III-13. SCHEMATIC DIAGRAM FOR PROBABILITY DENSITY ANALYSIS

CORRELATION OF EXPERIMENTAL RESULTS WITH
NINE-BAY ANALYTICAL RESULTS

The analytical section presented both a simple panel and a nine-bay panel analytical development. The results of the simple panel analysis were correlated with the test data to yield the empirical equations of Section IV and the design nomographs of Section V.

The nine-bay analytical development resulted in more complex equations which are not readily solved without the aid of a computer. The nine-bay analytical results were correlated with the experimental data, and a digital computer program was developed to simplify solution for routine design problems.

A. Room Temperature Fundamental Frequency

The room temperature fundamental mode frequency of the center bay is given by Equation (46) with $r = 0$, or

$$f_o = \frac{1}{2\pi} \left[\frac{K_1(0)}{M_1} \right]^{1/2} \tag{IV-1}$$

The mass, M_1, is the total combined mass of the skin and supporting structure, as defined by Equation (43). It was assumed for this development that the analytical mass relation was realistic, since only alloy density and specimen configuration are involved. The structural stiffness is more difficult to represent analytically; hence, the measured and calculated frequencies were correlated to provide an empirical modification of the total stiffness.

The stiffness is defined by Equation (44) which, for $r = 0$, becomes

$$K_1(0) = \frac{\pi^4 D}{4 a_2 b_2} \left[F_1^* + K_{sx} + K_{sy} \right] \tag{IV-2}$$

The parameter F_1^* represents the skin stiffness, and K_{sx} and K_{sy} represent the substructure stiffness.

The use of these equations, without modification, to calculate natural frequencies for the test specimen configurations produced frequencies 15 to 20 times higher than the measured values. Comparison of the skin and substructure terms revealed that the substructure terms were 35 to 1435 times higher than the skin stiffness terms.

A constant C_1 was, therefore, introduced into the stiffness $K_1(0)$ as follows:

$$K_1(0) = \frac{\pi^4 D}{4a_2 b_2} \left[F_1^* + \frac{K_{sx} + K_{sy}}{C_1} \right] \tag{IV-3}$$

The constant C_1 was varied from 100 to 1200, the frequencies calculated and plotted versus measured data, and standard deviation and correlation coefficient computed for each case. The constant $C_1 = 400$ was selected as the value which minimized the standard deviation (or maximized the correlation coefficient). Figure IV-1 shows the correlation of calculated and measured frequencies for $C_1 = 400$, and includes the least squares regression line (A). The approximate regression line (B), plotted through the origin and the data centroid, was selected for the empirical equation, since the differences between the two lines are insignificant. The following empirical equation for the natural frequency results:

$$f_{o_e} = \frac{1.03}{2\pi} \left[\frac{K_1(0)}{M_1} \right]^{1/2} = 0.164 \left[\frac{K_1(0)}{M_1} \right]^{1/2} \tag{IV-4}$$

where M_1 remains as defined and

$$K_1(0) = \frac{\pi^4 D}{4a_2 b_2} \left[F_1^* + .0025 (K_{sx} + K_{sy}) \right] \tag{IV-5}$$

Comparison of Figure IV-1 with the same plot for the simple panel (see Figure 71, Section IV) shows the following differences in statistical properties:

	Standard Deviation	Correlation Coefficient
Simple Panel Equation	20.69	0.915
Nine-Bay Panel Equation	27.03	0.850

Although there is a slightly greater variance in the nine-bay results, frequency calculations using either method will provide comparable predictions.

B. Buckling Amplitude

The measured buckling amplitudes were correlated with analytical buckling amplitudes given by Equation (51), or

$$\frac{W_o}{h} = \left[\frac{F_2^* r - F_1 - (K_{sx} + K_{sy})}{R^*} \right]^{1/2} \quad (r \geq r_o) \tag{IV-6}$$

From Equation (57)

$$F_1^* + K_{sx} + K_{sy} = F_2^* \ r_o$$

165
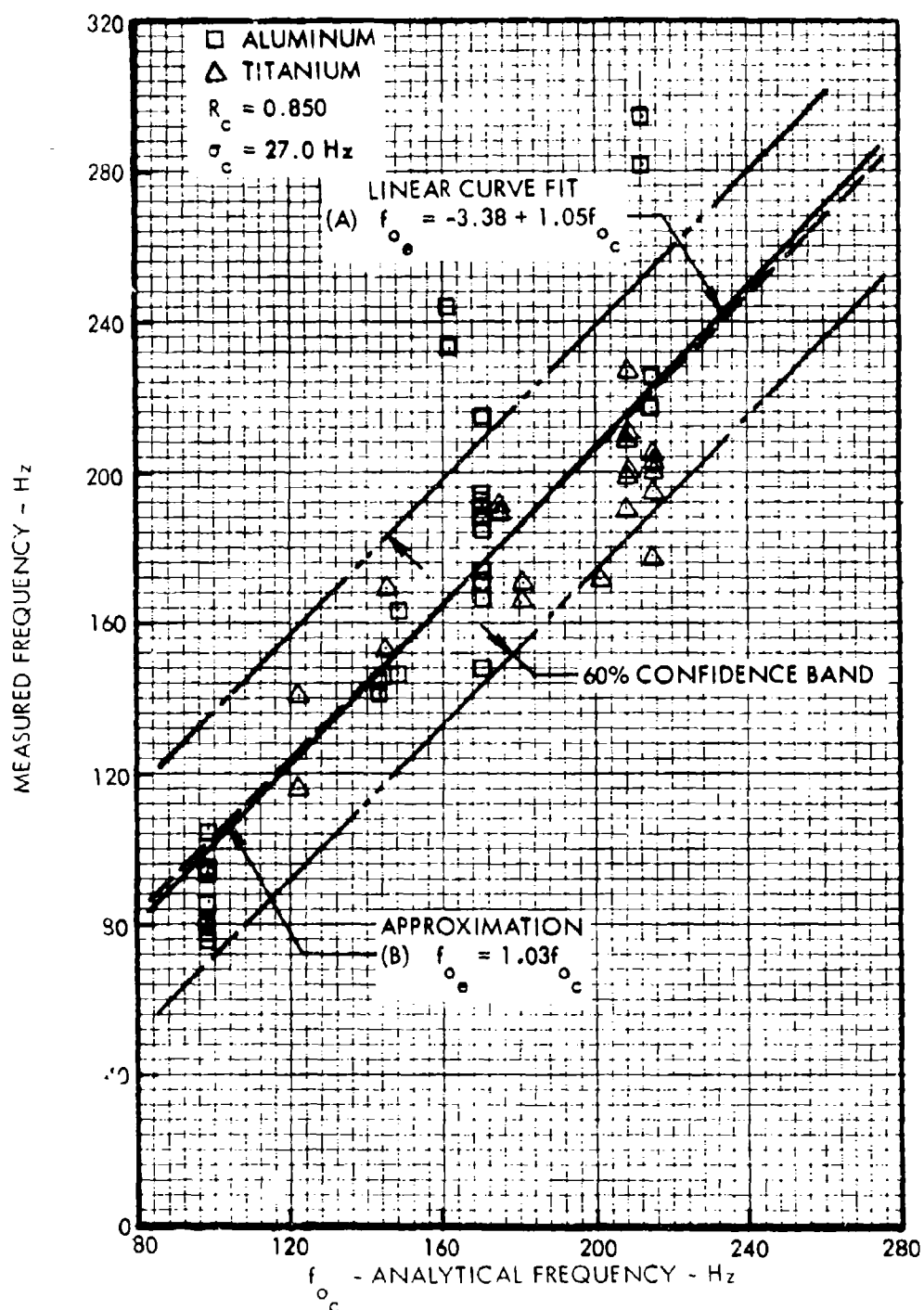
FIGURE IV-1. FUNDAMENTAL MODE FREQUENCY CORRELATION
NINE-BAY ANALYSIS, AMBIENT TEMPERATURE

166

and the buckling amplitude becomes, upon substitution,

$$\frac{W_o}{h} = 2\left[\frac{F_2^*}{R^*} \; r_o \left(\frac{r}{r_o} - 1\right)\right]^{1/2} \qquad \text{(IV-7)}$$

As defined, the term r_o is the temperature ratio at which the strain energy becomes zero. It is thus a parameter by which the simple panel buckling temperature, t_{c_s}, may be multiplied to obtain the buckling temperature, T_{c_m}, of the center bay of a multi-bay panel (where the sizes of the two panels are identical). Hence, the parameter, r, in the above equation is the temperature ratio of an equivalent simple panel. For instance,

$$T_{c_m} = r_o \, T_{c_s}$$

$$r = \frac{T}{T_{c_s}} = \frac{T}{T_{c_m}} \, r_o = r_m \, r_o$$

where r_m is the temperature ratio for the center bay of a nine-bay (or multi-bay) panel. Since the empirical expression for buckling temperature is based on multi-bay panel test data, the buckling amplitude can be redefined as

$$\frac{W_o}{h} = 2\left[\frac{F_2^* \; r_o}{R^*} \; (r_m - 1)\right]^{1/2} \qquad (r_m \geq 1) \qquad \text{(IV-8)}$$

where $r_m = \dfrac{T}{T_{c_m}}$, and T_{c_m} is given by Equation (60) or the nomograph of Figure 78.

Calculated displacement ratios were plotted versus measured displacement ratios for each panel configuration, and the slope of the regression line computed for each plot. The analytical expression dod not match the measured data for all aspect ratios; therefore, the regression line slopes were plotted versus the various parameters in the analytical equation and found to correlate best with the temperature parameter, r_o. This result, shown in Figure IV-2, revealed a trend of decreasing slope with increasing values of the parameter r_o. Both linear and exponential curve fits were plotted through the data points to determine the best analytical representation. Both equations were used to calculate the buckling amplitude, and the resulting curves were compared with the measured displacement ratios. The linear equation was found to produce the best agreement with the test data; hence, the displacement ratio for the multi-bay panel is expressed by the following empirical relation:

$$\frac{W_o}{h} = (3.37 - 0.20 \, r_o) \left[\frac{F_2^* \; r_o}{R^*} \; (r_m - 1)\right]^{1/2} \qquad (r_m \geq 1) \qquad \text{(IV-9)}$$

Unlike the simple panel results, the buckling amplitudes given by this equation are not constant for fixed aspect ratios since the parameter r_o varies with changes in substructure or skin stiffness.

167
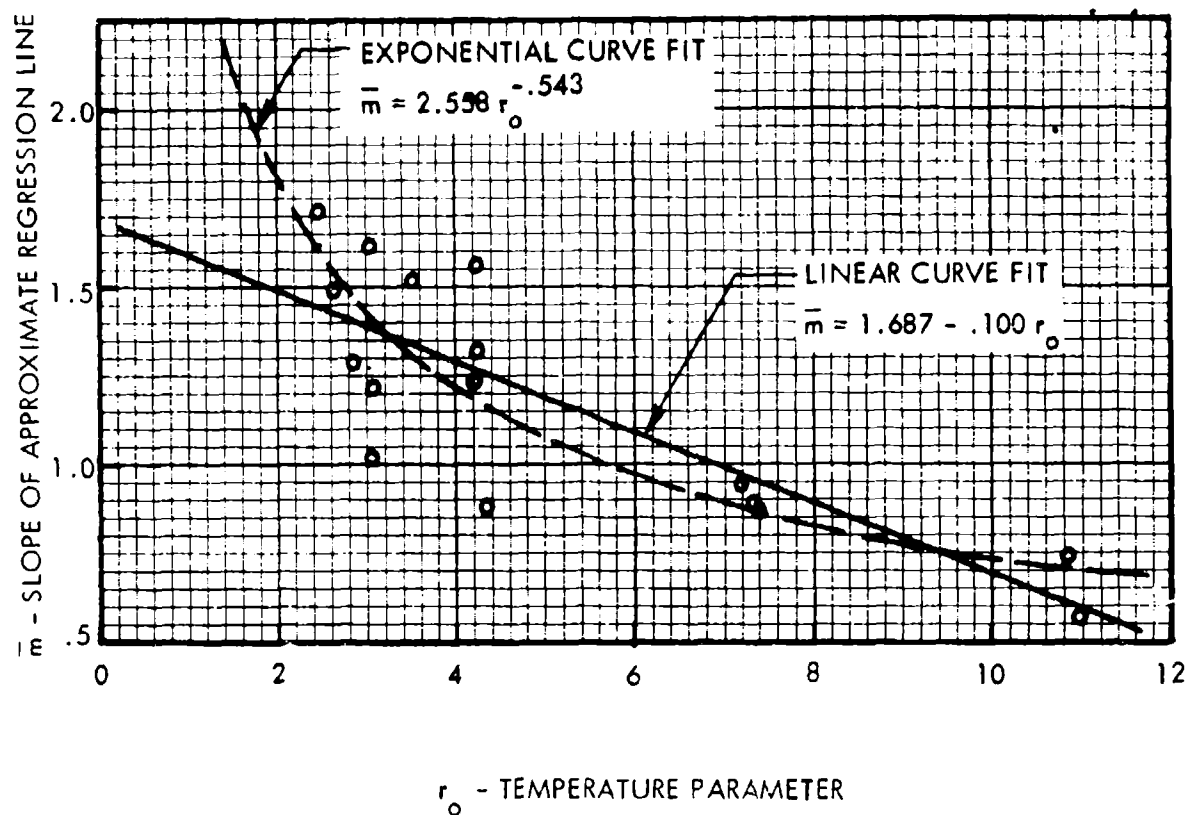
FIGURE IV-2. CONFIGURATION EFFECTS ON REGRESSION LINE SLOPE
NINE-BAY ANALYSIS

C. Thermal Stress

The thermal stresses for a multi-bay panel are defined by the same relations used for the simple panel. Since the only parameter that differs between the two forms of analysis is the buckling amplitude, thermal strains due to skin buckling were isolated for comparison with the measured data. This is identical to the correlation describe' for the simple panel in Section IV.

Measured buckling strains were plotted versus calculated buckling strains as shown in Figures IV-3 and IV-4. The data for the x-direction strains, Locations 1 and 2, were combined as shown in Figure IV-3. The slope of the approximate curve fit was used to develop the following thermal stress relations:

o   Midpoint of panel bay long side $(y = b/2)$

$$\sigma_{x_e} = - \frac{E\alpha T}{1-\nu} + \frac{0.81 \, E \, W_o^2}{a_2 b_2 (1-\nu^2)} \left[\frac{b_2}{a_2}(2-\nu^2) + \nu \frac{a_2}{b_2} \right] \qquad (IV-10)$$

o   Midpoint of panel bay short side $(x = a/2)$

$$\sigma_{y_e} = - \frac{E\alpha T}{1-\nu} + \frac{1.36 \, E \, W_o^2}{a_2 b_2 (1-\nu^2)} \left[\frac{a_2}{b_2}(2-\nu^2) + \nu \frac{b_2}{a_2} \right] \qquad (IV-11)$$

The results of this analysis compare favorably with the simple panel thermal strains presented in Section IV.

D. Elevated Temperature Frequency Response

The elevated temperature frequency response is given by Equations (59) as

$$f(r) = f_o \left[1 - \frac{r}{r_o} \right]^{1/2} \qquad (0 \le r \le r_o)$$

$$= f_o \left[2 \left(\frac{r}{r_o} - 1 \right) \right]^{1/2} \qquad (r \ge r_o)$$

As explained previously, r is the temperature ratio for an equivalent simple panel; substituting the multi-bay temperature ratio, r_m, for r gives

$$f(r) = f_o \left[1 - r_m \right]^{1/2} \qquad (0 \le r_m \le 1) \qquad (IV-12)$$

$$= f_o \left[2(r_m - 1) \right]^{1/2} \qquad (r_m \ge 1)$$

169
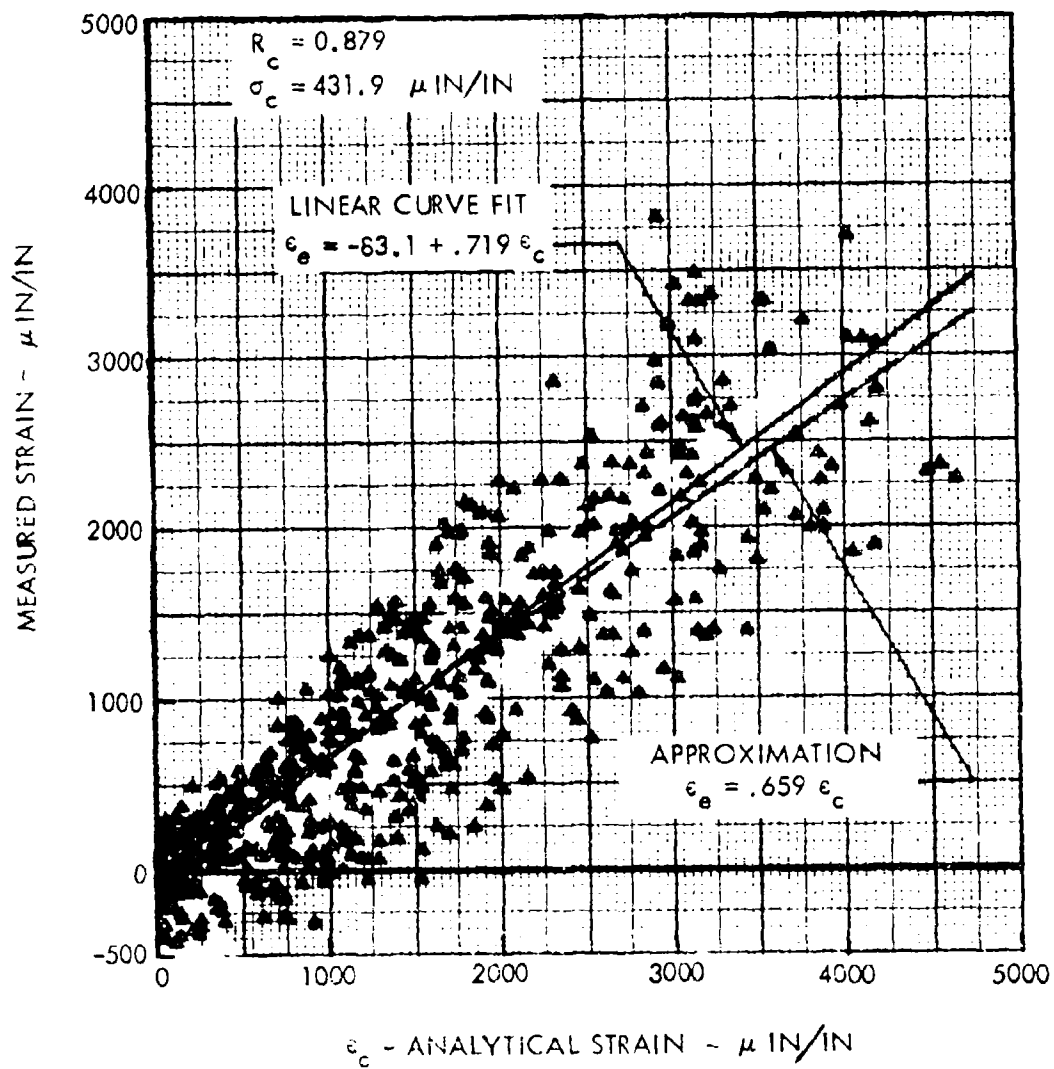
FIGURE IV-3. THERMAL BUCKLING STRAIN CORRELATION
LOCATION 1 & 2 – PANEL LONG LENGTH MIDPOINT
NINE – BAY ANALYSIS

170
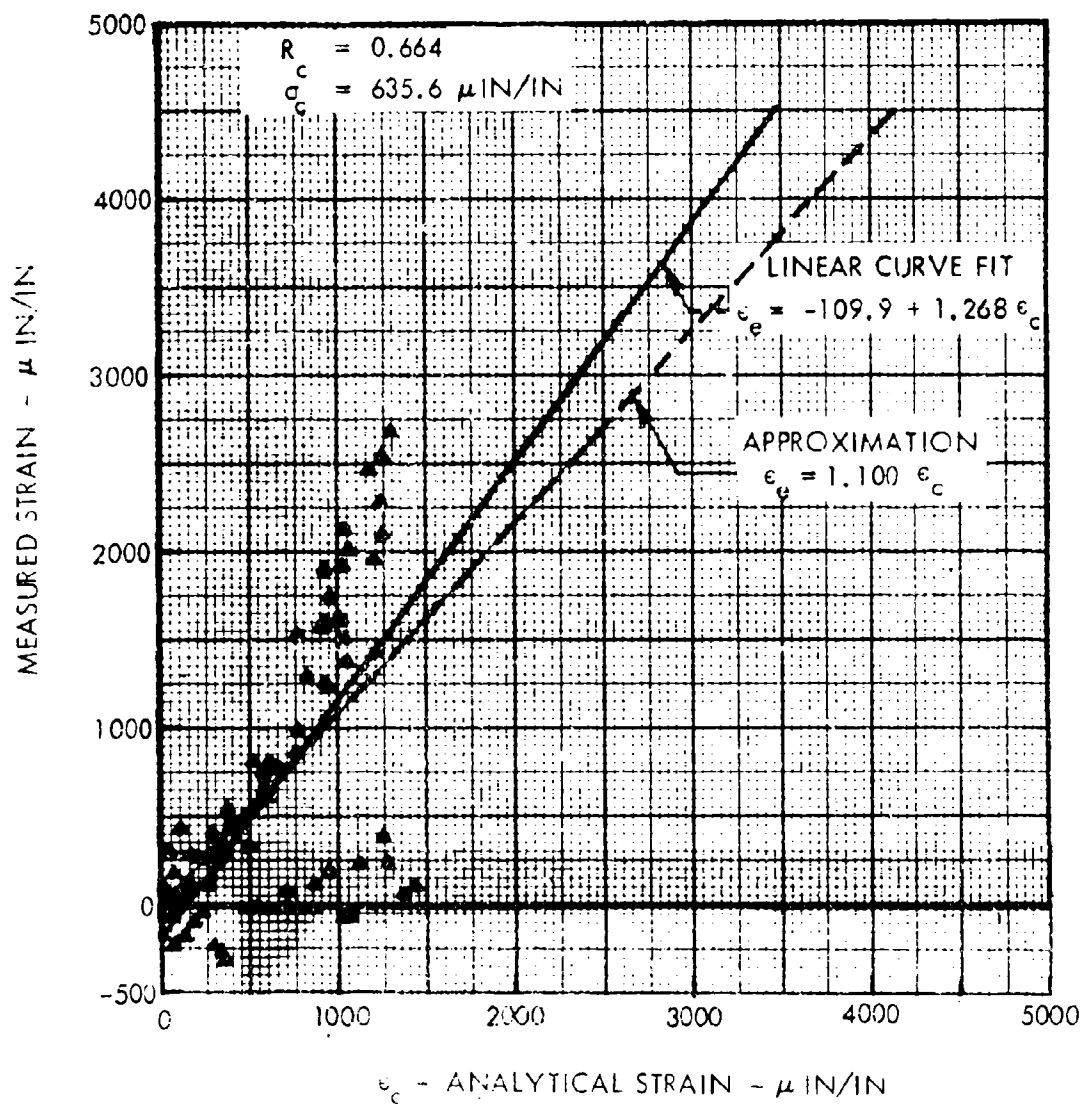
FIGURE IV-4. THERMAL BUCKLING STRAIN CORRELATION
LOCATION 3 PANEL SHORT LENGTH MIDPOINT
NINE - BAY ANALYSIS

171

These equations are identical to the simple panel analytical frequency relations given in Section II, where the temperature ratio for the multi-boy panel is now used in lieu of the temperature ratio for the simple panel; hence, the empirical equations given previously in Section IV are valid for the multi-bay panel.

E. Computer Program

Since the nine-bay panel analysis involves extensive computation, a digital computer program was developed to simplify solution. The program was developed for the Univac 1106 computer, in Fortran V; however, the program can readily be adapted to any digital computer. The input data format is shown in Table IV-I, while Table IV-II contains a definition of input parameters. The computer program is tabulated in Table IV-III and Table IV-IV shows a sample output, using specimen Al-4 data.

1. Subprograms

The following subprograms are required to run the dynamic analysis computer program:

> ETEMP (T, IFF)
>
> ALPHA (T, IFF)
>
> SN (SDYN, STEMP, TEMP, CTF, IFF)
>
> CTEMP (TCALP, TC, IFF)
>
> PROP (OPT, B, H, T, A, RJ, GAMAT, XIP)

Subprograms ETEMP, ALPHA, and SN are presented in Appendix V. Subprograms CTEMP and PROP were developed to compute skin buckling temperatures and stiffener properties, respectively, as discussed in the following subsections.

a. Subprogram CTEMP - This program computes the skin critical buckling temperature using the individual alloy curve for coefficient of thermal expansion versus temperature. The product of critical buckling temperature, T_c, and coefficient of thermal expansion, α, is calculated from Equation (60), or

$$T_c \alpha = 5.25 \frac{h^2 F_{11}}{a_2 b_2 (1 + \alpha)}$$

The program then uses a mathematical representation for α, as defined in Appendix V, to iterate for the actual value of α to be used in computing T_c. The value of T_c is then returned to the calling program.

TABLE IV-1

DYNAMIC ANALYSIS COMPUTER PROGRAM INPUT FORMAT

CARD 1

NAME	NCASE	IFF
COL(FORMAT)	1(I2)	3(I2)

CARD 2

NAME	OPTX	BX	HX	TX
COL(FORMAT)	1(I2)	3(F8.4)	11(F8.4)	19(F8.4)

CARD 3

NAME	OPTY	BY	HY	TY
COL(FORMAT)	1(I2)	3(F8.4)	11(F8.4)	19(F8.4)

CARD 4

NAME	A1	A2	B2	B1
COL.(FORMAT)	1(F8.4)	9(F8.4)	17(F8.4)	25(F8.4)

CARD 5

NAME	TS	RHO	RNU	DAMP
COL(FORMAT)	1(F8.4)	9(F8.4)	17(F8.4)	25(F8.4)

CARD 6

NAME	PSL	T
COL(FORMAT)	1(F8.4)	9(F8.4)

TABLE IV-11

DYNAMIC ANALYSIS COMPUTER PROGRAM
INPUT PARAMETER DEFINITION

NCASE	Two-digit identification number
IFF	Alloy identification code
	=1 Titanium Alloy (6A1-4V Annealed)
	=2 Aluminum Alloy (7075-T6)

OPTX	
BX	Input parameters defining stiffening member parallel to
HX	x-direction - see Subprogram PROP for definition.
TX	

OPTY	
BY	Input parameters defining stiffening member parallel to
HY	y-direction - see Subprogram PROP for definition.
TY	

A1	
A2	Panel bay dimensions
B1	
B2	

TS	Skin thickness - inch
RHO	Weight density of skin and stiffening member alloy - lb/in^3
RNU	Poisson's ratio for structure alloy.
DAMP	Damping ratio for structure.
PSL	Spectrum sound pressure level - dB.
T	Structure temperature rise - °F above ambient.

174

TABLE IV-III

COMPUTER PROGRAM FOR ELEVATED TEMPERATURE
DYNAMIC RESPONSE OF STIFFENED STRUCTURE

```
 1     C          THIS PROGRAM CALCULATES THE DYNAMIC RESPONSE OF
 2     C          A NINE-BAY FLAT STIFFENED PANEL EXPOSED TO A
 3     C          UNIFORM ACOUSTIC PRESSURE AND A UNIFORM TEMP-
 4     C          ERATURE RISE. ROOM TEMPERATURE IS 80 DEGREES F.
 5     C
 6     C          T IS A TEMPERATURE RISE, ABOVE ROOM TEMPERATURE
 7     C
 8     C          SUBPROGRAMS REQUIRED: ALPHA(T,IFF), ETEMP(T,IF),
 9     C             SN(SDYN,STEMP,T,CTF,IFF), CTEMP(TCALP,TC,IF),
10     C             AND PROP(OPT,B,H,T,A,ZJ,WC,PIM)
11     C
12     C          FUNCTION DEFINATION
13     C
14              F(B,A)=B/A+A/B
15              R(B,A,PR)=3.*((5.-PR**2)*(B/A+A/B)**2-2.*(5.+PP)
16            1               *(1.-PR))
17       200    READ(5,301)NCASE,IFF
18              READ(5,302)OPTX,BX,HX,TX
19              READ(5,302)OPTY,BY,HY,TY
20              READ(5,301)KY
21              READ(5,303)A1,A2,B2,B1
22              READ(5,303)TS,RHO,RNU,DAMP
23              READ(5,303)PSL,T
24     C        INPUT DATA FORMAT STATEMENTS
25       301    FORMAT(2I2)
26       302    FORMAT(I2,3F8.4)
27       303    FORMAT(4F8.4)
28     C            CALCULATE SUBSTRUCTURE PROPERTIES
29              CALL PROP(OPTX,BX,HX,TX,AX,YJ,WCX,XI)
30              CALL PROP(OPTY,BY,HY,TY,AY,YJ,WCY,YI)
31              H=TS
32              GM=RHO
33              PR=RNU
34     C        CALCULATE STIFFENER STIFFNESS AND MASS
35              RX1=0.05066*A1*A1*XJ/(WCX*(1.+PR))
36              RX2=0.05066*A2*A2*XJ/(WCX*(1.+PR))
37              RY1=0.05066*B1*B1*YJ/(WCY*(1.+PR))
38              RY2=0.05066*B2*B2*YJ/(WCY*(1.+PR))
39              SKX=WCX*(1.+RX2+2.*(A2/A1)*(1.+RX1))/A2
40              SKY=WCY*(1.+RY2+2.*(B2/B1)*(1.+RY1))/B2
41              H3=H*H*H
42              STR=473.7408*(1.-PR*PR)*(SKX+SKY)/(H3*A2*B2)
43              STR=STR/400.0
44              A3=(A1/A2)**3
45              B3=(B1/B2)**3
```

TABLE IV-III (CONT'D)

```
46            GM=GM/386.
47            SKM=0.25*GM*H*A2*B2*(1.+2.*A3+2.*B3+4.*A3*B3)
48           1    +9.8696*GM*(XI*A2*(1.+2.*A3)/(B2*B2)
49           2    +YI*B2*(1.+2.*B3)/(A2*A2))
50      C       CALCULATE COVER SHEET STIFFNESS AND MASS
51            F22=F(B2,A2)
52            F21=F(B2,A1)
53            F12=F(B1,A2)
54            F11=F(B1,A1)
55            F1S=F22*F22+2.*(A1/A2)*F21*F21
56           1    +2.*(B1/B2)*F12*F12+4.*(A1/A2)*(B1/B2)*F11*F11
57      C       ROOM TEMP STIFFNESS
58            SKO=2.02937*ETEMP(80.,IFF)*H3*(F1S+STR)/((1.-PR*PR)
59           1    *A2*B2)
60      C       ROOM TEMP FREQUENCY
61            F0=5.164*SQRT(SKO/SKM)
62      C       CALCULATE ROOM TEMP MEAN SQUARE STRESS RESPONSE
63            AR=3.*(B2/A2)**2+3.*(A2/B2)**2+2.
64      C       CONVERT DB TO PSI
65            SPL=2.91*10.**(PSL/20.-9.)
66      C       CALCULATE ROOM TEMP DYNAMIC STRESS AT X=0,Y=B2/2
67            SXO=0.36*B2*B2*SQRT(F0/DAMP)*SPL/(H*H*AR)
68      C       CALCULATE ROOM TEMP DYNAMIC STRESS AT X=A2/2,Y=0
69            SYO=1.30*A2*A2*SQRT(F0/DAMP)*SPL/(H*H*AR)
70      C       CONVERT STRESS FROM PSI TO KSI
71            SXO=SXO/1000.0
72            SYO=SYO/1000.0
73      C       CALCULATE ROOM TEMPERATURE LIFE
74            CALL SN(SXO,0.0,80.0,CTF1,IFF)
75            CALL SN(SYO,0.0,80.0,CTF2,IFF)
76            X1=A2/2.
77            Y1=0.0
78            X2=0.0
79            Y2=B2/2.
80            STEMP=0.0
81      C       PRINT ROOM TEMPERATURE RESPONSE
82            WRITE(6,400)
83            GO TO (201,202),IFF
84      201 WRITE(6,405) NCASE
85            GO TO 203
86      202 WRITE(6,406) NCASE
87      203 WRITE(6,410) PSL,T
88            WRITE(6,415)
89            WRITE(6,416) F0
```

TABLE IV-III (CONT'D)

```
90              WRITE(6,420)
91              WRITE(6,425)
92              WRITE(6,430) X2,Y2,SX0,STEMP,CTF1
93              WRITE(6,430) X1,Y1,SY0,STEMP,CTF2
94        C
95        C         THERMAL STRESS EFFECTS
96        C
97              R22=R(B2,A2,PR)
98              R21=R(B2,A1,PR)
99              R12=R(B1,A2,PR)
100             R11=R(B1,A1,PR)
101             F2S=F22*(F22+2.*(A1/A2)**2*F21+2.*(B1/B2)**2*F12
102            1    +4.*(A1/A2)**2*(B1/B2)**2*F11)
103             RST=R22+2.*A3*R12+2.*B3*R21+4.*A3*B3*R11
104             RO=(F1S+STR)/F2S
105       C         CALCULATE CRITICAL TEMPERATURE RISE, TCR
106             TCALP=5.25*H*H*F22/(A2*B2*(1.+PR))
107             CALL CTEMP(TCALP,TCR,IFF)
108       C        **NOTE** TCA AND RS ARE BUCKLING TEMPERATURE
109       C                 AND TEMPERATURE RATIO FOR AN EQUAL
110       C                 SIZE SIMPLE PANEL. R9 IS TEMP RATIO
111       C                 FOR NINE-BAY PANEL
112             TCA=TCR/RO
113             RS=T/TCA
114             R9=T/TCR
115             TACT=T+80.0
116       C         CALCULATE MATERIAL PROPERTIES AT TEMPERATURE
117             ES=ETEMP(TACT,IFF)
118             ALP=ALPHA(TACT,IFF)
119             D=0.0833*ES*H3/(1.-PR*PR)
120       C         CALCULATE RESPONSE FREQUENCY AT TEMPERATURE,T
121             SKT=D*F2S*RO/(A2*B2)
122             FQT=0.809*SQRT(SKT/SKM)
123       C        **NOTE** FQT=FO, ROOM TEMP FREQUENCY
124             STLIN=-ES*ALP*T/(1.-PR)/1000.0
125             IF(RS-RO)205,205,210
126       C         PRE-BUCKLED RESPONSE
127         205 FTEMP=FQT*(0.60+0.40*SQRT(1.-R9))
128             SXT=STLIN
129             SYT=STLIN
130             W0=0.0
131             GO TO 215
132       C         POST-BUCKLED RESPONSE
133         210 FTEMP=FQT*(0.60+0.44*SQRT(R9-1.))
134       C         CALCULATE PLATE BUCKLING AMPLITUDE, W0
135             W0=(3.37-0.20*RO)*H*SQRT(F2S*RO*(R9-1.)/RST)
```

177

TABLE IV-III (CONT'D)

```
136      C        CALCULATE THHERMAL STRESSES
137               C1=1./(A2*B2*(1.-PR*PR))
138               SXT=STLIN+0.81*ES*C1*((2.-PR*PR)*B2/A2+A2*PR/B2)
139            1     *W0*W0/1000.0
140               SYT=STLIN+1.36*ES*C1*(PR*B2/A2+(2.-PR*PR)*A2/B2)
141            1     *W0*W0/1000.0
142      C      CALCULATE DYNAMIC STRESS
143        215  CONTINUE
144               C2=SQRT(FTEMP/F0)
145               SX0=C2*SX0
146               SY0=C2*SY0
147      C        CALCULATE ELEVATED TEMPERATURE LIFE
148               CALL SN(SX0,SXT,TACT,CTF1,IFF)
149               CALL SN(SY0,SYT,TACT,CTF2,IFF)
150      C        PRINT ELEVATED TEMPERATURE RESPONSE
151               WRITE(6,435)
152               TA=TCR+80.0
153               WRITE(6,440) TCR
154               WRITE(6,445) W0
155               WRITE(6,416) FTEMP
156               WRITE(6,420)
157               WRITE(6,425)
158               WRITE(6,430) X2,Y2,SX0,SXT,CTF1
159               WRITE(6,430) X1,Y1,SY0,SYT,CTF2
160               GO TO 200
161      C        FORMAT STATEMENTS FOR OUTPUT DATA
162        400  FORMAT('1',25X,'DYNAMIC RESPONSE OF A',//,19X,
163            1'NINE-BAY STIFFENED PANEL EXPOSED TO',//,21X,
164            2'ACOUSTIC EXCITATION AND HEATING',/)
165        405  FORMAT(29X,'DATA CASE',I4,//,27X,'MATERIAL : TITANIUM')
166        406  FORMAT(29X,'DATA CASE',I4,//,27X,'MATERIAL : ALUMINUM')
167        410  FORMAT(5X,'EXCITATION SPECTRUM LEVEL = ',F4.0,1X,'DB',
168            13X,'TEMPERATURE INCREASE = ',F4.0,1X,'DEG. F',//)
169        415  FORMAT(24X,'ROOM TEMPERATURE RESPONSE',/)
170        416  FORMAT(20X,'FUNDAMENTAL FREQUENCY =',F7.1,' HZ',/)
171        420  FORMAT(5X,'STRESS AT POINT',3X,'DYNAMIC STRESS',3X,
172            1'THERMAL STRESS ',3X,'CYCLES TO FAILURE')
173        425  FORMAT(8X,'X',7X,'Y',11X,'KSI',14X,'KSI',/)
174        430  FORMAT(6X,F5.2,3X,F5.2,5X,F8.3,9X,F8.3,10X,1PE9.2,/)
175        435  FORMAT(////,23X,'ELEVATED TEMPERATURE RESPONSE',/)
176        440  FORMAT(10X,'BUCKLING TEMPERATURE =',F8.2,' DEG. F'
177            1,' ABOVE ROOM TEMPERATURE',/)
178        445  FORMAT(18X,'BUCKLING AMPLITUDE =',F8.4,
179            1'  INCHES',/)
180               END
```

TABLE IV-IV

OUTPUT FORMAT FOR DYNAMIC ANALYSIS COMPUTER PROGRAM

```
                    DYNAMIC RESPONSE OF A
              NINE-BAY STIFFENED PANEL EXPOSED TO
                ACOUSTIC EXCITATION AND HEATING

                      DAT  CASE   4

                    MATERIAL : ALUMINUM
      EXCITATION SPECTRUM LEVEL = 135. DB    TEMPERATURE INCREASE = 2 0. DEG. F


                   ROOM TEMPERATURE RESPONSE

                FUNDAMENTAL FREQUENCY =   175.. HZ
```

STRES AT POINT		DYNAMIC STRES	THERMAL STRES	CYCLES TO FAILURE
X	Y	KSI	KSI	
.0	6.0	6.075	.0	6.43+06
3.0	.0	5.485	.0	1.03+ 7

```
                  ELEVATED TEMPERATURE RESPONSE

         BUCKLING TEMPERATURE =   11.00 DEG. F ABOVE ROOM TEMPERATURE

                BUCKLING AMPLITUDE =   .2 5  INCHES

              FUNDAMENTAL FREQUENCY =   417.5 HZ
```

STRES AT POINT		DYNAMIC STRESS	THERMAL STRES	CYCLES TO FAILURE
X	Y	KSI	KSI	
.00	6.0	9.371	-16.83	1.32+05
3.00	.00	8.460	-24.342	1.40+ 5

The input parameters are:

TCALP - Product of critical buckling temperature and coefficient of thermal expansion.

IFF - Alloy Code

= 1 for Titanium Alloy (6Al-4V Annealed)

= 2 for Aluminum Alloy (7075-T6)

The output parameter is:

TC - Critical buckling temperature - °F above Ambient

The subprogram is listed in Table IV-V.

b. Subprogram PROP - This program computes stiffening member properties such as area and moment of inertia. The basic relations are from Reference 8, Appendix I. Two different sectional shapes are available, a zee or a channel section, with the parameters described in Figures A-1-1 and A-1-2, respectively, of the referenced report.

The input parameters are:

OPT - Option code to select sectional shape

= 0 for zee-section

= 1 for channel section

B - Flange width of stiffening member - in

H - Height of stiffening member - in

T - Thickness of stiffening member - in

The output parameters are:

A - Cross-sectional area - in^2

RJ - St. Venant's Torsion Constant - in^4

GAMAT - Warping constant for thin walled open section beam, with the pole taken at the shear center - in^6

XIP - Polar moment of inertia, referenced to rotation about the attachment point - in^4

The listing of this program is presented in Table IV-VI.

TABLE IV-V

COMPUTER PROGRAM FOR CALCULATING SKIN BUCKLING TEMPERATURE

```
1            SUBROUTINE CTEMP(TCALP,TC,IF )
2       C        THIS SUBROUTINE CALCULATES SKIN BUCKLING
3       C        TEMPERATURE FOR ALUMINUM OR TITANIUM ALLOY
4       C        STRUCTURAL PANELS.
5       C
6       C        TCALP - PRODUCT OF BUCKLING TEMPERATURE
7       C                AND ALPHA FROM CALLING PROGRAM
8       C        TC - BUCKLING TEMPERATURE - DEG F ABOVE
9       C             ROOM TEMPERATURE
10      C        IF  - ALLOY CODE
11      C              = 1 TITANIUM
12      C              = 2 ALUMINUM
13      C
14           TC=0.0
15           GO TO (100,200),IF
16      C  **********************************************
17      C        MATERIAL 6AL-4V TITANIUM ANNEALED
18      C        TEMPERATURE LIMITATION 100  DEG. F
19      C
20      100  C1=4.45E-06
21           C2=4.83E-09
22           I=1
23       1   C3=80.*C2+C1
24           TC=.5*SQRT((C3/C2)**2+4.*TCALP/C2)-.5*C3/C2
25           T=TC+80.
26           IF(T-260.) 50,50,2
27       2   IF(T-360.) 3,3,5
28       3   C1=4.9E-06
29           C2=2.5E-09
30           I=I+1
31           IF(I-2) 1,1,50
32       5   C1=5.80E-06
33           TC=TCALP/C1
34      50   TC=TC
35           RETURN
```

TABLE IV-V (CONT)

```
36      C    **********************************************************
37      C          MATERIAL 7075-T6 ALUMINUM ALLOY
38      C          TEMPERATURE LIMITATION 600 DEG. F
39      C
40      200  F1=12.4E-06
41           F2=5.0E-09
42           II=1
43      201  F3=80.*F2+F1
44           TC=0.50*SQRT((F3/F2)**2+4.0*TCALP/F2)+0.50*F3/F2
45           T=TC+80.
46           IF(T-100.)500,500,202
47      202  IF(T-300.)203,203,204
48      203  F1=10.625E-06
49           F2=0.75E-09
50           II=II+1
51           IF(II-2)201,201,500
52      204  IF(T-400.)205,205,206
53      205  F1=13.0E-06
54           F2=1.5E-09
55           II=II+1
56           IF(II-2)201,201,500
57      206  F1=13.6E-06
58           TC=TCALP/F1
59      500  TC=TC
60           RETURN
61           END
```

TABLE IV-VI
COMPUTER PROGRAM FOR CALCULATING SECTION PROPERTIES

```
1           SUBROUTINE PROP(OPT,B,H,T,A,RJ,GAMAT,XIP)
2     C
3     C        SECTION PROPERTIES
4     C          IF OPT = 0   ZEE SECTION
5     C          IF OPT = 1   CHANNEL SECTION
6     C          H= STRINGER HEIGHT, CL TO CL
7     C          B= FLANGE WIDTH
8     C          T= STRINGER THICKNESS
9     C        REFERENCE: AFFDL-TR-71-107
10    C        WC - WARPING CONSTANT ABOUT SHEAR CENTER
11    C        GAMAT - WARPING CONSTANT ABOUT ATTACH POINT
12    C        A - CROSS SECTIONAL AREA
13    C        RJ- ST. VENANTS TORSION CONSTANT - J
14    C        XIP - POLAR MOMENT OF INERTIA ABOUT ATTACH POINT
15          IF(OPT) 1,1,2
16    C        ZEE STIFFENER
17    1     A=T*(H+2.*B)
18          D=H**2*(6.*B+H)
19          D1=T**2*(3.*H+2.*B)
20          XXI=(T*(D+D1))/12.
21          D2=2.*B+T
22          D3=2.*B-T
23          XZI=-(T*H*D2*D3)/8.
24          ZZI=(T/12.)*(8.*B**3+H*T**2)
25          RJ=(T**3/3.)*(2.*B+H)
26          WC=T*B**3*H**2*(B+2.*H)/(12.*(2.*B+H))
27          SX=B/2.
28          SZ=-H/2.
29          D4=SX**2+SZ**2
30          D5=D4*A
31          XIP=(XXI+ZZI+D5)
32          GAMAT=WC+(SZ**2)*ZZI-2.*SX*SZ*XZI+(SX**2)*XXI
33          RETURN
34    C        CHANNEL SECTION
35    2     F=2.*B+H
36          XBAR=B**2/F
37          F1=6.*B+H
38          E=3.*B**2/F1
39          CX=E+XBAR
40          SX=E+(B/2.)
41          SZ=-H/2.
42          EX=CX-SX
43          A=T*(H+2.*B)
44          F2=3.*H+2.*B
45          XXI=T*(H**2*F1+T**2*F2)/12.
46          F3=12.*H*XBAR**2+8.*B**3
47          F4=B-XBAR
48          F5=B-2.*XBAR
49          ZZI=T*(F3-24.*XBAR*B*F4+12.*B*F5*T+6.*F4*T**2+T**3)/12.
50          RJ=T**3*F/3.
51          F6=3.*B+2.*H
52          WC=T*B**3*H**2*F6/(12.*F1)
53          GAMAT=WC+(SZ**2)*ZZI+(SX**2)*XXI
54          F7=(EX**2+SZ**2)*A
55          XIP=(XXI+ZZI+F7)
56          RETURN
57          END
```

183

APPENDIX V

TEMPERATURE DEPENDENCE OF MATERIAL PROPERTIES

The analytical development presented in Section II focused attention upon the temperature effects associated with the state of strain of the structure. The results obtained from these considerations indicate that the structural stiffness decreases with temperature rise up to the critical temperature, and that for a temperature rise above the critical temperature, the structural stiffness increases.

Beyond these considerations, certain alloy properties are temperature-dependent, and this dependency must be included to predict structural life accurately. Algorithms were developed to represent the temperature dependence of each property considered, and computer programs were written to expedite their use with the dynamic analysis computer program detailed in Appendix IV.

The material properties considered are the elastic (Young's) modulus, E, the coefficient of thermal expansion, α, and the characteristics of the fatigue curves for each alloy. Static properties were obtained from MIL-HDBK-5B[17], and generally agree with those of AFML-TR-68-115[20]. The analytical expression for fatigue life is based on the mean stress variation inferred from MIL-HDBK-5B and the fatigue characteristics, with temperature variation, resulting from the coupon fatigue testing discussed in Section III.3.

A. Static Material Properties

This discussion will concern the effect of temperature on the static material properties of 7075-T6 aluminum and 6A1-4V annealed titanium sheet material. The assumed ambient temperature for this development is 80°F.

1. Elastic Modulus

The effects of temperature on the elastic modulus of 7075-T6 aluminum and 6A1-4V annealed titanium alloys are shown in Figure V-1. These curves are reproduced from MIL-HDBK-5B, Figures 3.2.7.1.4 and 5.4.6.2.4, respectively.

The elastic modulus curve for 7075-T6 aluminum decreases steadily with increasing temperature. Since a single straight line representation would not suffice, the temperature range was broken into three regions. For each of these temperature regions, the elastic modulus was represented by a straight line element as follows:

a) Room temperature to 200°F $(80 \leq T \leq 200)$
$$E = \left| 1.020 - 0.0003\, T \right| E_o$$

b) 200° to 400°F $(200 \leq T \leq 400)$
$$E = \left| 0.960 - 0.0007\,(T - 200) \right| E_o$$

c) 400° to 600°F $(400 \leq T \leq 600)$
$$E = \left| 0.820 - 0.0016\,(T - 400) \right| E_o$$

184
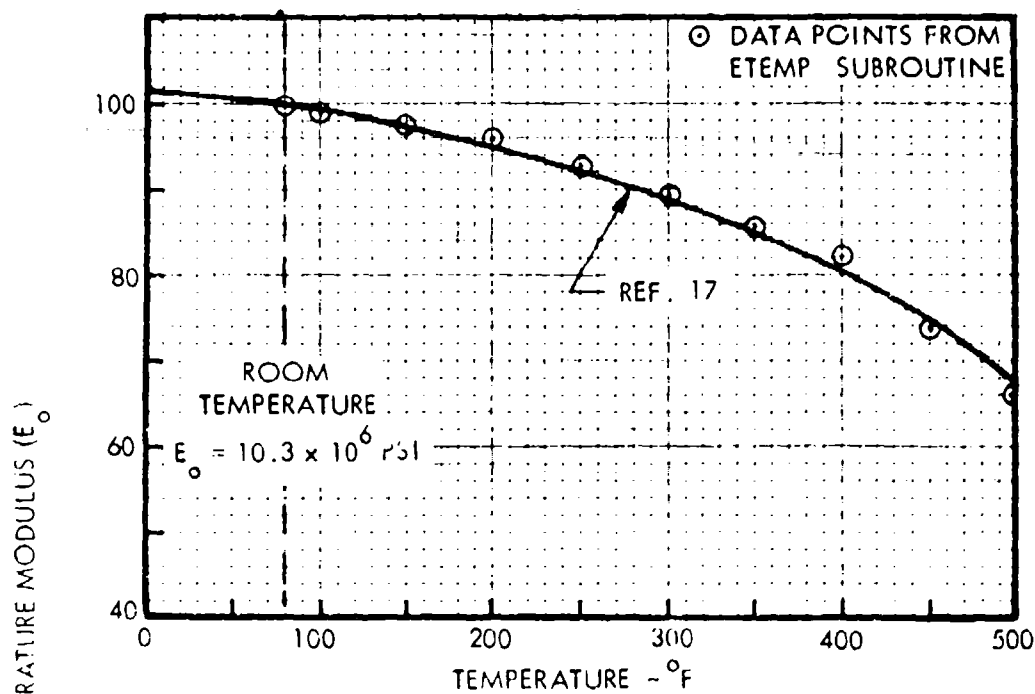
a) ALUMINUM ALLOY 7075-T6 SHEET
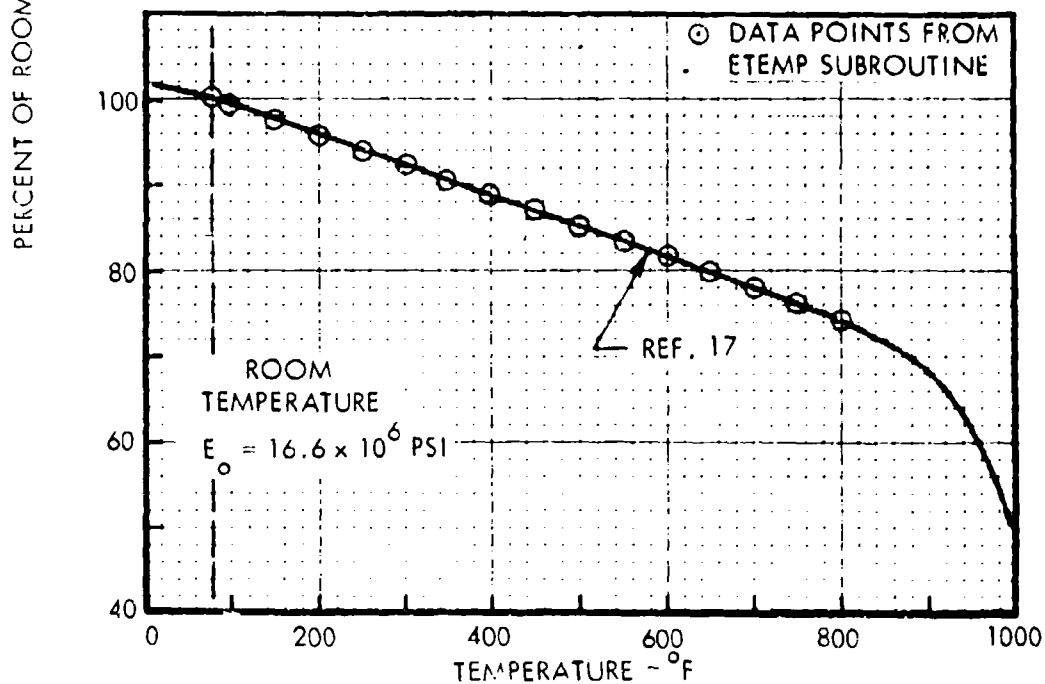
b) TITANIUM ALLOY 6Al-4V ANNEALED SHEET

FIGURE V-1. TEMPERATURE EFFECTS ON ELASTIC MODULUS
(FROM REFERENCE 17)

185

where $E_o = 10.3 \times 10^6$ psi is the room temperature elastic modulus.

The elastic modulus for titanium has a linear relationship with temperature below 800°F. Hence, the titanium modulus is represented by the following single relation:

a) Room temperature to 800°F (80 $\leq$ T $\leq$ 800)

$$E = (1.030 - 0.000375\ T)\ E_o$$

where the room temperature modulus is $E_o = 16.6 \times 10^6$ psi.

The above representations of the elastic modulus were developed into a digital computer program for use by the analytical program discussed in Appendix IV. This function, entitled "ETEMP", is presented in Table V-1. Since this program is a function, the input format is simply

$$ETEMP(T, IFF)$$

in the calling program, where

T - Input temperature at which the elastic modulus is desired - °F

IFF - Alloy code

  = 1 Titanium Alloy (6A1-4V annealed)

  = 2 Aluminum Alloy (7075-T6)

Data points calculated from this program, in temperature increments of 50°F, are compared with the MIL-HDBK-5B curves in Figure V-1.

2. Coefficient of Thermal Expansion

The effects of temperature on the thermal expansion of aluminum and titanium alloys are shown in Figure V-2. These curves are reproduced from MIL-HDBK-5B, Figures 3.2.7.0 and 5.4.6.1, respectively.

The coefficient of normal expansion, α, for aluminum alloy increases exponentially with increasing temperature as shown in Figure V-2. Hence, the temperature range was divided into three regions and the following representations were derived:

a) Room temperature to 100°F (80 $\leq$ T $\leq$ 100)

$$\alpha = \left| 12.4 + 0.0050\ T \right| 10^{-6}$$

b) 100° to 300°F (100 $\leq$ T $\leq$ 300)

$$\alpha = \left| 12.9 + 0.00275(T-100) \right| 10^{-6}$$

c) 300° to 400°F (300 $\leq$ T $\leq$ 400)

$$\alpha = \left| 13.45 + 0.0015(T-300) \right| 10^{-6}$$

TABLE V-I

COMPUTER PROGRAM FOR CALCULATING ELASTIC MODULUS

```
1           FUNCTION ETEMP(T,IFF)
2     C
3     C         THIS FUNCTION COMPUTES ELASTIC MODULUS FOR
4     C         ALUMINUM OR TITANIUM ALLOY AS A FUNCTION OF
5     C         TEMPERATURE
6     C
7     C         T - INPUT TEMPERATURE - DEG. F
8     C         IFF - ALLOY CODE
9     C               = 1 TITANIUM
10    C               = 2 ALUMINUM
11    C
12          GO TO (100,200),IFF
13    C ************************************************
14    C     MATERIAL 6AL-4V TITANIUM ANNEALED SHEET
15    C     REFERENCE MIL-HDBK-5B
16    C     TEMPERATURE LIMITATION 800 DEGREES F
17    C          RT<T<800 F
18    100   IF(800-T)180,190,150
19    190   ETEMP=(1.030-0.000375*T)*16.6E+06
20          RETURN
21    C          T>800 F
22    180   ETEMP=12.1E+06
23          WRITE(6,333)
24          RETURN
25    C ************************************************
26    C     MATERIAL 7075-T6 SHEET
27    C     REFERENCE MIL-HDBK-5B
28    C     TEMPERATURE LIMITATION 600 DEGREES F
29    C          RT<T<200 F
30    200   IF(200-T)220,210,210
31    210   ETEMP=(1.020-0.00030*T)*10.3E+06
32          RETURN
33    C          200<T<400 F
34    220   IF(400-T)240,230,230
35    230   ETEMP=(0.96-0.00070*(T-200))*10.3E+06
36          RETURN
37    C          400<T<600 F
38    240   IF(600-T)260,250,250
39    250   ETEMP=(0.82-0.0016*(T-400))*10.3E+06
40          RETURN
41    C          T>600 F
42    260   ETEMP=0.50*10.3E+06
43          WRITE(6,333)
44    333   FORMAT(/,5X,'UPPER TEMP LIMIT ON ELAST MODULUS',
45         1' EXCEEDED'/)
46          RETURN
47          END
```
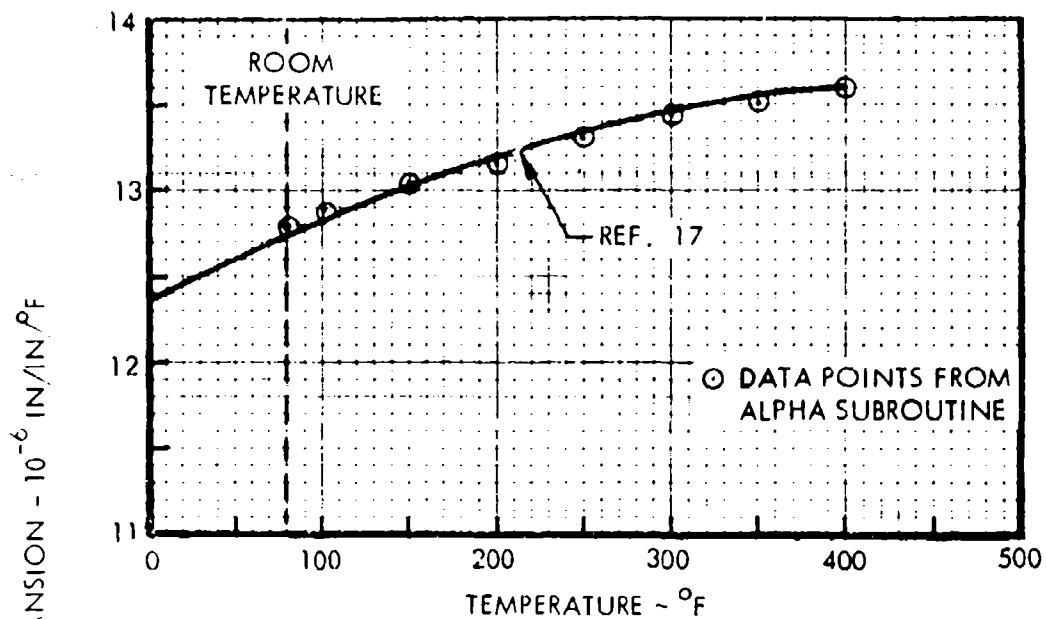
a) ALUMINUM ALLOY 7075-T6
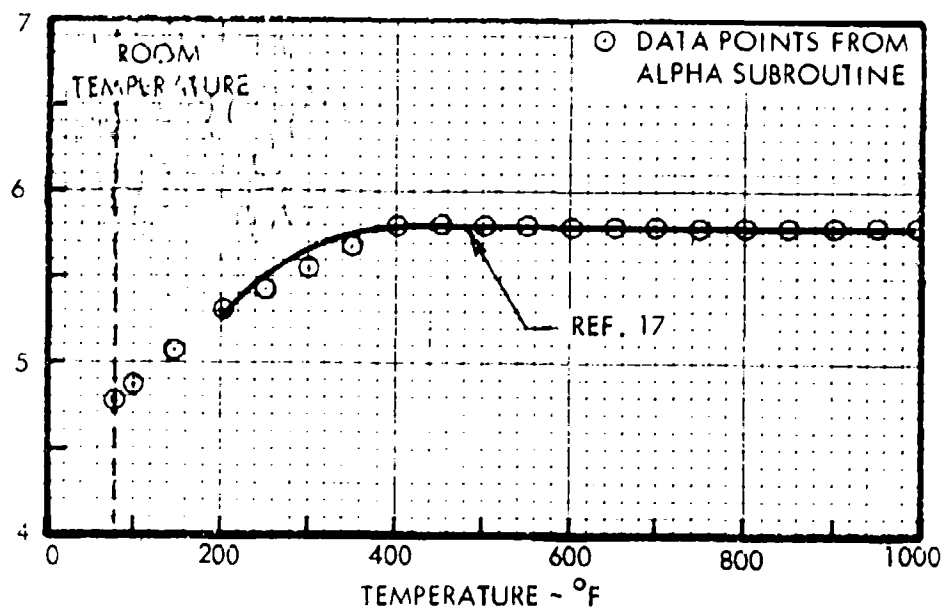
b) TITANIUM ALLOY 6AI-4V

FIGURE V-2. TEMPERATURE EFFECTS ON COEFFICIENT OF THERMAL EXPANSION (FROM REFERENCE 17)

188

The coefficient of thermal expansion for titanium increases from 200° to 400°F and is a constant thereafter. As no data were available for temperatures less than 200°F, the slope of the segment at 200°F was projected to room temperature to develop a relationship for the computer program. The resulting analytical representations are:

a)   Room temperature to 200°F (80 ≤ T ≤ 200)
$$\alpha = (4.45 + 0.00425 \, T) \quad 10^{-6}$$

b)   200° to 400°F (200 ≤ T ≤ 400)
$$\alpha = (4.80 + 0.0025T)10^{-6}$$

c)   400° to 1000°F (400 ≤ T ≤ 1000)
$$\alpha = 5.80 \times 10^{-6}$$

The preceding representations of the coefficient of thermal expansion were formulated into a digital computer program similar to that for the elastic modulus. This "ALPHA" function is presented in Table V-11. The input format is

     ALPHA (T, IFF)

in the calling program, where T and IFF are as defined in the preceding subsection.

B.   Fatigue Characteristics

The analytical description of the fatigue curves described here resulted from a review of fatigue data presented in MIL-HDBK-5B and the data from the coupon fatigue tests at room and elevated temperatures. It was assumed that for all values of mean stress, σ_m, dynamic stress, $\widetilde{\sigma}$, and temperature, T, the resulting fatigue curve would be linear when plotted on log-log scales.

1. Mean Stress Effects

The effect of increasing mean stress is basically a decrease in fatigue life at constant dynamic stress. Figures V-3 and V-4 present fatigue curves for axially loaded aluminum at room temperature, and titanium at room temperature and 600°F. These curves were obtained from MIL-HDBK-5B in the form of constant amplitude test data and were converted to an equivalent random amplitude fatigue curve by the method of Reference 1. Based on these room and elevated temperature curves, it was determined that the effect of increasing mean stress was to lower the RMS stress level by a constant amount from the zero mean stress curve. This decrease in dynamic stress was approximately 1 ksi for every 10 ksi increase in mean stress. Then, if only a zero mean stress fatigue curve were available, as is the case for the coupon fatigue data of Section III, the dynamic stress can be corrected by subtracting $0.1 \, \sigma_m$ from the dynamic stress, where σ_m is the mean stress. The equation for the zero mean stress fatigue curve is of the form

$$\log N = A + B \log \widetilde{\sigma} \qquad\qquad\qquad (V\text{-}1)$$

Then the equation, including mean stress effects, becomes

$$\log N = A + B \log (\widetilde{\sigma} - 0.1 \, \sigma_m) \qquad\qquad\qquad (V\text{-}2)$$

189

TABLE V-II

COMPUTER PROGRAM FOR CALCULATING COEFFICIENT OF THERMAL EXPANSION

```
 1              FUNCTION ALPHA(T,IFF)
 2      C
 3      C          THIS FUNCTION COMPUTES COEFFICIENT OF THERMAL
 4      C          EXPANSION FOR ALUMINUM OR TITANIUM ALLOY AS A
 5      C          FUNCTION OF TEMPERATURE
 6      C
 7      C          T - INPUT TEMPERATURE - DEG. F
 8      C          IFF - ALLOY CODE
 9      C                =1   TITANIUM
10      C                =2   ALUMINUM
11      C
12              GO TO (100,200),IFF
13      C  *****************************************************
14      C     MATERIAL 6AL-4V TITANIUM SHEET
15      C     ANNEALED
16      C     REFERENCE MIL-HDBK-5B
17      C     TEMPERATURE LIMITATION 1000 DEGREES F
18      C          RT<T<200 F
19        100   IF(200-T)180,150,150
20        150   ALPHA=(4.45+0.00425*T)*1.0E-06
21              RETURN
22      C          200<T<400 F
23        180   IF(400-T)185,190,190
24        190   ALPHA=(4.80+0.0025*T)*1.0E-06
25              RETURN
26      C          400<T<1000 F
27        185   IF(1000-T)195,198,198
28        195   WRITE(6,500)
29        500   FORMAT(X,5X,'UPPER TEMP LIMIT ON COEFF OF EXPAN ',
30            1'EXCEEDED',/)
31        198   ALPHA=5.8E-06
32              RETURN
33      C  *****************************************************
34      C     MATERIAL 7075-T6 SHEET
35      C     REFERENCE MIL-HDBK-5B
36      C     TEMPERATURE LIMITATION 600 DEGREES F
37      C          RT<T<100 F
38        200   IF(100-T)220,210,210
39        210   ALPHA=(12.4+0.0050*T)*1.0E-06
40              RETURN
41      C          100<T<300 F
42        220   IF(300-T)240,230,230
43        230   ALPHA=(12.9+0.00275*(T-100))*1.0E-06
44              RETURN
45      C          300<T<400 F
46        240   IF(400-T)260,250,250
47        250   ALPHA=(13.45+0.00150*(T-300))*1.0E-06
48              RETURN
49      C          T>400 F
50        260   ALPHA=13.6E-06
51              IF(600-T)280,270,270
52        280   WRITE(6,500)
53        270   RETURN
54              END
```
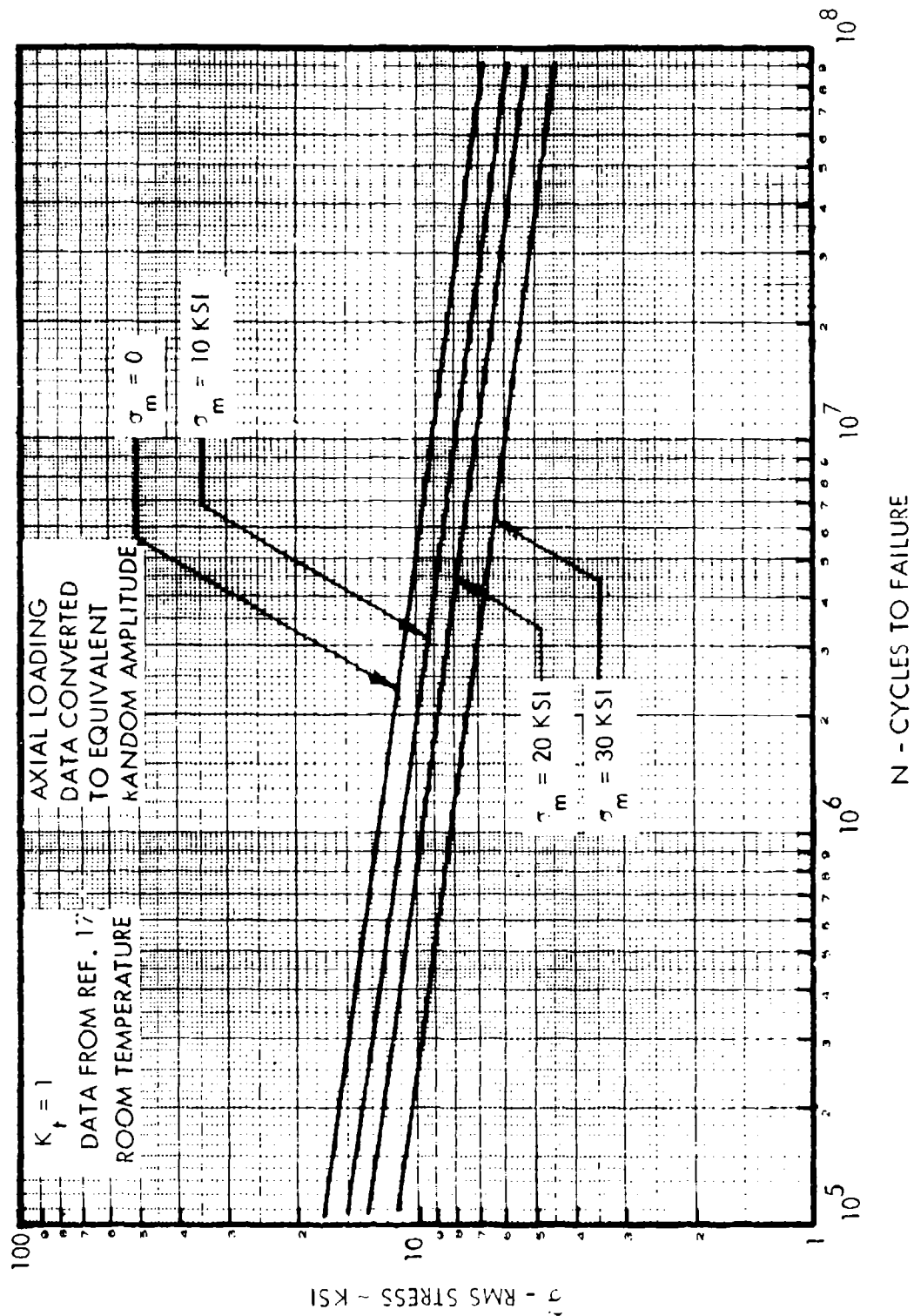
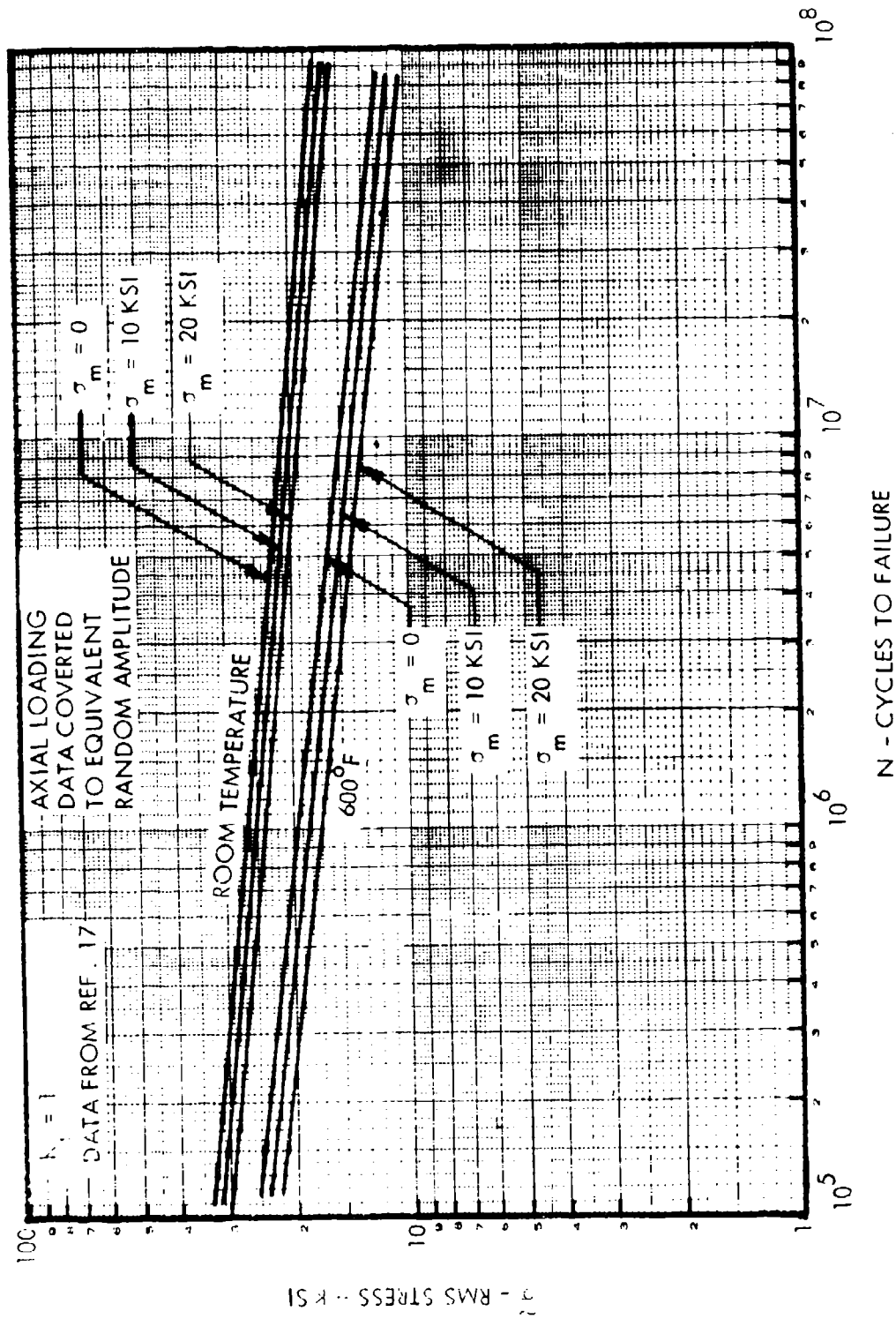FIGURE V-3. RANDOM AMPLITUDE FATIGUE CURVE
7075-T6 ALUMINUM

191

FIGURE V-4. RANDOM AMPLITUDE FATIGUE CURVE
6Al-4V TITANIUM

192

This relation was found to be valid for both the aluminum and titanium data of Figures V-3 and V-4.

From the riveted coupon fatigue tests of Section III, the equations for the regression lines of the room and 300°F temperature fatigue curves were as follows for the aluminum data:

$$\log N = 10.42 - 4.61 \log \tilde{\sigma} \qquad (80^\circ F)$$

$$\log N = 9.13 - 3.85 \log \tilde{\sigma} \qquad (300^\circ F) \tag{V-3}$$

Since only two temperature points were available, it was assumed that, if the regression line was linear on a log-log scale, then the slope and the intercept of each equation varied linearly with temperature. Therefore, the intercept, A, and slope, B, can be expressed as functions of temperature by

$$C_{11} + C_{12}T = A \qquad\qquad \text{and} \quad C_{21} + C_{22}T = B$$

Using the constants in Equations (V-3) gives

$$C_{11} + 80\, C_{12} = 10.42 \qquad\qquad C_{21} + 80\, C_{22} = -4.61$$

$$C_{11} + 300\, C_{12} = 9.13 \qquad\qquad C_{21} + 300\, C_{22} = -3.85 \tag{V-4}$$

Solving Equations (V-4) gives the constants

$$C_{11} = 10.89 \qquad\qquad C_{21} = -4.89$$

$$C_{12} = -0.00584 \qquad\qquad C_{22} = 0.00347$$

and the intercept and slope become

$$A = 10.89 - 0.00584\, T$$

$$B = -4.89 + 0.00347\, T$$

Then, the general expression for the fatigue curve, at zero mean stress, is

$$\log N = (10.89 - 0.00584T) - (4.89 - 0.00347T) \log \tilde{\sigma}$$

Introducing the mean stress variation as assumed for Equation (V-2), the fatigue curve is given by

$$\log N = (10.89 - 0.00584\, T) - (4.89 - 0.00347\, T) \log (\tilde{\sigma} - 0.1 \sigma_m) \tag{V-5}$$

where N = life in cycles to failure

$\tilde{\sigma}$ = dynamic stress, ksi rms

σ_m = mean stress, ksi

T = temperature in degrees Fahrenheit.

The equations of the regression lines for the titanium alloy riveted coupon fatigue data of Section III are

$$\log N = 12.28 - 5.26 \log \tilde{\sigma} \qquad (80^\circ F)$$

$$\log N = 10.33 - 4.34 \log \tilde{\sigma} \qquad (600^\circ F) \qquad (V-6)$$

Repeating the procedure given for the aluminum alloy gives the following constants:

$$C_{11} = 12.58 \qquad\qquad C_{21} = -5.40$$

$$C_{12} = -0.00376 \qquad\qquad C_{22} = 0.00176$$

and then

$$A = 12.58 - 0.00376\ T$$

$$B = -5.40 + 0.00176\ T$$

The fatigue curve for titanium alloy, at any mean stress or temperature, is then given by

$$\log N = (12.58 - 0.00376\ T) - (5.40 - 0.00176\ T) \log (\tilde{\sigma} - 0.1\ \sigma_m) \qquad (V-7)$$

where all parameters are as defined for the aluminum alloy.

These relations were formulated into a computer program for use with the general analysis program of Appendix IV. This program, in the form of a Subroutine, is presented in Table V-III and is entitled "SN." The input parameters are

SDYN – Dynamic Stress – ksi rms

STEMP – Thermal (or Mean) Stress – ksi

TEMP – Temperature – $^\circ F$

IFF – Alloy Code

     =   1 Titanium (6Al-4V annealed)

     =   2 Aluminum (7075-T6)

The output to the calling program is

CIF – Life in cycles to failure

TABLE V-III

COMPUTER PROGRAM FOR CALCULATING FATIGUE LIFE

```
1           SUBROUTINE SN(SDYN,STEMP,TEMP,CTF,IFF)
2     C
3     C     THIS SUBROUTINE CALCULATES FATIGUE LIFE FOR
4     C     ALUMINUM OR TITANIUM ALLOY AS A FUNCTION OF
5     C     TEMPERATURE AND MEAN STRESS.  THIS SUBROUTINE
6     C     IS BASED ON COUPON FATIGUE TEST DATA AT ROOM
7     C     AND ELEVATED TEMPERATURE.
8     C
9     C     ROOM TEMPERATURE IS 80 DEG. F
10    C
11    C        SDYN - DYNAMIC STRES  - KSI (RMS)
12    C        STEMP - THERMAL (OR MEAN) STRESS - KSI
13    C        TEMP - TEMPERATURE - DEG. F
14    C        CTF - LIFE IN CYCLES TO FAILURE
15    C        IFF - ALLOY CODE
16    C           = 1 TITANIUM
17    C           = 2 ALUMINUM
18    C
19          GO TO(100,200),IFF
20    C     ***************************************************
21    C        MATERIAL 6AL-4V TITANIUM SHEET ANNEALED
22    C        TEMPERATURE LIMITATION 600 DEG. F
23    C
24    100   C1=12.58-0.00376*TEMP
25          C2=-5.40+0.00276*TEMP
26          ARF=C1+C2*ALOG10(SDYN-0.1*STEMP)
27          CTF=10.**ARF
28          RETURN
29    C     ***************************************************
30    C        MATERIAL 7075-T6 ALUMINUM SHEET
31    C        TEMPERATURE LIMITATION 300 DEG. F
32    C
33    200   C1=10.89-0.00584*TEMP
34          C2=-4.89+0.00347*TEMP
35          ARF=C1+C2*ALOG10(SDYN-0.1*STEMP)
36          CTF=10.**ARF
37          RETURN
38          END
```

DOCUMENT CONTROL DATA - R & D

Security classification of title, body of abstract and indexing annotation must be entered when the overall report is classified)

1. ORIGINATING ACTIVITY (Corporate author)	2a. REPORT SECURITY CLASSIFICATION
Lockheed Aircraft Corp. Lockheed-Georgia Company Marietta Georgia 30063	Unclassified
	2b. GROUP

3. REPORT TITLE

ACOUSTIC FATIGUE OF AIRCRAFT STRUCTURES AT ELEVATED TEMPERATURES

4. DESCRIPTIVE NOTES (Type of report and inclusive dates)
Final - April 1972 - December 1973

5. AUTHOR(S) (First name, middle initial, last name)

Cecil W. Schneider

6. REPORT DATE	7a. TOTAL NO. OF PAGES	7b. NO. OF REFS
March 1974	195	20

8a. CONTRACT OR GRANT NO.	9a. ORIGINATOR'S REPORT NUMBER(S)
F33615-72-C-1141	LG73ER0182
b. PROJECT NO. 1471	
c. Task No. 147101	9b. OTHER REPORT NO(S) (Any other numbers that may be assigned this report)
d.	AFFDL-TR-73-155, Part I

10. DISTRIBUTION STATEMENT

Distribution limited to U. S. Government agencies only: test and evaluation; statement applied October 1973. Other requests for this document must be referred to Air Force Flight Dynamics Laboratory, AFFDL/FY, WPAFB, Ohio 45433.

11. SUPPLEMENTARY NOTES	12. SPONSORING MILITARY ACTIVITY
	Air Force Flight Dynamics Laboratory Wright-Patterson AFB, Ohio, 45433

13. ABSTRACT

An analytical and experimental program was conducted to develop acoustic fatigue design criteria for aircraft structures subjected to intense noise in a high temperature environment. Equations for the dynamic response of a buckled panel were formulated for simply supported boundary conditions using large deflection plate theory. Random amplitude acoustic fatigue testing of representative aircraft structure was accomplished at temperatures up to 600°F to provide data for correlation with the analytical results. Empirical design criteria are presented in the form of design equations and nomographs for predicting the combined thermal and dynamic response of aircraft structures.

DD FORM 1473
I NOV 65

KEY WORDS	LINK A		LINK B		LINK C	
	ROLE	WT	ROLE	WT	ROLE	WT
Acoustic Fatigue						
Dynamic Response						
Structural Design						
Structural Heating						
High Temperature Fatigue						
Curvature Effects						